Letter of Intent
for
KEK Super B Factory

Part I: Physics

edited by S. Hashimoto and M. Hazumi

March 10, 2004

Contents

Executive Summary **4**

1 Introduction **8**
1.1 Motivation for the Higher Luminosity B Factory 8
1.2 Belle Status and Prospects 10
1.2.1 Status of CP-Violation in $b \to c\bar{c}s$ Processes 10
1.2.2 Status of CP-Violation in $b \to sq\bar{q}$ Penguin Processes 13
1.2.3 Radiative B decays 15
1.2.4 Electroweak Rare B Decays 19
1.2.5 Prospects 23
References 23

2 Flavor Structure of the Standard Model **28**
2.1 Flavor Structure of the Standard Model 28
2.2 Low Energy Effective Hamiltonians 30
2.3 $B - \overline{B}$ Mixing 33
2.4 Time-dependent Asymmetries 34
2.4.1 Measurement of $\sin 2\phi_1$ 35
2.4.2 Measurement of ϕ_2 36
2.5 Theoretical Methods 37
2.5.1 Heavy Quark Symmetry 37
2.5.2 Heavy Quark Expansion 38
2.5.3 Perturbative Methods 38
2.5.4 Lattice QCD 39
References 41

3 Flavor Structure of the Physics beyond the Standard Model **47**
3.1 Motivation for New Physics 47
3.2 New Physics Scenarios 48
3.3 Supersymmetric Models 48
3.4 SUSY Effect on $b \to s$ Transitions 50
3.5 Lepton Flavor Violation 55
3.5.1 LFV in the Supersymmetric Models 55
3.5.2 SUSY Seesaw Mechanism and SUSY GUTs 58
3.5.3 Other Theoretical Models 60
References 60

4 Sensitivity at SuperKEKB **66**
4.1 Overview . . . 66
4.1.1 Goals of sensitivity studies . . . 66
4.1.2 Time-dependent CP asymmetries . . . 67
4.1.3 B tagging with full reconstruction . . . 69
4.2 New CP-violating phase in $b \to s\bar{q}q$ . . . 72
4.2.1 Introduction . . . 72
4.2.2 $B^0 \to \phi K^0_S$, $\eta' K^0_S$ and $K^+K^-K^0_S$ . . . 72
4.2.3 $B^0 \to K^0_S K^0_S K^0_S$ and $\pi^0 K^0_S$ . . . 76
4.2.4 $B^\pm \to \phi\phi X^\pm_s$ . . . 79
4.2.5 Discussion . . . 82
4.3 $b \to s\gamma$ and $b \to s\ell^+\ell^-$ . . . 85
4.3.1 Introduction . . . 85
4.3.2 $B \to X_s\gamma$ branching fraction . . . 86
4.3.3 $B \to K^*\ell^+\ell^-$ forward-backward asymmetry . . . 87
4.3.4 $B \to K\mu^+\mu^-$ versus $B \to Ke^+e^-$ . . . 89
4.3.5 Mixing induced CP asymmetry in $B \to K^*\gamma$ . . . 90
4.3.6 $B \to X_s\gamma$ direct CP asymmetry . . . 91
4.3.7 $b \to d\gamma$ and $b \to d\ell^+\ell^-$ . . . 92
4.3.8 Summary . . . 92
4.4 More than one neutrino I: $B \to K^{(*)}\nu\bar{\nu}$ and $B \to \tau\nu$ . . . 93
4.4.1 Introduction . . . 93
4.4.2 Estimation of signal and background . . . 94
4.4.3 Discussion . . . 95
4.5 More than one neutrino II: $B \to \bar{D}\tau^+\nu_\tau$ . . . 99
4.5.1 Introduction . . . 99
4.5.2 $B \to \bar{D}\tau^+\nu_\tau$ Reconstruction . . . 99
4.5.3 Kinematic Event Selection . . . 101
4.5.4 Background Components . . . 102
4.5.5 Statistical Significance . . . 105
4.5.6 Systematic Uncertainty . . . 105
4.5.7 Constraints on the Charged Higgs Mass . . . 105
4.5.8 Summary . . . 106
4.6 $\sin 2\phi_1$ . . . 107
4.7 ϕ_2 . . . 110
4.7.1 Status of the $B^0 \to \pi^+\pi^-$ analysis . . . 110
4.7.2 Isospin analysis for $B \to \pi\pi$ . . . 110
4.7.3 Status of the $B^0 \to \rho\pi$ analysis . . . 113
4.7.4 Dalitz plot analysis of $B^0 \to \rho\pi$ . . . 113
4.8 ϕ_3 . . . 117
4.8.1 Introduction . . . 117
4.8.2 $D^{(*)-}\pi^+$ modes . . . 117
4.8.3 $B^\pm \to DK^{*\pm}$ (ADS method) . . . 121
4.8.4 $B^\pm \to DK^\pm$ (Dalitz analysis) . . . 123
4.9 $|V_{ub}|$ . . . 129
4.9.1 Introduction . . . 129
4.9.2 Theoretical formalisms for the semileptonic B decays . . . 129
4.9.3 Measurement of inclusive $b \to u$ semileptonic decays . . . 135

4.9.4 Mesurement of exclusive $b \to u$ semileptonic decays . . . 137
4.10 Tau decays . . . 141
4.10.1 Introduction . . . 141
4.10.2 Present experimental status . . . 141
4.10.3 Achievable sensitivity at SuperKEKB and physics reaches . . . 144
4.10.4 Summary . . . 149
4.11 Diversity of physics at Super-KEKB–other possibilities . . . 150
4.11.1 Charm physics . . . 150
4.11.2 Electroweak physics . . . 151
4.11.3 Charmonium physics . . . 155
4.12 Summary . . . 160
References . . . 161

5 Study of New Physics Scenarios at SuperKEKB 170
5.1 New Physics Case Study . . . 170
5.2 Model Independent Approaches . . . 171
5.3 The CKM Fit . . . 177
References . . . 182

Executive Summary

The grand challenge of elementary particle physics is to identify the fundamental elements of Nature and uncover the ultimate theory of their creation, interactions and annihilation. To this end, all elementary particles and the forces between them should be described in a unified picture. Such unification naturally requires a deep understanding of physical laws at a very high-energy scale; for instance the unification of electroweak and strong forces is expected to occur at around 10^{15} GeV, which is often called the GUT scale.

It is unlikely that the GUT scale will be realized at any accelerator-based experiment even in the distant future. However, there are a few very promising ways to promote our grand challenge. One such approach is to elucidate the nature of quantum loop effects by producing as many particles as possible. This provides the rationale to pursue the luminosity frontier.

There is no doubt that past experiments at the luminosity (or intensity) frontier of the age have yielded epoch-making results. This good tradition has been followed by Belle and BaBar, experiments at energy-asymmetric e^+e^- B factories KEKB and PEPII, which have observed CP violation in the neutral B meson system. The result is in good agreement with the constraints from the Kobayashi-Maskawa (KM) model of CP violation. We are now confident that the KM phase is the dominant source of CP violation. In 2003 the KEKB collider achieved its design luminosity of 1×10^{34} cm^{-2}s^{-1}. The Belle experiment will accumulate an integrated luminosity of 500 fb^{-1} within a few years. This will suffice to determine the Unitarity Triangle with a precision of $\mathcal{O}(10)\%$. Various other quantities in B meson decays will also become accessible. In particular, the first observation of direct CP violation in charmless B decays is anticipated.

Over the past thirty years, the success of the Standard Model, which incorporates the KM mechanism, has become increasingly firm. This strongly indicates that the Standard Model is *the* effective low-energy description of Nature. Yet there are several reasons to believe that physics beyond the Standard Model should exist. One of the most outstanding problems is the quadratically divergent radiative correction to the Higgs mass, which requires a fine tuning of the bare Higgs mass unless the cutoff scale is $\mathcal{O}(1)$ TeV. This suggests that the new physics lies at the energy scale of $\mathcal{O}(1)$ TeV. There is a good chance that LHC will discover new elementary particles such as supersymmetric (SUSY) particles. With this vision in mind, we raise an important question "what should be a role of the luminosity frontier in the LHC era ?"

To answer the question, we note that the flavor sector of the Standard Model is quite successful in spite of the problem in the Higgs sector. This is connected to the observation that Flavor-Changing-Neutral-Currents (FCNCs) are highly suppressed. Indeed, if one considers a general new physics model without any mechanism to suppress FCNC processes, present experimental results on B physics imply that the new physics energy scale should be larger than $\mathcal{O}(10^3)$ TeV. This apparent mismatch is called *the new physics flavor problem*. To overcome the problem, any new physics at the TeV scale should have a mechanism to suppress FCNC processes, which often results in a distinctive flavor structure at low energy. Therefore, the indispensable roles of the luminosity frontier are to observe deviations from the Standard Model

in flavor physics, and more importantly, to distinguish between different new physics models by a close examination of the flavor structure. Comprehensive studies of B meson decays in the clean e^+e^- environment provide the ideal solution for this purpose, which is not possible at LHC nor even at the future linear collider.

These provide the primary motivation for SuperKEKB, a major upgrade of KEKB. Its design luminosity is 5×10^{35} cm^{-2}s^{-1}, which is 50 times as large as the peak luminosity achieved by KEKB. Various FCNC processes, such as the radiative decay $b \to s\gamma$, the semileptonic decay $b \to sl^+l^-$, and the hadronic decays $b \to s\bar{q}q$ and $b \to d\bar{q}q$, can be studied with unprecedented precision. All of these processes are suppressed in the Standard Model by the GIM mechanism, and therefore the effect of new physics is relatively enhanced. New observables that are currently out of reach will also become accessible. In addition to B meson decays, FCNC processes in τ and charm decays will also be studied at SuperKEKB.

The Belle detector will be upgraded to take full advantage of the high luminosity of SuperKEKB. In spite of harsh beam backgrounds, the detector performance will be at least as good as the present Belle detector and improvements in several aspects are envisaged. Table 1 summarizes the physics reach at SuperKEKB. As a reference, measurements expected at LHCb are also listed. One of the big advantages of SuperKEKB is the capability to reconstruct rare decays that have γ's, π^0's or neutrinos in the final states. There are several key observables in Table 1 that require this capability. Also important are time-dependent CP asymmetry measurements using only a K^0_S and a constraint from the interaction point to determine the B decay vertices. Examples include $B^0 \to K^{*0}(\to K^0_S\pi^0)\gamma$, $\pi^0K^0_S$ and $K^0_SK^0_SK^0_S$. These fundamental measurements cannot be carried out at hadron colliders.

Figure 1(a) shows a comparison between time-dependent CP asymmetries in $B^0 \to J/\psi K^0_S$, which is dominated by the $b \to c\bar{c}s$ tree process, and $B^0 \to \phi K^0_S$, which is governed by the $b \to s\bar{s}s$ FCNC (penguin) process. It demonstrates how well a possible new CP-violating phase can be measured. Such a new source of CP violation may revolutionize the understanding of the origin of the matter-dominated Universe, which is one of the major unresolved issues in cosmology. Figure 1(b) shows correlations between time-dependent CP asymmetries in $B^0 \to K^{*0}\gamma$ and $B^0 \to \phi K^0_S$ decays in two representative new physics models with different SUSY breaking scenarios; the SU(5) SUSY GUT with right-handed neutrinos and the minimal supergravity model. The two can be clearly distinguished. This demonstrates that SuperKEKB is sensitive to a quantum phase even at the GUT scale. Note that these two models may have rather similar mass spectra. It will therefore be very difficult to distinguish one from the other at LHC. If SUSY particles are discovered at LHC, the origin of SUSY breaking will become one of the primary themes in elementary particle physics. SuperKEKB will play a leading role in such studies.

We emphasize that the example above is just one of several useful correlations that can be measured only at SuperKEKB. The true value of SuperKEKB is a capability to observe the pattern as a whole, which allows us to differentiate a variety of new physics scenarios. It is so to speak "*DNA identification of new physics*", in that each measurement does not yield a basic physical parameter of the new physics but provides an essential piece of the overall flavor structure. This strategy works better when we accumulate more data. Thus the target annual integrated luminosity of 5 ab^{-1} is not a luxury but necessity, and stable long-term operation of SuperKEKB is necessary to meet the requirements.

Determination of the Unitarity Triangle will also be pushed forward and will be incorporated in the global pattern mentioned above. This can be done at SuperKEKB using redundant measurements of all three angles and all three sides of the Unitarity Triangle. In particular, ϕ_2 measurements and V_{ub} measurements require the reconstruction of π^0 mesons and neutrinos and

Observable	SuperKEKB		LHCb
	(5 ab^{-1})	(50 ab^{-1})	(0.002ab^{-1})
$\Delta\mathcal{S}_{\phi K^0_S}$	0.079	0.031	0.2
$\Delta\mathcal{S}_{K^+K^-K^0_S}$	0.056	0.026	
$\Delta\mathcal{S}_{\eta' K^0_S}$	0.049	0.024	$\times$
$\Delta\mathcal{S}_{K^0_S K^0_S K^0_S}$	0.14	0.04	$\times$
$\Delta\mathcal{S}_{\pi^0 K^0_S}$	0.10	0.03	$\times$
$\sin 2\chi$ ($B_s \to J/\psi\phi$)	$\times$	$\times$	0.058
$\mathcal{S}_{K^{*0}\gamma}$	0.14	0.04	$\times$
$\mathcal{B}(B \to X_s\gamma)$	5%	5%	$\times$
$A_{CP}(B \to X_s\gamma)$	0.011	5×10^{-3}	$\times$
C_9 from $A_{FB}(B \to K^*\ell^+\ell^-)$	32%	10%	
C_{10} from $A_{FB}(B \to K^*\ell^+\ell^-)$	44%	14%	
$\mathcal{B}(B_s \to \mu^+\mu^-)$	$\times$	$\times$	4σ (3 years)
$\mathcal{B}(B^+ \to K^+\nu\nu)$		5.1σ	$\times$
$\mathcal{B}(B^+ \to D\tau\nu)$	8%	2.5%	$\times$
$\mathcal{B}(B^0 \to D\tau\nu)$	3.5σ	9%	$\times$
$\sin 2\phi_1$	0.019	0.014	0.022
ϕ_2 ($\pi\pi$ isospin)	3.9°	1.2°	$\times$
ϕ_2 ($\rho\pi$)	2.9°	0.9°	$\times$
ϕ_3 ($DK^{(*)}$)	4°	1.2°	8°
ϕ_3 ($B_s \to KK$)	$\times$	$\times$	5°
ϕ_3 ($B_s \to D_sK$)	$\times$	$\times$	14°
$\lvert V_{ub}\rvert$ (inclusive)	5.8%	4.4%	$\times$
$\mathcal{B}(\tau \to \mu\gamma)$	$< 1.8 \times 10^{-8}$		

Table 1: Summary of the physics reach at SuperKEKB. Expected errors for the key observables are listed for an integrated luminosity of 5 ab^{-1}, which corresponds to one year of operation, and with 50 ab^{-1}. $\Delta\mathcal{S}_f$ is defined by $\Delta\mathcal{S}_f \equiv (-\xi_f)\mathcal{S}_f - \mathcal{S}_{J/\psi K^0_S}$, where ξ_f is the CP eigenvalue of the final state f. For comparison, expected sensitivities at LHCb with one year of operation are also listed if available. The $\times$ marks indicate measurements that are very difficult or impossible.

are thus unique to a Super B-Factory. An inconsistency among these measurements implies new physics. Figure 2 shows the expected constraints at 50 ab^{-1}. An ultimate precision of $\mathcal{O}(1)\%$ will be obtained at SuperKEKB.

We thus conclude that the physics case at SuperKEKB is compelling. It will be the place to elucidate *the new physics flavor problem* in the LHC era. The physics program at SuperKEKB is not only complementary to the next-generation energy frontier programme, but is an essential element of the grand challenge in elementary particle physics.

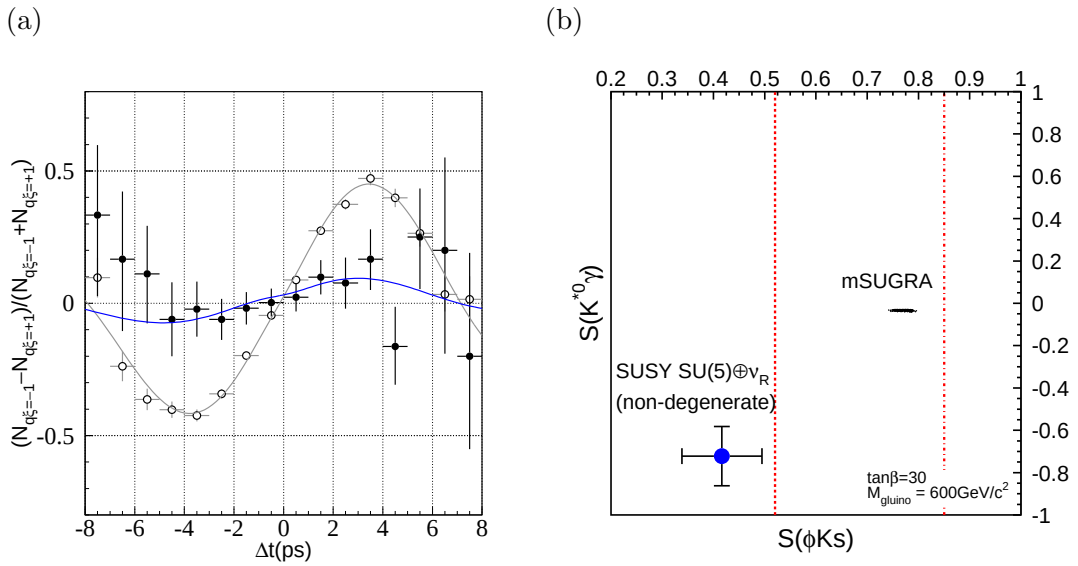

Figure 1: (a) Time-dependent CP asymmetries in $B^0 \to \phi K^0_S$ and $B^0 \to J/\psi K^0_S$ decays expected with one year of operation at SuperKEKB (5 ab^{-1}). The world average values (as of August 2003) for the modes governed by the $b \to s$ transition are used as the input values of $\mathcal{S}_{\phi K^0_S} = +0.24$ and $\mathcal{A}_{\phi K^0_S} = +0.07$. (b) A correlation between time-dependent CP asymmetries in $B^0 \to K^{*0}\gamma$ and $B^0 \to \phi K^0_S$. The dots show the range in the minimal supergravity model (mSUGRA). The circle corresponds to a possible point of supersymmetric SU(5) GUT model with right-handed neutrinos. Error bars associated with the circle indicate expected errors with one year of operation at SuperKEKB. The present experimental bound of $\mathcal{S}_{\phi K^0_S} < +0.52$ ($\mathcal{S}_{\phi K^0_S} < +0.85$) at the 2σ (3σ) level is also shown by the dashed (dot-dashed) vertical line.

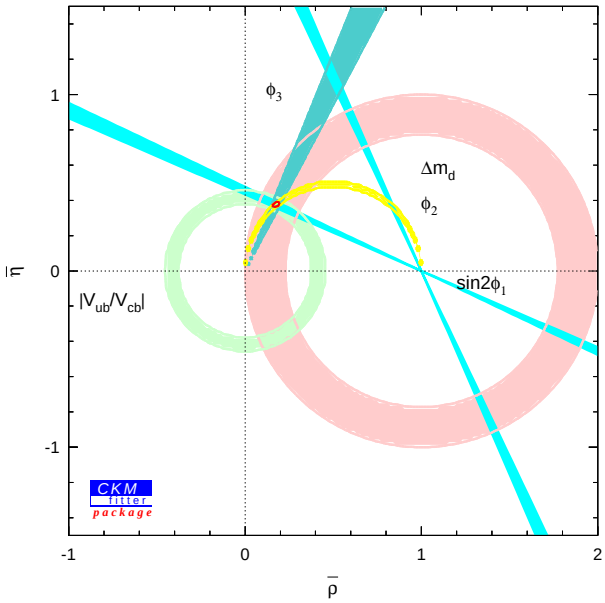

Figure 2: Constraints on the CKM unitarity triangle at 50 ab^{-1}.

Chapter 1

Introduction

1.1 Motivation for the Higher Luminosity B Factory

What are the most fundamental elements of the Universe? What is the law which governs their interactions? These are the questions that theoretical and experimental particle physicists have been working hard to answer for more than a century, and it was about thirty years ago that they reached the so-called Standard Model of elementary particles. The Standard Model contains three generations of quarks and leptons, and their interactions are mediated by gauge bosons according to the $SU(3)_C \times SU(2)_L \times U(1)_Y$ gauge field theory. Over the past thirty years the Standard Model has been confirmed by many precise experimental data.

Nevertheless, there are several reasons why the Standard Model is not completely satisfactory as *the* theory of elementary particles. First of all, it includes too many parameters, *i.e.* the masses and mixing of the quarks and leptons, all of which are a priori unknown. The hierarchy of quark and lepton masses and the flavor mixing matrices suggest that some hidden mechanism occurring at a higher energy scale governs their pattern. Secondly, due to quadratically divergent radiative corrections the Higgs mass is naturally of the same order as its cutoff scale, which means that some new physics should arise not far above the electroweak scale. From the astrophysical viewpoint, it is also a serious problem that the matter-antimatter asymmetry in the universe cannot be explained solely by the CP violation in the Standard Model, which originates from quark flavor mixing. These observations lead us to believe that new physics exists most likely at the TeV energy scale.

The most direct way to discover the new physics is to construct energy frontier machines, such as the Large Hadron Collider (LHC) or the Global Linear Collider (GLC), to realize TeV energy scale collisions in which new heavy particles may be produced. The history of particle physics implies, however, that this is not the only way. In fact, before its discovery, the existence of the charm quark was postulated in order to explain the smallness of strangeness changing neutral currents (the Glashow-Illiopolous-Maiani (GIM) mechanism [1]). The third family of quarks and leptons was predicted by Kobayashi and Maskawa to explain the small CP violation in kaon mixing [2]. These are examples of Flavor Changing Neutral Current (FCNC) processes, with which one can investigate the effect of heavier particles appearing only in quantum loop corrections.

The mechanism to suppress FCNC processes should also be present in new physics models if the new physics lies at the TeV energy scale, because otherwise such FCNC processes would violate current experimental limits. Information obtained from flavor physics experiments are thus essential to uncover the details of the physics beyond the Standard Model, even if energy frontier machines discover new particles.

A natural place to investigate a wide range of FCNC processes is in B meson decays, as the bottom quark belongs to the third generation and hence its decay involves all existing generations of quarks. In addition to $B^0 - \bar{B}^0$ mixing, which is an analog of the traditional $K^0 - \bar{K}^0$ mixing, there are many FCNC decay processes induced by so-called penguin diagrams, such as the radiative decay $b \to s\gamma$, the semileptonic decay $b \to s\ell^+\ell^-$, and the hadronic decays $b \to dq\bar{q}$ and $b \to sq\bar{q}$. All of these processes are suppressed in the Standard Model by the GIM mechanism, and therefore the effect of new physics may be relatively enhanced. The Higher Luminosity B Factory is a machine designed to explore such interesting B decay processes.

In the summer of 2001 the presence of CP violation in the B meson system was established by the Belle collaboration [3–6] (and simultaneously by the BaBar collaboration [7–10]) through the measurement of the time dependent asymmetry in the decay process $B^0(\bar{B}^0) \to J/\psi K^0_S$. This measurement was the main target of the present asymmetric e^+e^- B Factory, and it was achieved as originally planned. The experimental data indicated that the Kobayashi-Maskawa mechanism, which is now a part of the Standard Model of elementary particles, is indeed the dominant source of the observed CP violation in Nature.

The Belle experiment also proved its ability to measure a number of decay modes of the B meson and to extract Cabibbo-Kobayashi-Maskawa (CKM) matrix elements and other interesting observables. For instance, the precision of the measurement of the angle ϕ_1 of the unitarity triangle through the $B^0 \to J/\psi K^0_S$ time-dependent asymmetry reached the 10% level [11]; a CP asymmetry was observed in $B^0 \to \pi^+\pi^-$ decay, from which one can extract the angle ϕ_2 [12]; the angle ϕ_3 could also be measured through the processes $B \to DK$ and $D\pi$ [14–16]; the semi-leptonic FCNC processes $B \to K\ell^+\ell^-$ [17], $B \to K^*\ell^+\ell^-$ [18], and even the corresponding inclusive decay $B \to X_s\ell^+\ell^-$ [19] were observed. Furthermore, the recently observed disagreement between the values of the angle ϕ_1 measured in the penguin process $B \to \phi K^0_S$ and the precisely measured value in $B \to J/\psi K^0_S$ suggests the existence of a new CP phase in the penguin process $b \to sq\bar{q}$ [20]. By collecting many such observations we may probe new physics, and once its existence is established these measurements will determine the properties of the new physics. This is only possible by upgrading KEKB's luminosity by a substantial amount. As we discuss in the following sections, a factor of 50 improvement will greatly enhance the possibility to discover new physics.

In the program of quark flavor physics, one way to explore physics beyond the Standard Model is to substantially improve the measurement of the CKM matrix elements. Their determination can be done in many different ways, and any inconsistency with the Standard Model predictions would imply new physics. In this report we discuss the precision we expect to achieve at the Higher Luminosity B Factory for various determinations of the CKM matrix elements. These consist of measurements of the three angles and three sides of the Unitarity Triangle.

Another way to search for the effect of new physics is to look at loop-induced rare processes for which the Standard Model contribution is extremely suppressed. Such processes may provide an immediate signature of new physics, which also contributes through loops but in a different manner. We describe several such future measurements including the mixing induced $b \to s\gamma$ asymmetry, $b \to s\ell^+\ell^-$ forward-backward asymmetry, and flavor changing tau decay $\tau \to \mu\gamma$.

The B physics program is also being pursued at hadron machines including the ongoing Tevatron experiments [21] and the B physics programs at the Large Hadron Collider (LHC) [22], which is scheduled to start operation in 2007. Because of the very large $B\bar{B}$ production cross section in the hadron environment, some of the quantities we are planning to measure at the

e^+e^- B factory may be measured with better precision at the hadron colliders. The study of B_s mesons is also unique for the hadron machines. However, an e^+e^- machine provides a much cleaner environment, which is essential for some important observables. On the $\Upsilon(4S)$ resonance the $B\bar{B}$ pair is produced near threshold and there are no associated particles. This means that one can reconstruct the full energy-momentum vector of B ($\bar{B}$) meson from its daughter particles (so-called full reconstruction), and this may be used to infer the missing momentum in the decay of the other $\bar{B}$ (B) meson. This technique is essential for the measurement of channels including neutrino(s) in the final state. The measurement of the CKM element $|V_{ub}|$ through the semi-leptonic decay $b \to ul\bar{\nu}$, the search for a charged Higgs effect in $B \to D\tau\bar{\nu}$, and measurements of $B \to K\nu\bar{\nu}$, $B \to \tau\nu$ fall in this class.

1.2 Belle Status and Prospects

By the 2003 summer shutdown, Belle had accumulated data with an integrated luminosity of 140 fb^{-1} at the $\Upsilon(4S)$ resonance, corresponding to 152 million $B\overline{B}$ pairs. With modest improvements expected for the current KEKB accelerator, we expect an integrated luminosity of ~ 500 fb^{-1} in several years.

In this section, the current physics results are briefly reviewed for selected topics in order to give an overview of the present status. The status and future prospects for further topics are presented in the later sections.

1.2.1 Status of CP-Violation in $b \to c\bar{c}s$ Processes

Decays of B^0 to the following $b \to c\bar{c}s$ CP-eigenstates are reconstructed: $J/\psi K^0_S$, $\psi(2S)K^0_S$, $\chi_{c1}K^0_S$, $\eta_c K^0_S$ for $\xi_f = -1$ and $J/\psi K^0_L$ for $\xi_f = +1$ [1] The two classes ($\xi_f = \pm 1$) should have CP-asymmetries that are opposite in sign. $B^0 \to J/\psi K^{*0}[\to K^0_S\pi^0]$ decays are also used, where the final state is a mixture of even and odd CP. The CP content can, however, be determined from an angular analysis of other $J\psi K^*$ decays. The CP-odd fraction is found to be small (i.e. $(19 \pm 4)\%$).

The reconstructed samples with 140 fb^{-1} used for the $\sin 2\phi_1$ measurement [11] are shown in Figure 1.1. Table 1.1 lists the numbers of candidates, $N_{\rm ev}$, and the estimated signal purity for each f_{CP} mode. It is clear that the CP-eigenstate samples used for the CP-violation measurements in $b \to c\bar{c}s$ are large and clean.

Figure 1.2 shows the Δt distributions where a clear shift between B^0 and $\overline{B}^0$ tags is visible as well as the raw asymmetry plots in two bins of the flavor tagging quality variable r. For low quality tags ($0 < r < 0.5$), which have a large background dilution, only a modest asymmetry is visible while in the sub-sample with high quality tags ($0.5 < r < 1.0$), a very clear asymmetry with a sine-like time modulation is present. The final results are extracted from an unbinned maximum-likelihood fit to the Δt distributions that takes into account resolution, mistagging and background dilution. The result is

$$\sin 2\phi_1 = 0.733 \pm 0.057 \pm 0.028. \tag{1.1}$$

This result may be compared to the BaBar result with 82 fb^{-1} of $\sin 2\phi_1 = 0.741 \pm 0.067 \pm 0.03$ [10]. Both experiments are now in very good agreement. A new world average can be calculated from these results,

$$\sin 2\phi_1 = 0.736 \pm 0.049. \tag{1.2}$$

[1] The inclusion of the charge conjugate decay mode is implied unless otherwise stated.

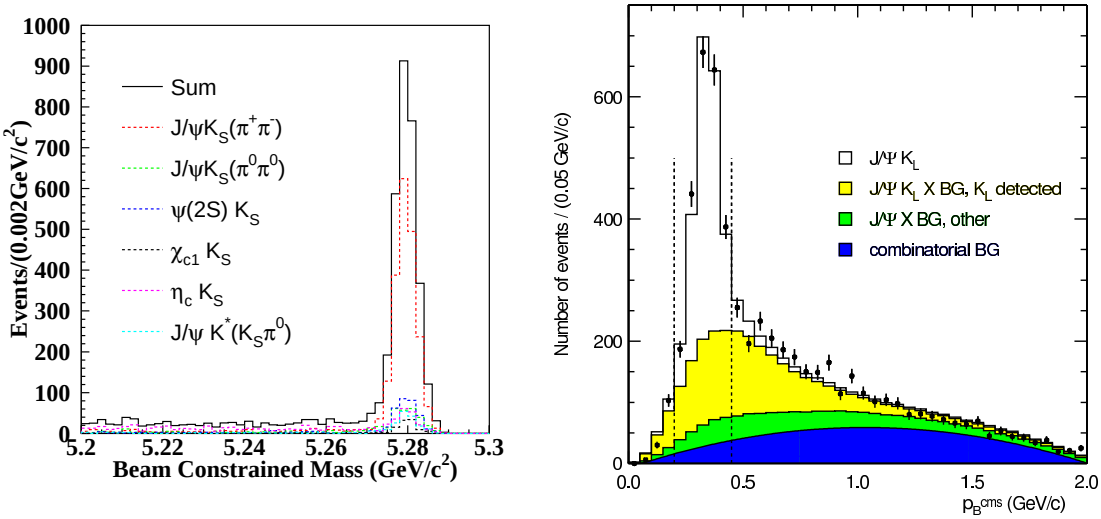

Figure 1.1: (Left) The fully reconstructed CP-eigenstate sample. (Right) The p_B^* (B momentum in the CM frame) distribution for the $B \to J/\psi K_L^0$ sample (right). The shaded portions show the contributions of different background components. The vertical dashed lines indicate the signal region.

Table 1.1: The yields for reconstructed $B \to f_{CP}$ candidates after flavor tagging and vertex reconstruction, $N_{\rm ev}$, and the estimated signal purity, p, in the signal region for each f_{CP} mode. J/ψ mesons are reconstructed in $J/\psi \to \mu^+\mu^-$ or e^+e^- decays. Candidate K_S^0 mesons are reconstructed in $K_S^0 \to \pi^+\pi^-$ decays unless explicitly stated otherwise.

Mode	ξ_f	$N_{\rm ev}$	p
$J/\psi K_S^0$	-1	1997	0.976 ± 0.001
$J/\psi K_S^0(\pi^0\pi^0)$	-1	288	0.82 ± 0.02
$\psi(2S)(\ell^+\ell^-)K_S^0$	-1	145	0.93 ± 0.01
$\psi(2S)(J/\psi\pi^+\pi^-)K_S^0$	-1	163	0.88 ± 0.01
$\chi_{c1}(J/\psi\gamma)K_S^0$	-1	101	0.92 ± 0.01
$\eta_c(K_S^0K^-\pi^+)K_S^0$	-1	123	0.72 ± 0.03
$\eta_c(K^+K^-\pi^0)K_S^0$	-1	74	0.70 ± 0.04
$\eta_c(p\overline{p})K_S^0$	-1	20	0.91 ± 0.02
All with $\xi_f = -1$	-1	2911	0.933 ± 0.002
$J/\psi K^{*0}(K_S^0\pi^0)$	$+1(81\%)$	174	0.93 ± 0.01
$J/\psi K_L^0$	$+1$	2332	0.60 ± 0.03

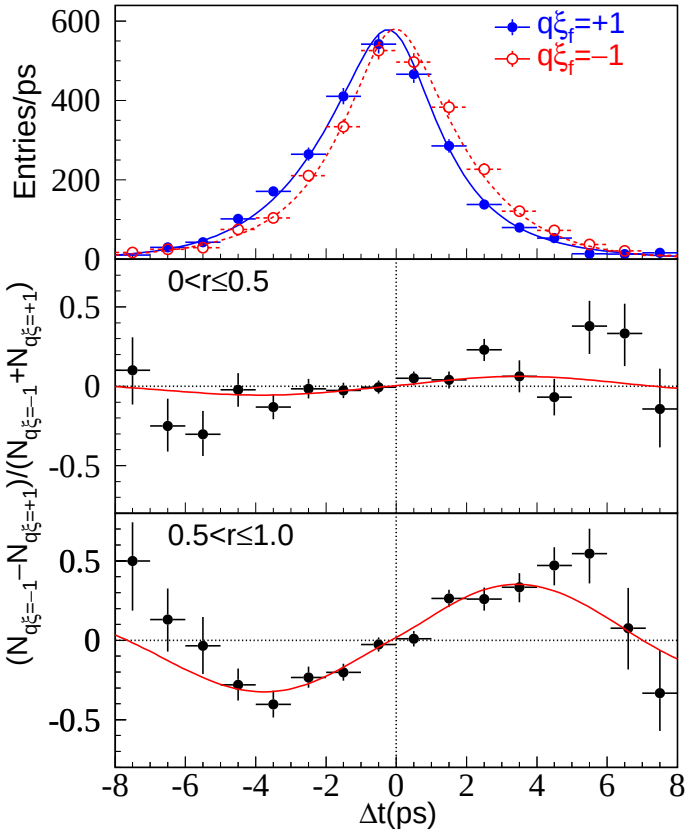

Figure 1.2: (a) Δt distributions for B^0 and $\overline{B}^0$ tags (b) raw asymmetry for low-quality tags and (c) raw asymmetry for high-quality tags. The smooth curves are projections of the unbinned likelihood fit.

This world average can be interpreted as a constraint on the CKM angle ϕ_1. This constraint can be compared with the indirect determinations of the unitarity triangle [23] and is consistent with the hypothesis that the Kobayashi-Maskawa phase is the source of CP violation. The measurement of $\sin 2\phi_1$ in $b \to c\bar{c}s$ modes, although still statistically limited, is becoming a precision measurement. The systematics are small and well-understood.

The presence of an asymmetry with a cosine dependence ($|\lambda| \neq 1$) would indicate direct CP-violation. In order to test for this possibility in $b \to c\bar{c}s$ modes, Belle also performed a fit with $a_{CP} \equiv -\xi_f \mathrm{Im}\lambda/|\lambda|$ and $|\lambda|$ as free parameters, keeping everything thing else the same. They obtain

$$|\lambda| = 1.007 \pm 0.041(\mathrm{stat}) \quad \text{and} \quad a_{CP} = 0.733 \pm 0.057(\mathrm{stat}), \tag{1.3}$$

for all the $b \to c\bar{c}s$ CP modes combined. This result is consistent with the assumption used in their primary analysis.

1.2.2 Status of CP-Violation in $b \to sq\bar{q}$ Penguin Processes

One of the promising ways to probe additional CP-violating phases from new physics beyond the Standard Model is to measure the time-dependent CP-asymmetry in penguin-dominated modes such as $B^0 \to \phi K^0_S$, $B^0 \to \eta' K^0_S$, where heavy new particles may contribute inside the loop, and compare it with the asymmetry in $B^0 \to J/\psi K^0_S$ and related $b \to c\bar{c}s$ charmonium modes. Belle has measured CP-violation in $B^0 \to \phi K^0_S$, $\eta' K^0_S$, and $K^+K^-K^0_S$ with 140 fb^{-1} [20].

The decay $B^0 \to \phi K^0_S$, which is dominated by the $b \to s\bar{s}s$ transition, is an especially unambiguous and sensitive probe of new CP-violating phases from physics beyond the Standard Model [24]. The Standard Model predicts that measurements of CP-violation in this mode should yield $\sin 2\phi_1$ to a very good approximation [25–27]. A significant deviation in the time-dependent CP-asymmetry in this mode from what is observed in $b \to c\bar{c}s$ decays would be evidence for a new CP-violating phase.

The $B \to \phi K^0_S$ sample is shown in Figure 1.3(a). The signal contains 68 ± 11 events. Figure 1.4(a,b) shows the raw asymmetries in two regions of the flavor-tagging parameter r.

The observed CP-asymmetry for $B^0 \to \phi K^0_S$ in the region $0.5 < r \leq 1.0$ (Figure 1.4 (b)) indicates a deviation from the Standard Model expectation (dashed curve). Note that these projections onto the Δt axis do not take into account event-by-event information (such as the signal fraction, the wrong tag fraction and the vertex resolution) that is used in the unbinned maximum likelihood fit. The contamination of $K^+K^-K^0_S$ events in the ϕK^0_S sample ($7.2 \pm 1.7\%$) is small. Finally, backgrounds from the decay $B^0 \to f_0(980)K^0_S$, which has the opposite CP-eigenvalue to ϕK^0_S, are found to be small ($1.6^{+1.9}_{-1.5}\%$). The influence of these backgrounds is treated as a source of systematic uncertainty.

The likelihood fit gives

$$\sin 2\phi_{1\mathrm{eff}}(B \to \phi K^0_S) = -0.96 \pm 0.5^{+0.09}_{-0.11}. \tag{1.4}$$

The likelihood function is parabolic and well-behaved. An evaluation of the significance of the result using the Feldman-Cousins method and allowing for systematic uncertainties shows that this result deviates by 3.5σ from the Standard Model expectation [20]. BaBar has analyzed a sample with an integrated luminosity of 110 fb^{-1}, containing 70 ± 9 events, and obtain $\sin 2\phi_{1\mathrm{eff}}(B \to \phi K^0_S) = 0.45 \pm 0.43 \pm 0.07$ [28]. This result differs from the Belle result by 2.1σ and the naive average, -0.14 ± 0.33, is still away from the $\sin 2\phi_1$ world average by 2.6σ.

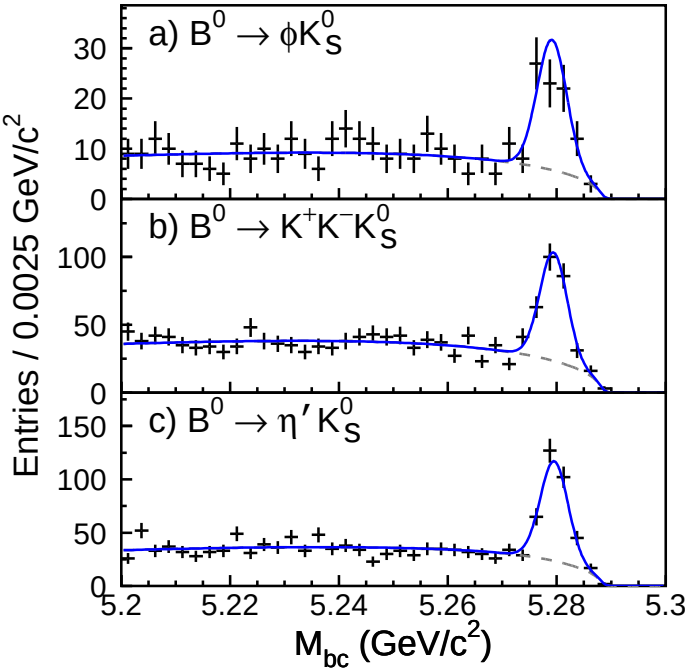

Figure 1.3: The beam-energy constrained mass distributions for (a) $B^0 \to \phi K^0_S$, (b) $B^0 \to K^+K^-K^0_S$, and (c) $B^0 \to \eta' K^0_S$ within the ΔE signal region. Solid curves show the fit to signal plus background distributions, and dashed curves show the background contributions. The background for $B^0 \to \eta' K^0_S$ decay includes an MC-estimated $B\overline{B}$ background component.

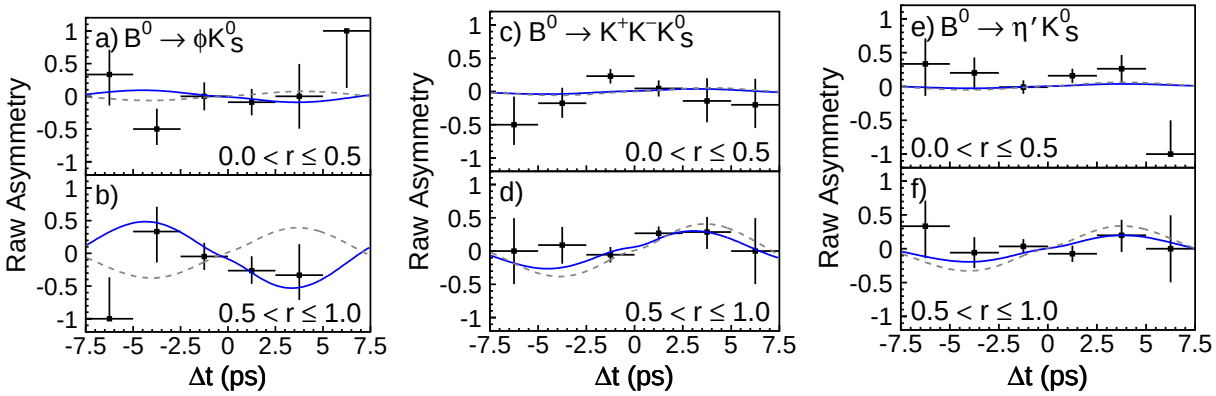

Figure 1.4: (a) The asymmetry, A, in each Δt bin for $B^0 \to \phi K^0_S$ with $0 < r \leq 0.5$, (b) with $0.5 < r \leq 1.0$, (c) for $B^0 \to K^+K^-K^0_S$ with $0 < r \leq 0.5$, (d) with $0.5 < r \leq 1.0$, (e) for $B^0 \to \eta' K^0_S$ with $0 < r \leq 0.5$, and (f) with $0.5 < r \leq 1.0$, respectively. The solid curves show the result of the unbinned maximum-likelihood fit. The dashed curves show the Standard Model expectation with $\sin 2\phi_1 = +0.731$ and $\mathcal{A} = 0$.

Table 1.2: $B \to K^*\gamma$ branching fractions

	$B^0 \to K^{*0}\gamma$ $[\times 10^{-5}]$	$B^+ \to K^{*+}\gamma$ $[\times 10^{-5}]$
CLEO	$4.55 \pm 0.70 \pm 0.34$	$3.76 \pm 0.86 \pm 0.28$
BaBar	$4.23 \pm 0.40 \pm 0.22$	$3.83 \pm 0.62 \pm 0.22$
Belle	$4.09 \pm 0.21 \pm 0.19$	$4.40 \pm 0.33 \pm 0.24$

The decay mode $B \to K^+K^-K^0_S$, where K^+K^- combinations consistent with the ϕ have been removed, is found to be dominantly CP-even [29] and thus can be treated as a CP-eigenstate and used for studies of time-dependent CP-violation in $b \to sq\overline{q}$ processes. The beam constrained mass distribution for the $B \to K^+K^-K^0_S$ sample used by Belle is shown in Figure 1.3(b). There are 199 ± 18 signal events. The result is

$$\sin 2\phi_{1\text{eff}}(B \to K^+K^-K^0_S) = 0.51 \pm 0.26 \pm 0.05^{+0.18}_{-0.00}, \tag{1.5}$$

where the third error is due to the uncertainty in the CP content of this final state [29]. The results for $B \to K^+K^-K^0_S$ are also consistent with $b \to c\bar{c}s$ decays. However, in this decay there is also the possibility of "tree-pollution", i.e. the contribution of a $b \to u\bar{u}s$ tree amplitude that may complicate the interpretation of the results [27].

The mode $B \to \eta' K^0_S$ is expected to include contributions from $b \to s\bar{u}u$ and $b \to s\bar{d}d$ penguin processes. The beam constrained mass distribution for the $B \to \eta' K^0_S$ sample is shown in Figure 1.3(c) and contains 244 ± 21 signal events [30]. The fit gives (Figure 1.4(e,f)),

$$\sin 2\phi_{1\text{eff}}(B \to \eta' K^0_S) = 0.43 \pm 0.27 \pm 0.05. \tag{1.6}$$

The average with the BaBar result ($0.02 \pm 0.34 \pm 0.03$ with 82 fb^{-1}) [31] is about 2.2σ from the $b \to c\bar{c}s$ measurement, which is the Standard Model expectation.

1.2.3 Radiative B decays

Exclusive $B \to K^*\gamma$

Measurement of the $B \to K^*\gamma$ exclusive branching fraction is straightforward, since one can use M_{bc}, ΔE and K^* mass constraints. (K^* denotes $K^*(892)$ throughout this section.) The latest Belle measurement (Figure 1.5) uses 78 fb^{-1} of data, with a total error of much less than 10% for each of the B^0 and B^+ decays. The results from CLEO [32], BaBar [33] and Belle [34] are in good agreement and are listed in Table 1.2. The world averages are calculated as

$$\mathcal{B}(B^0 \to K^{*0}\gamma) = (4.17 \pm 0.23) \times 10^{-5}, \tag{1.7}$$

$$\mathcal{B}(B^+ \to K^{*+}\gamma) = (4.18 \pm 0.32) \times 10^{-5}. \tag{1.8}$$

The corresponding theoretically predicted branching fraction is about $(7 \pm 2) \times 10^{-5}$, higher than the measurement with a large uncertainty [35, 36]. A better approach to exploit the $B \to K^*\gamma$ branching fraction measurements is to consider isospin asymmetry [37]. A small difference in the branching fractions between $B^0 \to K^{*0}\gamma$ and $B^+ \to K^{*+}\gamma$ tells us the sign of the combination of the Wilson coefficients, C_6/C_7. Belle has taken into account correlated systematic errors and obtains

$$\begin{aligned} \Delta_{+0} &\equiv \frac{(\tau_{B^+}/\tau_{B^0})\mathcal{B}(B^0 \to K^{*0}\gamma) - \mathcal{B}(B^+ \to K^{*+}\gamma)}{(\tau_{B^+}/\tau_{B^0})\mathcal{B}(B^0 \to K^{*0}\gamma) + \mathcal{B}(B^+ \to K^{*+}\gamma)} \\ &= (+0.003 \pm 0.045 \pm 0.018), \end{aligned} \tag{1.9}$$

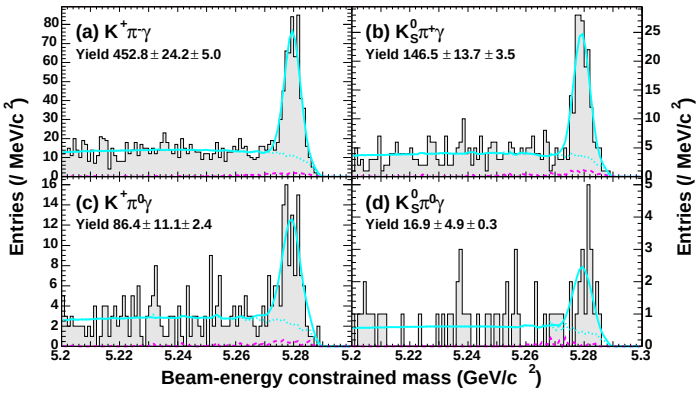

Figure 1.5: $B \to K^*\gamma$ signals from Belle.

which is consistent with zero. One cannot tell whether the Standard Model prediction ($\Delta_{+0} > 0$) is correct yet. Here, the lifetime ratio $\tau_{B^+}/\tau_{B^0} = 1.083 \pm 0.017$ is used, and the B^0 to B^+ production ratio is assumed to be unity. The latter is measured to be $f_0/f_+ = 1.072 \pm 0.057$ and is a source of additional systematic error.

Other Exclusive Radiative Decays

The dominant radiative decay channel $B \to K^*\gamma$ covers only 12.5% of the total $B \to X_s\gamma$ branching fraction (world average $(3.34 \pm 0.38) \times 10^{-4}$). The remainder has to be accounted for by decays with higher resonances or multi-body decays. Knowledge of these decay modes will eventually be useful to reduce the systematic error for the inclusive measurement.

Belle has extended the analysis into multi-body decay channels in addition to $B \to K_2^*(1430)[\to K\pi]\gamma$ decay [38]. Using 29 fb^{-1} of data, the decay $B^+ \to K^+\pi^+\pi^-\gamma$ is measured to have a branching fraction of $(24 \pm 5^{+4}_{-2}) \times 10^{-6}$ for $M(K\pi\pi) < 2.4$ GeV. The decay is dominated by $K^{*0}\pi^+\gamma$ and $K^+\rho^0\gamma$ final states that overlap each other as shown in Figure 1.6. At this moment, it is not possible to disentangle the resonant states that decay into $K^*\pi$ or $K\rho$, such as $K_1(1270)$, $K_1(1400)$, $K^*(1650)$, and so on. A clear $B^+ \to K^+\phi\gamma$ (5.5σ) signal was recently observed by Belle with 90 fb^{-1} of data (Figure 1.7), together with 3.3σ evidence for $B^0 \to K^0_S\phi\gamma$. There is no known $K\phi$ resonant state. This is the first example of a $s\bar{s}s\gamma$ final state. The branching fractions for $B \to K\phi\gamma$ are measured to be [39]

$$\begin{aligned} \mathcal{B}(B^+ \to K^+\phi\gamma) &= (3.4 \pm 0.9 \pm 0.4) \times 10^{-6} \\ \mathcal{B}(B^0 \to K^0\phi\gamma) &= (4.6 \pm 2.4 \pm 0.4) \times 10^{-6} \\ &< 8.3 \times 10^{-6} \quad (90\%\ \mathrm{CL}) \end{aligned} \tag{1.10}$$

With more data, one can perform a time-dependent CP-asymmetry measurement with the $K^0_S\phi\gamma$ decay channel.

At present, $(35 \pm 6)\%$ of the total $B \to X_s\gamma$ rate is measured to be either $B \to K^*\gamma$ (12.5%), $B \to K_2^*(1430)\gamma$ (4% after excluding $K\pi\pi\gamma$), $B \to K^*\pi\gamma$ (9%), $B \to K\rho\gamma$ (9%) or $B \to K\phi\gamma$ (1%). The remaining $(65 \pm 6)\%$ may be accounted for by decays with multi-body final states, baryonic decays, modes with η and η', multi-kaon final states other than $K\phi\gamma$ or in the large X_s mass range.

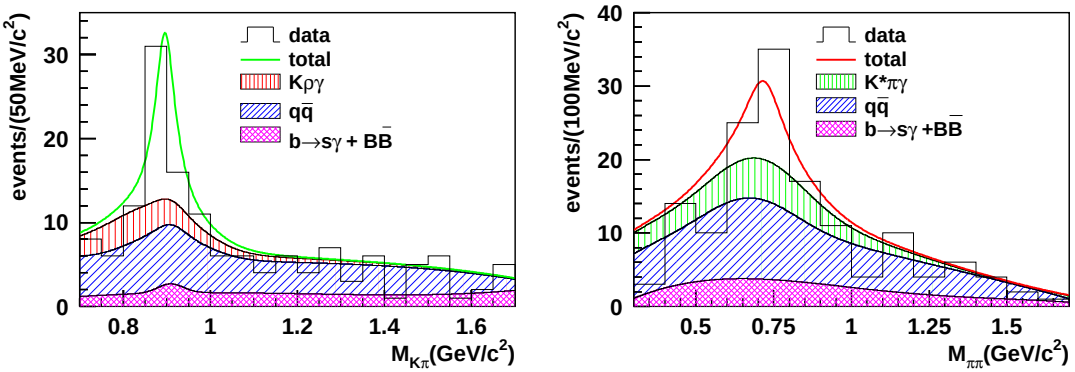

Figure 1.6: $B^+ \to K^{*0}\pi^+\gamma$ and $B \to K^+\rho^0\gamma$ from Belle.

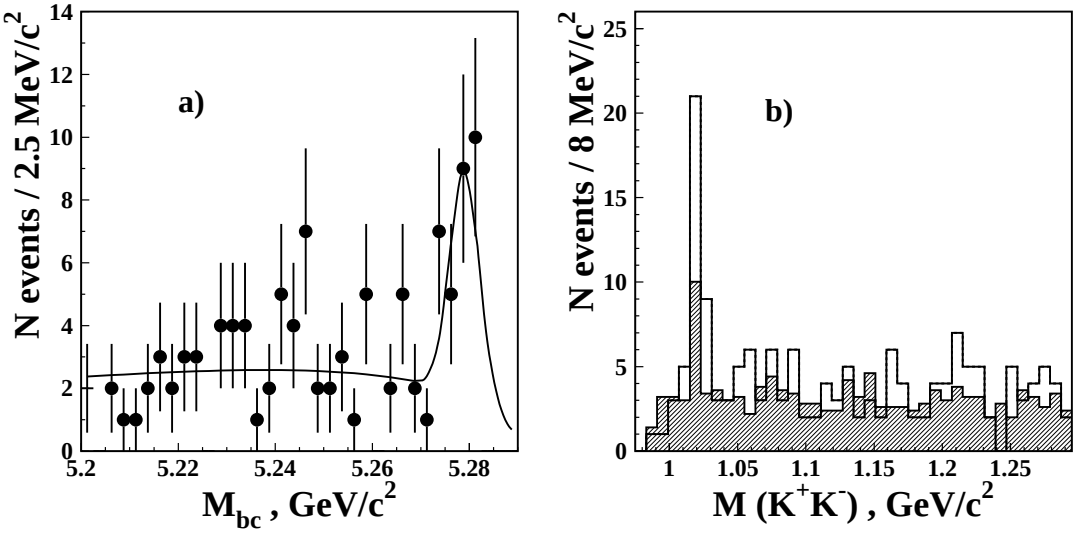

Figure 1.7: $B^+ \to K\phi\gamma$ from Belle.

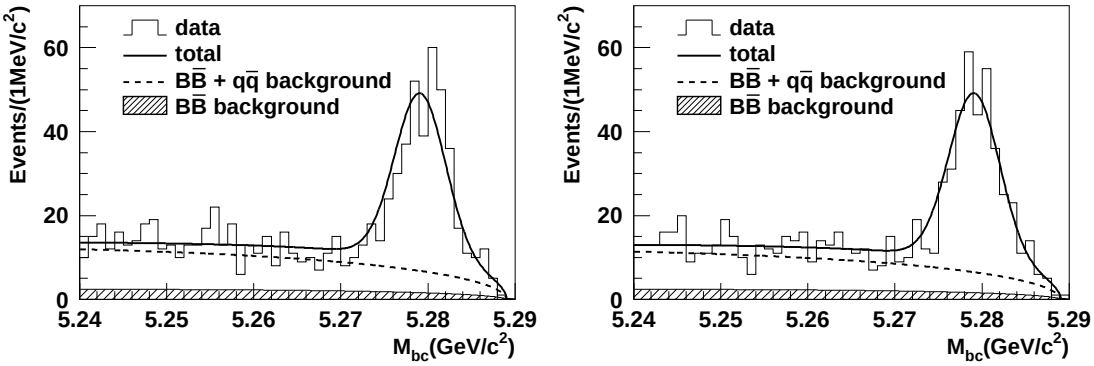

Figure 1.8: $\overline{B}$-tagged (top-left), B-tagged (top-right) $B \to X_s\gamma$ signals from Belle.

Search for Direct CP-Asymmetry

The direct CP-asymmetry in $B \to X_s\gamma$ is predicted to be 0.6% in the Standard Model with a small error [40, 41]. A large CP-asymmetry would be a clear sign of new physics.

An $A_{CP}(B \to X_s\gamma)$ measurement was performed by Belle [42], by summing up the exclusive modes of one kaon plus up to four pions and modes with three kaon plus up to one pion. This result eliminates $B \to X_d\gamma$ by exploiting particle identification devices for the tagged hadronic recoil system. $M(X_s) < 2.1$ GeV is required, which roughly corresponds to $E_\gamma^{\rm min} \sim 2.25$ GeV. Events are self-tagged as B candidates (B^0 or B^+) or $\overline{B}$ candidates ($\overline{B}^0$ or B^-), except for ambiguous modes with a K_S^0 and zero net charge. In order to correct the imperfect knowledge of the hadronic final state, the signal yields for each exclusive mode are used to correct the Monte Carlo multiplicity distribution. The resulting $\overline{B}$-tagged ($342 \pm 23\,^{+7}_{-14}$ events), B-tagged ($349 \pm 23\,^{+7}_{-14}$ events) signals are shown in Figure 1.8. Using the wrong-tag fractions of 0.019 ± 0.014 between B- and $\overline{B}$-tagged, 0.240 ± 0.192 from ambiguous to B- or $\overline{B}$-tagged, and 0.0075 ± 0.0079 from B- or $\overline{B}$-tagged to ambiguous samples, the asymmetry is measured to be

$$A_{CP}(B \to X_s\gamma) = 0.004 \pm 0.051 \pm 0.038. \tag{1.11}$$

The result corresponds to a 90% confidence level limit of $-0.107 < A_{CP}(B \to X_s\gamma) < 0.099$, and therefore already constrains part of the new physics parameter space.

For exclusive radiative decays, it is straightforward to extend the analysis to search for the direct CP-asymmetry [32–34]. Particle identification devices at Belle and BaBar resolve the possible ambiguity between $K^{*0} \to K^+\pi^-$ and $\overline{K}^{*0} \to K^-\pi^+$ to an almost negligible level with a reliable estimation of the wrong-tag fraction (0.9% for Belle). The results of the asymmetry measurements are listed in Table 1.3, whose average is

$$A_{CP}(B \to K^*\gamma) = (-0.5 \pm 3.7) \times 10^{-2}. \tag{1.12}$$

It is usually thought that large CP-violation in $B \to K^*\gamma$ is not allowed in the Standard Model and the above result may be used to constrain new physics. However, as the involved strong phase difference may not be reliably calculated for exclusive decays, the interpretation may be model dependent.

Search for $b \to d\gamma$ Final States

There are various interesting aspects of the $b \to d\gamma$ transition. Within the Standard Model, most of the diagrams are the same as those for $b \to s\gamma$, except for the replacement of the CKM

Table 1.3: $B \to K^*\gamma$ direct CP-asymmetry

CLEO (9.1 fb^{-1})	$(8 \pm 13 \pm 3) \times 10^{-2}$
BaBar (20.7 fb^{-1})	$(-4.4 \pm 7.6 \pm 1.2) \times 10^{-2}$
Belle (78 fb^{-1})	$(-0.1 \pm 4.4 \pm 0.8) \times 10^{-2}$

Table 1.4: 90% confidence level upper limits on the $B \to \rho\gamma$ and $\omega\gamma$ branching fractions.

	$\rho^+\gamma$	$\rho^0\gamma$	$\omega\gamma$
CLEO (9.1 fb^{-1})	13×10^{-6}	17×10^{-6}	9.2×10^{-6}
Belle (78 fb^{-1})	2.7×10^{-6}	2.6×10^{-6}	4.4×10^{-6}
BaBar (78 fb^{-1})	2.1×10^{-6}	1.2×10^{-6}	1.0×10^{-6}

matrix element V_{ts} with V_{td}. A measurement of the $b \to d\gamma$ process will therefore provide the ratio $|V_{td}/V_{ts}|$ without large model dependent uncertainties. This mode is also the place where a large direct CP-asymmetry is predicted within and beyond the Standard Model.

The search for the exclusive decay $B \to \rho\gamma$ is as straightforward as the measurement of $B \to K^*\gamma$, except for its small branching fraction, the enormous combinatorial background from copious ρ mesons and random pions, and the huge $B \to K^*\gamma$ background that overlaps with the $B \to \rho\gamma$ signal window. $B \to \omega\gamma$ is not affected by $B \to K^*\gamma$ background, but it is still unobserved. The upper limits obtained by BaBar [43], Belle [44] and CLEO [32] are summarized in Table 1.4. The upper limits are still about twice as large as the Standard Model predictions [**?**] $(9.0 \pm 3.4) \times 10^{-7}$ for $\rho^+\gamma$, and $(4.9 \pm 1.8) \times 10^{-7}$ for $\rho^0\gamma$ and $\omega\gamma$.

From these upper limits the bound $|V_{td}/V_{ts}| < 0.34$ can be obtained, which is still weaker than the corresponding bound derived from $\Delta m_s/\Delta m_d$.

1.2.4 Electroweak Rare B Decays

Observation of $B \to K^*\ell^+\ell^-$

The first signal for $B \to K\ell^+\ell^-$ was observed by Belle [17] using 29 fb^{-1} of data and confirmed by BaBar [45] with 78 fb^{-1}, while the $B \to K^*\ell^+\ell^-$ signal, whose branching fraction is expected to be larger, was not significant with those data samples.

The $B \to K^{(*)}\ell^+\ell^-$ signal is identified using $M_{\rm bc}$, ΔE (and $M(K\pi)$ for $K^*\ell^+\ell^-$). Belle has updated the analysis using a 140 fb^{-1} data sample, with a number of improvements in the analysis procedure [18]. The most significant improvement is a lower minimum lepton momentum of 0.7 (0.4) GeV for muons (electrons) from 1.0 (0.5) GeV to gain 12% (7%) in the total efficiency. In addition, a $K^*\ell^+\ell^-$ combinations are removed if there can be an unobserved photon along with one of the leptons that can form a $B \to J/\psi K \to \ell^+\ell^-\gamma K$ decay. As a result, the first $B \to K^*\ell^+\ell^-$ signal was observed with a statistical significance of 5.7 from a fit to $M_{\rm bc}$, as shown in Figure 1.9, together with an improved $B \to K\ell^+\ell^-$ signal with a significance of 7.4.

The branching fractions obtained are summarized in Table 1.5, together with the BaBar results [46]. For the combined $B \to K^*\ell^+\ell^-$ results, $\mathcal{B}(B \to K^*\ell^+\ell^-) = \mathcal{B}(B \to K^*\mu^+\mu^-) = 0.75\mathcal{B}(B \to K^*e^+e^-)$ is assumed which compensates for the enhancement at the $q^2 = 0$ pole that appears more significantly in $K^*e^+e^-$, using the expected Standard Model ratio [**?**]. The measured branching fractions are in agreement with the Standard Model, for example [47, 48] $(3.5 \pm 1.2) \times 10^{-7}$ for $B \to K\ell^+\ell^-$ and $(11.9 \pm 3.9) \times 10^{-7}$ for $B \to K^*\ell^+\ell^-$. We note that the

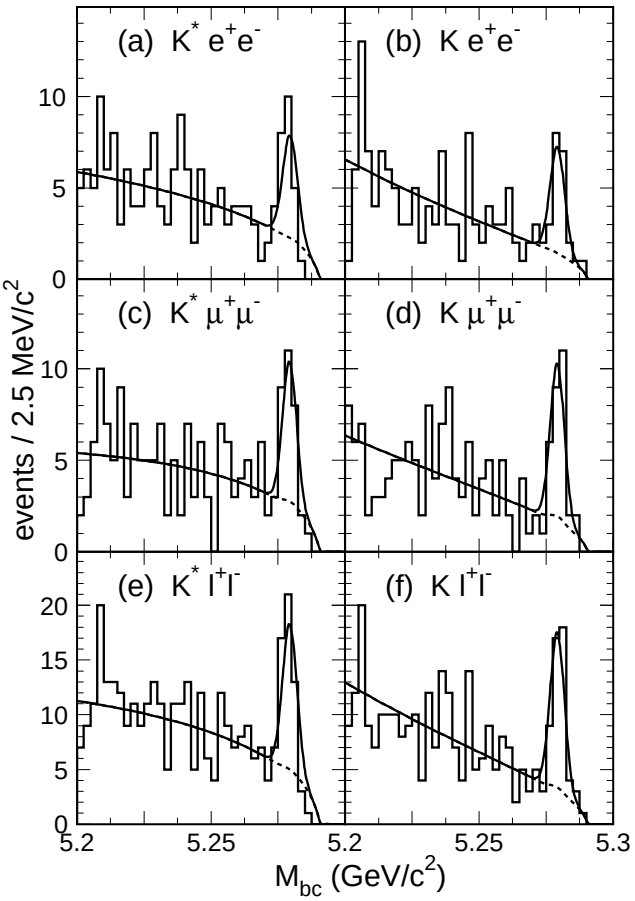

Figure 1.9: The $B \to K^{(*)}\ell^+\ell^-$ signal observed by Belle.

Table 1.5: $B \to K^{(*)}\ell^+\ell^-$ branching fractions.

Mode	Belle (140 fb^{-1}) [$\times 10^{-7}$]	BaBar (113 fb^{-1}) [$\times 10^{-7}$]
$B \to Ke^+e^-$	$4.8^{+1.5}_{-1.3} \pm 0.3 \pm 0.1$	$7.9^{+1.9}_{-1.7} \pm 0.7$
$B \to K\mu^+\mu^-$	$4.8^{+1.3}_{-1.1} \pm 0.3 \pm 0.2$	$4.8^{+2.5}_{-2.0} \pm 0.4$
$B \to K\ell^+\ell^-$	$4.8^{+1.0}_{-0.9} \pm 0.3 \pm 0.1$	$6.9^{+1.5}_{-1.3} \pm 0.6$
$B \to K^*e^+e^-$	$14.9^{+5.2+1.1}_{-4.6-1.3} \pm 0.3$	$10.0^{+5.0}_{-4.2} \pm 1.3$
$B \to K^*\mu^+\mu^-$	$11.7^{+3.6}_{-3.1} \pm 0.8 \pm 0.6$	$12.8^{+7.8}_{-6.2} \pm 1.7$
$B \to K^*\ell^+\ell^-$	$11.5^{+2.6}_{-2.4} \pm 0.7 \pm 0.4$	$8.9^{+3.4}_{-2.9} \pm 1.1$

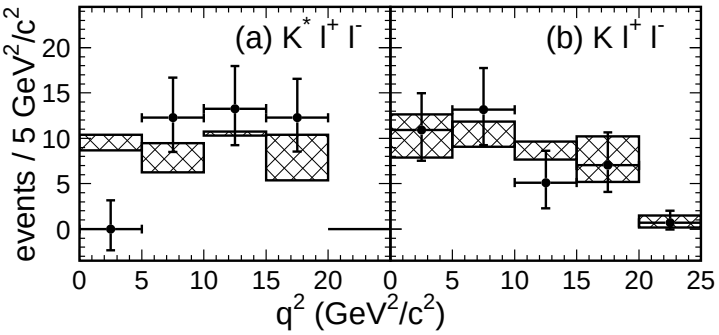

Figure 1.10: q^2 distributions for $B \to K^{(*)}\ell^+\ell^-$ from Belle.

experimental errors are already much smaller than both the uncertainties in the theoretical predictions of the Standard Model and the variations due to different model-dependent assumptions used to account for the hadronic uncertainties [49–53].

It is still too early to fit the q^2 distribution to constrain new physics. First attempts to extract the q^2 distribution using the individual $M_{\rm bc}$ signal yields in q^2 bins have been performed by Belle as shown in Figure 1.10.

Measurement of $B \to X_s\ell^+\ell^-$

The first measurements of the $B \to K^{(*)}\ell^+\ell^-$ branching fractions are consistent with the Standard Model predictions. However since these predictions have uncertainties that are already larger than the measurement errors, the inclusive rate for $B \to X_s\ell^+\ell^-$ becomes more important in terms of the search for a deviation from the Standard Model. In contrast to $B \to X_s\gamma$, the lepton pair alone does not provide a sufficient constraint to suppress the largest background from semi-leptonic decays. Therefore, it is only possible to use the semi-inclusive method to sum up the exclusive modes for now.

Belle has successfully measured the inclusive $B \to X_s\ell^+\ell^-$ branching fraction [19] from a 60 fb^{-1} data sample by applying a method that reconstructs the X_s final state with one kaon (K^+ or K^0_S) and up to four pions, of which one pion is allowed to be a π^0. Assuming the K^0_L contribution is the same as the K^0_S, this set of final states covers $82 \pm 2\%$ of the signal. In addition, $M(X_s)$ is required to be below 2.1 GeV in order to reduce backgrounds. For leptons, a minimum momentum of 0.5 GeV for electrons, 1.0 GeV for muons and $M(\ell^+\ell^-) > 0.2$ GeV

Table 1.6: $B \to X_s \ell^+ \ell^-$ branching fractions.

Mode	Belle (60 fb^{-1}) [$\times 10^{-6}$]	BaBar (78 fb^{-1}) [$\times 10^{-6}$]
$X_s e^+ e^-$	$5.0 \pm 2.3 \,^{+1.3}_{-1.1}$	$6.6 \pm 1.9 \,^{+1.9}_{-1.6}$
$X_s \mu^+ \mu^-$	$7.9 \pm 2.1 \,^{+2.1}_{-1.5}$	$5.7 \pm 2.8 \,^{+1.7}_{-1.4}$
$X_s \ell^+ \ell^-$	$6.1 \pm 1.4 \,^{+1.4}_{-1.1}$	$6.3 \pm 1.6 \,^{+1.8}_{-1.5}$

are required. Background sources and the suppression techniques are similar to those for the exclusive decays. The signal of 60 ± 14 events from Belle with a statistical significance of 5.4 is shown in Figure 1.11. Corresponding branching fractions are given in Table 1.6, together with the BaBar results [54]. The branching fraction results are for the dilepton mass range above $M(\ell^+\ell^-) > 0.2$ GeV and are interpolated in the J/ψ and ψ' regions that are removed from the analysis, assuming no interference with these charmonium states.

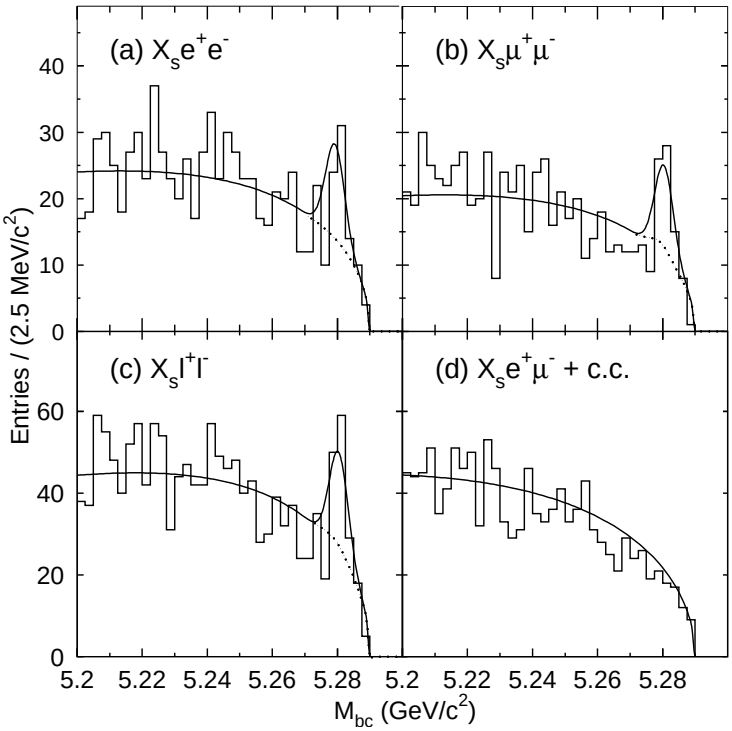

Figure 1.11: $B \to X_s \ell^+ \ell^-$ signal measured by Belle. The $X_s e^+ \mu^-$ sample, which is prohibited in the Standard Model, represents the combinatorial backgrounds.

The results may be compared with the Standard Model prediction [47] of $(4.2 \pm 0.7) \times 10^{-6}$ integrated over the same dilepton mass range of $M(\ell^+\ell^-) > 0.2$ GeV. With this requirement, the effect of the $q^2 = 0$ pole becomes insignificant, giving almost equal branching fractions for the electron and muon modes. The measured branching fractions are in agreement with the Standard Model, considering the large error in the measurement. It should be noted that the large systematic error is dominated by the uncertainty in the $M(X_s)$ distribution, in particular the fraction of $B \to K^{(*)} \ell^+ \ell^-$, which will be reduced with more statistics. Distributions for

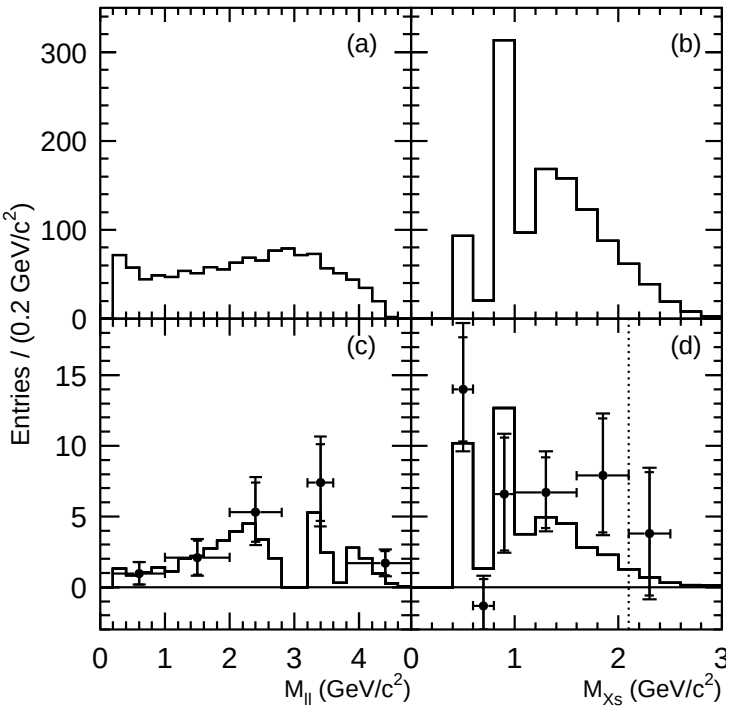

Figure 1.12: $M(\ell^+\ell^-)$ (left) and $M(X_s)$ (right) distributions for $B \to X_s\ell^+\ell^-$ from Belle (points with error bars), compared with the Standard Model predictions before (top) and after (bottom) including detector acceptance effects.

$M(X_s)$ and $M(\ell^+\ell^-)$ are shown in Figure 1.12, in which no significant deviation from the Standard Model is observed.

1.2.5 Prospects

With a data sample of ~ 500 fb^{-1}, the statistical errors will be reduced to about half of the present errors. The value of $\sin 2\phi_1$ will be measured with an accuracy less than 5% using $b \to c\bar{c}s$ processes. Though uncertainties are still large, ϕ_2 and ϕ_3 will be measured. Together with some improvement in $|V_{cb}|$ and $|V_{ub}|$ measurements, the KM scheme for CP-violation will be further confirmed. Direct CP-violation will be observed in several decay modes, which also strongly supports the KM scheme.

Results will be available for new measurements that are sensitive to new physics, such as measurements of forward-backward asymmetry of lepton-pairs in $B \to K^{(*)}\ell^+\ell^-$, time-dependent CP-violation of radiative decays, *etc.* If the effect of new physics is large, it may manifest itself in the above ways in a similar fashion to the current indication of as the CP-violation in $b \to s\bar{q}q$ decays (if it remains as currently measured). However, the confirmation of the new physics effects and understanding its nature will require much larger data samples, which will be the primary goal of the proposed SuperKEKB and upgraded Belle detector in this LoI.

References

[1] S. L. Glashow, J. Iliopoulos and L. Maiani, "Weak Interactions With Lepton – Hadron Symmetry," Phys. Rev. D **2**, 1285 (1970).

[2] M. Kobayashi and T. Maskawa, "CP Violation In The Renormalizable Theory Of Weak Interaction," Prog. Theor. Phys. **49**, 652 (1973).

[3] A. Abashian *et al.* [BELLE Collaboration], "Measurement of the CP violation parameter $\sin(2\phi_1)$ in B^0_d meson decays," Phys. Rev. Lett. **86**, 2509 (2001) [arXiv:hep-ex/0102018].

[4] K. Abe *et al.* [Belle Collaboration], "Observation of large CP violation in the neutral B meson system," Phys. Rev. Lett. **87**, 091802 (2001) [arXiv:hep-ex/0107061].

[5] K. Abe *et al.* [Belle Collaboration], "Observation of mixing-induced CP violation in the neutral B meson system," Phys. Rev. D **66**, 032007 (2002) [arXiv:hep-ex/0202027].

[6] K. Abe *et al.* [Belle Collaboration], "An improved measurement of mixing-induced CP violation in the neutral B meson system. ((B))," Phys. Rev. D **66**, 071102 (2002) [arXiv:hep-ex/0208025].

[7] B. Aubert *et al.* [BABAR Collaboration], "Measurement of CP violating asymmetries in B^0 decays to CP eigenstates," Phys. Rev. Lett. **86**, 2515 (2001) [arXiv:hep-ex/0102030].

[8] B. Aubert *et al.* [BABAR Collaboration], "A study of time dependent CP-violating asymmetries and flavor oscillations in neutral B decays at the $\Upsilon(4S)$," Phys. Rev. D **66**, 032003 (2002) [arXiv:hep-ex/0201020].

[9] B. Aubert *et al.* [BABAR Collaboration], "Observation of CP violation in the B^0 meson system," Phys. Rev. Lett. **87**, 091801 (2001) [arXiv:hep-ex/0107013].

[10] B. Aubert *et al.* [BABAR Collaboration], "Measurement of the CP-violating asymmetry amplitude $\sin 2\beta$. ((B))," Phys. Rev. Lett. **89**, 201802 (2002) [arXiv:hep-ex/0207042].

[11] K. Abe *et al.* [Belle Collaboration], "Measurement of CP-violation parameter $\sin(2\phi_1)$ with 152 million $B\bar{B}$ pairs," arXiv:hep-ex/0308036.

[12] K. Abe *et al.* [Belle Collaboration], "Measurement of CP-violating asymmetries in $B0 \to \pi^+\pi^-$ decays," Phys. Rev. Lett. **89**, 071801 (2002) [arXiv:hep-ex/0204002].

[13] K. Abe *et al.* [Belle Collaboration], "Evidence for CP-violating asymmetries $B^0 \to \pi^+\pi^-$ decays and constraints on the CKM angle ϕ_2," Phys. Rev. D **68**, 012001 (2003) [arXiv:hep-ex/0301032].

[14] S. K. Swain *et al.* [Belle Collaboration], "Measurement of branching fraction ratios and CP asymmetries in $B^\pm \to D_{CP}K^\pm$," Phys. Rev. D **68**, 051101 (2003) [arXiv:hep-ex/0304032].

[15] K. Abe *et al.* [Belle Collaboration], "Measurement of the angle ϕ_3 with Dalitz analysis of three-body D^0 decay from $B \to D^0K$ process," arXiv:hep-ex/0308043.

[16] K. Abe *et al.* [BELLE Collaboration], "Study of CP violating effects in time dependent $B^0(\bar{B}^0) \to D^{(*)\mp}\pi^\pm$ decays," arXiv:hep-ex/0308048.

[17] K. Abe *et al.* [BELLE Collaboration], "Observation of the decay $B \to K\mu^+\mu^-$," Phys. Rev. Lett. **88**, 021801 (2002) [arXiv:hep-ex/0109026].

[18] A. Ishikawa *et al.* [Belle Collaboration], "Observation of the electroweak penguin decay $B \to K^*l^+l^-$," Phys. Rev. Lett. **91**, 261601 (2003) [arXiv:hep-ex/0308044].

[19] J. Kaneko *et al.* [Belle Collaboration], Phys. Rev. Lett. **90**, 021801 (2003) [arXiv:hep-ex/0208029].

[20] K. Abe *et al.* [Belle Collaboration], "Measurement of time-dependent CP-violating asymmetries in $B0 \to \phi K^0_S$, $K^+K^-K^0_S$, and $\eta' K^0_S$ decays," Phys. Rev. Lett. **91**, 261602 (2003) [arXiv:hep-ex/0308035].

[21] K. Anikeev *et al.*, "B physics at the Tevatron: Run II and beyond," arXiv:hep-ph/0201071.

[22] P. Ball *et al.*, "B decays at the LHC," arXiv:hep-ph/0003238.

[23] A. Hocker, H. Lacker, S. Laplace and F. Le Diberder, "A new approach to a global fit of the CKM matrix," Eur. Phys. J. C **21**, 225 (2001) [arXiv:hep-ph/0104062].

[24] Y. Grossman and M. P. Worah, "CP asymmetries in B decays with new physics in decay amplitudes," Phys. Lett. B **395**, 241 (1997) [arXiv:hep-ph/9612269].

[25] D. London and A. Soni, "Measuring the CP angle β in hadronic $b \to s$ penguin decays," Phys. Lett. B **407**, 61 (1997) [arXiv:hep-ph/9704277].

[26] Y. Grossman, G. Isidori and M. P. Worah, "CP asymmetry in $B_d \to \phi K_S$: Standard model pollution," Phys. Rev. D **58**, 057504 (1998) [arXiv:hep-ph/9708305].

[27] Y. Grossman, Z. Ligeti, Y. Nir and H. Quinn, "SU(3) relations and the CP asymmetries in B decays to $\eta' K_S$, ϕK_S and $K^+K^-K_S$," Phys. Rev. D **68**, 015004 (2003) [arXiv:hep-ph/0303171].

[28] BaBar Collaboration, B. Aubert *et al.*, BABAR-PLOT-0053; BABAR-PLOT-0056.

[29] A. Garmash *et al.* [Belle Collaboration], "Study of B meson decays to three-body charmless hadronic final states," Phys. Rev. D **69**, 012001 (2004) [arXiv:hep-ex/0307082].

[30] K. F. Chen *et al.* [Belle Collaboration], "Measurement of CP-violating parameters in $B \to \eta' K$ decays. ((B))," Phys. Lett. B **546**, 196 (2002) [arXiv:hep-ex/0207033].

[31] B. Aubert *et al.* [BABAR Collaboration], "Measurements of CP-violating asymmetries and branching fractions in B meson decays to $\eta' K$," Phys. Rev. Lett. **91**, 161801 (2003) [arXiv:hep-ex/0303046].

[32] T. E. Coan *et al.* [CLEO Collaboration], "Study of exclusive radiative B meson decays," Phys. Rev. Lett. **84**, 5283 (2000) [arXiv:hep-ex/9912057].

[33] B. Aubert *et al.* [BABAR Collaboration], "Measurement of $B \to K^* \gamma$ branching fractions and charge asymmetries," Phys. Rev. Lett. **88**, 101805 (2002) [arXiv:hep-ex/0110065].

[34] Belle Collaboration, K. Abe *et al.*, Belle-CONF-0319.

[35] A. Ali and A. Y. Parkhomenko, "Branching ratios for $B \to \rho \gamma$ decays in next-to-leading order in α_s including hard spectator corrections," Eur. Phys. J. C **23**, 89 (2002) [arXiv:hep-ph/0105302].

[36] S. W. Bosch and G. Buchalla, "The radiative decays $B \to V \gamma$ at next-to-leading order in QCD," Nucl. Phys. B **621**, 459 (2002) [arXiv:hep-ph/0106081].

[37] A. L. Kagan and M. Neubert, "Isospin breaking in $B \to K^*\gamma$ decays," Phys. Lett. B **539**, 227 (2002) [arXiv:hep-ph/0110078].

[38] S. Nishida *et al.* [Belle Collaboration], "Radiative B meson decays into $K\pi\gamma$ and $K\pi\pi\gamma$ final states," Phys. Rev. Lett. **89**, 231801 (2002) [arXiv:hep-ex/0205025].

[39] A. Drutskoy *et al.* [BELLE Collaboration], "Observation of radiative $B \to \phi K\gamma$ decays," Phys. Rev. Lett. **92**, 051801 (2004) [arXiv:hep-ex/0309006].

[40] J. M. Soares, "CP violation in radiative b decays," Nucl. Phys. B **367**, 575 (1991).

[41] A. L. Kagan and M. Neubert, "Direct CP violation in $B \to X_s\gamma$ decays as a signature of new physics," Phys. Rev. D **58**, 094012 (1998) [arXiv:hep-ph/9803368].

[42] K. Abe *et al.* [BELLE Collaboration], "Measurement of the CP asymmetry in $B \to X_s\gamma$," arXiv:hep-ex/0308038.

[43] B. Aubert *et al.* [BABAR Collaboration], "Search for the radiative decays $B \to \rho\gamma$ and $B^0 \to \omega\gamma$," arXiv:hep-ex/0306038.

[44] M. Nakao for the Belle Collaboration, talk given at 2nd Workshop on the CKM Unitarity Triangle, Durham, England, Apr. 2003, "Belle results on $b \to sl^+l^-$ and $b \to \gamma$," eConf **C0304052**, WG208 (2003) [arXiv:hep-ex/0307031].

[45] B. Aubert *et al.* [BABAR Collaboration], "Evidence for the flavor changing neutral current decays $B \to Kl^+l^-$ and $B \to K^*l^+l^-$. ((B))," arXiv:hep-ex/0207082.

[46] B. Aubert *et al.* [BABAR Collaboration], "Evidence for the rare decay $B \to K^*l^+l^-$ and measurement of the $B \to Kl^+l^-$ branching fraction," Phys. Rev. Lett. **91**, 221802 (2003) [arXiv:hep-ex/0308042].

[47] A. Ali, E. Lunghi, C. Greub and G. Hiller, "Improved model-independent analysis of semileptonic and radiative rare B decays," Phys. Rev. D **66**, 034002 (2002) [arXiv:hep-ph/0112300].

[48] E. Lunghi, "Improved model-independent analysis of semileptonic and radiative rare B decays," arXiv:hep-ph/0210379.

[49] W. Jaus and D. Wyler, "The Rare Decays Of $B \to Kl\bar{l}$ And $B \to K * l\bar{l}$," Phys. Rev. D **41**, 3405 (1990).

[50] D. Melikhov, N. Nikitin and S. Simula, "Rare decays $B \to (K, K^*)(l^+l^-, \nu\bar{\nu})$ in the quark model," Phys. Lett. B **410**, 290 (1997) [arXiv:hep-ph/9704268].

[51] P. Colangelo, F. De Fazio, P. Santorelli and E. Scrimieri, "QCD Sum Rule Analysis of the Decays $B \to K\ell + \ell -$ and $B \to K * \ell + \ell -$," Phys. Rev. D **53**, 3672 (1996) [Erratum-ibid. D **57**, 3186 (1998)] [arXiv:hep-ph/9510403].

[52] T. M. Aliev, C. S. Kim and Y. G. Kim, "A systematic analysis of the exclusive $B \to K^*l^+l^-$ decay," Phys. Rev. D **62**, 014026 (2000) [arXiv:hep-ph/9910501].

[53] M. Zhong, Y. L. Wu and W. Y. Wang, "Exclusive B meson rare decays and new relations of form factors in effective field theory of heavy quarks," Int. J. Mod. Phys. A **18**, 1959 (2003) [arXiv:hep-ph/0206013].

[54] B. Aubert *et al.* [BABAR Collaboration], "Measurement of the $B \to X_s l^+ l^-$ branching fraction using a sum over exclusive modes," arXiv:hep-ex/0308016.

Chapter 2

Flavor Structure of the Standard Model

2.1 Flavor Structure of the Standard Model

In the Standard Model of elementary particles there are three generations of leptons and quarks

$$\begin{pmatrix} \nu_e \\ e \end{pmatrix} \quad \begin{pmatrix} \nu_\mu \\ \mu \end{pmatrix} \quad \begin{pmatrix} \nu_\tau \\ \tau \end{pmatrix}, \tag{2.1}$$

$$\begin{pmatrix} u \\ d \end{pmatrix} \quad \begin{pmatrix} c \\ s \end{pmatrix} \quad \begin{pmatrix} t \\ b \end{pmatrix}, \tag{2.2}$$

and their interactions are described by a gauge field theory with the gauge group $SU(3)_C \times SU(2)_L \times U(1)_Y$. The group $SU(3)$ denotes Quantum Chromodynamics (QCD), which governs the strong interaction among quarks. The transformation property under the electroweak gauge group $SU(2)_L \times U(1)_Y$ differs for the left and right chiralities of fermions. The right-handed components of the leptons and quarks are singlets under the weak $SU(2)_L$, and the weak hypercharge Y is 0, -1, 2/3, $-1/3$ for neutrinos, leptons, up-type quarks and down-type quarks, respectively. The left-handed components of leptons transform as doublets under the weak $SU(2)_L$ while the weak doublets of quarks differ slightly from (2.2) and are given by

$$\begin{pmatrix} u \\ d' \end{pmatrix}_L \quad \begin{pmatrix} c \\ s' \end{pmatrix}_L \quad \begin{pmatrix} t \\ b' \end{pmatrix}_L. \tag{2.3}$$

The weak eigenstates (d', s', b') are a linear combination of the mass eigenstates (d, s, b), being related by a 3×3 unitary matrix, referred to as the Cabibbo-Kobayashi-Maskawa (CKM) matrix $\hat{V}_{\rm CKM}$ [1, 2], as follows

$$\begin{pmatrix} d' \\ s' \\ b' \end{pmatrix} = \hat{V}_{\rm CKM} \begin{pmatrix} d \\ s \\ b \end{pmatrix} \equiv \begin{pmatrix} V_{ud} & V_{us} & V_{ub} \\ V_{cd} & V_{cs} & V_{cb} \\ V_{td} & V_{ts} & V_{tb} \end{pmatrix} \begin{pmatrix} d \\ s \\ b \end{pmatrix}. \tag{2.4}$$

The charged current interactions of quarks mediated by the W boson are described by an interaction Lagrangian

$$\mathcal{L}^{\rm CC} = -\frac{g_2}{\sqrt{2}} \begin{pmatrix} \overline{u} & \overline{c} & \overline{t} \end{pmatrix}_L \gamma^\mu \begin{pmatrix} d' \\ s' \\ b' \end{pmatrix}_L W_\mu^\dagger + \text{h.c.}$$

$$= -\frac{g_2}{\sqrt{2}} \begin{pmatrix} \overline{u} & \overline{c} & \overline{t} \end{pmatrix}_L \gamma^\mu \hat{V}_{\rm CKM} \begin{pmatrix} d \\ s \\ b \end{pmatrix}_L W_\mu^\dagger + \text{h.c.}, \tag{2.5}$$

where W_μ denotes the W boson, and g_2 is the gauge coupling corresponding to the gauge group $SU(2)_L$. In the low energy effective Hamiltonian it appears as the Fermi constant $G_F/\sqrt{2} = g_2^2/8M_W^2$. Due to the misalignment between the up-type and down-type quark fields, the charged current induces transitions among different generations.

In contrast, the neutral current is flavor-conserving, which is ensured by the unitarity of the CKM matrix, and thus Flavor Changing Neutral Currents (FCNC) are absent at the tree level in the Standard Model. This is the Glashow-Iliopoulos-Maiani (GIM) mechanism [3]. Even including loop corrections, the FCNC interaction vanishes in the limit of degenerate (up-type) quark masses, due to the unitarity of the CKM matrix.

The CKM matrix is a unitary $N \times N$ matrix with $N(=3)$ number of generations, and thus contains N^2 parameters in general. However, $2N-1$ phases may be absorbed by rephasing the $2N$ quark fields (one overall phase is related to the total baryon number conservation and is irrelevant for the quark mixing), and $(N-1)^2$ independent parameters remain. Of these, $\frac{1}{2}N(N+1)$ are real parameters, which correspond to rotation angles among different generations, while $\frac{1}{2}N(N-1)$ are imaginary parameters, which are sources of CP-violation. In the three-generation Standard Model, there are 3 mixing angles and 1 CP-phase.

The standard parametrization of the CKM matrix is the following: [4]

$$V_{\rm CKM} = \begin{pmatrix} c_{12}c_{13} & s_{12}c_{13} & s_{13}e^{-i\delta} \\ -s_{12}c_{23} - c_{12}s_{23}s_{13}e^{i\delta} & c_{12}c_{23} - s_{12}s_{23}s_{13}e^{i\delta} & s_{23}c_{13} \\ s_{12}s_{23} - c_{12}c_{23}s_{13}e^{i\delta} & s_{23}c_{12} - s_{12}c_{23}s_{13}e^{i\delta} & c_{23}c_{13} \end{pmatrix}, \tag{2.6}$$

where $c_{ij} = \cos\theta_{ij}$ and $s_{ij} = \sin\theta_{ij}$ with θ_{ij} ($ij = 12$, 13 and 23) the mixing angles, and δ is the complex phase. It is known experimentally that the angles are small and exhibit the hierarchy $1 \gg s_{12} \gg s_{23} \gg s_{13}$. To make this structure manifest, the Wolfenstein parametrization [5] is often used, in which one sets $\lambda = |V_{us}| \simeq 0.22$ and

$$V_{\rm CKM} = \begin{pmatrix} 1-\lambda^2/2 & \lambda & A\lambda^3(\rho - i\eta) \\ -\lambda & 1-\lambda^2/2 & A\lambda^2 \\ A\lambda^3(1-\rho-i\eta) & -A\lambda^2 & 1 \end{pmatrix} + O(\lambda^4), \tag{2.7}$$

with A, ρ and η being real parameters of order unity. In this parametrization the source of CP-violation is carried by the most off-diagonal elements V_{ub} and V_{td}.

Among these four parameters, λ and A are relatively well known from corresponding semi-leptonic decays: $|V_{us}| = 0.2196 \pm 0.0026$ from K_{l3} decays and $|V_{cb}| = (41.2 \pm 2.0) \times 10^{-3}$ from inclusive and exclusive $b \to c l \overline{\nu}_l$ decays [4]. The determination of the other two parameters ρ and η is conveniently depicted as a contour in the plane of (ρ, η). It corresponds to the unitarity relation of the CKM matrix applied to the first and third columns

$$V_{ud}V_{ub}^* + V_{cd}V_{cb}^* + V_{td}V_{tb}^* = 0. \tag{2.8}$$

This relation may be presented in the complex place as in Fig. 2.1 (a), which is called the "unitarity triangle" Since $V_{cd}V_{cb}^*$ is real to a good approximation (up to $O(\lambda^7)$), it is convenient to normalize the triangle by $|V_{cd}V_{cb}^*| = A\lambda^3$ so that the apex has the coordinate $(\overline{\rho}, \overline{\eta})$ where

$$\overline{\rho} = \rho(1-\lambda^2/2), \quad \overline{\eta} = \eta(1-\lambda^2/2), \tag{2.9}$$

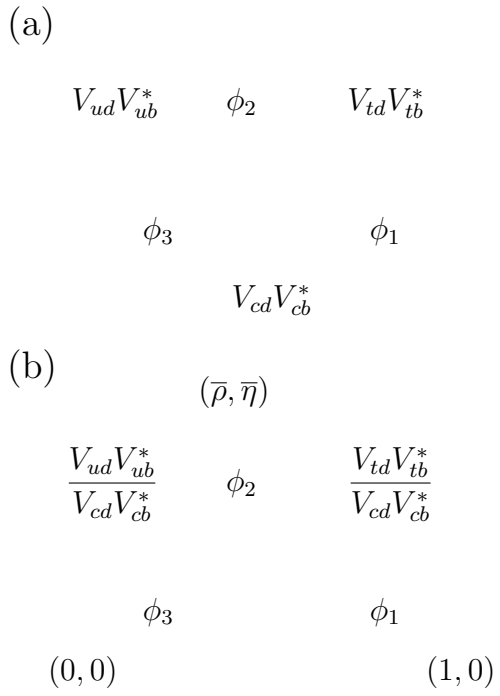

Figure 2.1: Unitarity triangle

(Fig. 2.1 (b)). The three angles of the unitarity triangle represent the complex phase of the combinations

$$\phi_1 = \arg\left[-\frac{V_{cd}V_{cb}^*}{V_{td}V_{tb}^*}\right], \quad \phi_2 = \arg\left[-\frac{V_{td}V_{tb}^*}{V_{ud}V_{ub}^*}\right], \quad \phi_3 = \arg\left[-\frac{V_{ud}V_{ub}^*}{V_{cd}V_{cb}^*}\right]. \tag{2.10}$$

The notation $\alpha \equiv \phi_2$, $\beta \equiv \phi_1$, $\gamma \equiv \phi_3$ is also used in the literature.

The present constraints on the parameter (ρ, η) are summarized in Fig. 2.2, which is taken from the CKM fitter group (http://ckmfitter.in2p3.fr/). Details of the input parameters are discussed, for instance, in [6]. Prospects with Super-KEKB will be discussed in the following sections.

2.2 Low Energy Effective Hamiltonians

In B decays the exchange of a W boson and virtual loops involving the top quark are effectively point-like interactions, since the relevant length scale of B meson decays is at least $O(1/m_b)$ while W exchange takes place at a short distance scale $O(1/M_W)$. It is theoretically inefficient to calculate the physical amplitudes using the entire W and top quark propagators, and one may instead introduce a low energy effective Hamiltonian. This framework is based on the Operator Product Expansion (OPE) [7], which allows one to separate the long distance physics from the short distance interactions, occurring at a length scale of $1/M_W$, up to the corrections of order m_b/M_W, which can be safely neglected in many cases.

For instance, $B^0 - \overline{B}^0$ mixing occurs through the box diagrams shown in Fig. 2.3. The interaction can be described in terms of the $\Delta B = 2$ effective Hamiltonian

$$\mathcal{H}_{eff}^{\Delta B=2} = \frac{G_F^2}{16\pi^2}(V_{tb}V_{td}^*)^2 M_W^2 S_0(m_t^2/M_W^2) C^{\Delta B=2}(\mu_b) Q^{\Delta B=2}(\mu), \tag{2.11}$$

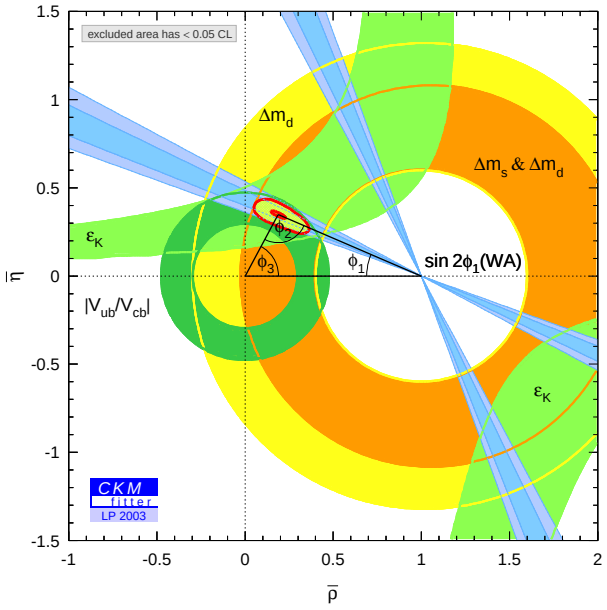

Figure 2.2: A fit of the parameters (ρ, η) using several experimental constraints as of Lepton-Photon 2003. The plot is taken from the CKM fitter page http://ckmfitter.in2p3.fr/.

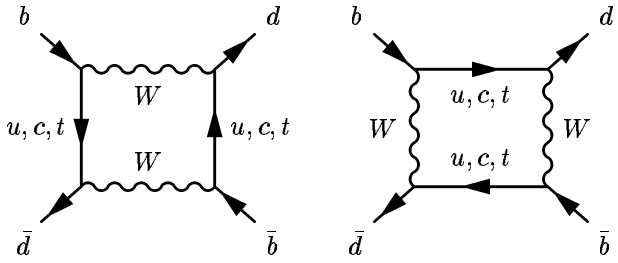

Figure 2.3: Box diagrams to produce the $\Delta B = 2$ four-quark operator

where the $\Delta B = 2$ effective four-quark operator is

$$Q^{\Delta B=2} = \bar{d}\gamma_\mu(1-\gamma_5)b\,\bar{d}\gamma_\mu(1-\gamma_5)b. \tag{2.12}$$

The operator is defined at the renormalization scale μ_b and the corresponding Wilson coefficient $C^{\Delta B=2}(\mu_b)$ is calculated using the renormalization group technique as $C^{\Delta B=2}(\mu_b) = [\alpha_s^{(5)}(\mu_b)]^{-6/23}$ to leading order. The function $S_0(m_t^2/M_W^2)$ is called the Inami-Lim function [8] and represents the loop effect through the box diagrams.

The $\Delta B = 1$ transitions are described by the following effective Hamiltonian

$$\mathcal{H}_{eff}^{\Delta B=1} = \frac{4G_F}{\sqrt{2}} V_{\rm CKM} \sum_i C_i(\mu_b) O_i(\mu_b) + \text{h.c.},$$

where $V_{\rm CKM}$ is the corresponding CKM matrix element. The operators $O_i(\mu_b)$ defined at the scale μ_b are listed below, and the couplings $C_i(\mu_b)$ are the Wilson coefficients.

The effective operators representing the tree-level W exchange diagram depicted in Fig. 2.4 are

$$O_1^q = \bar{d}^\alpha\gamma_\mu(1-\gamma_5)q^\beta\,\bar{q}^\beta\gamma_\mu(1-\gamma_5)b^\alpha, \quad q = u, c, \tag{2.13}$$
$$O_2^q = \bar{d}^\alpha\gamma_\mu(1-\gamma_5)q^\alpha\,\bar{q}^\beta\gamma_\mu(1-\gamma_5)b^\beta, \quad q = u, c. \tag{2.14}$$

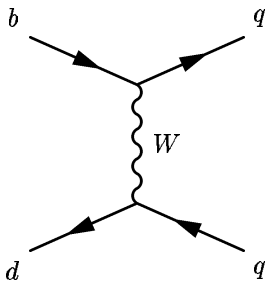

Figure 2.4: Tree-type W boson exchange diagram.

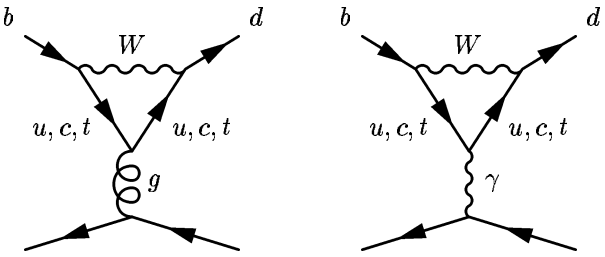

Figure 2.5: Penguin diagrams. The fermion line on the bottom are quarks for the gluon penguin diagram (left), while either quarks or leptons can be involved in the electro-weak penguin (right).

Here the superscripts α and β specify the color contraction. There is another set of operators obtained by replacing d by s.

Many important FCNC decays occur through the so-called penguin diagrams. Some examples are shown in Fig. 2.5.

The gluon penguin diagram (Fig. 2.5 (left)) produces the following operators

$$O_3 = \sum_{q=u,d,s,c} \overline{d}^{\alpha}\gamma_{\mu}(1-\gamma_5)b^{\alpha}\,\overline{q}^{\beta}\gamma_{\mu}(1-\gamma_5)q^{\beta}, \tag{2.15}$$

$$O_4 = \sum_{q=u,d,s,c} \overline{d}^{\alpha}\gamma_{\mu}(1-\gamma_5)b^{\beta}\,\overline{q}^{\beta}\gamma_{\mu}(1-\gamma_5)q^{\alpha}, \tag{2.16}$$

$$O_5 = \sum_{q=u,d,s,c} \overline{d}^{\alpha}\gamma_{\mu}(1-\gamma_5)b^{\alpha}\,\overline{q}^{\beta}\gamma_{\mu}(1+\gamma_5)q^{\beta}, \tag{2.17}$$

$$O_6 = \sum_{q=u,d,s,c} \overline{d}^{\alpha}\gamma_{\mu}(1-\gamma_5)b^{\beta}\,\overline{q}^{\beta}\gamma_{\mu}(1+\gamma_5)q^{\alpha}. \tag{2.18}$$

There are also diagrams in which the gluon or photon is not attached to the fermion line and directly appears in the final state. Such diagrams produce

$$O_{7\gamma} = \frac{e}{8\pi^2} m_b \overline{d}\sigma^{\mu\nu}(1+\gamma_5)F_{\mu\nu}b, \tag{2.19}$$

$$O_{8g} = \frac{g}{8\pi^2} m_b \overline{d}\sigma^{\mu\nu}(1+\gamma_5)G^a_{\mu\nu}T^a b, \tag{2.20}$$

where $F_{\mu\nu}$ and $G_{\mu\nu}$ are electromagnetic and QCD field strength tensors, respectively. These operators are responsible for the $b \to d\gamma$ and $b \to dg$ transitions. The operators relevant to the $b \to s\gamma$ and $b \to sg$ transitions are obtained by replacing d by s in (2.19) and (2.20).

The electroweak penguin diagram (Fig. 2.5 (right)) gives a higher order contribution in the electromagnetic coupling constant α and is thus very small in general. However, since it

may become a source of isospin symmetry breaking, in some cases it could be relevant. The corresponding operators are

$$O_7 = \frac{3}{2}\sum_{q=u,d,s,c} e_q\,\overline{d}^{\alpha}\gamma_\mu(1-\gamma_5)b^{\alpha}\,\overline{q}^{\beta}\gamma_\mu(1+\gamma_5)q^{\beta}, \tag{2.21}$$

$$O_8 = \frac{3}{2}\sum_{q=u,d,s,c} e_q\,\overline{d}^{\alpha}\gamma_\mu(1-\gamma_5)b^{\beta}\,\overline{q}^{\beta}\gamma_\mu(1+\gamma_5)q^{\alpha}, \tag{2.22}$$

$$O_9 = \frac{3}{2}\sum_{q=u,d,s,c} e_q\,\overline{d}^{\alpha}\gamma_\mu(1-\gamma_5)b^{\alpha}\,\overline{q}^{\beta}\gamma_\mu(1-\gamma_5)q^{\beta}, \tag{2.23}$$

$$O_{10} = \frac{3}{2}\sum_{q=u,d,s,c} e_q\,\overline{d}^{\alpha}\gamma_\mu(1-\gamma_5)b^{\beta}\,\overline{q}^{\beta}\gamma_\mu(1-\gamma_5)q^{\alpha}. \tag{2.24}$$

e_q is the electromagnetic change of quarks: $2/3$ for up-type quarks and $-1/3$ for down-type quarks. When the fermion line in the bottom of Fig. 2.5 (right) is a lepton (e, μ or τ), we obtain

$$O_{9V} = \frac{e^2}{16\pi^2}\overline{d}\gamma_\mu(1-\gamma_5)b\,\bar{l}\gamma_\mu l, \tag{2.25}$$

$$O_{10A} = \frac{e^2}{16\pi^2}\overline{d}\gamma_\mu(1-\gamma_5)b\,\bar{l}\gamma_\mu\gamma_5 l. \tag{2.26}$$

They give rise to the $b \to d(s)l^+l^-$ transitions.

The Wilson coefficients in (2.2) are calculated using perturbation theory to next-to-leading order (NLO) [9–12].

2.3 $B - \overline{B}$ Mixing

Neutral B meson mixing is one of the most important FCNC processes in B physics. In the Standard Model it involves the CKM matrix element V_{td} and thus gives a CP-violating amplitude, which induces a variety of CP-violating observables through its quantum mechanical interference with other amplitudes.

A B^0 meson produced as an initial state may evolve into its antiparticle $\overline{B}^0$ through the interaction given by the $\Delta B = 2$ effective Hamiltonian (2.11). In quantum mechanics the state $|B^0(t)\rangle$ at time t is a superposition of two states $|B^0\rangle$ and $|\overline{B}^0\rangle$. The time evolution is described by a Shrödinger equation

$$i\frac{d}{dt}|B(t)\rangle = \left(M - i\frac{\Gamma}{2}\right)|B(t)\rangle, \tag{2.27}$$

where the two-by-two Hermite matrices M and Γ denote mass and decay matrices, respectively. The diagonal parts are constrained from CPT invariance $M_{11} = M_{22}$ and $\Gamma_{11} = \Gamma_{22}$, and the off-diagonal parts M_{12} (M_{21}) and $\Gamma_{12}/2$ ($\Gamma_{21}/2$) are disparsive and absorptive parts of the $\Delta B = 2$ transition. The eigenstates of the matrix $M - i\Gamma/2$ are given by

$$|B_H\rangle = p|B^0\rangle + q|\overline{B}^0\rangle, \tag{2.28}$$

$$|B_L\rangle = p|B^0\rangle - q|\overline{B}^0\rangle, \tag{2.29}$$

and their coefficients p and q are obtained by solving

$$\frac{q}{p} = -\sqrt{\frac{M_{12}^* - i\Gamma_{12}^*/2}{M_{12} - i\Gamma_{12}/2}} \tag{2.30}$$

together with the normalization condition $|p|^2 + |q|^2 = 1$. The eigenvalues $M_{H,L} - i\Gamma_{H,L}/2$ are related to observables as follows: the B meson mass $M = (M_H + M_L)/2$, the B meson width $\Gamma = (\Gamma_H + \Gamma_L)/2$, the $B^0 - \overline{B}^0$ mixing frequency $\Delta M = M_H - M_L$, and the width difference $\Delta\Gamma = \Gamma_L - \Gamma_H$.

In the B meson system there is a relation $\Delta\Gamma \ll \Delta M$, which follows from $\Gamma_{12} \ll M_{12}$. We may then appoximately obtain

$$\Delta M = 2|M_{12}| \left[1 + O\left(\left|\frac{\Gamma_{12}}{M_{12}}\right|^2\right)\right], \tag{2.31}$$

$$\Delta\Gamma = 2|\Gamma_{12}| \cos\phi \left[1 + O\left(\left|\frac{\Gamma_{12}}{M_{12}}\right|^2\right)\right], \tag{2.32}$$

and

$$\frac{q}{p} = -\sqrt{\frac{M_{12}^*}{M_{12}}} \left[1 - \frac{1}{2}\left|\frac{\Gamma_{12}}{M_{12}}\right| \sin\phi + O\left(\left|\frac{\Gamma_{12}}{M_{12}}\right|^2\right)\right]. \tag{2.33}$$

The angle ϕ is the CP violating phase difference between M_{12} and Γ_{12}

$$\mathrm{Im}\frac{\Gamma_{12}}{M_{12}} = \left|\frac{\Gamma_{12}}{M_{12}}\right| \sin\phi. \tag{2.34}$$

The time evolution of the state $|B^0\rangle$ and $|\overline{B}^0\rangle$ produced at time $t = 0$ is then given by

$$|B^0(t)\rangle = g_+(t)|B^0\rangle + \frac{q}{p} g_-(t)|\overline{B}^0\rangle, \tag{2.35}$$

$$|\overline{B}^0(t)\rangle = g_+(t)|\overline{B}^0\rangle + \frac{p}{q} g_-(t)|B^0\rangle, \tag{2.36}$$

with

$$g_+(t) = e^{-iMt-\Gamma t/2}\left[\cosh\frac{\Delta\Gamma t}{4}\cos\frac{\Delta M t}{2} - i\sinh\frac{\Delta\Gamma t}{4}\sin\frac{\Delta M t}{2}\right], \tag{2.37}$$

$$g_-(t) = e^{-iMt-\Gamma t/2}\left[-\sinh\frac{\Delta\Gamma t}{4}\cos\frac{\Delta M t}{2} + i\cosh\frac{\Delta\Gamma t}{4}\sin\frac{\Delta M t}{2}\right]. \tag{2.38}$$

As the initial B^0 (or $\overline{B}^0$) state evolves, it oscillates between B^0 and $\overline{B}^0$ states with the frequency ΔM. The CP-violating phase arises in the mixing parameter q/p, which carries the phase of M_{12} as shown in (2.33).

2.4 Time-dependent Asymmetries

One of the key observables in the asymmetric B factory is the time-dependent asymmetry between B^0 and $\overline{B}^0$ decays.

Let us consider a decay of the B meson to a final state f. The decay rate $\Gamma(B^0(t) \to f)$ is time dependent, since the decaying state is a time-dependent superposition of $|B^0\rangle$ and $|\overline{B}^0\rangle$, as discussed in the previous section. We write the decay amplitude of flavor eigenstates as $A_f = \langle f|B^0\rangle$ and $\overline{A}_f = \langle f|\overline{B}^0\rangle$, and define a parameter

$$\lambda_f = \frac{q}{p}\frac{\overline{A}_f}{A_f}. \tag{2.39}$$

If the final state is a CP-eigenstate $CP|f\rangle = \eta_f|f\rangle$ with an eigenvalue $\eta_f = \pm 1$, then the time dependent asymmetry

$$a_f(t) = \frac{\Gamma(\overline{B}^0(t) \to f) - \Gamma(B^0(t) \to f)}{\Gamma(\overline{B}^0(t) \to f) + \Gamma(B^0(t) \to f)} \tag{2.40}$$

becomes

$$a_f(t) = \mathcal{A}_f \cos(\Delta M t) + \mathcal{S}_f \sin(\Delta M t), \tag{2.41}$$

neglecting the small width difference of the B meson. Here, the direct and indirect (or mixing-induced) CP asymmetries are written as

$$\mathcal{A}_f = \frac{|\lambda_f|^2 - 1}{|\lambda_f|^2 + 1}, \tag{2.42}$$

$$\mathcal{S}_f = \frac{2\,\mathrm{Im}\lambda_f}{1 + |\lambda_f|^2}. \tag{2.43}$$

Since the absolute value of q/p is approximately 1, direct CP-violation $|\mathcal{A}_f| \neq 0$ requires $|A_f| \neq |\overline{A}_f|$, which could happen if A_f is a sum of (more than one) decay amplitudes having different CP-phases. Indirect CP-violation, on the other hand, proves the quantum mechanical interference between the mixing and decay amplitudes.

2.4.1 Measurement of $\sin 2\phi_1$

The mixing-induced asymmetry provides a variety of methods to measure the angles of the Unitarity Triangle (Fig. 2.1). It was first proposed by Bigi, Carter, and Sanda in 1980–1981 [13–15], and gave strong motivation to construct the present KEK B Factory. The best known example is the case where the final state is $J/\psi K^0_S$, whose quark level process is $\overline{b} \to \overline{c}c\overline{s}$ followed by $K^0 - \overline{K}^0$ mixing. Provided that the decay is dominated by a single amplitude, the ratio of decay amplitudes is given by

$$\frac{\overline{A}_{J/\psi K^0_S}}{A_{J/\psi K^0_S}} = \left(\frac{V_{cb}V^*_{cs}}{V^*_{cb}V_{cs}}\right)\left(\frac{V_{cs}V^*_{cd}}{V^*_{cs}V_{cd}}\right), \tag{2.44}$$

The overall sign is $(-1)^2 = 1$, where one minus sign appears from a phase convention for the B and $\overline{B}$ meson states, and the other is due to the CP odd final state $J/\psi K^0_S$. Together with the phase in the mixing

$$\frac{q}{p} \simeq -e^{-i\phi_M} = -\left(\frac{V^*_{tb}V_{td}}{V_{tb}V^*_{cd}}\right), \tag{2.45}$$

the entire ratio $\lambda_{J/\psi K^0_S}$ becomes

$$\lambda_{J/\psi K^0_S} = -\left(\frac{V^*_{tb}V_{td}}{V_{tb}V^*_{td}}\right)\left(\frac{V_{cb}V^*_{cs}}{V^*_{cb}V_{cs}}\right)\left(\frac{V_{cs}V^*_{cd}}{V^*_{cs}V_{cd}}\right) = -e^{2i\phi_1}. \tag{2.46}$$

Thus, one can precisely measure the angle ϕ_1 from the time-dependent asymmetry

$$a_{J/\psi K^0_S}(t) = -\sin(2\phi_1)\sin(\Delta M t). \tag{2.47}$$

There exists an additional decay amplitude through the penguin diagram $\overline{b} \to \overline{s}c\overline{c}$, which involves the CKM factor $V_{ts}V^*_{tb}$. Using the unitarity of the CKM matrix $V_{ts}V^*_{tb} = -V_{cs}V^*_{cb} - V_{us}V^*_{ub}$, the

weak phase of the penguin contribution is the same as that of the tree amplitude $V_{cs}V_{cb}^*$ up to a doubly Cabibbo-suppressed correction. Therefore, the relation (2.47) holds to an excellent approximation ($\sim 1\%$), and the mode $J/\psi K_S^0$ is called the "gold-plated" mode. The precision expected at SuperKEKB is discussed in Section 4.6.

There are other decay modes which develop the same weak phase. Namely, the penguin decays $\overline{b} \to \overline{s}s\overline{s}$ are accompanied by the CKM factor $V_{ts}V_{tb}^*$ just as the penguin contribution to $\overline{b} \to \overline{s}c\overline{c}$. Since there is no direct tree diagram for $\overline{b} \to \overline{s}s\overline{s}$, measurement of the same angle $\sin 2\phi_1$ through its time dependent asymmetry can be a probe of any new physics phase in the penguin loop process [16]. At the hadron level, the corresponding modes are $B^0 \to \phi K_S^0$ and $B^0 \to \eta' K_S^0$. These asymmetries have already been measured as described in Section 1.2, and the expected sensitivity at SuperKEKB is studied in Section 4.2. Possible contamination from the tree-level process $\overline{b} \to \overline{u}u\overline{s}$ with a rescattering of $u\overline{u}$ to $s\overline{s}$ may distort the measurement. However, such a contribution is expected to be small ($O(\lambda^2) \sim 5\%$) [17], and a model independent bound can be obtained using $SU(3)$ relations provided that the related modes are observed at higher luminosity B factories [18].

2.4.2 Measurement of ϕ_2

If a decay can occur through more than one amplitude with different weak phases, the analysis is more involved. For example, let us consider $B^0 \to \pi^+\pi^-$, whose decay amplitude can be parametrized as

$$A(B^0 \to \pi^+\pi^-) = T_{\pi\pi} + P_{\pi\pi}. \tag{2.48}$$

The first term represents an amplitude for the tree level W exchange process $\overline{b} \to \overline{u}u\overline{d}$, which picks up the CKM matrix elements $V_{ud}V_{ub}^*$, while the second term is a penguin diagram contribution $\overline{b} \to \overline{d}u\overline{u}$ containing the CKM factor $V_{td}V_{tb}^*$. If the penguin contribution can be neglected, the ratio $\lambda_{\pi^+\pi^-}$ in (2.39) reads as

$$\lambda_{\pi^+\pi^-} = -\left(\frac{V_{tb}^*V_{td}}{V_{tb}V_{td}^*}\right)\left(\frac{V_{ud}^*V_{ub}}{V_{ud}V_{ub}^*}\right) = -e^{2i\phi_2}, \tag{2.49}$$

and the time-dependent asymmetry could be used to determine the angle ϕ_2. However, both amplitudes in (2.48) are the same order in λ ($\sim \lambda^3$), and the penguin contribution is not so suppressed compared to the tree level contribution. In fact, the ratio of amplitudes $|P_{\pi\pi}/T_{\pi\pi}|$ is roughly estimated to be around 0.3 from $B \to K\pi$ decays assuming the flavor $SU(3)$ symmetry.

One solution to the problem is to consider isospin symmetry [19]. The $B \to \pi\pi$ decay amplitudes are written as

$$A(B^0 \to \pi^+\pi^-) = \sqrt{2}(A_2 - A_0), \tag{2.50}$$
$$A(B^0 \to \pi^0\pi^0) = 2A_2 + A_0, \tag{2.51}$$
$$A(B^+ \to \pi^+\pi^0) = 3A_2. \tag{2.52}$$

A_0 and A_2 are amplitudes for isospin 0 and 2 of two-pion final state, respectively. The tree diagram contributes to both A_0 and A_2, while the penguin diagram gives A_0 only. Then, one obtains a relation

$$A(B^0 \to \pi^+\pi^-) + \sqrt{2}A(B^0 \to \pi^0\pi^0) = \sqrt{2}A(B^+ \to \pi^+\pi^0). \tag{2.53}$$

and its CP-conjugate

$$\overline{A}(B^0 \to \pi^+\pi^-) + \sqrt{2}\overline{A}(B^0 \to \pi^0\pi^0) = \sqrt{2}\overline{A}(B^+ \to \pi^+\pi^0). \tag{2.54}$$

By measuring the branching ratios of the three decay modes and the time dependent asymmetry of $\pi^+\pi^-$, one can determine the absolute values $|A_0|$ and $|A_2|$ and their relative phase difference $\arg(A_0 A_2^*)$, through a simple geometric reconstruction. Then, the angle ϕ_2 can be determined up to a four-fold ambiguity.

Another solution is to consider the isospin relations among $B \to \rho\pi$ decays [20]. There are three possible decay chains $B^0 \to \{\rho^+\pi^-, \rho^0\pi^0, \rho^-\pi^+\} \to \pi^+\pi^-\pi^0$. Together with their CP-conjugate amplitudes, there exist six different amplitudes, each of which has contributions from both tree and penguin diagrams. By combining the time-dependent asymmetry of this process in the Dalitz plot one may extract the pure tree amplitude, and thus the angle ϕ_2.

If there is non-negligible contribution from the electroweak penguin diagram, the isospin relations are violated, since up and down quarks have different charges [21]. However, such a contribution is suppressed compared to the gluon penguin by a factor $\alpha_{[\mathrm{weak}}(m_t^2/m_Z^2)]/\alpha_s \ln(m_t^2/m_c^2)] \sim 0.1$ [22]. At Super-KEKB, the actual size of the electroweak penguin amplitude can be estimated from the analysis of $K\pi$ decays [22–26].

The prospects of measuring the angle ϕ_2 at Super-KEKB using these methods are discussed in Section 4.7.

2.5 Theoretical Methods

In order to extract fundamental parameters, such as the quark masses and CKM matrix elements, from B decay experiments, one needs model independent calculations of the decay amplitudes. However, since B meson decays accompany complicated QCD interactions, which are highly non-perturbative in general, the theoretical calculation of physical amplitudes is a non-trivial task.

2.5.1 Heavy Quark Symmetry

One useful theoretical method with which one can avoid the hadronic uncertainty is to use symmetries. Using isospin or $SU(3)$ flavor symmetries, different decay amplitudes can be related to each other. This approach is widely used in B decay analyses, *e.g.* the isospin analysis of $\pi\pi$ decays to extract $\sin 2\phi_2$ discussed in Section 2.4.2.

Another symmetry which is especially important in B physics is the heavy quark symmetry [27, 28]. In the limit of an infinitely heavy quark mass, the heavy quark behaves as a static color source and the QCD interaction cannot distinguish different flavors, *i.e.* charm or bottom. Consequently the decay amplitudes (or form factors) of b and c hadrons are related to each other (heavy quark flavor symmetry). Moreover, since the spin-dependent interaction decouples in the infinitely heavy quark mass limit, some form factors become redundant (heavy quark spin symmetry). The most famous example is the heavy-to-heavy semi-leptonic decay $\overline{B} \to D^{(*)}\ell\overline{\nu}_\ell$ form factors. In general there are 6 independent form factors for these exclusive decay modes, but in the heavy quark limit they reduce to one: the Isgur-Wise function, and its normalization in the zero-recoil limit is determined.

A more general formalism has also been developed in the language of effective field theory, *i.e.* Heavy Quark Effective Theory (HQET) [29–31]. It provides a systematic expansion in terms of $\Lambda_{\mathrm{QCD}}/m_Q$.

2.5.2 Heavy Quark Expansion

The inclusive decay rate of a B meson to the final state X can be written as

$$\Gamma(B \to X) = \frac{1}{2m_B} \sum_X (2\pi)^4 \delta^4(p_B - p_X) |\langle X|\mathcal{H}_{\mathit{eff}}^{\Delta B=1}|B\rangle|^2, \tag{2.55}$$

where the sum runs over all possible final states and momentum configurations. The effective Hamiltonian $\mathcal{H}_{\mathit{eff}}^{\Delta B=1}$ is proportional to $\bar{c}\gamma^\mu P_L b \bar{l}\gamma_\mu P_L \nu_l$ when the $b \to c$ semileptonic decay is considered, or to $\bar{u}\gamma^\mu P_L b \bar{l}\gamma_\mu P_L \nu_l$ if we are interested in the $b \to u$ semileptonic decay to determine $|V_{ub}|$. It could also describe non-leptonic decay by considering a four-quark operator $\bar{c}\gamma^\mu P_L b \bar{q}\gamma_\mu P_L q'$. Using the optical theorem (2.55) can be rewritten in terms of an absorptive part of a B meson matrix element

$$\Gamma(B \to X) = \frac{1}{m_B} \mathrm{Im}\, \langle B|\mathcal{T}|B\rangle, \tag{2.56}$$

where the operator $\mathcal{T}$ is

$$\mathcal{T} = i \int d^4x T \left(\mathcal{H}_{\mathit{eff}}^{\Delta B=1}(x) \mathcal{H}_{\mathit{eff}}^{\Delta B=1}(0) \right). \tag{2.57}$$

Since the momentum flowing into the final state quark propagator is large ($\sim m_b$), one can expand the time-ordered product of operators in terms of local operators, using the Operator Product Expansion (OPE) technique [7]. It gives an expansion in terms of the inverse heavy quark mass and is called the Heavy Quark Expansion (HQE) [32–36].

The lowest dimensional operator is $\bar{b}b$, whose matrix element is unity up to $(\Lambda_{\mathrm{QCD}}/m_b)^2$ corrections. The first non-trivial higher order correction appears at $1/m_b^2$ with the chromomagnetic operator $\bar{b}\sigma_{\mu\nu} g_s G^{\mu\nu} b$. Therefore, at $O((\Lambda_{\mathrm{QCD}}/m_b)^2)$ the heavy quark expansion can be expresssed in terms of two non-perturbative parameters

$$\lambda_1 = \frac{1}{2m_B} \langle B(v)|\bar{h}_v (i\vec{D})^2 h_v|B(v)\rangle, \tag{2.58}$$

$$3\lambda_2 = \frac{g_s}{2m_B} \langle B(v)|\frac{1}{2}\bar{h}_v \sigma_{\mu\nu} G^{\mu\nu} h_v|B(v)\rangle, \tag{2.59}$$

where the operators are defined with the HQET field h_v and the B meson state is also defined in the heavy quark limit. λ_2 is known from the hyper-fine splitting of the B meson (B-B^* splitting) to be $\lambda_2 \simeq 0.12$ GeV^2, while λ_1 has to be calculated using non-perturbative methods, such as QCD sum rules [37, 38] or lattice QCD [39–42], or to be fitted with experimental data of inclusive B decays [43–47].

2.5.3 Perturbative Methods

Model independent theoretical calculations of exclusive non-leptonic decay amplitudes are known to be very challenging, as they involve both soft and hard gluon exchanges and clear separation of the perturbative (hard) and non-perturbative (soft) parts is intractable. In the heavy quark limit, however, a formulation to realize such separation of short and long distance physics has recently been developed, ameliorating the perturbative calculation of decay amplitudes.

The intuitive idea is the color transparency argument due to Bjorken [48]. An energetic light meson emitted from B decay resembles a color dipole, and its soft interaction with the remaining decay products is suppressed by $\Lambda_{\mathrm{QCD}}/m_b$. A systematic formulation of such an idea is provided

by QCD factorization [49–51]. In this formalism, the decay matrix elements of $B \to \pi\pi$ can be factorized in the form

$$\begin{aligned}\langle \pi(p')\pi(q)|Q_i|\overline{B}(p)\rangle &= f^{B\to\pi}(q^2)\int_0^1 du\, T_i^I(u)\Phi_\pi(u) \\ &\quad + \int_0^1 d\xi du dv\, T_i^{II}(\xi,u,v)\Phi_B(\xi)\Phi_\pi(u)\Phi_\pi(v), \end{aligned} \tag{2.60}$$

for a four-quark operator Q_i. The first term represents a factorization of the amplitude into the $B \to \pi$ form factor and an out-going pion wave function $\Phi_\pi(u)$ convoluted with the hard scattering kernel $T_i^I(u)$. Here, the term "factorization" is used for two meanings: one is the factorization of the diagram to $\langle\pi|V|\overline{B}\rangle\langle\pi|A|0\rangle$, while the other is the separation of hard, collinear and soft interactions. The kernel $T_i^I(u)$ describes the hard interaction only and thus is calculable using perturbation theory. The second term in (2.60) describes a factorization of the amplitude into three pieces: $\overline{B} \to 0$, $0 \to \pi$, and $0 \to \pi$ convoluted with a hard interaction kernel $T_i^{II}(\xi,u,v)$. To make the factorization of collinear and soft degrees of freedom more explicit, an effective theory has also been developed, which is called the Soft Collinear Effective Theory (SCET) [52–55].

The form factor $f^{B\to\pi}(q^2)$ and the light-cone distribution function (or wave function) $\Phi_B(\xi)$ and $\Phi_\pi(u)$ contain long-distance dynamics, which has to be treated with non-perturbative methods.

Another method of factorization, Perturbative QCD (PQCD) [56–61], has also been proposed and is being used for the analysis of various B decay modes. It relies on the Sudakov suppression of the tail of the wave function, in which the first term (2.60) becomes subleading and the input of the form factor is unnecessary.

2.5.4 Lattice QCD

Lattice QCD provides a method to calculate non-perturbative hadronic matrix elements from the first principles of QCD [62]. It is a regularization of QCD on a four-dimensional hypercubic lattice, which enables numerical simulation on the computer. Since the calculation is numerically so demanding, one has to introduce several approximations in the calculation, which leads to systematic uncertainties.

For more than a decade, lattice QCD has been applied to the calculation of matrix elements relevant to B physics. The best-known quantity is the B meson leptonic decay constant f_B, for which the systematic uncertainty is now under control at the level of 10–15% accuracy. The important tools to achieve this goal are the following.

- *Effective theories for heavy quarks.* Since the Compton wave-length of the b quark is shorter than the lattice spacing a, the discretization error is out of control with the usual lattice fermion action for relativistic particles. Instead, Heavy Quark Effective Theory (HQET) [29] or Non-relativistic QCD (NRQCD) [63–65] is formulated on the lattice and used to simulate the b quark. Another related effective theory is the so-called Fermilab action [66, 67], which covers the entire (light to heavy) mass regime with the same lattice action. For the B meson the next-to-leading $(1/m_Q)$ order calculation provides $\lesssim 5\%$ accuracy [68].

- *Effective theories to describe discretization errors.* The discretization effect can be expressed in terms of the Lagrangian language, *i.e.* Symanzik effective theory [69, 70]. It

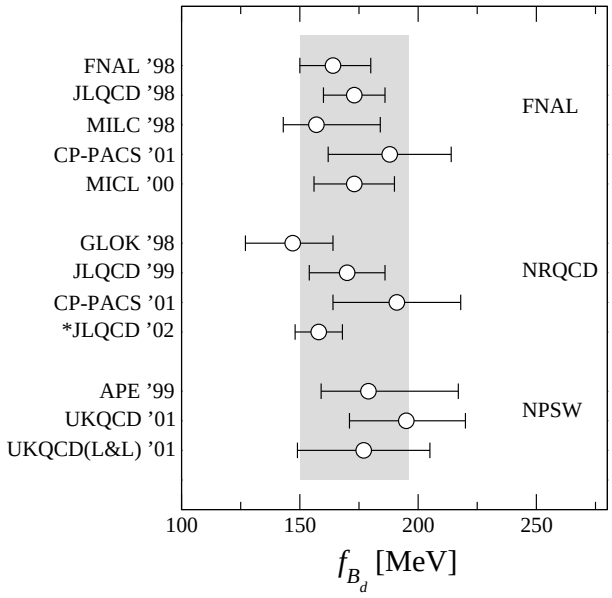

Figure 2.6: Recent quenched lattice calculations of f_B. Figure from [75].

also provides a method to eliminate the error by adding irrelevant operators to the lattice action. The $O(a)$ error existing in the Wilson fermion action can be removed by adding a dimension-five operator [71]. The cancellation of the $O(a)$ error can also be done non-perturbatively [72, 73], so that the remaining discretization error is $O(a^2)$ and not $O(\alpha_s^n a)$.

- *Renormalized perturbation theory.* To relate the lattice operators to their continuum counterparts, one has to rely on perturbation theory. For a long time lattice perturbation had bad convergence behavior and the perturbative error was too large if one calculated only the one-loop terms. This problem was cured by Lepage and Mackenzie by taking a renormalized coupling constant as an expansion parameter [74].

A summary of recent lattice calculations of f_B in the quenched approximation is shown in Fig. 2.6. Results of many groups obtained with different discretizations for heavy quarks agree very well within the error band of $\sim 13\%$.

The above results are obtained within the approximation of neglecting the pair creation and annihilation of quarks in the vacuum, which is called the quenched approximation. To include such dynamical quark effects requires much more computer power, and it has only recently become feasible. A recent calculation by the JLQCD collaboration [76] is shown in Fig. 2.7, which represents the light quark mass dependence of f_B in two-flavor QCD. A major uncertainty in the unquenched simulation comes from the chiral extrapolation, as the present unquenched simulation is limited to relatively heavy sea quark masses ($m_q \gtrsim m_s/2$). Because chiral perturbation theory predicts the chiral logarithm $m_q \ln m_q$ [77], the chiral extrapolation may bend downwards near the chiral limit as shown by dashed curves in Fig. 2.7. To control such extrapolation one needs simulations with much smaller sea quark masses as adopted in the recent simulations using staggered fermions for sea quarks [78].

Lattice QCD calculations can be applied to several other important quantities:

- B_B. The B parameter in $B^0 - \overline{B}^0$ mixing has been calculated in unquenched QCD [76], with the result $f_B\sqrt{\hat{B}_B} = 215(11)(^{+\ 0}_{-23})(15)$ MeV. Here the first error is statistical, the

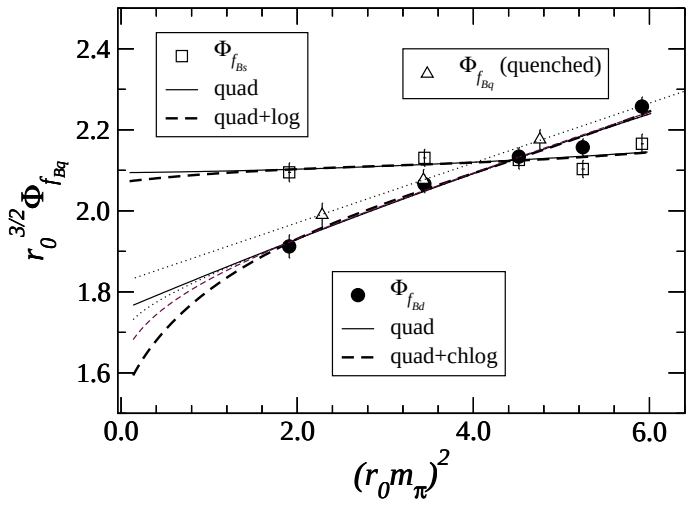

Figure 2.7: Chiral extrapolation of unquenched f_B. The plot is for $\Phi_{f_B} \equiv f_B\sqrt{m_B}$ normalized with a Sommer scale r_0. Figure from [76].

second is uncertainty from the chiral extrapolation and the third is from other systematic errors.

- *heavy-to-heavy semileptonic decay.* The zero recoil form factor of the semileptonic decay $B \to D^{(*)}l\nu$ has been calculated rather precisely using a double-ratio technique [79, 80].
- *heavy-to-light semileptonic decay.* The $B \to \pi\ell\nu$ form factor has been calculated in quenched QCD to an accuracy of order 20% [81–84].

These and other recent results have been reviewed at recent conferences [75, 85–87].

References

[1] N. Cabibbo, "Unitary Symmetry And Leptonic Decays," Phys. Rev. Lett. **10** (1963) 531.

[2] M. Kobayashi and T. Maskawa, "CP Violation In The Renormalizable Theory Of Weak Interaction," Prog. Theor. Phys. **49**, 652 (1973).

[3] S. L. Glashow, J. Iliopoulos and L. Maiani, "Weak Interactions With Lepton – Hadron Symmetry," Phys. Rev. D **2**, 1285 (1970).

[4] K. Hagiwara *et al.* [Particle Data Group Collaboration], "Review Of Particle Physics," Phys. Rev. D **66**, 010001 (2002).

[5] L. Wolfenstein, "Parametrization Of The Kobayashi-Maskawa Matrix," Phys. Rev. Lett. **51**, 1945 (1983).

[6] M. Battaglia *et al.*, "The CKM matrix and the unitarity triangle," Proceedings of the First Workshop on the CKM Unitarity Triangle, CERN 13-16 February 2002; arXiv:hep-ph/0304132.

[7] K. G. Wilson, "Nonlagrangian Models Of Current Algebra," Phys. Rev. **179** (1969) 1499.

[8] T. Inami and C. S. Lim, "Effects Of Superheavy Quarks And Leptons In Low-Energy Weak Processes $K_L \to \mu\bar{\mu}$, $K^+ \to \pi^+\nu\bar{\nu}$ and $K^0 \leftrightarrow \bar{K}^0$," Prog. Theor. Phys. **65**, 297 (1981) [Erratum-ibid. **65**, 1772 (1981)].

[9] G. Altarelli, G. Curci, G. Martinelli and S. Petrarca, "QCD Nonleading Corrections To Weak Decays As An Application Of Regularization By Dimensional Reduction," Nucl. Phys. B **187**, 461 (1981).

[10] A. J. Buras and P. H. Weisz, "QCD Nonleading Corrections To Weak Decays In Dimensional Regularization and 't Hooft-Veltman Schemes," Nucl. Phys. B **333**, 66 (1990).

[11] A. J. Buras, M. Jamin, M. E. Lautenbacher and P. H. Weisz, "Effective Hamiltonians for $\Delta S = 1$ and $\Delta B = 1$ nonleptonic decays beyond the leading logarithmic approximation," Nucl. Phys. B **370**, 69 (1992) [Addendum-ibid. B **375**, 501 (1992)].

[12] A. J. Buras, M. Jamin, M. E. Lautenbacher and P. H. Weisz, "Two loop anomalous dimension matrix for $\Delta S = 1$ weak nonleptonic decays. 1. $O(\alpha_s^2)$," Nucl. Phys. B **400**, 37 (1993) [arXiv:hep-ph/9211304].

[13] A. B. Carter and A. I. Sanda, "CP Violation In Cascade Decays Of B Mesons," Phys. Rev. Lett. **45**, 952 (1980).

[14] A. B. Carter and A. I. Sanda, "CP Violation In B Meson Decays," Phys. Rev. D **23**, 1567 (1981).

[15] I. I. Y. Bigi and A. I. Sanda, "Notes On The Observability Of CP Violations In B Decays," Nucl. Phys. B **193**, 85 (1981).

[16] D. London and A. Soni, "Measuring the CP angle beta in hadronic $b \to s$ penguin decays," Phys. Lett. B **407**, 61 (1997) [arXiv:hep-ph/9704277].

[17] Y. Grossman, G. Isidori and M. P. Worah, "CP asymmetry in $B_d \to \phi K_S$: Standard model pollution," Phys. Rev. D **58**, 057504 (1998) [arXiv:hep-ph/9708305].

[18] Y. Grossman, Z. Ligeti, Y. Nir and H. Quinn, "SU(3) relations and the CP asymmetries in B decays to $\eta' K_S$, ϕK_S and $K^+K^-K_S$," Phys. Rev. D **68**, 015004 (2003) [arXiv:hep-ph/0303171].

[19] M. Gronau and D. London, "Isospin Analysis Of CP Asymmetries In B Decays," Phys. Rev. Lett. **65**, 3381 (1990).

[20] A. E. Snyder and H. R. Quinn, "Measuring CP asymmetry in $B \to \rho\pi$ decays without ambiguities," Phys. Rev. D **48**, 2139 (1993).

[21] N. G. Deshpande and X. G. He, "Isospin structure of penguins and their consequences in B physics," Phys. Rev. Lett. **74**, 26 (1995) [Erratum-ibid. **74**, 4099 (1995)] [arXiv:hep-ph/9408404].

[22] M. Gronau, O. F. Hernandez, D. London and J. L. Rosner, "Electroweak penguins and two-body B decays," Phys. Rev. D **52**, 6374 (1995) [arXiv:hep-ph/9504327].

[23] M. Neubert, "Model-independent analysis of $B \to \pi K$ decays and bounds on the weak phase gamma," JHEP **9902**, 014 (1999) [arXiv:hep-ph/9812396].

[24] T. Yoshikawa, "A possibility of large electro-weak penguin contribution in $B \to K\pi$modes," Phys. Rev. D **68**, 054023 (2003) [arXiv:hep-ph/0306147].

[25] M. Gronau and J. L. Rosner, "Rates and asymmetries in $B \to K\pi$ decays," Phys. Lett. B **572**, 43 (2003) [arXiv:hep-ph/0307095].

[26] A. J. Buras, R. Fleischer, S. Recksiegel and F. Schwab, "The $B \to \pi K$ puzzle and its relation to rare B and K decays," arXiv:hep-ph/0309012.

[27] N. Isgur and M. B. Wise, "Weak Decays Of Heavy Mesons In The Static Quark Approximation," Phys. Lett. B **232**, 113 (1989).

[28] N. Isgur and M. B. Wise, "Weak Transition Form-Factors Between Heavy Mesons," Phys. Lett. B **237**, 527 (1990).

[29] E. Eichten and B. Hill, "An Effective Field Theory For The Calculation Of Matrix Elements Involving Heavy Quarks," Phys. Lett. B **234**, 511 (1990).

[30] H. Georgi, "An Effective Field Theory For Heavy Quarks At Low-Energies," Phys. Lett. B **240**, 447 (1990).

[31] B. Grinstein, "The Static Quark Effective Theory," Nucl. Phys. B **339**, 253 (1990).

[32] J. Chay, H. Georgi and B. Grinstein, "Lepton Energy Distributions In Heavy Meson Decays From QCD," Phys. Lett. B **247**, 399 (1990).

[33] I. I. Y. Bigi, N. G. Uraltsev and A. I. Vainshtein, "Nonperturbative corrections to inclusive beauty and charm decays: QCD versus phenomenological models," Phys. Lett. B **293**, 430 (1992) [Erratum-ibid. B **297**, 477 (1993)] [arXiv:hep-ph/9207214].

[34] I. I. Y. Bigi, M. A. Shifman, N. G. Uraltsev and A. I. Vainshtein, "QCD predictions for lepton spectra in inclusive heavy flavor decays," Phys. Rev. Lett. **71**, 496 (1993) [arXiv:hep-ph/9304225].

[35] A. V. Manohar and M. B. Wise, "Inclusive semileptonic B and polarized Lambda(b) decays from QCD," Phys. Rev. D **49**, 1310 (1994) [arXiv:hep-ph/9308246].

[36] B. Blok, L. Koyrakh, M. A. Shifman and A. I. Vainshtein, "Differential distributions in semileptonic decays of the heavy flavors in QCD," Phys. Rev. D **49**, 3356 (1994) [Erratum-ibid. D **50**, 3572 (1994)] [arXiv:hep-ph/9307247].

[37] P. Ball and V. M. Braun, "Next-to-leading order corrections to meson masses in the heavy quark effective theory," Phys. Rev. D **49**, 2472 (1994) [arXiv:hep-ph/9307291].

[38] M. Neubert, "QCD sum-rule calculation of the kinetic energy and chromo-interaction of heavy quarks inside mesons," Phys. Lett. B **389**, 727 (1996) [arXiv:hep-ph/9608211].

[39] M. Crisafulli, V. Gimenez, G. Martinelli and C. T. Sachrajda, "First lattice calculation of the B meson binding and kinetic energies," Nucl. Phys. B **457**, 594 (1995) [arXiv:hep-ph/9506210].

[40] V. Gimenez, G. Martinelli and C. T. Sachrajda, "A high-statistics lattice calculation of λ_1 and λ_2 in the B meson," Nucl. Phys. B **486**, 227 (1997) [arXiv:hep-lat/9607055].

[41] A. S. Kronfeld and J. N. Simone, "Computation of $\bar{\Lambda}$ and λ_1 with lattice QCD," Phys. Lett. B **490**, 228 (2000) [Erratum-ibid. B **495**, 441 (2000)] [arXiv:hep-ph/0006345].

[42] S. Aoki *et al.* [JLQCD Collaboration], "Heavy quark expansion parameters from lattice NRQCD," arXiv:hep-lat/0305024.

[43] R. D. Dikeman, M. A. Shifman and N. G. Uraltsev, "$b \to s + \gamma$: A QCD consistent analysis of the photon energy distribution," Int. J. Mod. Phys. A **11**, 571 (1996) [arXiv:hep-ph/9505397].

[44] A. Kapustin and Z. Ligeti, "Moments of the photon spectrum in the inclusive $B \to X_s\gamma$ decay," Phys. Lett. B **355**, 318 (1995) [arXiv:hep-ph/9506201].

[45] A. F. Falk, M. E. Luke and M. J. Savage, "Hadron spectra for semileptonic heavy quark decay," Phys. Rev. D **53**, 2491 (1996) [arXiv:hep-ph/9507284].

[46] A. F. Falk, M. E. Luke and M. J. Savage, "Phenomenology of the $1/m_Q$ Expansion in Inclusive B and D Meson Phys. Rev. D **53**, 6316 (1996) [arXiv:hep-ph/9511454].

[47] M. Gremm, A. Kapustin, Z. Ligeti and M. B. Wise, "Implications of the $B \to X\ell\bar{\nu}_\ell$ lepton spectrum for heavy quark theory," Phys. Rev. Lett. **77**, 20 (1996) [arXiv:hep-ph/9603314].

[48] J. D. Bjorken, "Topics In B Physics," Nucl. Phys. Proc. Suppl. **11**, 325 (1989).

[49] M. Beneke, G. Buchalla, M. Neubert and C. T. Sachrajda, "QCD factorization for $B \to \pi\pi$ decays: Strong phases and CP violation in the heavy quark limit," Phys. Rev. Lett. **83**, 1914 (1999) [arXiv:hep-ph/9905312].

[50] M. Beneke, G. Buchalla, M. Neubert and C. T. Sachrajda, "QCD factorization for exclusive, non-leptonic B meson decays: General arguments and the case of heavy-light final states," Nucl. Phys. B **591**, 313 (2000) [arXiv:hep-ph/0006124].

[51] M. Beneke, G. Buchalla, M. Neubert and C. T. Sachrajda, "QCD factorization in $B \to \pi K$, $\pi\pi$ decays and extraction of Wolfenstein parameters," Nucl. Phys. B **606**, 245 (2001) [arXiv:hep-ph/0104110].

[52] C. W. Bauer, S. Fleming and M. E. Luke, "Summing Sudakov logarithms in B $\to$ X/s gamma in effective field theory," Phys. Rev. D **63**, 014006 (2001) [arXiv:hep-ph/0005275].

[53] C. W. Bauer, S. Fleming, D. Pirjol and I. W. Stewart, "An effective field theory for collinear and soft gluons: Heavy to light decays," Phys. Rev. D **63**, 114020 (2001) [arXiv:hep-ph/0011336].

[54] C. W. Bauer and I. W. Stewart, "Invariant operators in collinear effective theory," Phys. Lett. B **516**, 134 (2001) [arXiv:hep-ph/0107001].

[55] C. W. Bauer, D. Pirjol and I. W. Stewart, Phys. Rev. D **65**, 054022 (2002) [arXiv:hep-ph/0109045].

[56] H. n. Li and H. L. Yu, "Extraction of V(ub) from decay $B \to \pi l\nu$," Phys. Rev. Lett. **74**, 4388 (1995) [arXiv:hep-ph/9409313].

[57] H. N. Li and H. L. Yu, "PQCD Analysis Of Exclusive Charmless B Meson Decay Spectra," Phys. Lett. B **353** (1995) 301.

[58] H. n. Li and H. L. Yu, "Perturbative QCD analysis of B meson decays," Phys. Rev. D **53**, 2480 (1996) [arXiv:hep-ph/9411308].

[59] Y. Y. Keum, H. n. Li and A. I. Sanda, "Fat penguins and imaginary penguins in perturbative QCD," Phys. Lett. B **504**, 6 (2001) [arXiv:hep-ph/0004004].

[60] Y. Y. Keum, H. N. Li and A. I. Sanda, "Penguin enhancement and $B \to K\pi$ decays in perturbative QCD," Phys. Rev. D **63**, 054008 (2001) [arXiv:hep-ph/0004173].

[61] Y. Y. Keum and H. n. Li, "Nonleptonic charmless B decays: Factorization vs. perturbative QCD," Phys. Rev. D **63**, 074006 (2001) [arXiv:hep-ph/0006001].

[62] K. G. Wilson, "Confinement Of Quarks," Phys. Rev. D **10**, 2445 (1974).

[63] W. E. Caswell and G. P. Lepage, "Effective Lagrangians For Bound State Problems In QED, QCD, And Other Field Theories," Phys. Lett. B **167**, 437 (1986).

[64] B. A. Thacker and G. P. Lepage, "Heavy Quark Bound States In Lattice QCD," Phys. Rev. D **43**, 196 (1991).

[65] G. P. Lepage, L. Magnea, C. Nakhleh, U. Magnea and K. Hornbostel, "Improved nonrelativistic QCD for heavy quark physics," Phys. Rev. D **46**, 4052 (1992) [arXiv:hep-lat/9205007].

[66] A. X. El-Khadra, A. S. Kronfeld and P. B. Mackenzie, "Massive Fermions in Lattice Gauge Theory," Phys. Rev. D **55**, 3933 (1997) [arXiv:hep-lat/9604004].

[67] A. S. Kronfeld, "Application of heavy-quark effective theory to lattice QCD. I: Power corrections," Phys. Rev. D **62**, 014505 (2000) [arXiv:hep-lat/0002008].

[68] K. I. Ishikawa, H. Matsufuru, T. Onogi, N. Yamada and S. Hashimoto, "f_B with lattice NRQCD including $O(1/m_Q^2)$ corrections," Phys. Rev. D **56**, 7028 (1997) [arXiv:hep-lat/9706008].

[69] K. Symanzik, "Continuum Limit And Improved Action In Lattice Theories. 1. Principles And Φ^4 Theory," Nucl. Phys. B **226**, 187 (1983).

[70] K. Symanzik, "Continuum Limit And Improved Action In Lattice Theories. 2. $O(N)$ Nonlinear Sigma Model In Perturbation Theory," Nucl. Phys. B **226**, 205 (1983).

[71] B. Sheikholeslami and R. Wohlert, "Improved Continuum Limit Lattice Action For QCD With Wilson Fermions," Nucl. Phys. B **259**, 572 (1985).

[72] K. Jansen *et al.*, "Non-perturbative renormalization of lattice QCD at all scales," Phys. Lett. B **372**, 275 (1996) [arXiv:hep-lat/9512009].

[73] M. Luscher, S. Sint, R. Sommer, P. Weisz and U. Wolff, "Non-perturbative $O(a)$ improvement of lattice QCD," Nucl. Phys. B **491**, 323 (1997) [arXiv:hep-lat/9609035].

[74] G. P. Lepage and P. B. Mackenzie, "On the viability of lattice perturbation theory," Phys. Rev. D **48**, 2250 (1993) [arXiv:hep-lat/9209022].

[75] N. Yamada, "Heavy quark physics and lattice QCD," Nucl. Phys. Proc. Suppl. **119**, 93 (2003) [arXiv:hep-lat/0210035].

[76] S. Aoki *et al.* [JLQCD Collaboration], "$B^0 - \bar{B}^0$ mixing in unquenched lattice QCD," Phys. Rev. Lett. **91**, 212001 (2003) [arXiv:hep-ph/0307039].

[77] B. Grinstein, E. Jenkins, A. V. Manohar, M. J. Savage and M. B. Wise, Nucl. Phys. B **380**, 369 (1992) [arXiv:hep-ph/9204207].

[78] C. T. H. Davies *et al.* [HPQCD Collaboration], "High-precision lattice QCD confronts experiment," arXiv:hep-lat/0304004.

[79] S. Hashimoto, A. X. El-Khadra, A. S. Kronfeld, P. B. Mackenzie, S. M. Ryan and J. N. Simone, "Lattice QCD calculation of $\bar{B} \to Dl\bar{\nu}$ decay form factors at zero recoil," Phys. Rev. D **61**, 014502 (2000) [arXiv:hep-ph/9906376].

[80] S. Hashimoto, A. S. Kronfeld, P. B. Mackenzie, S. M. Ryan and J. N. Simone, "Lattice calculation of the zero recoil form factor of $\bar{B} \to D^* l\bar{\nu}$: Toward a model independent determination of $|V_{cb}|$," Phys. Rev. D **66**, 014503 (2002) [arXiv:hep-ph/0110253].

[81] K. C. Bowler *et al.* [UKQCD Collaboration], "Improved $B \to \pi l \nu_l$ form factors from the lattice," Phys. Lett. B **486** (2000) 111 [arXiv:hep-lat/9911011].

[82] A. Abada, D. Becirevic, P. Boucaud, J. P. Leroy, V. Lubicz and F. Mescia, "Heavy $\to$ light semileptonic decays of pseudoscalar mesons from lattice QCD," Nucl. Phys. B **619** (2001) 565 [arXiv:hep-lat/0011065].

[83] A. X. El-Khadra, A. S. Kronfeld, P. B. Mackenzie, S. M. Ryan and J. N. Simone, "The semileptonic decays $B \to \pi l \nu$ and $D \to \pi l \nu$ from lattice QCD," Phys. Rev. D **64** (2001) 014502 [arXiv:hep-ph/0101023].

[84] S. Aoki *et al.* [JLQCD Collaboration], "Differential decay rate of $B \to \pi l \nu$ semileptonic decay with lattice NRQCD," Phys. Rev. D **64** (2001) 114505 [arXiv:hep-lat/0106024].

[85] L. Lellouch, "Phenomenology from lattice QCD," Nucl. Phys. Proc. Suppl. **117**, 127 (2003) [arXiv:hep-ph/0211359].

[86] D. Becirevic, "Lattice results relevant to the CKM matrix determination," arXiv:hep-ph/0211340.

[87] A. S. Kronfeld, "Heavy quarks and lattice QCD," arXiv:hep-lat/0310063.

Chapter 3

Flavor Structure of the Physics beyond the Standard Model

3.1 Motivation for New Physics

The Standard Model of elementary particles has been very successful in explaining a wide variety of existing experimental data. It covers a range of phenomena from low energy (less than a GeV) physics, such as kaon decays, to high energy (a few hundred GeV) processes involving real weak gauge bosons (W and Z) and top quarks. There is, therefore, little doubt that the present Standard Model is a theory to describe the physics below the energy scale of several hundred GeV, which has been explored so far.

However, the Standard Model is not satisfactory as *the* theory of elementary particles beyond the TeV energy scale. First of all, it does not explain the characteristic pattern of the mass spectrum of quarks and leptons. The second generation quarks and leptons are several orders of magnitude heavier than the corresponding first generation particles, and the third generation is even heavier by another order of magnitude. The quark flavor mixing matrix — the CKM matrix — also has a striking hierarchical structure, *i.e.* the diagonal terms are close to unity and $1 \ll \theta_{12} \ll \theta_{23} \ll \theta_{13}$, where θ_{ij} denotes a mixing angle between the i-th and j-th generation. The recent observation of neutrino oscillations implies there is also a rich flavor structure in the lepton sector. All of these masses and mixings are free parameters in the Standard Model, but ideally they should be explained by higher scale theories.

The particles in the Standard Model acquire masses from the Higgs mechanism. The Higgs potential itself is described by a scalar field theory, which contains a quadratic mass divergence. This means that a Higgs mass of order 100 GeV is realized only after a huge cancellation between the bare Higgs mass squared μ_0^2 and the quadratically divergent mass renormalization, both of which are quantities of order Λ^2 where Λ is the cutoff scale. If Λ is of the order of the Planck scale, then a cancellation of more than 30 orders of magnitude is required. This is often called the hierarchy problem [1–3]. Therefore it would be highly unnatural if the Standard Model were *the* theory valid at a very high energy scale, such as the Planck scale. Instead, the Standard Model should be considered as an effective theory of some more fundamental theory, which most likely lies in the TeV energy region.

CP-violation is needed in order to produce the observed baryon number (or matter-antimatter) asymmetry in the universe. In the Standard Model, the complex phase of the CKM matrix provides the only source of the CP-violation[1], but models of baryogenesis suggest that it is

[1]The θ parameter in the QCD Lagrangian is another possible source of the CP-violation, but its value has to

quantitatively insufficient (for a review, see [4]). This is further motivation to consider new physics models.

3.2 New Physics Scenarios

Several scenarios have been proposed for the physics beyond the Standard Model. They introduce new particles, dynamics, symmetries or even extra-dimensions at the TeV energy scale. In the supersymmetry (SUSY) scenarios, one introduces a new symmetry between bosons and fermions, and a number of new particles that form supersymmetric pairs with the existing Standard Model particles. The quadratic divergence of the Higgs mass term then cancels out among superpartners (for reviews, see [5, 6]. The Technicolor-type scenario assumes new strong dynamics (like QCD) at the TeV scale and the Higgs field is realized as a composite state of more fundamental particles (for a recent review, see [7]). The large extra space-time dimension models [8,9] cure the problem by extending the number of spacetime dimensions beyond four (a recent review can be found in [10]). In Little Higgs models the Higgs is a pseudo-Nambu-Goldstone boson, and thus naturally light [11].

Flavor Changing Neutral Current (FCNC) processes, such as $B^0 - \overline{B}^0$ mixing and the $b \to s\gamma$ transition, provide strong constraints on new physics models. If there is no suppression mechanism for FCNC processes, such as the GIM mechanism in the Standard Model, the new physics contribution can easily become too large to be consistent with the experimental data. In fact, if one introduces a FCNC interaction as a higher dimensional operator to represent some new physics interaction, the associated energy scale is typically of order 10^3 TeV, which is much higher than the expected scale of the new physics ($\sim$ TeV). Therefore, one has to introduce some flavor structure in new physics models.

3.3 Supersymmetric Models

Here, let us consider the supersymmetric (SUSY) model as an example of new physics models at the TeV scale. The SUSY model is attractive not only because it solves the Higgs mass hierarchy problem. It is also consistent with Grand Unification [12, 13], *i.e.* the renormalization group running of the three gauge couplings is modified by the supersymmetric partners, causing them to intersect at the same point at $\Lambda_{\rm GUT} \simeq 10^{16}$ GeV.

The general SUSY models have a number of free parameters corresponding to the masses and mixings of the superpartners for each Standard Model particle. Even in the minimal model — the Minimal Supersymmetric Standard Model (MSSM) — the number is more than a hundred. These mass and mixing parameters are, at least partly, governed by the soft supersymmetry breaking mechanism, which is necessary to make the superpartners heavy enough such that they are not detected at existing collider experiments. Therefore, to predict the mass spectrum and flavor mixing of the SUSY particles one has to specify the details of the SUSY breaking mechanism, which should be given at energy scales higher than the TeV scale.

The Minimal Supersymmetric Standard Model (MSSM) is a minimal supersymmetric extension of the Standard Model, containing a superpartner for each particle in the Standard Model and two Higgs doublets. Its matter contents are written in terms of the chiral super-fields as

$$Q_i(3, 2, 1/6), \;\; \overline{U}_i(\overline{3}, 1, -2/3), \;\; \overline{D}_i(\overline{3}, 1, 1/3) \tag{3.1}$$

be unnaturally small $\theta \leq 10^{-10}$ in order to be consistent with the neutron electron dipole moment experiment. This is another problem — the strong CP problem.

for the left-handed (Q) and right-handed (U and D) quark sector,

$$L_i(1,2,-1/2), \quad \overline{E}_i(1,1,1) \tag{3.2}$$

for the left-handed (L) and right-handed (E) lepton sector, and

$$H_1(1,2,-1/2), \quad H_2(1,2,1/2) \tag{3.3}$$

for the Higgs fields. The representation (or charge) for the gauge group $SU(3)_C \times SU(2)_L \times U(1)_Y$ is given in parentheses, and i (= 1, 2, or 3) is a generation index. Under the assumption of R-parity conservation, which is required to avoid an unacceptably large proton decay rate, the superpotential is written as

$$\mathcal{W}_{\rm MSSM} = f_D^{ij}\overline{D}_i Q_j H_1 + f_U^{ij}\overline{U}_i Q_j H_2 + f_E^{ij}\overline{E}_i L_j H_1 + \mu H_1 H_2, \tag{3.4}$$

where f_U and f_D are the quark Yukawa couplings. The soft supersymmetry breaking terms are

$$\begin{aligned} -\mathcal{L}_{\rm soft} \;=\; & (m_Q^2)^i{}_j \tilde{q}_i \tilde{q}^{\dagger j} + (m_D^2)_i{}^j \tilde{d}^{\dagger i}\tilde{d}_j + (m_U^2)_i{}^j \tilde{u}^{\dagger i}\tilde{u}_j + (m_E^2)^i{}_j \tilde{e}_i \tilde{e}^{\dagger j} + (m_L^2)_i{}^j \tilde{l}^{\dagger i}\tilde{l}_j \\ & + \Delta_1^2 h_1^\dagger h_1 + \Delta_2^2 h_2^\dagger h_2 - (B\mu h_1 h_2 + \text{h.c.}) \\ & + A_D^{ij}\tilde{d}_i \tilde{q}_j h_1 + A_U^{ij}\tilde{u}_i \tilde{q}_j h_2 + A_L^{ij}\tilde{u}_i \tilde{q}_j h_2 \\ & + \frac{M_1}{2}\overline{\tilde{B}}\tilde{B} + \frac{M_2}{2}\overline{\tilde{W}}\tilde{W} + \frac{M_3}{2}\overline{\tilde{g}}\tilde{g}. \end{aligned} \tag{3.5}$$

These consist of mass terms for scalar fields ($\tilde{q}_i$, $\tilde{u}_i$, $\tilde{d}_i$, $\tilde{l}_i$, $\tilde{e}_i$, h_1, and h_2), Higgs mixing terms, trilinear scalar couplings, and gaugino ($\tilde{B}$, $\tilde{W}$, and $\tilde{g}$) mass terms.

Flavor physics already places strong restrictions on the possible structure of the SUSY breaking sector, since arbitrary terms would induce many flavor violating processes which are easily ruled out by present experimental data. Therefore, in order to comply with the requirement of highly suppressed FCNC interactions one has to introduce some structure in the soft SUSY breaking terms. Several scenarios have been proposed.

- *Universality.* The SUSY breaking terms have a universal flavor structure at a very high energy scale, such as the Planck scale ($\sim 10^{18}$ GeV) or the GUT scale ($\sim 10^{16}$ GeV). It could also be a lower scale ($\sim 10^{4-6}$ GeV). The universality comes from mediation of the SUSY breaking effect by flavor-blind interactions, such as gravity (for a review of gravity mediation see [5]), the Standard Model gauge interaction (gauge mediation [14–16] the gaugino mediation [17–19]), or the super-Weyl anomaly (anomaly mediation [20, 21]). Since the soft SUSY breaking terms are flavor-blind, the squark masses are degenerate at the high energy scale where those terms are generated. The GIM mechanism then works as long as the scalar triple coupling (squark-squark-Higgs), the A term, is proportional to the Yukawa couplings in the Standard Model. An additional flavor violating effect could appear through the renormalization group running of the squark masses to the low energy scale, which depends on the flavor [22]. For the gauge mediation scenario the effect on FCNC processes is extremely suppressed, since the SUSY breaking scale is low and there is not enough room for the running.

- *Alignment.* Squark and slepton mass matrices could be diagonalized (no flavor changing interaction) in the same basis as quarks and leptons, if one assumes some symmetries involving different generations [23, 24]. Flavor violation is then suppressed and flavor violating processes are induced by incomplete alignment.

- *Decoupling.* The squarks and sleptons of the first and second generations are sufficiently heavy, 10–100 TeV, so that flavor violation in the first and second generations is suppressed [25–31]. In general such models predict large FCNC effects in the third generation, *i.e.* the b quark and τ lepton decays.

Signals for FCNC processes and CP-violation largely depend on the structure of the soft SUSY breaking terms.

The Grand Unified Theory (GUT) [12,13] is one of the motivations for introducing supersymmetry. Besides the unification of couplings, GUTs also relate the Yukawa couplings of the quark and lepton sectors. Since the particle content and symmetry are modified above the GUT scale, they could generate different FCNC effects even if universal soft SUSY breaking is assumed. GUTs also predicts some correlation between quark and lepton flavor violation processes. Such studies have been done by several authors [32–40]

3.4 SUSY Effect on $b \to s$ Transitions

Here we discuss the possible effects of SUSY particles on $b \to s$ transitions. The $b \to s$ processes are especially interesting, since the time-dependent CP-violation measured in $B \to \phi K_S^0$ significantly deviates from its Standard Model expectation $\mathcal{S}_{\phi K_S^0} = \mathcal{S}_{J/\psi K_S^0}$ [41] although the measurement by BaBar is still consistent with the Standard Model [42]. In the Standard Model the $B \to \phi K_S^0$ transition is induced by the $b \to s$ penguin diagram, in which there is room for new physics effects to compete with the Standard Model contribution. Supersymmetric GUT models also predict large effects in $b \to s$ transitions as a large mixing angle is observed in the neutrino sector between the second and third generations.

We parametrize the effect of soft SUSY breaking terms applying the mass insertion approximation (MIA) [22]. In the MIA, one adopts a basis where the fermion and sfermion mass matrices are rotated in the same way to diagonalize the fermion mass matrix (the super-CKM basis). In this basis, the couplings of fermions and sfermions to neutral gauginos are flavor diagonal, leaving all the sources of flavor violation in the off-diagonal terms of the sfermion mass matrix. These terms are denoted by $(\Delta^q_{AB})^{ij}$, where $A, B = (L, R)$ and $q = (u, d)$. The sfermion propagator can then be expanded as

$$\langle \tilde{q}^a_A \tilde{q}^{b*}_B \rangle = i(k^2 \mathbf{1} - \tilde{m}^2 \mathbf{1} - \Delta^q_{AB})^{-1}_{ab} \simeq \frac{i\delta_{ab}}{k^2 - \tilde{m}^2} + \frac{i(\Delta^q_{AB})_{ab}}{(k^2 - \tilde{m}^2)^2} + \cdots, \tag{3.6}$$

where $\mathbf{1}$ is the unit matrix and $\tilde{m}$ is the averaged squark mass. Here we keep only the first term of the expansion. In this way, the flavor violation in SUSY models can be parameterized in a model independent way by the dimensionless parameters $(\delta^q_{AB})_{ij} = (\Delta^q_{AB})_{ij}/\tilde{m}^2$, where $\tilde{m}$ is an average squark mass. Constraints on these parameters from presently available data have been analyzed in [43–45] (also see [46] for a summary).

Using the MIA, the $b \to s\bar{s}s$ transition accompanied by SUSY particles occurs through the diagrams shown in Figure 3.1, and the $B \to \phi K_S^0$ data provide a constraint on the mass insertions $(\delta^d_{AB})_{23}$ where $(A, B) = (L, R)$. In fact, the absolute value of $(\delta^d_{AB})_{23}$ is constrained by the branching ratio of $B \to X_s\gamma$ as

$$|(\delta^d_{LL(RR)})_{23}| < 8.2, \quad |(\delta^d_{LR(RL)})_{23}| < 1.6 \times 10^{-2}, \tag{3.7}$$

for $m_{\tilde{g}} = 300$ GeV and $m_{\tilde{q}} = 500$ GeV [45] [2] Thus, an interesting question is whether the

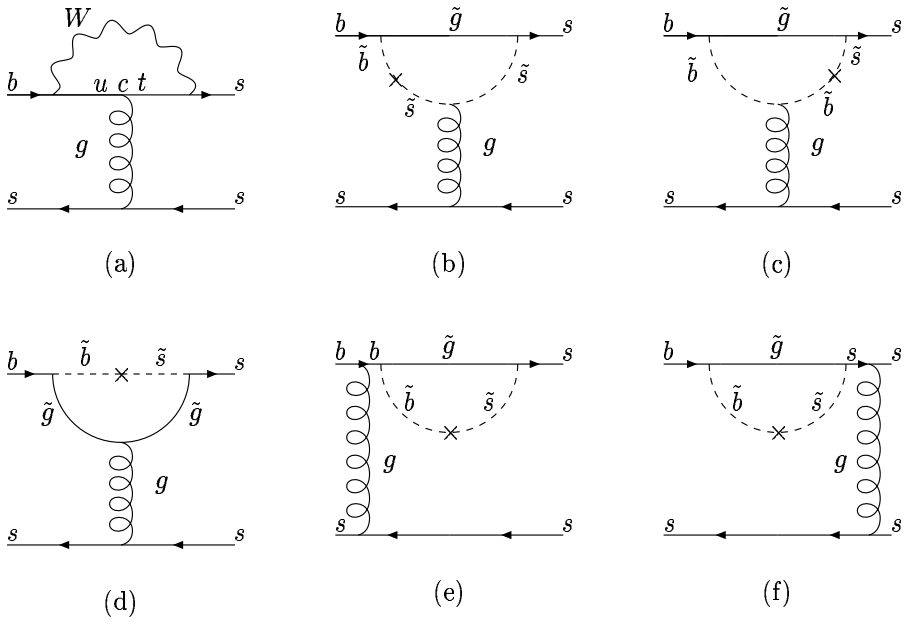

Figure 3.1: The Standard Model contribution (a) and the gluino–down squark contributions (b)–(f) to $B \to \phi K_S^0$ decay. The cross represents the mass insertions $(\delta^d_{AB})_{23}$.

observed deviation of $\mathcal{S}_{\phi K_S^0}$ from $\mathcal{S}_{J/\psi K_S^0}$ can be obtained while satisfying (3.7).

Here we parameterize the Standard Model and SUSY amplitudes as

$$A^{\rm SM}(\phi K_S^0) = |A^{\rm SM}| e^{i\delta_{\rm SM}}, \qquad A^{\rm SUSY}(\phi K_S^0) = |A^{\rm SUSY}| e^{i\theta_{\rm SUSY}} e^{i\delta_{\rm SUSY}}, \tag{3.8}$$

$$\overline{A}^{\rm SM}(\phi K_S^0) = |\overline{A}^{\rm SM}| e^{i\delta_{\rm SM}}, \qquad \overline{A}^{\rm SUSY}(\phi K_S^0) = |\overline{A}^{\rm SUSY}| e^{-i\theta_{\rm SUSY}} e^{i\delta_{\rm SUSY}}, \tag{3.9}$$

where $\delta_{\rm SM(SUSY)}$ is the strong (CP-conserving) phase and $\theta_{\rm SUSY}$ is the weak (CP-violating) phase. Then, we obtain

$$\mathcal{S}_{\phi K_S^0} = \frac{\sin 2\phi_1 + 2\left(\frac{|A^{\rm SUSY}|}{|A^{\rm SM}|}\right)\cos\delta_{12}\sin(\theta_{\rm SUSY}+2\phi_1) + \left(\frac{|A^{\rm SUSY}|}{|A^{\rm SM}|}\right)^2 \sin(2\theta_{\rm SUSY}+2\phi_1)}{1 + 2\left(\frac{|A^{\rm SUSY}|}{|A^{\rm SM}|}\right)\cos\delta_{12}\cos\theta_{\rm SUSY} + \left(\frac{|A^{\rm SUSY}|}{|A^{\rm SM}|}\right)^2}, \tag{3.10}$$

where $\delta_{12} \equiv \delta_{\rm SM} - \delta_{\rm SUSY}$. Let us first see how large $|A^{\rm SUSY}/A^{\rm SM}|$ needs to be in order to have $\mathcal{S}_{\phi K_S^0}$ as small as the experimental central value. Using (3.10), we plot $\mathcal{S}_{\phi K_S^0}$ in terms of $\theta_{\rm SUSY}$ for different values of $|A^{\rm SUSY}/A^{\rm SM}|$ in Figure 3.2, by fixing $\delta_{12} = 0$ for simplicity and using the central value of the observed $\sin 2\phi_1$. We can see that the deviation of $\mathcal{S}_{\phi K_S^0}$ from $\mathcal{S}_{J/\psi K_S^0}$ becomes maximal at around $\theta_{\rm SUSY} = -\pi/2$ and $|A^{\rm SUSY}/A^{\rm SM}| \gtrsim 0.4$ is required in order to have a negative value of $\mathcal{S}_{\phi K_S^0}$.

The effective Hamiltonian for the penguin process can be expressed as

$$\mathcal{H}_{\rm eff}^{\Delta B=1} = -\frac{G_F}{\sqrt{2}} V_{tb} V_{ts}^* \left[\sum_{i=3}^{6} C_i O_i + C_g O_g + \sum_{i=3}^{6} \tilde{C}_i \tilde{O}_i + \tilde{C}_g \tilde{O}_g \right] \tag{3.11}$$

[2]In the following analysis we use $|(\delta^d_{LL(RR)})_{23}| < 1$ instead, as the mass insertion approximation does not converge for > 1 and the entire analysis become unreliable.

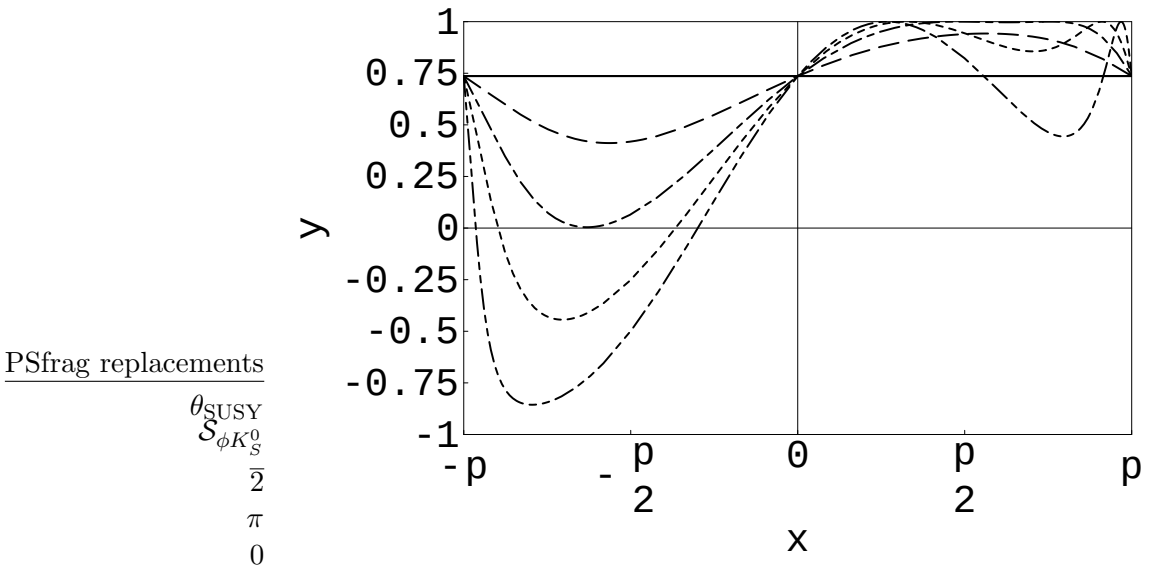

Figure 3.2: $\mathcal{S}_{\phi K^0_S}$ including SUSY contributions (3.10) as a function of $\theta_{\rm SUSY}$ for different values of $|A^{\rm SUSY}/A^{\rm SM}|$: 0.2 (dashed), 0.4 (dashed-dotted), 0.6 (dotted), 0.8 (dashed-double-dotted). The solid line represents the central value of $\mathcal{S}_{J/\psi K^0_S}$. Here we assume that the strong phase difference between SUSY and Standard Model is negligible $\delta_{12} \simeq 0$.

with

$$O_3 = \overline{s}_\alpha \gamma^\mu L b_\alpha \overline{s}_\beta \gamma^\mu L s_\beta, \tag{3.12}$$

$$O_4 = \overline{s}_\alpha \gamma^\mu L b_\beta \overline{s}_\beta \gamma^\mu L s_\alpha, \tag{3.13}$$

$$O_5 = \overline{s}_\alpha \gamma^\mu L b_\alpha \overline{s}_\beta \gamma^\mu L s_\beta, \tag{3.14}$$

$$O_6 = \overline{s}_\alpha \gamma^\mu L b_\beta \overline{s}_\beta \gamma^\mu R s_\alpha, \tag{3.15}$$

$$O_g = \frac{g_s}{8\pi^2} m_b \overline{s}_\alpha \sigma^{\mu\nu} R \frac{\lambda^A_{\alpha\beta}}{2} b_\beta G^A_{\mu\nu}, \tag{3.16}$$

where $L \equiv (1-\gamma_5)/2$ and $R \equiv (1+\gamma_5)/2$. The terms with a tilde are obtained from $C_{i,g}$ and $O_{i,g}$ by exchanging $L \leftrightarrow R$. The Wilson coefficient $C_{i(g)}$ includes both Standard Model and SUSY contributions. In the following analysis, we neglect the effect of the operator $O_\gamma = \frac{e}{8\pi^2} m_b \overline{s}_\alpha \sigma^{\mu\nu} R b_\alpha F_{\mu\nu}$ and the electroweak penguin operators, which give very small contributions. The matrix elements are computed in the naive factorization approximation in the following[3]. The SUSY amplitude $A^{\rm SUSY}(\phi K)$ contains gluino and chargino contributions although the latter is negligible. The Wilson coefficients for the gluino contributions that come from box and penguin diagrams are computed in [43]. We note that the dominant SUSY contribution to $B \to \phi K^0_S$ comes from the chromo-magnetic operator, O_g and $\tilde{O}_g$.

The numerical result for the ratio of the Standard Model to SUSY amplitude for $m_{\tilde{g}} \simeq m_{\tilde{q}} = 500$ GeV is as follows [49]

$$\frac{A^{\rm SUSY}(\phi K^0_S)}{A^{\rm SM}(\phi K^0_S)} \simeq (0.14 + 0.02i)[(\delta^d_{LL})_{23} + (\delta^d_{RR})_{23}] + (65 + 11i)[(\delta^d_{LR})_{23} + (\delta^d_{RL})_{23}]. \tag{3.17}$$

[3]The matrix element of $B \to \phi K^0_S$ can also be computed using more recent methods: the QCD factorization and the pQCD approach method. Application of these to analyse the SUSY effect on $S_{\phi K^0_S}$ can be found in [38,47] for the former and [48] for the latter.

The tiny imaginary parts in (3.17) are the strong phases coming from the QCD correction terms in the effective Wilson coefficient in [50]. We shall consider SUSY models where one mass insertion is dominant, which is often the case in minimal flavour violation models. Let us start with the models in which $LL(RR)$ dominates and the remaining mass insertions, $(\delta^d_{LR})_{23}, (\delta^d_{RL})_{23}$ and $(\delta^d_{RR(LL)})_{23}$ are all negligible. Taking into account the constraints from the $B \to X_s\gamma$ branching ratio in (3.7), we obtain a maximum SUSY contribution of $(|A^{\rm SUSY}|/|A^{\rm SM}|)_{LL(RR)} \simeq 0.14$, which can lead to only a small deviation between $\mathcal{S}_{\phi K^0_S}$ and $\mathcal{S}_{J/\psi K^0_S}$ as we learned in Figure 3.2. On the other hand, even if LR and RL dominated models are more severely constrained by $B \to X_s\gamma$, the SUSY contribution can reach $(|A^{\rm SUSY}/A^{\rm SM}|)_{LR(RL)} \simeq 1.1$, which gives a negative value of $\mathcal{S}_{\phi K^0_S}$ for a large range of $\theta_{\rm SUSY}$. Smaller gluino and squark masses, $m_{\tilde g} \simeq m_{\tilde q} = 300$ GeV, result in a larger SUSY contribution:

$$\frac{A^{\rm SUSY}(\phi K^0_S)}{A^{\rm SM}(\phi K^0_S)} \simeq (0.39 + 0.07i)[(\delta^d_{LL})_{23} + (\delta^d_{RR})_{23}] + (110 + 18i)[(\delta^d_{LR})_{23} + (\delta^d_{RL})_{23}]. \quad (3.18)$$

In this case, all LL, RR, LR and RL dominated models can lead to a negative value of $\mathcal{S}_{\phi K^0_S}$. We see that in order to have a significant differance between $\mathcal{S}_{\phi K^0_S}$ and $\mathcal{S}_{J/\psi K^0_S}$, LL and RR dominated models require small gluino and squark masses. Thus, some LL and RR dominated models with large $m_{\tilde g}$ and $m_{\tilde q}$ may be excluded by measurements of $\mathcal{S}_{\phi K^0_S}$; for instance, an observation of $\mathcal{S}_{\phi K^0_S} < 0$ would exclude $m_{\tilde g} \simeq m_{\tilde q} \gtrsim$ 300 GeV.

Once more precise experimental data are available and the existence of a new physics contribution in $\mathcal{S}_{\phi K^0_S}$ is confirmed, it will be necessary to find further evidence to prove that $\mathcal{S}_{\phi K^0_S}$ indeed includes a SUSY contribution. For this purpose, we are able to benefit from other $b \to s$ transitions, which can also be described by the mass insertion $(\delta^d_{AB})_{23}$. In the rest of this section, we shall discuss the process $B \to \eta' K^0_S$.

CP-violation in $B \to \eta' K^0_S$ was first reported by the Belle collaboration in summer 2002 [51]. Averaging with the result from the BaBar collaboration reported in spring 2003 [52], we obtain $S_{\eta' K^0_S} = 0.33 \pm 0.34$. The η' meson is known to be composed of $u\bar{u}$, $d\bar{d}$ and $s\bar{s}$ accompanied by a small amount of other particles such as gluonium and $c\bar{c}$ *etc.* [4]. Apart from the exotic particles, the $B \to \eta' K^0_S$ process comes from the $B^0_d - \overline{B}^0_d$ mixing box diagram and the penguin and tree decay diagrams. While there are two penguin diagrams $b \to s\bar{s}s$ and $b \to d\bar{d}d$, there is only one tree diagram, which furthermore is Cabbibo suppressed. As a result, the tree contribution is very small and estimated to be less than 1%. Thus, $B \to \eta' K^0_S$ and $B \to \phi K^0_S$ are approximately the same apart from the parity of the final states. In the following, we shall investigate whether this parity difference can lead to the experimental observation $\mathcal{S}_{\phi K^0_S} < 0 < \mathcal{S}_{\eta' K^0_S} < \mathcal{S}_{J/\psi K^0_S}$.

Let us first see the consequence of this parity difference in the SUSY contributions by comparing the computation of the matrix elements for $B \to \phi K^0_S$ and $B \to \eta' K^0_S$ in the case of the $b \to s\bar{s}s$ transition. In the naive factorization approximation, the amplitudes are written as a product of Wilson coefficients, form factors and decay constants:

$$A(B \to \phi(\eta')K) \propto C_{\rm Wilson}\ F^{B\to K} f_{\phi(\eta')}. \quad (3.19)$$

The decay constants appear in the calculation by sandwiching the $V \pm A$ current, corresponding to O_i and $\tilde{O}_i$ contributions, respectively, between $\phi(\eta')$ and the vacuum:

$$\langle 0|\bar{s}\gamma_\mu(1 \pm \gamma_5)s|\phi\rangle = +m_\phi f_\phi \epsilon_\mu \quad (3.20)$$

$$\langle 0|\bar{s}\gamma_\mu(1 \pm \gamma_5)s|\eta'\rangle = \pm i f_{\eta'} p_\mu \quad (3.21)$$

[4] We do not consider contributions from exotic particles here. However, since an unexpectedly large branching ratio is observed in the $B \to \eta' K$ processes, possible large contributions from such particles have been considered. The gluonium contributions to $B \to \eta' K^0_S$ including the possibility that SUSY effects also enhance the branching ratio of $B \to \eta' K$ is discussed in [53].

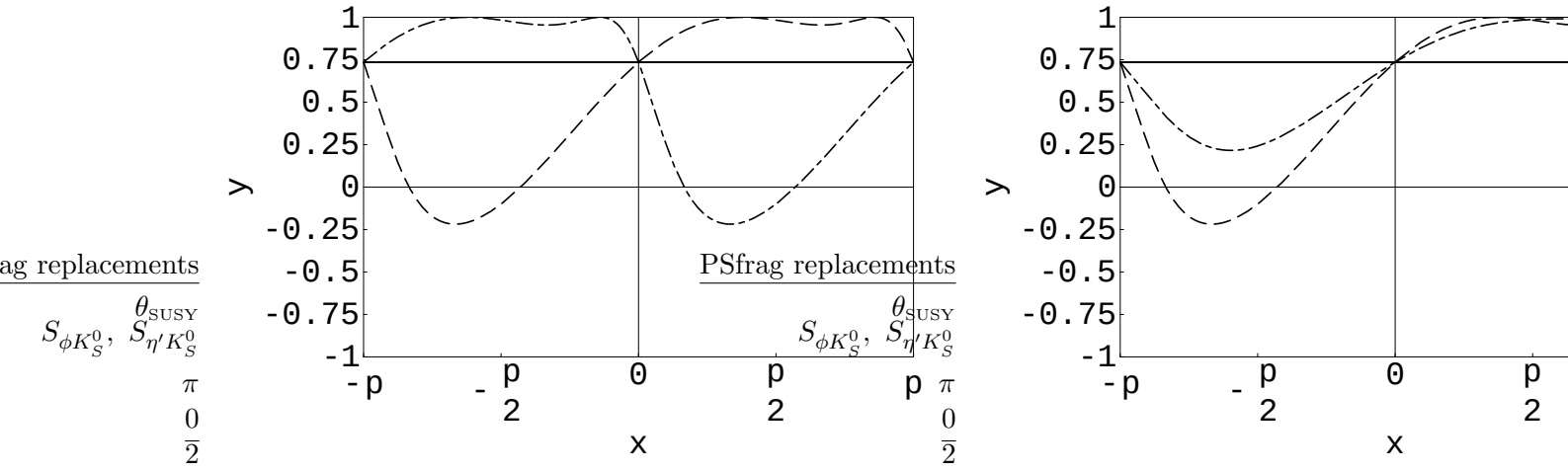

Figure 3.3: Possible solution for the puzzle of $\mathcal{S}_{\phi K_S^0} < 0 < \mathcal{S}_{\eta' K_S^0} < \mathcal{S}_{J/\psi K_S^0}$. Dashed and dashed-dotted lines are results for $\mathcal{S}_{\phi K_S^0}$ and $\mathcal{S}_{\eta' K_S^0}$, respectively. Left figure is for the case that RR and/or RL are dominant. Right figure is for the case that there are both LL (and/or LR) and RR (and/or RL) contributions and the LL (and/or LR) amplitude is 4 times larger than RR (and/or RL) one whereas the phase of the former is equal to the phase of the latter. For both cases, we fix $|A^{\rm SUSY}(\phi K_S^0)/A^{\rm SM}(\phi K_S^0)| \simeq 0.5$.

As can be seen from (3.21), the overall sign flips for the $V+A$ and $V-A$ currents in the case of η'. Thus, the contributions for $\mathcal{S}_{\eta' K_S^0}$ coming from $\tilde{O}_i$ and O_i have opposite signs. Accordingly, the numerical results are found to be [53]

$$\frac{A^{\rm SUSY}(\eta' K_S^0)}{A^{\rm SM}(\eta' K_S^0)} \simeq (0.15+0.03i)[(\delta^d_{LL})_{23} - (\delta^d_{RR})_{23}] + (69+12i)[(\delta^d_{LR})_{23} - (\delta^d_{RL})_{23}], \quad (3.22)$$

$$\frac{A^{\rm SUSY}(\eta' K_S^0)}{A^{\rm SM}(\eta' K_S^0)} \simeq (0.41+0.08i)[(\delta^d_{LL})_{23} - (\delta^d_{RR})_{23}] + (115+20i)[(\delta^d_{LR})_{23} - (\delta^d_{RL})_{23}] \quad (3.23)$$

for $m_{\tilde{g}} \simeq m_{\tilde{q}} = 500$ GeV and 300 GeV, respectively. As expected, the result is very similar to those for $B \to \phi K_S^0$ in (3.17) and (3.18) except for the overall signs of the RR and RL mass insertions. Thus, if $\mathcal{S}_{\phi K_S^0}$ and $\mathcal{S}_{\eta' K_S^0}$ differ, one would need some contributions from the RR and/or RL mass insertion.

Now we shall discuss how we could reproduce the relation $\mathcal{S}_{\phi K_S^0} < 0 < \mathcal{S}_{\eta' K_S^0} < \mathcal{S}_{J/\psi K_S^0}$ as indicated by experiment. Let us first consider RR and/or RL dominated models with $A^{\rm SUSY}(\phi K_S^0)/A^{\rm SM}(\phi K_S^0) \simeq 0.5\ e^{i\theta_{\rm SUSY}}$. In this case, the overall sign flips for $\eta' K_S^0$, so we obtain $A^{\rm SUSY}(\eta' K_S^0)/A^{\rm SM}(\eta' K_S^0) \simeq -0.5\ e^{i\theta_{\rm SUSY}}$. The results for $S_{\phi K_S^0}$ and $S_{\eta' K_S^0}$ are shown in Figure 3.3 (left). In this way, $\mathcal{S}_{\phi K_S^0}$ and $\mathcal{S}_{\eta' K_S^0}$ may differ and we can obtain $\mathcal{S}_{\phi K_S^0} < 0 < \mathcal{S}_{\eta' K_S^0}$. However, $\mathcal{S}_{\eta' K_S^0}$ is rather large compared to $\mathcal{S}_{J/\psi K_S^0}$. To solve this problem, we need to consider models with both sizable LL (and/or LR) and RR (and/or RL) mass insertions. Let us give an example: the amplitude of the LL (and/or LR) mass insertion is 4 times larger than the one for RR (and/or RL) whereas their phases are equal. In this case with the same SUSY contributions to $\mathcal{S}_{\phi K_S^0}$, $A^{\rm SUSY}(\phi K_S^0)/A^{\rm SM}(\phi K_S^0) \simeq 0.5 e^{i\theta_{\rm SUSY}}$, we obtain $A^{\rm SUSY}(\eta' K_S^0)/A^{\rm SM}(\eta' K_S^0) \simeq 0.3 e^{i\theta_{\rm SUSY}}$. In this way, we are able to reproduce the pattern $\mathcal{S}_{\phi K_S^0} < 0 < \mathcal{S}_{\eta' K_S^0} < \mathcal{S}_{J/\psi K_S^0}$ (see Figure 3.3 (right)).

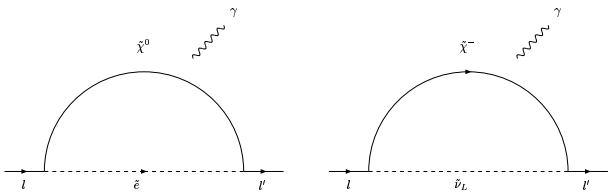

Figure 3.4: Feynman diagrams to generate $l^- \to l'^-\gamma$ in the SUSY models with conserved R parity. $\tilde{e}$, $\tilde{\nu}$, $\tilde{\chi}^0$ and $\tilde{\chi}^-$ represent charged slepton, sneutrino, chargino, and neutralino, respectively.

3.5 Lepton Flavor Violation

Strictly speaking, the Standard Model already has to be modified by introducing tiny neutrino masses, in order to incorporate the Lepton Flavor Violating (LFV) phenomena observed in the neutrino sector. Neutrino mixing ν_μ-ν_τ was first discovered in atmospheric neutrino experiments [54], and it is being further confirmed by the K2K experiment [55]. The neutrino oscillation was also confirmed in solar neutrinos, which comes from ν_e-ν_μ mixing, by both the Super-Kamiokande [56] and SNO [57,58] experiments. More recently, the Kamland experiment pinned down the explanation of the solar neutrino problem to the large mixing angle (LMA) solution [59]. Thus, neutrino oscillation experiments are providing high precision measurements in the neutrino sector. It is very interesting that the ν_e-ν_μ and ν_μ-ν_τ mixing angles are found to be almost maximal and the neutrino mass structure is quite different from that of the quark sector.

Now it is known that lepton-flavor symmetries are not exact in Nature. However, the magnitude of LFV processes in the charged lepton sector is not obvious. The tiny neutrino masses do not lead to sizable LFV processes in the charged lepton sector, since the event rates are suppressed by the fourth power of (m_ν/m_W). Thus, searches for LFV in the charged lepton sector will probe physics beyond the Standard Model and the origin of the neutrino masses.

The τ lepton is a member of the third generation and is the heaviest charged lepton. It can decay into quarks and leptons in the first and second generations. This may imply that τ lepton physics could provide some clues to puzzles in the family structure. In fact, one naively expects the heavier quarks and leptons to be more sensitive to the dynamics responsible for fermion mass generation.

In the following we discuss LFV τ lepton decay in SUSY models, especially in the supersymmetric seesaw mechanism and SUSY GUTs, and other models such as extra-dimension models and R parity violating SUSY models.

3.5.1 LFV in the Supersymmetric Models

The LFV in the SUSY extension of the Standard Model comes from the soft SUSY breaking terms, since the supersymmetric interactions have the same flavor structure as in the Standard Model. The soft SUSY breaking terms in lepton sector are as follows,

$$-\mathcal{L} = (m_E^2)_{ij}\tilde{e}^\dagger_{Ri}\tilde{e}_{Rj} + (m_L^2)_{ij}\tilde{l}^\dagger_{Li}\tilde{l}_{Lj} + \left\{(A_e)_{ij}H_1\tilde{e}^\dagger_{Ri}\tilde{l}_{Lj} + h.c.\right\} \tag{3.24}$$

where $(m_E^2)_{ij}$ and $(m_L^2)_{ij}$ are mass matrices for the right-handed sleptons $\tilde{e}_{Rj}$ and the left-handed sleptons $\tilde{l}_{Lj}(\equiv(\tilde{\nu}_{Lj}, \tilde{e}_{Lj}))$, respectively. $(A_e)_{ij}$ is the trilinear scalar coupling matrix.

LFV processes for charged leptons are radiative if R parity is conserved, since the SUSY interactions must be bilinears of the SUSY fields. Thus, $\tau^- \to \mu^-(e^-)\gamma$ and $\mu^- \to e^-\gamma$ are the

most sensitive to the flavor structure of the soft SUSY breaking terms except for some exceptional cases. These processes are generated by diagrams in Figure 3.4. The effective operators relevant to $l^- \to l'^- \gamma$ are flavor-violating magnetic moment operators,

$$\mathcal{H} = \sum_{l>l'} \frac{4G_F}{\sqrt{2}} \left[m_l A_R^{ll'} \bar{l} \sigma^{\mu\nu} P_R l' + m_l A_L^{ll'} \bar{l} \sigma^{\mu\nu} P_L l' \right] F_{\mu\nu} + h.c., \tag{3.25}$$

where $P_{L/R} = (1 \mp \gamma_5)/2$, and the branching ratios are given as

$$Br(l^- \to l'^- \gamma) = 384\pi^2 (|A_R^{ll'}|^2 + |A_L^{ll'}|^2)\ Br(l^- \to l'^- \nu_l \overline{\nu}_{l'}). \tag{3.26}$$

Here, $Br(\tau^- \to \mu^-(e^-)\nu_\tau \overline{\nu}_{\mu(e)}) \simeq 0.17$ and $Br(\mu^- \to e^- \nu_\mu \overline{\nu}_e) = 1$.

The coefficients in Eq. (3.25) are approximately given as

$$A_R^{\tau l'} = \frac{\sqrt{2}e}{4G_F} \frac{\alpha_Y}{4\pi} \frac{\tan\beta}{m_{SUSY}^2} \left[-\frac{1}{120} \delta_{\tau l'}^R \right], \tag{3.27}$$

$$A_L^{\tau l'} = \frac{\sqrt{2}e}{4G_F} \frac{\alpha_2}{4\pi} \frac{\tan\beta}{m_{SUSY}^2} \left[(\frac{1}{30} + \frac{t_W^2}{24}) \delta_{\tau l'}^L \right], \tag{3.28}$$

$$A_R^{\mu e} = \frac{\sqrt{2}e}{4G_F} \frac{\alpha_Y}{4\pi} \frac{\tan\beta}{m_{SUSY}^2} \left[-\frac{1}{120} \delta_{\mu e}^R + \frac{1}{120} \delta_{\mu\tau}^R \delta_{\tau e}^R - \frac{1}{60} \frac{m_\tau}{m_\mu} \delta_{\mu\tau}^L \delta_{\tau e}^R \right], \tag{3.29}$$

$$A_L^{\mu e} = \frac{\sqrt{2}e}{4G_F} \frac{\alpha_2}{4\pi} \frac{\tan\beta}{m_{SUSY}^2} \left[(\frac{1}{30} + \frac{t_W^2}{24}) \delta_{\mu e}^L - (\frac{1}{80} + \frac{7t_W^2}{240}) \delta_{\mu\tau}^L \delta_{\tau e}^L - \frac{t_W^2}{60} \frac{m_\tau}{m_\mu} \delta_{\mu\tau}^R \delta_{\tau e}^L \right], \tag{3.30}$$

assuming for simplicity that all SUSY particle masses are equal to m_{SUSY} and $\tan\beta \gg 1$. Here, $t_W \equiv \tan\theta_W$, where θ_W is the Weinberg angle, and the mass insertion parameters are given as

$$\delta_{ll'}^R = \left(\frac{(m_E^2)_{ll'}}{m_{SUSY}^2} \right), \qquad \delta_{ll'}^L = \left(\frac{(m_L^2)_{ll'}}{m_{SUSY}^2} \right). \tag{3.31}$$

When both the 13 and 23 generation components of the slepton mass matrices are non-vanishing, $\mu^- \to e^- \gamma$ is generated via scalar tau lepton exchange. In particular, if both the left-handed and right-handed mixings are sizable, the branching ratio is enhanced by $(m_\tau/m_\mu)^2$ compared to the case where only left-handed or right-handed mixing angles are non-vanishing. The off-diagonal components in $(A_e)_{ij}$ are sub-dominant in these processes since the contribution is not proportional to $\tan\beta$.

We list constraints on $\delta_{ll'}^R$ and $\delta_{ll'}^L$ from current experimental bounds on $Br(\tau^- \to \mu^-(e^-)\gamma)$, which are derived by the Belle experiment, and $Br(\mu^- \to e^-\gamma)$ in Table 3.1. In this table, we take $\tan\beta = 10$ and $m_{\rm SUSY} = 100$ GeV and 300 GeV. The constraints from $\mu^- \to e^-\gamma$ on the slepton mixings are quite stringent. On the other hand, the current bounds on the LFV τ lepton decay modes independently give sizable constraints on $|\delta_{\tau\mu}^L|$ and $|\delta_{\tau e}^L|$. Furthermore, while the current constraint on $|\delta_{\mu\tau}^L \delta_{\tau e}^L|$ from the LFV τ lepton decay is weaker than that from the LFV muon decay, improvement of the LFV τ lepton decay modes by about an order of magnitude will give a bound on $|\delta_{\mu\tau}^L \delta_{\tau e}^L|$ competitive with that from LFV muon decay.

The flavor structure of the soft SUSY breaking terms depends on the origin of the SUSY breaking and the physics beyond the MSSM, as discussed in Section 3.3. Even in the Universal

m_{SUSY}	$\lvert\delta^L_{\tau\mu}\rvert$	$\lvert\delta^L_{\tau e}\rvert$	$\lvert\delta^L_{\mu e}\rvert$	$\lvert\delta^L_{\mu\tau}\delta^L_{\tau e}\rvert$	$\lvert\delta^R_{\mu\tau}\delta^L_{\tau e}\rvert$
100 GeV	2×10^{-2}	2×10^{-2}	4×10^{-5}	1×10^{-4}	2×10^{-5}
				(3×10^{-4})	(7×10^{-3})
300 GeV	2×10^{-1}	2×10^{-1}	4×10^{-4}	9×10^{-4}	2×10^{-4}
				(3×10^{-2})	(6×10^{-1})
m_{SUSY}	$\lvert\delta^R_{\tau\mu}\rvert$	$\lvert\delta^R_{\tau e}\rvert$	$\lvert\delta^R_{\mu e}\rvert$	$\lvert\delta^R_{\mu\tau}\delta^R_{\tau e}\rvert$	$\lvert\delta^L_{\mu\tau}\delta^R_{\tau e}\rvert$
100 GeV	3×10^{-1}	3×10^{-1}	9×10^{-4}	9×10^{-4}	2×10^{-5}
				(1×10^{-1})	(7×10^{-3})
300 GeV	3	3	8×10^{-3}	8×10^{-3}	2×10^{-4}
				(9)	(6×10^{-1})

Table 3.1: Constraints on $\delta^R_{ll'}$ and $\delta^L_{ll'}$ from current experimental bounds on $Br(l^-\to l'^-\gamma)$. Here, we use the results of the LFV tau decay search from the Belle experiment. We take $\tan\beta = 10$ and $m_{\rm SUSY} = 100$ GeV and 300 GeV. The numbers in parentheses are derived from constraints on $|\delta^{(L/R)}_{\tau\mu}|$ and $|\delta^{(L/R)}_{\tau e}|$.

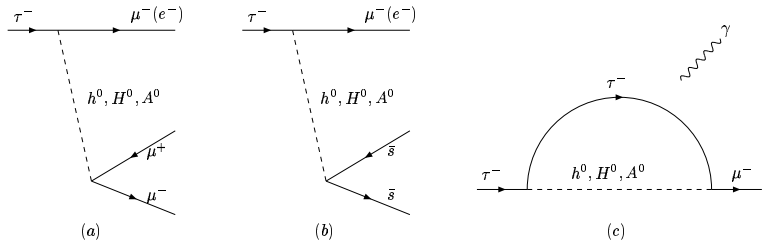

Figure 3.5: Feynman diagrams to generate (a) $\tau^-\to\mu^-(e^-)\mu^+\mu^-$, (b) $\tau^-\to\mu^-(e^-)\eta$, (c) $\tau^-\to\mu^-(e^-)\mu^-\gamma$, induced by anomolous Higgs boson couplings.

scalar mass scenario, the LFV Yukawa interaction may induce LFV slepton mass terms radiatively. If the heavier leptons have larger LFV Yukawa interactions, the τ lepton is the most sensitive to them. In the decoupling scenario, scalar τ leptons may be much lighter than other sleptons and have LFV interactions. Thus, the search for LFV τ lepton decay is important to probe such physics. In the next section we present predictions for LFV τ lepton decay in the SUSY seesaw model and SUSY GUTs.

Finally, we discuss other tau LFV processes in SUSY models. In a broader parameter space, $\tau^-\to\mu^-(e^-)\gamma$ are the largest tau LFV processes, unless they are suppressed by some accidental cancellation or much heavier SUSY particle masses. The LFV τ lepton decay modes to three leptons are dominantly induced by the photon-penguin contributions, and are correlated with $\tau^-\to\mu^-(e^-)\gamma$ as follows

$$Br(\tau^-\to\mu^-e^+e^-)/Br(\tau^-\to\mu^-\gamma) \simeq 1/94, \tag{3.32}$$
$$Br(\tau^-\to\mu^-\mu^+\mu^-)/Br(\tau^-\to\mu^-\gamma) \simeq 1/440, \tag{3.33}$$
$$Br(\tau^-\to e^-e^+e^-)/Br(\tau^-\to e^-\gamma) \simeq 1/94, \tag{3.34}$$
$$Br(\tau^-\to e^-\mu^+\mu^-)/Br(\tau^-\to e^-\gamma) \simeq 1/440. \tag{3.35}$$

The LFV τ decay modes into pseudoscalar mesons tend to be smaller than those to three leptons since the branching ratios are not proportional to $\tan^2\beta$.

When sleptons are much heavier than the weak scale, $Br(\tau^- \to \mu^-(e^-)\gamma)$ is suppressed. In this case, the modes $\tau^- \to \mu^-(e^-)\mu^+\mu^-$ and $\tau^- \to \mu^-(e^-)\eta$ induced by Higgs boson exchange become relatively important [60]. The LFV anomalous Yukawa coupling for the Higgs bosons is generated by radiative corrections, and it is not suppressed by powers of the slepton masses. While these processes are suppressed by a small Yukawa coupling constant for muons or strange quarks, they may acquire sizable branching ratios when $\tan\beta$ is large since the branching ratios are proportional to $\tan^6\beta$. When $\delta^L_{\tau\mu}$ is non-vanishing, the approximate formula for $Br(\tau^- \to \mu^-\mu^+\mu^-)$ is given as [60, 61]

$$\begin{aligned} Br(\tau^- \to \mu^-\mu^+\mu^-) &= \frac{m_\mu^2 m_\tau^2 \epsilon_2^2 |\delta^L_{\tau\mu}|^2}{8\cos^6\beta} Br(\tau^- \to \mu^-\nu_\tau\overline{\nu}_\mu) \\ &\quad \times \left[\left(\frac{\sin(\alpha-\beta)\cos\alpha}{M^2_{H^0}} - \frac{\cos(\alpha-\beta)\sin\alpha}{M^2_{h^0}} \right)^2 + \frac{\sin^2\beta}{M^4_{A^0}} \right], \\ &\simeq 3.8\times 10^{-7} \times |\delta^L_{\tau\mu}|^2 \left(\frac{\tan\beta}{60} \right)^6 \left(\frac{M_{A^0}}{100\ \mathrm{GeV}} \right)^{-4}, \end{aligned} \tag{3.36}$$

and $Br(\tau^- \to \mu^-\eta)$ is 8.4 times larger than $Br(\tau^- \to \mu^-\mu^+\mu^-)$ [62]. Here, ϵ_2 is a function of the SUSY particle masses. We take limits of large $\tan\beta$ and equal SUSY breaking mass parameters in the last step in Eq. (3.36). Notice that $\tau^- \to \mu^-\gamma$ also has a comparable branching ratio to them since the Higgs loop diagram [Fig. 3.5(c)] is enhanced by the τ lepton Yukawa coupling constant [63]. As a result, the ratio of the branching ratios for these LFV τ lepton decay modes, which are induced by the Higgs boson exchange, is $Br(\tau^- \to \mu^-\eta) : Br(\tau^- \to \mu^-\gamma) : Br(\tau^- \to \mu^-\mu^+\mu^-) = 8.4 : 1.5 : 1$.

3.5.2 SUSY Seesaw Mechanism and SUSY GUTs

In general, in seesaw and GUT models, LFV Yukawa interactions are introduced. If the SUSY breaking mediation scale is higher than the GUT [64–66] or the right-handed neutrino mass scale [67–70], sizable LFV processes are predicted as mentioned in the previous section.

The most economical way to generate the tiny neutrino masses is the seesaw mechanism. In the seesaw model, a neutrino Yukawa coupling Y_ν is introduced, which is lepton-flavor violating. In the supersymmetric extension, the off-diagonal components of the left-handed slepton mass matrix are radiatively induced, and they are approximately given by

$$(\delta m^2_{\tilde{L}})_{ij} \simeq -\frac{1}{8\pi^2}(3m_0^2 + A_0^2) \sum_k (Y_\nu^\dagger)_{ki}(Y_\nu)_{kj} \log\frac{M_G}{M_{N_k}}, \tag{3.37}$$

where M_{N_i} are the i-th right-handed neutrino masses, and M_G is the Planck scale. Here we assume the gravity mediation scenario, and the parameters m_0 and A_0 are the universal scalar mass and the universal trilinear scalar coupling. The predicted small neutrino mass matrix is

$$(m_\nu)_{ij} = \sum_k \frac{(Y_\nu)_{ki}(Y_\nu)_{kj}\langle H_2\rangle^2}{M_{N_k}}. \tag{3.38}$$

(3.37) has a different structure from (3.38). Thus, we may obtain independent information about the seesaw mechanism from the charged LFV searches and the neutrino oscillation experiments.

In Figure 3.6 we show $Br(\tau^- \to \mu^-\gamma)$ and $Br(\tau^- \to e^-\gamma)$ in the SUSY seesaw mechanism, assuming the gravity mediation scenario for the SUSY breaking. We fix the neutrino Yukawa coupling using the neutrino oscillation data under assumptions for the neutrino Yukawa coupling

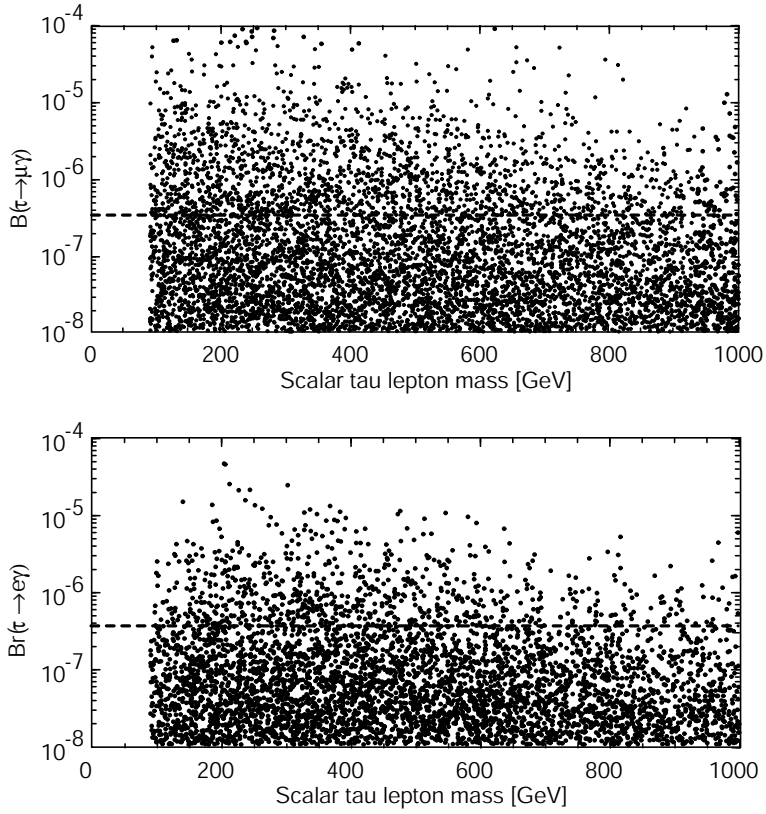

Figure 3.6: $Br(\tau^- \to \mu^-\gamma)$ and $Br(\tau^- \to e^-\gamma)$ in the SUSY seesaw mechanism, assuming the gravity mediation scenario for the SUSY breaking. Dashed lines show the current experimental bounds from the Belle experiment. Here, we take $\tan\beta = 30$, the $SU(2)_L$ gaugino mass 200 GeV, $A_0 = 0$, and positive Higgsino mass. We fix the neutrino Yukawa coupling by using the neutrino oscillation data under assumptions of the neutrino Yukawa coupling.

Y_ν, which suppresses $Br(\mu^- \to e^-\gamma)$. The experimental bounds on these τ processes have already excluded some of the parameter space. While a natural candidate for the largest LFV τ lepton decay mode is $\tau^- \to \mu^-\gamma$ from the atmospheric neutrino result, some model-parameters in the seesaw model predict larger $Br(\tau^- \to e^-\gamma)$ [71]. This is because (3.37) and (3.38) have different dependences on Y_ν and M_N as mentioned above.

In GUT models, even if the neutrino Yukawa contribution is negligible, LFV processes are predicted. In the $SU(5)$ SUSY GUT, the right-handed charged leptons are embedded in the **10**-dimensional multiplets with the left-handed quarks and the right-handed up-type quarks. The LFV SUSY breaking terms for the right-handed sleptons are generated by the top-quark Yukawa coupling Y_t above the GUT scale. The off-diagonal components in the right-handed slepton mass matrix are given as

$$(\delta m^2_{\tilde{E}})_{ij} \simeq -\frac{3}{8\pi^2}(3m_0^2 + A_0^2)V_{i3}V^\star_{j3}|Y_t|^2 \log\frac{M_G}{M_{\rm GUT}}, \tag{3.39}$$

where V_{ij} is the CKM matrix in the SUSY $SU(5)$ GUT and $M_{\rm GUT}$ is the GUT scale.

In the minimal $SU(5)$ SUSY GUT, in which the neutrino Yukawa coupling is negligible, $Br(\tau^- \to \mu^-\gamma)$ is smaller than $10^{-(9-10)}$. While the process is enhanced by the top-quark Yukawa coupling, it is suppressed by the CKM matrix element and the $U(1)_Y$ gauge coupling

constant. Furthermore, when the right-handed sleptons have LFV mass terms, an accidental cancellation among the diagrams tends to suppress the branching ratio. However, we notice that the CKM matrix elements at the GUT scale may not be the same as ones extrapolated from the low energy data. This is because the quark and lepton mass ratios are not well explained in this model. If V_{32} is larger, the processes are enhanced [72, 73].

3.5.3 Other Theoretical Models

In the previous subsections we discussed LFV τ lepton decays in SUSY models assuming that R parity is conserved. In this subsection we review some examples of other models which predict LFV τ lepton decays.

In extra-dimension models [8, 9] the "fundamental" scale is expected to be comparable to the weak scale, and the classical seesaw mechanism does not explain the tiny neutrino masses. Instead, singlet neutrinos in the bulk space are introduced [74–76]. The Yukawa couplings of the left-handed neutrinos with the bulk neutrinos are suppressed by an overlap of the wave functions, and small Dirac neutrino masses are predicted.

In this model the loop diagrams from the Kaluza-Klein states of the bulk neutrinos generate the LFV τ lepton and μ decay [77, 78]. On the other hand, this model is constrained by short baseline experiments and charged current universality, since the kinetic mixing term for neutrinos is not negligible. In the minimal model, in which the unique source of LFV is the Yukawa coupling of the left-handed neutrinos with the bulk neutrinos, $Br(\tau^- \to \mu^-\gamma) \lesssim 10^{-9}$ from the existing constraints, while $Br(\mu^- \to e^-\gamma) \lesssim 10^{-(11-13)}$ depending on U_{e3} [78]. In the non-minimal case, the constraints may be looser.

In R-parity violating SUSY models, there exist lepton flavor and baryon number non-conserving interactions at the tree level. Proton stability gives stringent bounds on such models, as well as other processes, such as the decays of charged leptons and B and D mesons, neutral current processes, and FCNC processes. Since the τ lepton is the heaviest lepton, various τ LFV modes can be induced. These include $\tau^- \to \mu^-\mu^+\mu^-$, $\mu^-e^+e^-$, $\mu^+e^-e^-$ and $\tau^- \to \mu^-M^0$, μ^-V^0. Here, M^0 and V^0 are pseudoscalar and vector mesons, respectively. Comprehensive studies of LFV τ lepton decay have been performed in [79].

If the masses of the right-handed neutrinos are $O(1-10)$ TeV in the seesaw mechanism, sizable LFV τ lepton decay might be possible [80]. It is found in [81] that $Br(\tau^- \to \mu^-\gamma)$ and $Br(\tau^- \to \mu^-\mu^+\mu^-)$ are smaller than 10^{-9} and 10^{-10}, respectively. It is also argued that $Br(\tau^- \to e^-\gamma)$ and $Br(\tau^- \to e^-e^+e^-)$ can reach 10^{-8} and 10^{-9}, respectively, in various models [81].

References

[1] S. Weinberg, "Implications Of Dynamical Symmetry Breaking," Phys. Rev. D **13**, 974 (1976).

[2] S. Weinberg, "Implications Of Dynamical Symmetry Breaking: An Addendum," Phys. Rev. D **19** (1979) 1277.

[3] L. Susskind, "Dynamics Of Spontaneous Symmetry Breaking In The Weinberg-Salam Theory," Phys. Rev. D **20**, 2619 (1979).

[4] A. G. Cohen, D. B. Kaplan and A. E. Nelson, "Progress in electroweak baryogenesis," Ann. Rev. Nucl. Part. Sci. **43**, 27 (1993) [arXiv:hep-ph/9302210].

[5] H. P. Nilles, "Supersymmetry, Supergravity And Particle Physics," Phys. Rept. **110**, 1 (1984).

[6] H. E. Haber and G. L. Kane, "The Search For Supersymmetry: Probing Physics Beyond The Standard Model," Phys. Rept. **117**, 75 (1985).

[7] C. T. Hill and E. H. Simmons, "Strong dynamics and electroweak symmetry breaking," Phys. Rept. **381**, 235 (2003) [arXiv:hep-ph/0203079].

[8] N. Arkani-Hamed, S. Dimopoulos and G. R. Dvali, "The hierarchy problem and new dimensions at a millimeter," Phys. Lett. B **429**, 263 (1998) [arXiv:hep-ph/9803315].

[9] L. Randall and R. Sundrum, "A large mass hierarchy from a small extra dimension," Phys. Rev. Lett. **83**, 3370 (1999) [arXiv:hep-ph/9905221].

[10] J. Hewett and M. Spiropulu, "Particle physics probes of extra spacetime dimensions," Ann. Rev. Nucl. Part. Sci. **52**, 397 (2002) [arXiv:hep-ph/0205106].

[11] N. Arkani-Hamed, A. G. Cohen and H. Georgi, "Electroweak symmetry breaking from dimensional deconstruction," Phys. Lett. B **513**, 232 (2001) [arXiv:hep-ph/0105239].

[12] H. Georgi and S. L. Glashow, "Unity Of All Elementary Particle Forces," Phys. Rev. Lett. **32**, 438 (1974).

[13] J. C. Pati and A. Salam, "Lepton Number As The Fourth Color," Phys. Rev. D **10**, 275 (1974).

[14] M. Dine, A. E. Nelson and Y. Shirman, "Low-energy dynamical supersymmetry breaking simplified," Phys. Rev. D **51**, 1362 (1995) [arXiv:hep-ph/9408384].

[15] M. Dine, A. E. Nelson, Y. Nir and Y. Shirman, "New tools for low-energy dynamical supersymmetry breaking," Phys. Rev. D **53**, 2658 (1996) [arXiv:hep-ph/9507378].

[16] M. Dine, Y. Nir and Y. Shirman, "Variations on minimal gauge mediated supersymmetry breaking," Phys. Rev. D **55**, 1501 (1997) [arXiv:hep-ph/9607397].

[17] D. E. Kaplan, G. D. Kribs and M. Schmaltz, "Supersymmetry breaking through transparent extra dimensions," Phys. Rev. D **62**, 035010 (2000) [arXiv:hep-ph/9911293].

[18] Z. Chacko, M. A. Luty, A. E. Nelson and E. Ponton, "Gaugino mediated supersymmetry breaking," JHEP **0001**, 003 (2000) [arXiv:hep-ph/9911323].

[19] M. Schmaltz and W. Skiba, "Minimal gaugino mediation," Phys. Rev. D **62**, 095005 (2000) [arXiv:hep-ph/0001172].

[20] L. Randall and R. Sundrum, "Out of this world supersymmetry breaking," Nucl. Phys. B **557**, 79 (1999) [arXiv:hep-th/9810155].

[21] G. F. Giudice, M. A. Luty, H. Murayama and R. Rattazzi, "Gaugino mass without singlets," JHEP **9812**, 027 (1998) [arXiv:hep-ph/9810442].

[22] L. J. Hall, V. A. Kostelecky and S. Raby, "New Flavor Violations In Supergravity Models," Nucl. Phys. B **267**, 415 (1986).

[23] Y. Nir and N. Seiberg, "Should squarks be degenerate?," Phys. Lett. B **309**, 337 (1993) [arXiv:hep-ph/9304307].

[24] M. Leurer, Y. Nir and N. Seiberg, "Mass matrix models: The Sequel," Nucl. Phys. B **420**, 468 (1994) [arXiv:hep-ph/9310320].

[25] M. Dine, A. Kagan and S. Samuel, "Naturalness In Supersymmetry, Or Raising The Supersymmetry Breaking Scale," Phys. Lett. B **243**, 250 (1990).

[26] M. Dine, R. G. Leigh and A. Kagan, "Flavor symmetries and the problem of squark degeneracy," Phys. Rev. D **48**, 4269 (1993) [arXiv:hep-ph/9304299].

[27] S. Dimopoulos and G. F. Giudice, "Naturalness constraints in supersymmetric theories with nonuniversal soft terms," Phys. Lett. B **357**, 573 (1995) [arXiv:hep-ph/9507282].

[28] A. Pomarol and D. Tommasini, "Horizontal symmetries for the supersymmetric flavor problem," Nucl. Phys. B **466**, 3 (1996) [arXiv:hep-ph/9507462].

[29] A. G. Cohen, D. B. Kaplan and A. E. Nelson, "The more minimal supersymmetric standard model," Phys. Lett. B **388**, 588 (1996) [arXiv:hep-ph/9607394].

[30] J. Hisano, K. Kurosawa and Y. Nomura, "Large squark and slepton masses for the first-two generations in the anomalous U(1) SUSY breaking models," Phys. Lett. B **445**, 316 (1999) [arXiv:hep-ph/9810411].

[31] J. Hisano, K. Kurosawa and Y. Nomura, "Natural effective supersymmetry," Nucl. Phys. B **584**, 3 (2000) [arXiv:hep-ph/0002286].

[32] T. Moroi, "CP violation in $B_d \to \phi K_S$ in SUSY GUT with right-handed neutrinos," Phys. Lett. B **493**, 366 (2000) [arXiv:hep-ph/0007328].

[33] N. Akama, Y. Kiyo, S. Komine and T. Moroi, "CP violation in kaon system in supersymmetric SU(5) model with seesaw-induced neutrino masses," Phys. Rev. D **64**, 095012 (2001) [arXiv:hep-ph/0104263].

[34] S. Baek, T. Goto, Y. Okada and K. i. Okumura, "Muon anomalous magnetic moment, lepton flavor violation, and flavor changing neutral current processes in SUSY GUT with right-handed neutrino," Phys. Rev. D **64**, 095001 (2001) [arXiv:hep-ph/0104146].

[35] T. Goto, Y. Okada, Y. Shimizu, T. Shindou and M. Tanaka, "Exploring flavor structure of supersymmetry breaking at B factories," Phys. Rev. D **66**, 035009 (2002) [arXiv:hep-ph/0204081].

[36] T. Goto, Y. Okada, Y. Shimizu, T. Shindou and M. Tanaka, "Exploring flavor structure of supersymmetry breaking from rare B decays and unitarity triangle," arXiv:hep-ph/0306093.

[37] D. Chang, A. Masiero and H. Murayama, Phys. Rev. D **67**, 075013 (2003) [arXiv:hep-ph/0205111].

[38] M. Ciuchini, E. Franco, A. Masiero and L. Silvestrini, Phys. Rev. D **67**, 075016 (2003) [Erratum-ibid. D **68**, 079901 (2003)] [arXiv:hep-ph/0212397].

[39] J. Hisano and Y. Shimizu, "GUT relation in neutrino induced flavor physics in SUSY SU(5) GUT," Phys. Lett. B **565**, 183 (2003) [arXiv:hep-ph/0303071].

[40] M. Ciuchini, A. Masiero, L. Silvestrini, S. K. Vempati and O. Vives, "Grand unification of quark and lepton FCNCs," arXiv:hep-ph/0307191.

[41] K. Abe *et al.* [Belle Collaboration], "Measurement of time-dependent CP-violating asymmetries in $B^0 \to \phi K^0_S$, $K^+K^-K^0_S$, and $\eta' K^0_S$ decays," arXiv:hep-ex/0308035.

[42] S.M. Spanier [BABAR Collaboration], BABAR-PLOT-0056,

`https://oraweb.slac.stanford.edu:8080/pls/slacquery/BABAR_DOCUMENTS.DetailedIndex?P_BP_`

Contributed to 21st International Symposium on Lepton and Photon Interactions at High Energies(LP 03), Batavia, Illinois, 11-16 Aug 2003.

[43] F. Gabbiani, E. Gabrielli, A. Masiero and L. Silvestrini, "A complete analysis of FCNC and CP constraints in general SUSY extensions of the standard model," Nucl. Phys. B **477**, 321 (1996) [arXiv:hep-ph/9604387].

[44] M. Ciuchini *et al.*, "ΔM_K and ϵ_K in SUSY at the next-to-leading order," JHEP **9810**, 008 (1998) [arXiv:hep-ph/9808328].

[45] M. B. Causse and J. Orloff, "Supersymmetric penguin contributions to the decay $b \to s\gamma$ with non-universal squarks masses," Eur. Phys. J. C **23**, 749 (2002) [arXiv:hep-ph/0012113].

[46] A. Masiero and O. Vives, "Flavour And CP Violation In Supersymmetry," New J. Phys. **4**, 4 (2002).

[47] G.L. Kane, P. Ko, H.B. Wang, C. Kolda, J.H. Park and L.T. Wang, "$B_d \to \phi K_S$ CP asymmetries as an important probe of supersymmetry," Phys. Rev. Lett. **90** (2003) 141803; [arXiv:hep-ph/0304239].

[48] S. Mishima and A. I. Sanda, "An analysis of supersymmetric effects on $B \to \phi K$ decays in PQCD approach," arXiv:hep-ph/0311068.

[49] S. Khalil and E. Kou, "On supersymmetric contributions to the CP asymmetry of the $B \to \phi K_S$," Phys. Rev. D **67** (2003) 055009 [arXiv:hep-ph/0212023].

[50] A. Ali and C. Greub, "An analysis of two-body non-leptonic B decays involving light mesons in the standard model," Phys. Rev. D **57** (1998) 2996; [arXiv:hep-ph/9707251].

[51] K. F. Chen *et al.*, [Belle Collaboration], "Measurement of CP-violating parameters in $B \to \eta' K$ decays. ((B))," Phys. Lett. B **546**, 196 (2002) [arXiv:hep-ex/0207033].

[52] B. Aubert *et al.* [BABAR Collaboration], "Observation of B meson decays to $\eta\pi$ and ηK," arXiv:hep-ex/0303039.

[53] S. Khalil and E. Kou, "A possible supersymmetric solution to the discrepancy between $B \to \phi K_S$ and $B \to \eta' K_S$ CP asymmetries," Phys. Rev. Lett. **91**, 241602 (2003) [arXiv:hep-ph/0303214].

[54] Y. Fukuda *et al.* [Super-Kamiokande Collaboration], "Evidence for oscillation of atmospheric neutrinos," Phys. Rev. Lett. **81**, 1562 (1998) [arXiv:hep-ex/9807003].

[55] M. H. Ahn *et al.* [K2K Collaboration], "Indications of neutrino oscillation in a 250-km long-baseline experiment," Phys. Rev. Lett. **90**, 041801 (2003) [arXiv:hep-ex/0212007].

[56] S. Fukuda *et al.* [Super-Kamiokande Collaboration], Phys. Rev. Lett. **86**, 5651 (2001) [arXiv:hep-ex/0103032].

[57] Q. R. Ahmad *et al.* [SNO Collaboration], "Direct evidence for neutrino flavor transformation from neutral-current interactions in the Sudbury Neutrino Observatory," Phys. Rev. Lett. **89**, 011301 (2002) [arXiv:nucl-ex/0204008].

[58] Q. R. Ahmad *et al.* [SNO Collaboration], "Measurement of day and night neutrino energy spectra at SNO and constraints on neutrino mixing parameters," Phys. Rev. Lett. **89**, 011302 (2002) [arXiv:nucl-ex/0204009].

[59] K. Eguchi *et al.* [KamLAND Collaboration], "First results from KamLAND: Evidence for reactor anti-neutrino disappearance," Phys. Rev. Lett. **90**, 021802 (2003) [arXiv:hep-ex/0212021].

[60] K. S. Babu and C. Kolda, "Higgs-mediated $\tau \to 3\mu$ in the supersymmetric seesaw model," Phys. Rev. Lett. **89**, 241802 (2002) [arXiv:hep-ph/0206310].

[61] A. Dedes, J. R. Ellis and M. Raidal, "Higgs mediated $B^0_{s,d} \to \mu\tau$, $e\tau$ and $\tau \to 3\mu$, $e\mu\mu$ decays in supersymmetric seesaw models," Phys. Lett. B **549** (2002) 159 [arXiv:hep-ph/0209207].

[62] M. Sher, "$\tau \to \mu\eta$ in supersymmetric models," Phys. Rev. D **66**, 057301 (2002) [arXiv:hep-ph/0207136].

[63] J. Hisano and Y. Shimizu, in preparation.

[64] R. Barbieri and L. J. Hall, "Signals for supersymmetric unification," Phys. Lett. B **338**, 212 (1994) [arXiv:hep-ph/9408406].

[65] R. Barbieri, L. J. Hall and A. Strumia, "Violations of lepton flavor and CP in supersymmetric unified theories," Nucl. Phys. B **445**, 219 (1995) [arXiv:hep-ph/9501334].

[66] J. Hisano, T. Moroi, K. Tobe and M. Yamaguchi, "Exact event rates of lepton flavor violating processes in supersymmetric SU(5) model," Phys. Lett. B **391**, 341 (1997) [Erratum-ibid. B **397**, 357 (1997)] [arXiv:hep-ph/9605296].

[67] F. Borzumati and A. Masiero, "Large Muon And Electron Number Violations In Supergravity Theories," Phys. Rev. Lett. **57**, 961 (1986).

[68] J. Hisano, T. Moroi, K. Tobe, M. Yamaguchi and T. Yanagida, "Lepton flavor violation in the supersymmetric standard model with seesaw induced neutrino masses," Phys. Lett. B **357**, 579 (1995) [arXiv:hep-ph/9501407].

[69] J. Hisano, T. Moroi, K. Tobe and M. Yamaguchi, "Lepton-Flavor Violation via Right-Handed Neutrino Yukawa Couplings in Supersymmetric Standard Model," Phys. Rev. D **53**, 2442 (1996) [arXiv:hep-ph/9510309].

[70] J. A. Casas and A. Ibarra, "Oscillating neutrinos and $\mu \to e\gamma$," Nucl. Phys. B **618**, 171 (2001) [arXiv:hep-ph/0103065].

[71] J. R. Ellis, J. Hisano, M. Raidal and Y. Shimizu, "A new parametrization of the seesaw mechanism and applications in supersymmetric models," Phys. Rev. D **66**, 115013 (2002) [arXiv:hep-ph/0206110].

[72] N. Arkani-Hamed, H. C. Cheng and L. J. Hall, "Flavor mixing signals for realistic supersymmetric unification," Phys. Rev. D **53**, 413 (1996) [arXiv:hep-ph/9508288].

[73] J. Hisano, D. Nomura, Y. Okada, Y. Shimizu and M. Tanaka, "Enhancement of $\mu \to e\gamma$ in the supersymmetric SU(5) GUT at large $\tan\beta$," Phys. Rev. D **58**, 116010 (1998) [arXiv:hep-ph/9805367].

[74] N. Arkani-Hamed, S. Dimopoulos, G. R. Dvali and J. March-Russell, "Neutrino masses from large extra dimensions," Phys. Rev. D **65**, 024032 (2002) [arXiv:hep-ph/9811448].

[75] K. R. Dienes, E. Dudas and T. Gherghetta, "Light neutrinos without heavy mass scales: A higher-dimensional seesaw mechanism," Nucl. Phys. B **557**, 25 (1999) [arXiv:hep-ph/9811428].

[76] Y. Grossman and M. Neubert, "Neutrino masses and mixings in non-factorizable geometry," Phys. Lett. B **474**, 361 (2000) [arXiv:hep-ph/9912408].

[77] A. E. Faraggi and M. Pospelov, "Phenomenological issues in TeV scale gravity with light neutrino masses," Phys. Lett. B **458**, 237 (1999) [arXiv:hep-ph/9901299].

[78] A. De Gouvea, G. F. Giudice, A. Strumia and K. Tobe, "Phenomenological implications of neutrinos in extra dimensions," Nucl. Phys. B **623**, 395 (2002) [arXiv:hep-ph/0107156].

[79] J. P. Saha and A. Kundu, "Constraints on R-parity violating supersymmetry from leptonic and semileptonic τ, B_d and B_s decays," Phys. Rev. D **66**, 054021 (2002) [arXiv:hep-ph/0205046].

[80] A. Ilakovac and A. Pilaftsis, "Flavor violating charged lepton decays in a GUT and superstring inspired standard model," Nucl. Phys. B **437** (1995) 491 [arXiv:hep-ph/9403398].

[81] G. Cvetic, C. Dib, C. S. Kim and J. D. Kim, "On lepton flavor violation in tau decays," Phys. Rev. D **66**, 034008 (2002) [Erratum-ibid. D **68**, 059901 (2003)] [arXiv:hep-ph/0202212].

Chapter 4

Sensitivity at SuperKEKB

4.1 Overview

4.1.1 Goals of sensitivity studies

As described in Chapter 1, the primary purpose of SuperKEKB is to perform a comprehensive study of B decays governed by quark transitions induced by quantum loops, where sizable effects from physics beyond the Standard Model are expected. If the study leads to a conclusion that an observed pattern is inconsistent with the Standard Model expectation, we further proceed to identify underlying flavor structure.

One of major goals of sensitivity studies is to clarify the meaning of the statement above quantitatively. To this end, we estimate statistical, systematic and theoretical errors on key observables at SuperKEKB. As fully explained in the acclerator part of this Letter of Intent, the target luminosity of SuperKEKB is 5×10^{35} cm^{-2}s^{-1}, which corresponds to an annual integrated luminosity of 5 ab^{-1}. Therefore we estimate expected errors at 5 ab^{-1} to describe what will be achieved at an early stage of the SuperKEKB experiment. We also provide errors at 50 ab^{-1} as ultimate measurements that can be performed at SuperKEKB. Although this looks rather ambitious, our experience at the Belle experiment tells that an integrated luminosity that is 10 times as large as a target annual luminosity is not a mere dream.

There are a huge number of observables that can be measured at SuperKEKB. It is not the main purpose of our sensitivity studies to cover all of them. Instead, our strategy is to concentrate on observables that are indispensable to reach the primary goal mentioned above. The following points are considered to select such observables:

- A sizable deviation from a prediction of the Standard Model is expected.
- A hadronic uncertainty is negligible or very small.
- A measurement at SuperKEKB is (much) superior to others, in particular to LHCb, whose expected physics performance is regarded as the benchmark of next-generation B physics programs at hadron colliders.

Selected topics do not necessarily satisfy all of these criteria, but do have clear advantages over others not covered in this chapter.

As discussed in the detector part of this Letter of Intent, at SuperKEKB we expect a background level that is about 20 times larger than what we currently observe at Belle. Our investigation leads to a conclusion that under such conditions there is a feasible detector design that guarantees performance equivalent to the present Belle detector. Therefore, throughout our

studies, we assume a detector that has the same performance as the present Belle detector unless otherwise noticed. Any possible gain from an improved detector performance is regarded as a bonus, and our aim is to demonstrate that most of physics goals at SuperKEKB are achieved even without any improvement in the detector performance. One important exception, however, is B meson vertex reconstruction using the K^0_S. Here we clearly need to introduce a larger vertex detector to increase vertex reconstruction efficiencies. Therefore we incorporate the proposed detector design in this case.

One of the biggest advantages of the sensitivity studies for Super-KEKB compared with those for hadron collider experiments is that we can fully utilize information obtained by analyzing Belle data. In particular, many of studies described in this chapter rely on Monte Carlo pseudo-experiments (also called "toy Monte Carlo experiments") in which PDFs are constructed from data. A clear advantage of this approach over genuine Monte Carlo simulations (e.g. GEANT simulation) is that background fractions and detector resolutions are more reliable. For some topics for which pseudo-experiments are not available, however, we also use GEANT simulation and/or FSIM, a parametric Monte Carlo simulator that requires much less CPU power than GEANT.

In the rest of this section we overview two important analysis techniques that are used repeatedly in our studies. One is the procedure to fit a proper-time difference distribution for a time-dependent CP asymmetry measurement. The other is to reconstruct one B meson exclusively (or semi-inclusively) so as to study decays of an accompanying B meson in the cleanest environment. This is called "full reconstruction B tagging".

4.1.2 Time-dependent CP asymmetries

In the decay chain $\Upsilon(4S) \to B^0\overline{B}^0 \to f_{CP}f_{\rm tag}$, where one of the B mesons decays at time t_{CP} to a final state f_{CP} and the other decays at time $t_{\rm tag}$ to a final state $f_{\rm tag}$ that distinguishes between B^0 and $\overline{B}^0$, the decay rate has a time dependence given by [1]

$$\mathcal{P}(\Delta t) = \frac{e^{-|\Delta t|/\tau_{B^0}}}{4\tau_{B^0}}\left\{1 + q\cdot\Big[\mathcal{S}\sin(\Delta m_d\Delta t) + \mathcal{A}\cos(\Delta m_d\Delta t)\Big]\right\}, \tag{4.1}$$

where τ_{B^0} is the B^0 lifetime, Δm_d is the mass difference between the two B^0 mass eigenstates, $\Delta t = t_{CP} - t_{\rm tag}$, and the b-flavor charge $q = +1$ (-1) when the tagging B meson is a B^0 $(\overline{B}^0)$. $\mathcal{S}$ and $\mathcal{A}$ are CP-violation parameters. For example, to a good approximation, the Standard Model predicts $\mathcal{S} = -\xi_f \sin 2\phi_1$, where $\xi_f = +1(-1)$ corresponds to CP-even (-odd) final states, and $\mathcal{A} = 0$ for both $b \to c\bar{c}s$ and $b \to s\bar{s}s$ transitions.

We determine q and Δt for each event. Charged leptons, pions, kaons, and Λ baryons that are not associated with a reconstructed CP eigenstate decay are used to identify the b-flavor of the accompanying B meson. The tagging algorithm is described in detail elsewhere [2]. We use two parameters, q and r, to represent the tagging information. The first, q, is already defined above. The parameter r is an event-by-event Monte Carlo-determined flavor-tagging dilution parameter that ranges from $r = 0$ for no flavor discrimination to $r = 1$ for an unambiguous flavor assignment. It is used only to sort data into six intervals of r, according to estimated flavor purity. We determine directly from data the average wrong-tag probabilities, $w_l \equiv (w_l^+ + w_l^-)/2$ $(l = 1, 6)$, and differences between B^0 and $\overline{B}^0$ decays, $\Delta w_l \equiv w_l^+ - w_l^-$, where $w_l^{+(-)}$ is the wrong-tag probability for the $B^0(\overline{B}^0)$ decay in each r interval. The event fractions and wrong-tag fractions are summarized in Table 4.1. The total effective tagging efficiency is determined to be $\epsilon_{\rm eff} \equiv \sum_{l=1}^{6}\epsilon_l(1-2w_l)^2 = 0.287 \pm 0.005$, where ϵ_l is the event fraction for each r interval. The error includes both statistical and systematic uncertainties.

l	r interval	ϵ_l	w_l	Δw_l	$\epsilon^l_{\rm eff}$
1	0.000 – 0.250	0.398	0.464 ± 0.006	-0.011 ± 0.006	0.002 ± 0.001
2	0.250 – 0.500	0.146	0.331 ± 0.008	$+0.004 \pm 0.010$	0.017 ± 0.002
3	0.500 – 0.625	0.104	0.231 ± 0.009	-0.011 ± 0.010	0.030 ± 0.002
4	0.625 – 0.750	0.122	0.163 ± 0.008	-0.007 ± 0.009	0.055 ± 0.003
5	0.750 – 0.875	0.094	0.109 ± 0.007	$+0.016 \pm 0.009$	0.057 ± 0.002
6	0.875 – 1.000	0.136	0.020 ± 0.005	$+0.003 \pm 0.006$	0.126 ± 0.003

Table 4.1: The event fractions ϵ_l, wrong-tag fractions w_l, wrong-tag fraction differences Δw_l, and average effective tagging efficiencies $\epsilon^l_{\rm eff} = \epsilon_l(1-2w_l)^2$ for each r interval. The errors include both statistical and systematic uncertainties. The event fractions are obtained from the $J/\psi K^0_S$ simulation.

The vertex position for the f_{CP} decay is reconstructed using leptons from J/ψ decays or charged hadrons from η_c decays, and that for $f_{\rm tag}$ is obtained with well reconstructed tracks that are not assigned to f_{CP}. Tracks that are consistent with coming from a $K^0_S \to \pi^+\pi^-$ decay are not used. Each vertex position is required to be consistent with the interaction region profile, determined run-by-run, smeared in the r-ϕ plane to account for the B meson decay length. With these requirements, we are able to determine a vertex even with a single track; the fraction of single-track vertices is about 10% for z_{CP} and 22% for $z_{\rm tag}$. The proper-time interval resolution function $R_{\rm sig}(\Delta t)$ is formed by convolving four components: the detector resolutions for z_{CP} and $z_{\rm tag}$, the shift in the $z_{\rm tag}$ vertex position due to secondary tracks originating from charmed particle decays, and the kinematic approximation that the B mesons are at rest in the cms [3]. A small component of broad outliers in the Δz distribution, caused by mis-reconstruction, is represented by a Gaussian function. We determine fourteen resolution parameters from the aforementioned fit to the control samples. We find that the average Δt resolution is ~ 1.43 ps (rms). The width of the outlier component is determined to be (39 ± 2) ps; the fractions of the outlier components are $(2.1 \pm 0.6) \times 10^{-4}$ for events with both vertices reconstructed with more than one track, and $(3.1 \pm 0.1) \times 10^{-2}$ for events with at least one single-track vertex.

We determine $\mathcal{S}$ and $\mathcal{A}$ for each mode by performing an unbinned maximum-likelihood fit to the observed Δt distribution. The probability density function (PDF) expected for the signal distribution, $\mathcal{P}_{\rm sig}(\Delta t; \mathcal{S}, \mathcal{A}, q, w_l, \Delta w_l)$, is given by Eq. (4.1) incorporating the effect of incorrect flavor assignment. The distribution is also convolved with the proper-time interval resolution function $R_{\rm sig}(\Delta t)$, which takes into account the finite vertex resolution. We determine the following likelihood value for each event:

$$\begin{aligned} P_i &= (1 - f_{\rm ol}) \int_{-\infty}^{\infty} \Big[f_{\rm sig} \mathcal{P}_{\rm sig}(\Delta t') R_{\rm sig}(\Delta t_i - \Delta t') \\ &+ (1 - f_{\rm sig}) \mathcal{P}_{\rm bkg}(\Delta t') R_{\rm bkg}(\Delta t_i - \Delta t') \Big] d(\Delta t') \\ &+ f_{\rm ol} P_{\rm ol}(\Delta t_i) \end{aligned} \tag{4.2}$$

where $P_{\rm ol}(\Delta t)$ is a broad Gaussian function that represents an outlier component with a small fraction $f_{\rm ol}$. The signal probability $f_{\rm sig}$ depends on the r region and is calculated on an event-by-event basis as a function of ΔE and $M_{\rm bc}$. $\mathcal{P}_{\rm bkg}(\Delta t)$ is a PDF for background events, which is modeled as a sum of exponential and prompt components, and is convolved with a sum of two Gaussians $R_{\rm bkg}$. All parameters in $\mathcal{P}_{\rm bkg}(\Delta t)$ and $R_{\rm bkg}$ are determined by the fit to the Δt distribution of a background-enhanced control sample; i.e. events away from the ΔE-$M_{\rm bc}$ signal

region. We fix τ_{B^0} and Δm_d at their world-average values. The only free parameters in the final fit are $\mathcal{S}$ and $\mathcal{A}$, which are determined by maximizing the likelihood function $L = \prod_i P_i(\Delta t_i; \mathcal{S}, \mathcal{A})$ where the product is over all events.

4.1.3 B tagging with full reconstruction

At SuperKEKB, $B\bar{B}$ meson pairs will be produced from $\Upsilon(4S)$ decays. To study B meson decays that include neutrinos, photons, π^0 mesons in the final states, it is useful to tag one of the B mesons through the full reconstruction. This method has the following attractive features:

- The momentum vector and flavor of the other B meson can be identified, i.e. single B meson beams can practically be obtained offline.
- Continuum and combinatoric $B\bar{B}$ backgrounds can be significantly reduced.

If we take advantage of these features, it will be possible to measure the B decays listed in Table 4.2. Some of these decays have more than one neutrino in the final states. Therefore, it is very difficult to perform such studies even in the clean environment of e^+e^- collider unless the full reconstruction B tagging is applied.

Since the tagging efficiency is very low [$\mathcal{O}(0.1\%)$], this method has not been extensively applied at the current B factory experiments. However, a very large B meson sample at SuperKEKB will make it possible to extract useful results.

Decay mode	Motivation
$B \to X_u l\nu$	Precise measurement of $\|V_{ub}\|$
$B \to \tau\nu$	Measurement of f_B
$B \to K\nu\bar{\nu}$, $D\tau\nu$	Search for new physics
Inclusive B decays	Detailed study, model independent analysis etc.

Table 4.2: Physics topics that will be studied with the fully-reconstructed B sample.

Hadronic B Tagging

Most B meson decays are hadronic decays. However, the branching fraction of each individual mode is less than $\mathcal{O}(1\%)$. Therefore, we need to collect as many modes as possible to achieve a high efficiency. In Fig. 4.1, the beam-constrained mass distribution for the main decay modes, $B \to D^{(*)}(\pi, \rho, a_1)^-$, are shown. The yields including other decay modes are also shown in Table 4.3. With a 152 million $B\bar{B}$ sample, we already have a sample of more than 10^5 fully-reconstructed B meson tags. The tagging efficiency is around 0.2 (0.1) % for charged (neutral) B mesons with a purity around 80% [4].

If a B meson is reconstructed semi-inclusively, we can further improve the efficiency. At BaBar, the $B \to D^{(*)}(n_1\pi^{\pm}n_2K^{\pm}n_3K_Sn_4\pi^0)^-$ process is reconstructed, where $n_1 + n_2 \leq 5$, $n_3 \leq 2$ and $n_4 \leq 2$. As a result, the higher efficiency, 0.5 (0.3) % for charged (neutral) B mesons, is obtained. However, due to combinatoric backgrounds, the purity is only around 25 %. These samples are used for the $|V_{ub}|$ measurement using $B \to X_u l\nu$ decays, where the background can be reduced by requiring a lepton in the recoil side [5] [6].

	decay mode	yield	eff. (%)	purity(%)
Charged B	$B^- \to D^{(*)0}(\pi, \rho, a_1)^-$	132723	0.17	79
	$B^- \to D^{(*)0} D_s^{(*)-}$	8700	0.01	60
	$B^- \to J/\psi K^-$	9373	0.01	96
	total	150796	0.20	78
Neutral B	$\bar{B^0} \to D^{(*)+}(\pi, \rho, a_1)^-$	56898	0.07	85
	$\bar{B^0} \to D^{(*)+} D_s^{(*)-}$	4390	0.006	60
	$\bar{B^0} \to (J/\psi, \psi(2s), \chi_{c1}) K_S$, $J/\psi K^{*0}$	7275	0.01	94
	total	68563	0.09	83

Table 4.3: Full reconstructed B events for hadronic modes with 152 million $B\bar{B}$ sample.

Semileptonic B tagging

In semileptonic B decays, we cannot use information about the B momentum vector due to the missing neutrino. However, we still have relatively clean tagged samples. Semileptonic B decays are dominated by $B \to Dl\nu$ and $D^*l\nu$, with a total branching fraction of around 15%. At Belle, these samples were used for a $|V_{ub}|$ measurement with inclusive $B \to X_u l\nu$ decays. If we require a semileptonic decay on the recoil side, we can apply a kinematical constraint, and the B momentum vector can be determined with a two-fold ambiguity. The background contribution is significantly suppressed in this case. This method yields a $B \to D^*l\nu$ efficiency of 0.3 (0.2)% for charged (neutral) B decays [7].

It is also notable that we can utilize other $B \to DXl\nu$ decays as B tags in the $Dl\nu$ mode, because the signal in the missing mass spectrum is too broad for separation. The missing mass distribution for $B^- \to D^0 l\nu$ is shown in Fig. 4.2. Tagging efficiency is estimated to be 1.7% including the contribution from the $B^- \to D^{(*)0} l\nu$ decays of around 15% [4]. Other background is mostly combinatoric. Although the tagging quality is not good in this case, it is still useful for the study of rare B decays with low track multiplicities in the final states. In BaBar, this method was used to search for the $B \to K\nu\bar{\nu}$ and $\tau\nu$ decays [8] [9] to provide improved upper limits.

Conclusions

In summary, the tagging efficiency will be around 0.2% for the clean hadronic B tagging and around 1% for the semileptonic B tagging that has a lower purity. With 1 ab^{-1} of data, there will be 2 million clean tags and 10 million semileptonic tags. With these samples, the physics topics listed in Table 4.2 will be studied.

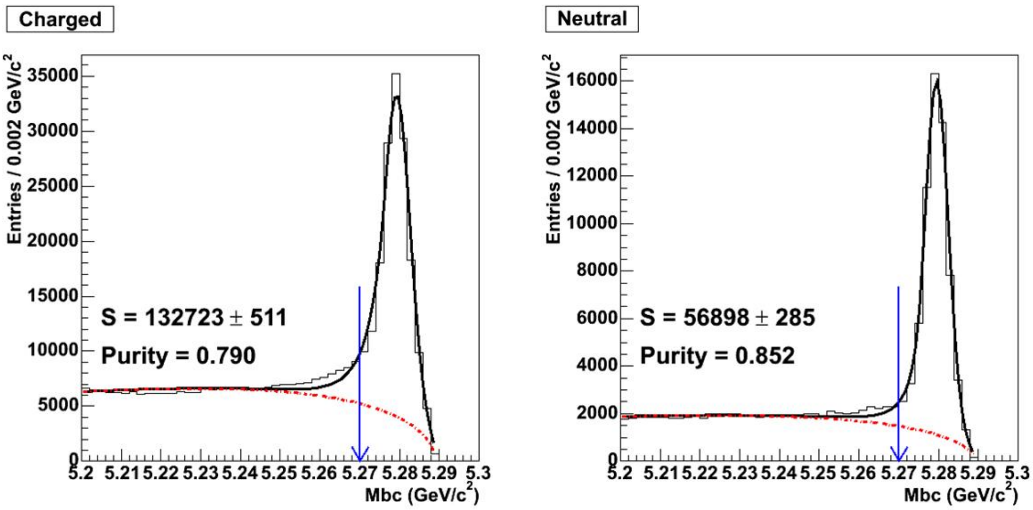

Figure 4.1: Beam-constrained mass distribution for $B \to D^{(*)}(\pi, \rho, a_1)^-$ with the 152 million $B\bar{B}$ sample recorded by Belle.

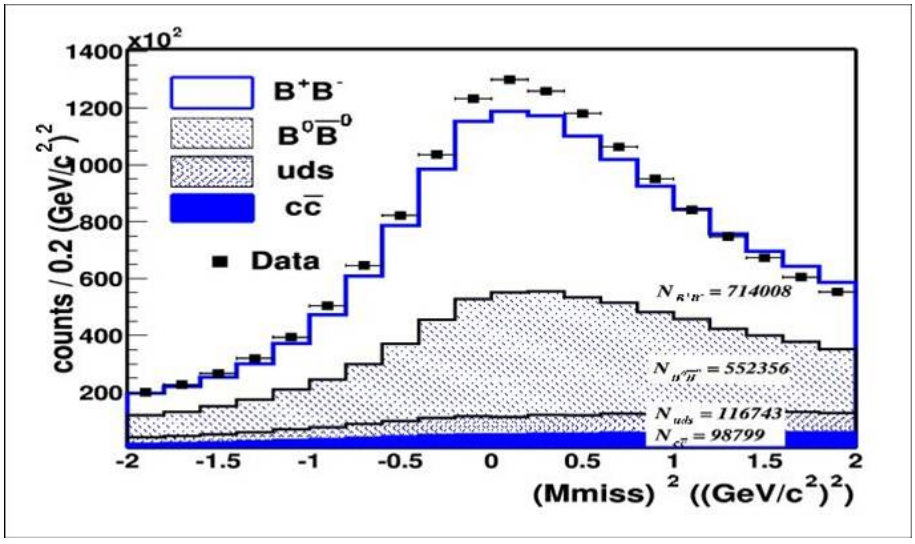

Figure 4.2: Missing mass squared distribution for $B^- \to D^0 l\nu$ with a sample of 85×10^6 $B\bar{B}$ pairs.

4.2 New CP-violating phase in $b \to s\overline{q}q$

4.2.1 Introduction

Despite the great success of the KM mechanism, additional CP-violating phases are inevitable in most theories involving new physics (NP) beyond the SM [10]. Some of them allow large deviations from the SM predictions for B meson decays. Examples of such theories include supersymmetric grand-unified theories with the see-saw mechanism that can accommodate large neutrino mixing [11]. Therefore it is of fundamental importance to measure CP asymmetries that are sensitive to the difference between the SM and NP. Additional sources of CP violation are also highly desirable to understand the origin of the matter-antimatter asymmetry of the universe; detailed studies have found no way that CP violation in the SM alone could explain baryogenesis [12]. Many methods to search for a new source of CP violation in B meson decays have been proposed up to now. One of the most promising ways is to compare the mixing-induced CP asymmetries in the $B \to \phi K^0_S$ decay [13], which is dominated by the $b \to s\bar{s}s$ transition that is known to be sensitive to possible NP effects, with those in the $B^0 \to J/\psi K^0_S$ decay [14]. Ignoring a strong phase difference between the amplitude of NP ($A_{\rm NP}$) and SM ($A_{\rm SM}$)[1], we obtain

$$\mathcal{S}_{\phi K^0_S} = \frac{\sin 2\phi_1 + 2\rho \sin(2\phi_1 + \Theta_{\rm NP}) + \rho^2 \sin(2\phi_1 + 2\Theta_{\rm NP})}{1 + \rho^2 + 2\rho \cos\Theta_{\rm NP}}, \tag{4.3}$$

where $\rho \equiv A_{\rm NP}/A_{\rm SM}$ is an amplitude ratio of NP to the SM. Since $\mathcal{S}_{J/\psi K^0_S} \simeq \sin 2\phi_1$ is expected in many extensions of the SM, the difference $\Delta\mathcal{S}_{\phi K^0_S} \equiv (-\xi_f)\mathcal{S}_{\phi K^0_S} - \mathcal{S}_{J/\psi K^0_S}$ is a gold-plated observable to search for a new CP-violating phase.

Recent measurements by Belle [15] and BaBar [16] collaborations yield values smaller than the SM expectation; a difference by 2.6 standard deviations is obtained when two results are combined. The other charmless decays $B^0 \to \eta' K^0_S$ and $B^0 \to K^+K^-K^0_S$, which are mediated by $b \to s\bar{s}s$, $s\bar{u}u$ and $s\bar{d}d$ transitions, also provide additional information [15, 16]. The present world average with $B^0 \to \phi K^0_S$, $\eta' K^0_S$ and $K^+K^-K^0_S$ combined is different from the average with $B^0 \to J/\psi K^0_S$ and related modes by 3.1 standard deviations [17] as shown in Fig. 4.3. Possible theoretical implications of these measurements are already discussed in Section 3.4.

In this section we describe the expected sensitivities for $\mathcal{S}(\phi K^0_S)$, $\mathcal{S}(\eta' K^0_S)$ and $\mathcal{S}(K^+K^-K^0_S)$ based on the measurements performed with the present Belle detector. It will be crucial to measure as many observables as possible and to check correlations among them. Therefore we also describe several other new methods to access a new CP-violating phase in the $b \to s$ transition.

4.2.2 $B^0 \to \phi K^0_S$, $\eta' K^0_S$ and $K^+K^-K^0_S$

As mentioned in the previous section, the $B^0 \to \phi K^0_S$ decay is one of the most promising decays in which to search for a new CP-violating phase in $b \to s\bar{s}s$ transitions. The other charmless decays $B^0 \to \eta' K^0_S$ and $B^0 \to K^+K^-K^0_S$ provide additional information. As most of the experimental procedure for these three modes is common, we discuss them here together. Note that the theoretical uncertainties for $\Delta\mathcal{S}$ within the SM depend on the decay mode. We discuss this issue in Section 4.2.5. Note also that the three-body decay $B^0 \to K^+K^-K^0_S$ is in general a mixture of CP-even and CP-odd eigenstates. The Belle collaboration finds that the $K^+K^-K^0_S$ state is primarily $\xi_f = +1$; a measurement of the $\xi_f = +1$ fraction with a 140 fb^{-1} data set

[1] The formula with the strong phase is given in Section 3.4 [Eq. 3.10].

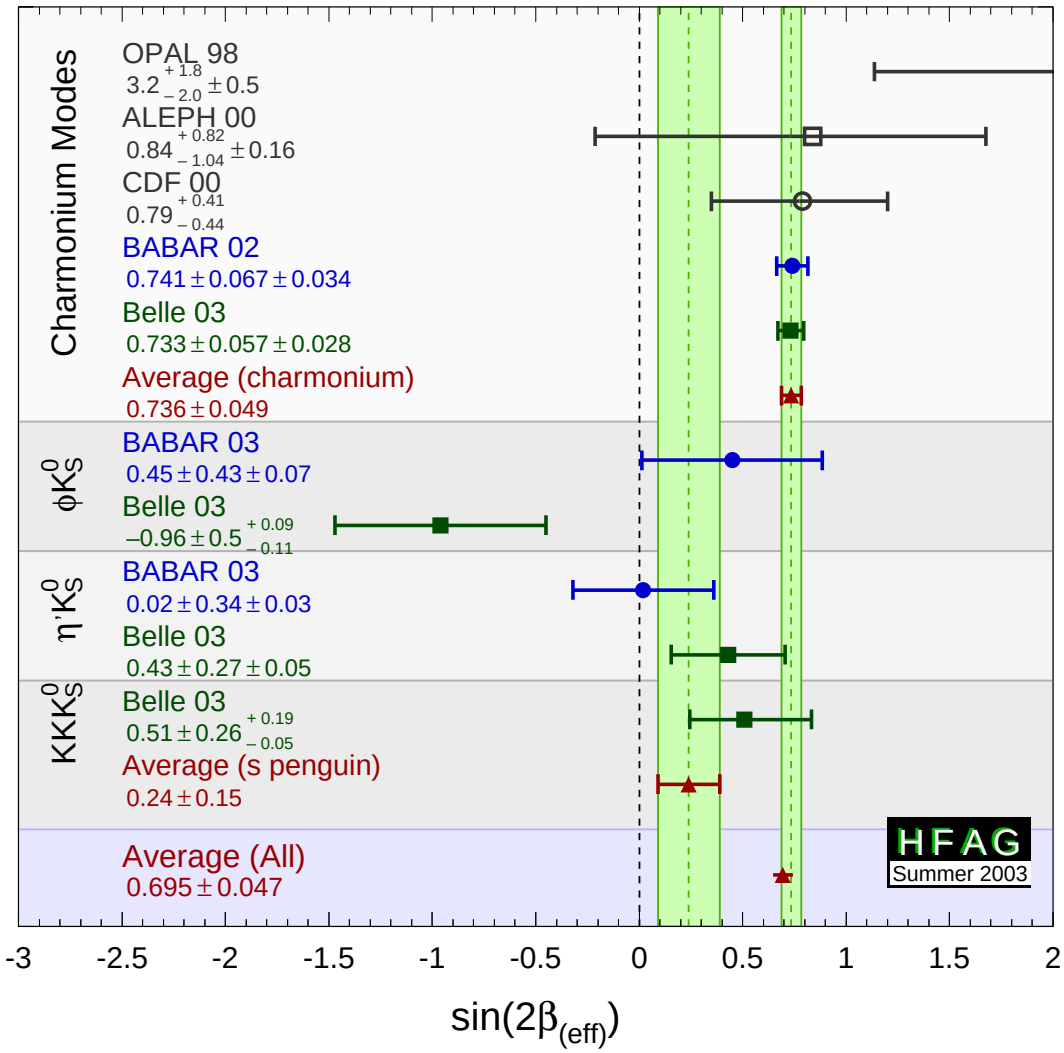

Figure 4.3: $\mathcal{S}$ terms measured with decay modes governed by $b \to c\bar{c}s$ or $b \to s\bar{s}s$ transitions.

yields $1.03 \pm 0.15(\text{stat}) \pm 0.05(\text{syst})$ [15]. The uncertainty in the CP-asymmetry parameters, which arises from the $\xi_f = -1$ component, is included in the systematic error.

We estimate the expected sensitivities at SuperKEKB by extrapolating the present experimental results. Therefore we first explain Belle's analysis with a data sample of 140 fb^{-1} [15]. We reconstruct B^0 decays to ϕK^0_S and $\eta' K^0_S$ final states for $\xi_f = -1$, and $B^0 \to K^+K^-K^0_S$ decays that are a mixture of $\xi_f = +1$ and -1. K^+K^- pairs that are consistent with $\phi \to K^+K^-$ decay are excluded from the $B^0 \to K^+K^-K^0_S$ sample. We find that the $K^+K^-K^0_S$ state is primarily $\xi_f = +1$; a measurement of the $\xi_f = +1$ fraction with a 140 fb^{-1} data set yields $1.03 \pm 0.15(\text{stat}) \pm 0.05(\text{syst})$. In the following determination of $\mathcal{S}$ and $\mathcal{A}$, we fix $\xi_f = +1$ for this mode. The intermediate meson states are reconstructed from the following decay chains: $\eta' \to \rho^0(\to \pi^+\pi^-)\gamma$ or $\eta' \to \pi^+\pi^-\eta(\to \gamma\gamma)$, $K^0_S \to \pi^+\pi^-$, and $\phi \to K^+K^-$. Pairs of oppositely charged tracks are used to reconstruct $K^0_S \to \pi^+\pi^-$ decays. The $\pi^+\pi^-$ vertex is required to be displaced from the IP by a minimum transverse distance of 0.22 cm for high momentum (> 1.5 GeV/c) candidates and 0.08 cm for those with momentum less than 1.5 GeV/c. The direction of the pion pair momentum must agree with the direction defined by the IP and the vertex displacement within 0.03 rad for high-momentum candidates, and within 0.1 rad for the remaining candidates. Candidate $\phi \to K^+K^-$ decays are found by selecting pairs of oppositely charged tracks that are not pion-like ($P(K/\pi) > 0.1$), where a kaon likelihood ratio, $P(K/\pi) = \mathcal{L}_K/(\mathcal{L}_K + \mathcal{L}_\pi)$, has values between 0 (likely to be a pion) and 1 (likely to be a kaon). The likelihood $\mathcal{L}_{K(\pi)}$ is derived from dE/dx, ACC and TOF measurements. The vertex of the candidate charged tracks is required to be consistent with the interaction point (IP) to suppress poorly measured tracks. In addition, candidates are required to have a K^+K^- invariant mass that is less than 10 MeV/c^2 from the nominal ϕ meson mass. Since the ϕ meson selection is effective in reducing background events, we impose only minimal kaon-identification requirements. We use more stringent kaon-identification requirements to select non-resonant K^+K^- candidates for the $B^0 \to K^+K^-K^0_S$ decay. We reject K^+K^- pairs that are consistent with $D^0 \to K^+K^-$, $\chi_{c0} \to K^+K^-$, or $J/\psi \to K^+K^-$ decay. $D^+ \to K^0_S K^+$ candidates are also removed. To reconstruct η' candidates, we first require that all of the tracks have associated SVD hits and radial impact parameters $|dr| < 0.1$ cm projected on the r-ϕ plane. Particle identification information from the ACC, TOF and CDC dE/dx measurements are used to form a likelihood ratio in order to distinguish pions from kaons with at least 2.5σ separation for laboratory momenta up to 3.5 GeV/c. Candidate photons from $\eta_{\gamma\gamma}$ ($\eta'_{\rho\gamma}$) decays are required to be isolated and have $E_\gamma > 50$ (100) MeV from the ECL measurement. The invariant mass of $\eta_{\gamma\gamma}$ candidates is required to be between 500 MeV/c^2 and 570 MeV/c^2. A kinematic fit with an η mass constraint is performed using the fitted vertex of the $\pi^+\pi^-$ tracks from the η' as the decay point. For $\eta'_{\rho\gamma}$ decays, the candidate ρ^0 mesons are reconstructed from pairs of vertex-constrained $\pi^+\pi^-$ tracks with an invariant mass between 550 and 920 MeV/c^2. The η' candidates are required to have a reconstructed mass from 940 to 970 MeV/c^2 for the $\eta'_{\eta\pi\pi}$ mode and 935 to 975 MeV/c^2 for $\eta'_{\rho\gamma}$ mode. Charged $K^\pm$ candidates are selected for the decay $B^\pm \to \eta' K^\pm$ based on the particle identification information. We also reconstruct events where only one of the charged pions has associated SVD hits. In this case, the requirement on the impact parameter is relaxed for the track without SVD hits, while a higher threshold is imposed on the likelihood ratio. For reconstructed $B \to f_{CP}$ candidates, we identify B meson decays using the energy difference $\Delta E \equiv E_B^{\rm cms} - E_{\rm beam}^{\rm cms}$ and the beam-energy constrained mass $M_{\rm bc} \equiv \sqrt{(E_{\rm beam}^{\rm cms})^2 - (p_B^{\rm cms})^2}$, where $E_{\rm beam}^{\rm cms}$ is the beam energy in the cms, and $E_B^{\rm cms}$ and $p_B^{\rm cms}$ are the cms energy and momentum of the reconstructed B candidate, respectively. The B meson signal region is defined as $|\Delta E| < 0.06$ GeV for $B^0 \to \phi K^0_S$, $|\Delta E| < 0.04$ GeV for $B^0 \to K^+K^-K^0_S$, $|\Delta E| < 0.06$ GeV for $B^0 \to \eta'(\to \rho\gamma)K^0_S$, or -0.10 GeV $< \Delta E < 0.08$ GeV

Mode	ξ_f	$N_{\rm sig}$	Purity	Statistical error	
				$\mathcal{S}$	$\mathcal{A}$
ϕK^0_S	-1	2400	0.64	0.074	0.051
$K^+K^-K^0_S$	$+1(100\%)$	7100	0.55	0.040	0.028
$\eta' K^0_S$	-1	8700	0.58	0.042	0.028

Table 4.4: Expected numbers of $B^0 \to f_{CP}$ signal events, $N_{\rm sig}$, and estimated signal purities in the ΔE-$M_{\rm bc}$ signal region for each f_{CP} mode at 5 ab^{-1}.

for $B^0 \to \eta'(\to \pi^+\pi^-\eta)K^0_S$, and 5.27 GeV/$c^2$ $< M_{\rm bc} <$ 5.29 GeV/c^2 for all decays. In order to suppress background from the $e^+e^- \to u\bar{u}$, $d\bar{d}$, $s\bar{s}$, or $c\bar{c}$ continuum, we form signal and background likelihood functions, $\mathcal{L}_{\rm S}$ and $\mathcal{L}_{\rm BG}$, from a set of variables that characterize the event topology, and impose thresholds on the likelihood ratio $\mathcal{L}_{\rm S}/(\mathcal{L}_{\rm S} + \mathcal{L}_{\rm BG})$. The threshold value depends both on the decay mode and on the flavor-tagging quality.

The vertex reconstruction, flavor tagging and the unbinned maximum likelihood fit to the Δt distributions are the same as those described for the $\sin 2\phi_1$ measurement (Section 4.6) with $B^0 \to J/\psi K^0_S$ decays. By using the identical procedure for both cases, we can reduce the systematic uncertainties in the differences $\Delta\mathcal{S}_{\phi K^0_S} \equiv \mathcal{S}_{\phi K^0_S} - \mathcal{S}_{J/\psi K^0_S}$ etc.

After flavor tagging and vertex reconstruction, we expect the signal yields and the purities listed in Table 4.4. Figure 4.4 shows the $M_{\rm bc}$ distributions for the reconstructed B candidates that have ΔE values within the signal region. Unbinned maximum likelihood fits yield expected

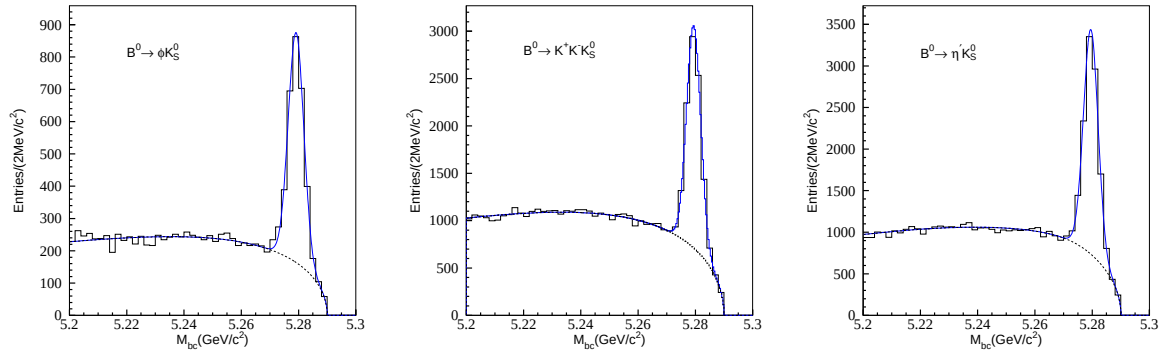

Figure 4.4: Beam-constrained mass ($M_{\rm bc}$) distributions for (left) $B^0 \to \phi K^0_S$, (middle) $B^0 \to K^+K^-K^0_S$, and (right) $B^0 \to \eta' K^0_S$ decays within the ΔE signal region expected at 5 ab^{-1}. Solid curves show results of fits to signal plus background distributions, and dashed curves show the background contributions.

statistical errors on $\mathcal{S}$ and $\mathcal{A}$ shown also in Table 4.4. It is seen that errors are rather small even for these rare B decays. Hence systematic uncertainties become crucial.

Major sources of the systematic uncertainties on $\mathcal{S}$ and $\mathcal{A}$ are common to those for $B^0 \to J/\psi K^0_S$, which will be described in Section 4.6. For the $K^+K^-K^0_S$ mode, the CP-even fraction is expected to be determined more precisely as the integrated luminosity increases. Therefore we assume that the systematic uncertainty due to the uncertainty in the CP-even fraction is *reducible*; e.g. it is proportional to $1/\sqrt{\mathcal{L}_{\rm tot}}$. An additional systematic error for $B^0 \to \phi K^0_S$ arises from the $B^0 \to f_0 K^0_S$ and $K^+K^-K^0_S$ backgrounds. These background fractions

Mode	5 ab^{-1}		50 ab^{-1}	
	$\Delta\mathcal{S}$	$\Delta\mathcal{A}$	$\Delta\mathcal{S}$	$\Delta\mathcal{A}$
ϕK^0_S	0.079	0.055	0.031	0.024
$K^+K^-K^0_S$	0.056	0.036	0.026	0.020
$\eta' K^0_S$	0.049	0.035	0.024	0.019

Table 4.5: Expected total errors on $\Delta\mathcal{S}$ and $\Delta\mathcal{A}$ at 5 ab^{-1} and 50 ab^{-1}.

are estimated at 140 fb^{-1} from the K^+K^- invariant mass distribution to be $1.6^{+1.9}_{-1.5}$% and 7.2 ± 1.7%, respectively. We assume that the errors on these fractions will be reduced as the integrated luminosity increases. We also assume that the CP-violating parameters for these decays are also determined experimentally with errors that will also decrease as the integrated luminosity increases. Therefore, the systematic errors on $\mathcal{S}$ and $\mathcal{A}$ due to these backgrounds are also assumed to be *reducible*.

Some of the systematic errors cancel when we calculate $\Delta\mathcal{A}$ or $\Delta\mathcal{S}$. For example, the effect of the tag-side interference cancels in $\Delta\mathcal{A}_{\phi K^0_S}$ and $\Delta\mathcal{S}_{\phi K^0_S}$ since it causes a bias in the same direction for $\mathcal{S}_{\phi K^0_S}$ and $\mathcal{S}_{J/\psi K^0_S}$ measurements. On the other hand, a special care on the systematic bias from the tag-side interference needs to be taken for $\Delta\mathcal{A}_{K^+K^-K^0_S}$. In this case, the effect does not cancel because the bias has the opposite sign to each other. We use information from $B^0 \to J/\psi K^0_L$ decays to reduce this uncertainty on $\Delta\mathcal{A}_{K^+K^-K^0_S}$.

Figure 4.5 shows the resulting total errors on $\Delta\mathcal{S}$ and $\Delta\mathcal{A}$ as a function of integrated luminosity. Table 4.5 also shows the corresponding values at 5 ab^{-1} and 50 ab^{-1}.

Based on the above estimates, we perform Feldman-Cousins analyses to obtain 5σ discovery regions at 5 ab^{-1} and at 50 ab^{-1} in the 2-dimensional plane of $\mathcal{A}$ and $\mathcal{S}$. Results are shown in Fig. 4.6. At SuperKEKB, even a small deviation of $\Delta\mathcal{S} \sim 0.1$ can be established with a 5σ significance as far as the statistical and systematic errors are concerned. Therefore it is important to understand levels of theoretical uncertainties within the SM very well. This issue will be discussed in Section 4.2.5.

4.2.3 $B^0 \to K^0_S K^0_S K^0_S$ and $\pi^0 K^0_S$

In this section we discuss the feasibility of time-dependent CP asymmetry measurements using only a K^0_S and a constraint from the interaction point to determine the B decay vertices. In particular, we consider $B^0 \to K^0_S K^0_S K^0_S$ and $\pi^0 K^0_S$ decays as the most promising modes in this class of decays to study a new CP-violating phase in $b \to s$ transitions. Recently, the BaBar collaboration has succeeded in measuring the B decay vertex in $B^0 \to K^0_S \pi^0$ [18]. The possibility of obtaining B vertex information from K^0_S mesons makes time-dependent analyses of these decays feasible.

$B^0 \to K^0_S K^0_S K^0_S$

Recently it was pointed out [19] that in decays of the type $B^0 \to P^0 Q^0 X^0$, where P^0, Q^0 and X^0 represent any CP eigenstate spin-0 neutral particles, the final state is a CP eigenstate. First we give a brief proof of this statement. In what follows, L denotes the angular momentum of the P^0Q^0 system, and L' denotes the angular momentum of X^0 relative to the P^0Q^0 system. By conservation of angular momentum in the decay $B^0 \to P^0Q^0X^0$, we obtain

$$\mathbf{J}_{B^0} \;=\; \mathbf{L} + \mathbf{L}' + \mathbf{S}_{P^0} + \mathbf{S}_{Q^0} + \mathbf{S}_{X^0} \tag{4.4}$$

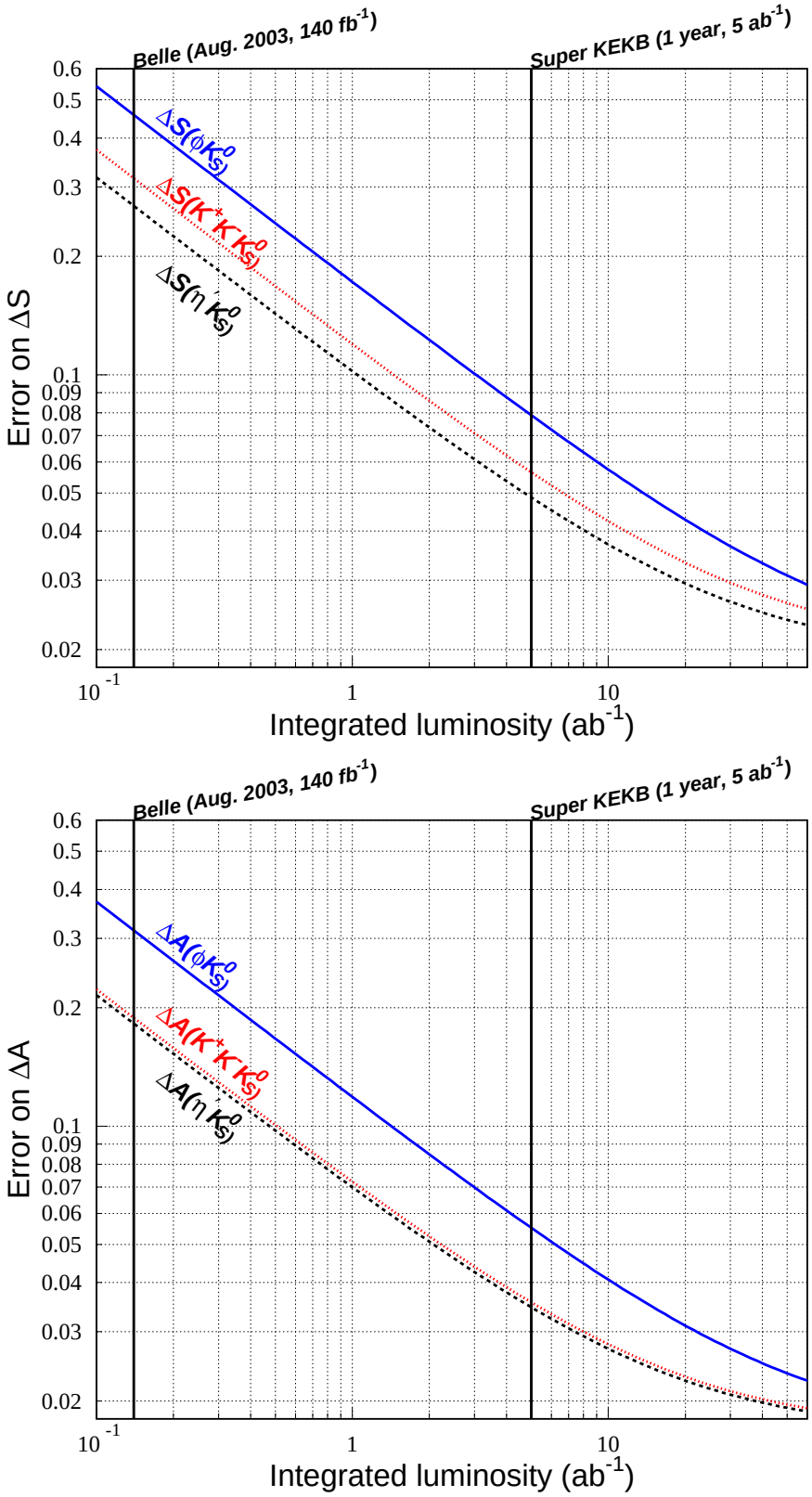

Figure 4.5: Expected total errors on $\Delta\mathcal{S}$ (top) and $\Delta\mathcal{A}$ (bottom) as a function of integrated luminosity.

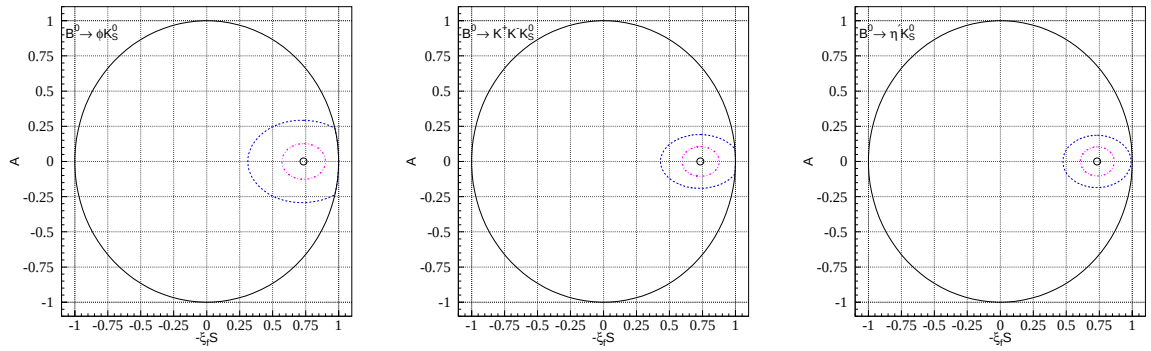

Figure 4.6: 5σ confidence regions for $\mathcal{A}$ and $\mathcal{S}$ in (left) $B^0 \to \phi K^0_S$, (middle) $B^0 \to K^+K^-K^0_S$ and (right)$B^0 \to \eta' K^0_S$ decays at 5 ab^{-1} and 50 ab^{-1}. Input values are $\mathcal{S} = 0.73$ and $\mathcal{A} = 0$.

$$\mathbf{0} \quad = \quad \mathbf{L} + \mathbf{L}', \tag{4.5}$$

since the neutral B meson is a spin-0 particle, as are P^0, Q^0 and X^0. In the above equations, $\mathbf{J}$, $\mathbf{L}$ and $\mathbf{S}$ represent the total, orbital and intrinsic angular momentum, respectively (and elsewhere J, L and S represent their magnitudes). Therefore, the angular momentum between the P^0Q^0 system and X^0 (L') must be equal to L, and we can write down the CP of the $P^0P^0X^0$ system:

$$\begin{aligned} CP\left(P^0Q^0X^0\right) &= CP\left(P^0\right) \times CP\left(Q^0\right) \times CP\left(X^0\right) \times (-1)^L \times (-1)^{L'} & (4.6) \\ &= CP\left(P^0\right) \times CP\left(Q^0\right) \times CP\left(X^0\right). & (4.7) \end{aligned}$$

Thus there are many three-body B decays that can be used in time-dependent CP asymmetry measurements *without any angular analysis*. In particular, the decay $B^0 \to K^0_S K^0_S K^0_S$ is promissing. In terms of phenomenology, it has an advantage over $B^0 \to K^+K^-K^0_S$, since the latter includes a contribution from the $b \to u$ tree diagram, which has a different weak phase. Although this contribution ("tree pollution") is expected to be small as will be discussed in Section 4.2.5, it might be an issue at SuperKEKB. In the case of $B^0 \to K^0_S K^0_S K^0_S$, however, there is no u quark in the final state. The $b \to s\bar{u}u$ tree diagram followed by rescattering into $s\bar{d}d$ or $s\bar{s}s$ is OZI-suppressed. Therefore these are almost pure penguin decays. There can be contributions from both $b \to s\bar{s}s$ with additional $d\bar{d}$ production, and $b \to s\bar{d}d$ with additional $s\bar{s}$ production, but these diagrams have the same weak phase. Any new physics contribution expected in the $B^0 \to \phi K^0_S$ decay can also affect $B^0 \to K^0_S K^0_S K^0_S$, and in the absence of new physics it should exhibit the same CP violating effects as $J/\psi K^0_S$.

Turning to experimental considerations, we note that this mode has been observed at Belle [20]. From 78 fb^{-1} of data recorded on the $\Upsilon(4S)$ resonance, $12.2^{+4.5}_{-3.8}$ signal events are found. From Fig. 4.7 (left), we can count the number of candidates in the region -0.1 GeV $< \Delta E < 0.1$ GeV, to estimate the signal purity. There are 21 candidates in this region giving a purity of $\sim$0.6, which is approximately the same purity as $\eta' K^0_S$. The efficiency to reconstruct a K^0_S vertex reflects the probability for the K^0_S to decay inside the vertex detector, and so depends on the K^0_S momentum and on the size of the vertex detector. In a three body $B^0 \to K^0_S K^0_S K^0_S$ decay, at least one K^0_S must have fairly low momentum in the B^0 rest frame. Therefore, we expect a high vertex efficiency for $B^0 \to K^0_S K^0_S K^0_S$, if the vertex efficiency for $B^0 \to K^0_S \pi^0$ (where the K^0_S has high momentum) is moderate. In the time-dependent analysis

of $B^0 \to K^0_S\pi^0$ by the BaBar collaboration, a vertex efficiency of 65% is obtained [18]. Since the size of SuperKEKB vertex detector is comparable to the BaBar SVT, we expect that vertex efficiencies for $B^0 \to K^0_S K^0_S K^0_S$ of close to 100% may be obtained. Using these assumptions, we estimate the statistical error on $\mathcal{S}_{K^0_S K^0_S K^0_S}$) to be

$$\begin{aligned} \delta\mathcal{S}_{K^0_S K^0_S K^0_S} &= 0.14 \text{ (at 5 ab}^{-1}\text{)} \\ \delta\mathcal{S}_{K^0_S K^0_S K^0_S} &= 0.04 \text{ (at 50 ab}^{-1}\text{)}. \end{aligned} \tag{4.8}$$

$B^0 \to \pi^0 K^0_S$

The authors in Ref. [21] claim that $K_S\pi^0$ is one of the gold-plated modes to study a new CP-violating phase in the $b \to s$ transition. As mentioned before, the BaBar group recently showed a preliminary result on the time-dependent CP asymmetries in this decay, demonstrating the feasibility of measuring the B meson decay point using only a K^0_S and the interaction point constraint.

Belle's result based on 78 fb^{-1} of data is shown in Fig. 4.7 (right). The signal yield is 72.6 ± 14.0. Since this estimation includes the tail region in the ΔE distribution where rare B decay backgrounds are not negligible, a more stringent selection is necessary for the time-dependent CP asymmetry measurements. Using $|\Delta E| < 0.1$ GeV and assuming a vertex reconstruction efficiency of 50%, the signal yield with reconstructed vertices at 5 ab^{-1} is ∼1900 for a purity of 0.46. Based on these numbers, we obtain

$$\begin{aligned} \delta\mathcal{S}_{\pi^0 K^0_S} &= 0.10 \text{ (at 5 ab}^{-1}\text{)} \\ \delta\mathcal{S}_{\pi^0 K^0_S} &= 0.03 \text{ (at 50 ab}^{-1}\text{)}. \end{aligned} \tag{4.9}$$

4.2.4 $B^\pm \to \phi\phi X^\pm_s$

In this section we discuss a new method to study direct CP violation that arises from a new CP-violating phase in $B^\pm \to \phi\phi X^\pm_s$ decays [23]. Here $X^\pm_s$ represents a final state with a specific strange flavor such as $K^\pm$ or $K^{*\pm}$. These non-resonant direct decay amplitudes are dominated by the $b \to s\bar{s}s\bar{s}s$ transition. A contribution from the $b \to u\bar{u}s$ transition followed by rescattering into $s\bar{s}s$ is expected to be below 1% because of CKM suppression and the OZI rule [23]. In these decays, when the invariant mass of the $\phi\phi$ system is within the η_c resonance region, they interfere with the $B^\pm \to \eta_c(\to \phi\phi)X^\pm_s$ decay that is dominated by the $b \to c\bar{c}s$ transition. The decay width of η_c is sufficiently large [24, 25] to provide a sizable interference. Within the SM, this interference does not cause sizable direct CP violation because there is no weak phase difference between the $b \to s\bar{s}s\bar{s}s$ and the $b \to c\bar{c}s$ transitions. On the other hand, a NP contribution with a new CP-violating phase can create a large weak phase difference. Thus large CP asymmetries can appear only from NP amplitudes, and an observation of direct CP violation in these decays is an unambiguous manifestation of physics beyond the SM. Although the same argument so far is applicable to the $B^\pm \to \phi X^\pm_s$ decays, there is no guaranteed strong phase difference that is calculable reliably for these decays. In contrast, the Breit-Wigner resonance provides the maximal strong phase difference in the case of $B^\pm \to (\phi\phi)_{m\sim m_{\eta_c}} X^\pm_s$ decays. Since present experimental knowledge of the decay rate for $b \to s\bar{s}s$ is still limited, a large CP asymmetry up to 0.4 is allowed.

The Belle Collaboration recently announced evidence for $B \to \phi\phi K$ decays [26]. The signal purity is close to 100% when the $\phi\phi$ invariant mass is within the η_c mass region. Belle [25] has

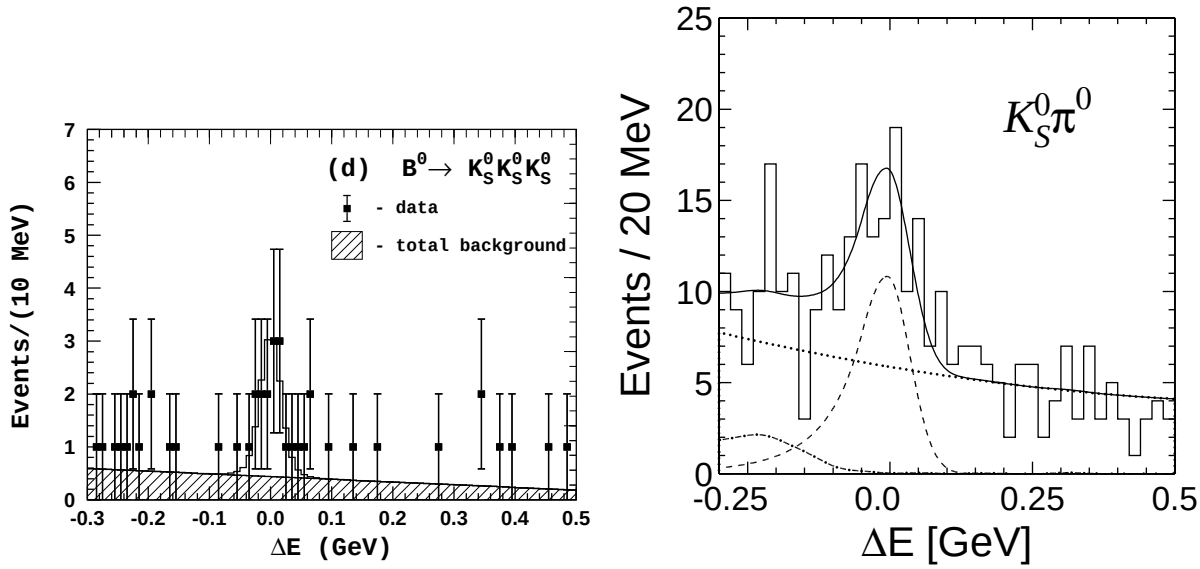

Figure 4.7: (left) Observation of $B^0 \to K^0_S K^0_S K^0_S$ [20]. From 78 fb^{-1} of data recorded on the $\Upsilon(4S)$ resonance, a signal yield of $12.2^{+4.5}_{-3.8}$ is obtained, leading to a branching fraction of $\mathcal{B}\left(B^0 \to K^0_S K^0_S K^0_S\right) = \left(4.2^{+1.6}_{-1.3} \pm 0.8\right) \times 10^{-6}$. (right) Observation of $B^0 \to K^0_S \pi^0$ [22]. From 78 fb^{-1} of data recorded on the $\Upsilon(4S)$ resonance, a signal yield of 72.6 ± 14.0 is obtained, leading to a branching fraction of $\mathcal{B}\left(B^0 \to K^0_S K^0_S K^0_S\right) = (11.7 \pm 2.3^{+1.2}_{-1.3}) \times 10^{-6}$.

also reported the first observation of the $B^0 \to \eta_c K^{*0}$ decay. This implies that other modes such as $B^+ \to \eta_c K^{*+}$ will also be seen with a similar branching fraction, so that we will be able to study semi-inclusive $B^\pm \to \eta_c X_s^\pm$ transitions experimentally. The semi-inclusive branching fraction of $B^\pm \to \eta_c X_s^\pm$ is not yet measured, but is expected to be comparable to the branching fraction of the semi-inclusive decay $B^\pm \to J/\psi X_s^\pm$ [27].

We have performed Monte Carlo simulation for the $B^\pm \to \phi\phi K^\pm$ decay and estimated statistical errors on the CP asymmetry parameter. The procedure and the fit parameters are the same as those described in Ref. [23]. The reconstruction efficiency and the $\phi\phi$ mass resolution are estimated using a GEANT-based detector simulator for the present Belle detector [30]. We perform an unbinned maximum-likelihood fit to the differential decay rate distribution. Figure. 4.8 shows the 5σ search regions at 5 ab^{-1} (dotted line) and at 50 ab^{-1} (solid line), where r^2 is the ratio between the NP amplitude and the SM amplitude, and $\Theta_{\rm NP}$ is the CP-violating phase from NP. Direct CP violation can be observed in a large parameter space with significance above 5σ.

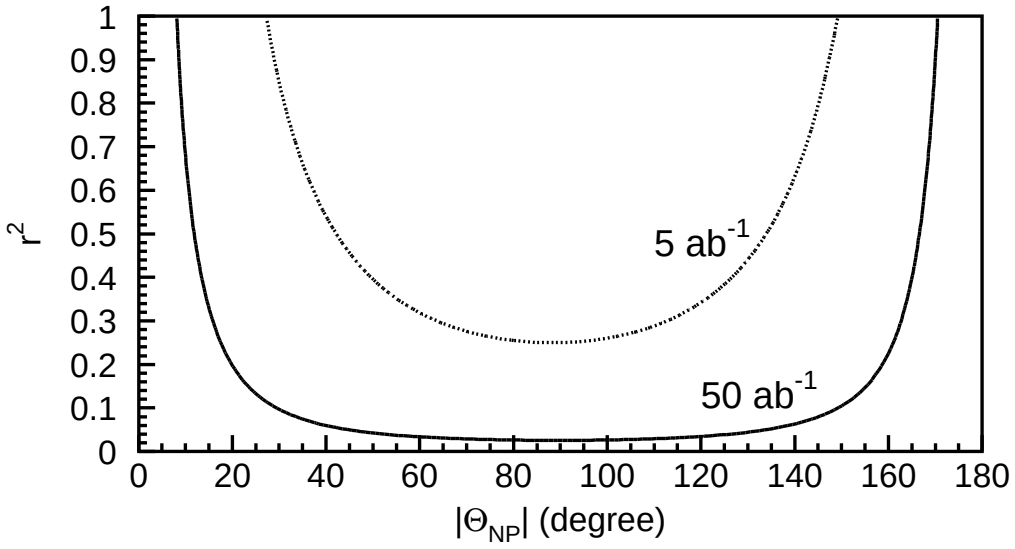

Figure 4.8: Expected sensitivities on direct CP violation in the $B^\pm \to \phi\phi K^\pm$ decay at 5 ab^{-1} (dotted line) and at 50 ab^{-1} (solid line). In the regions above the curves, direct CP violation can be measured with a 5σ significance or larger.

Figure. 4.9 shows the expected significance of the new phase $\Theta_{\rm NP}$ at 5 ab^{-1} for $B^\pm \to \phi\phi K^\pm$ decay ($r^2 = 0.5$) and for time-dependent CP violation in the $B^0 \to \phi K_S^0$ decay ($|A_{\rm NP}/A_{\rm SM}|^2 = 0.5$). The significance for $\Delta\mathcal{S}_{\phi K_S^0}$ depends on the sign of $\Theta_{\rm NP}$, which is not the case for the $B^\pm \to \phi\phi K^\pm$ decay. The sign dependence arises from an asymmetric range for $\Delta\mathcal{S}_{\phi K_S^0}$; to a good approximation, we have $-1-\sin 2\phi_1 \leq \Delta\mathcal{S} \leq 1-\sin 2\phi_1$ where $\sin 2\phi_1 = +0.736 \pm 0.049$ [17]. Therefore the $B^\pm \to \phi\phi K^\pm$ decay plays a unique role in searching for a new CP-violating phase.

Experimental sensitivities can be improved by adding more final states. The technique to reconstruct X_s, which has been successfully adopted for the measurements of semi-inclusive $B \to X_s \ell\ell$ transitions [31], can be used for this purpose. Flavor-specific neutral B meson decays,

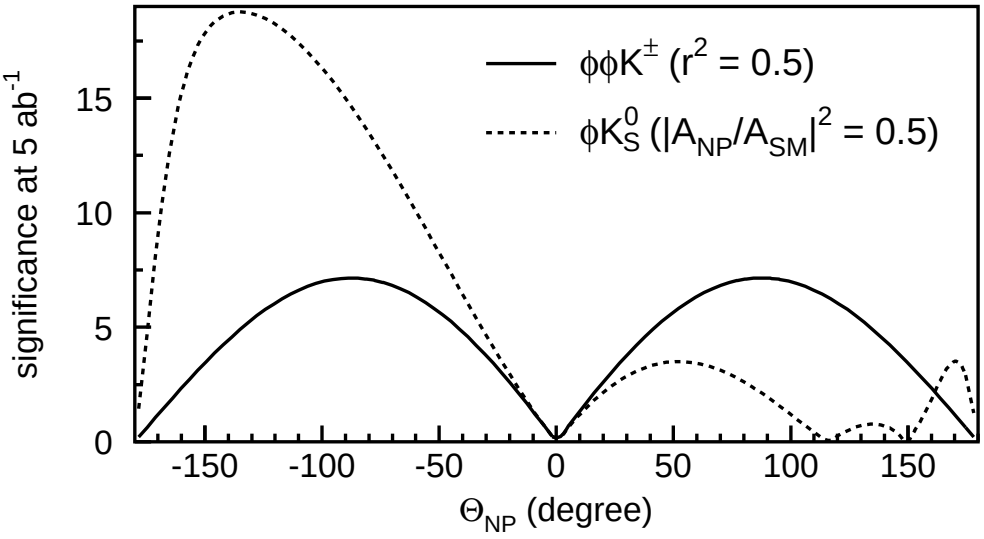

Figure 4.9: Expected statistical significance of deviations from the SM for direct CP violation in the $B^{\pm} \to \phi\phi K^{\pm}$ decay with $r^2 = 0.5$ (solid line) and for time-dependent CP violation in the $B^0 \to \phi K^0_S$ decay with $|A_{\rm NP}/A_{\rm SM}|^2 = 0.5$ (dashed line). For each case, significance is calculated at 5 ab^{-1}.

such as $B^0 \to \phi\phi K^{*0}(\to K^+\pi^-)$, and other charmonia such as the $\chi_{c0} \to \phi\phi$ decay can also be included.

4.2.5 Discussion

As is shown in the previous sections, statistical errors in new phase measurements can be at the few percent level at SuperKEKB. Figure 4.10 shows an example of a fit to events in a MC pseudo-experiment for the $B^0 \to \phi K^0_S$ and $J/\psi K^0_S$ decays at 5 ab^{-1}, where the input value of $\mathcal{S}(\phi K^0_S) = +0.24$ is chosen to be the world average value of the $\mathcal{S}$ term for $B^0 \to \phi K^0_S$, $\eta' K^0_S$ and $K^+K^-K^0_S$. This level of large deviation can easily be observed only with a single decay channel $B^0 \to \phi K^0_S$ at SuperKEKB. Combining all the available modes described in the previous sections allows us to measure a deviation of ~ 0.1. At this level, even the SM may be able to create non-zero values of $\Delta\mathcal{S}$. Therefore it is important to evaluate $\Delta\mathcal{S}$ within the SM. Grossmann, Isidori and Worah [32] analyzed the possible pollution in the $B^0 \to \phi K^0_S$ decay, which comes from the $b \to u\bar{u}s$ transition that contains V_{ub}. They estimate that the pollution is at most $O(\lambda^2) \sim 5\%$. In addition, they claim that the upper limit of the pollution will be set experimentally from the ratios of branching fractions $\mathcal{B}(B^+ \to \phi\pi^+)/\mathcal{B}(B^0 \to \phi K_S)$ and $\mathcal{B}(B^+ \to K^*K^+)/\mathcal{B}(B^0 \to \phi K_S)$. This is due to the fact that enhancement of $b \to u\bar{u}s$ should also be detected in these modes. Therefore they conclude that new physics is guaranteed if $|\Delta\mathcal{S}(\phi K^0_S)| > 0.05$ is established.

For the $B^0 \to \eta' K^0_S$ decay, London and Soni [33] discussed the tree ($b \to u\bar{u}s$) pollution by evaluating $T(\eta' K_S)/P(\eta' K_S) = T(\eta' K_S)/T(\pi^+\pi^-) \times T(\pi^+\pi^-)/P(\eta' K_S)$, and concluded that manifestation of new physics is established if $|\Delta\mathcal{S}(\eta' K^0_S)| > 0.1$ is observed.

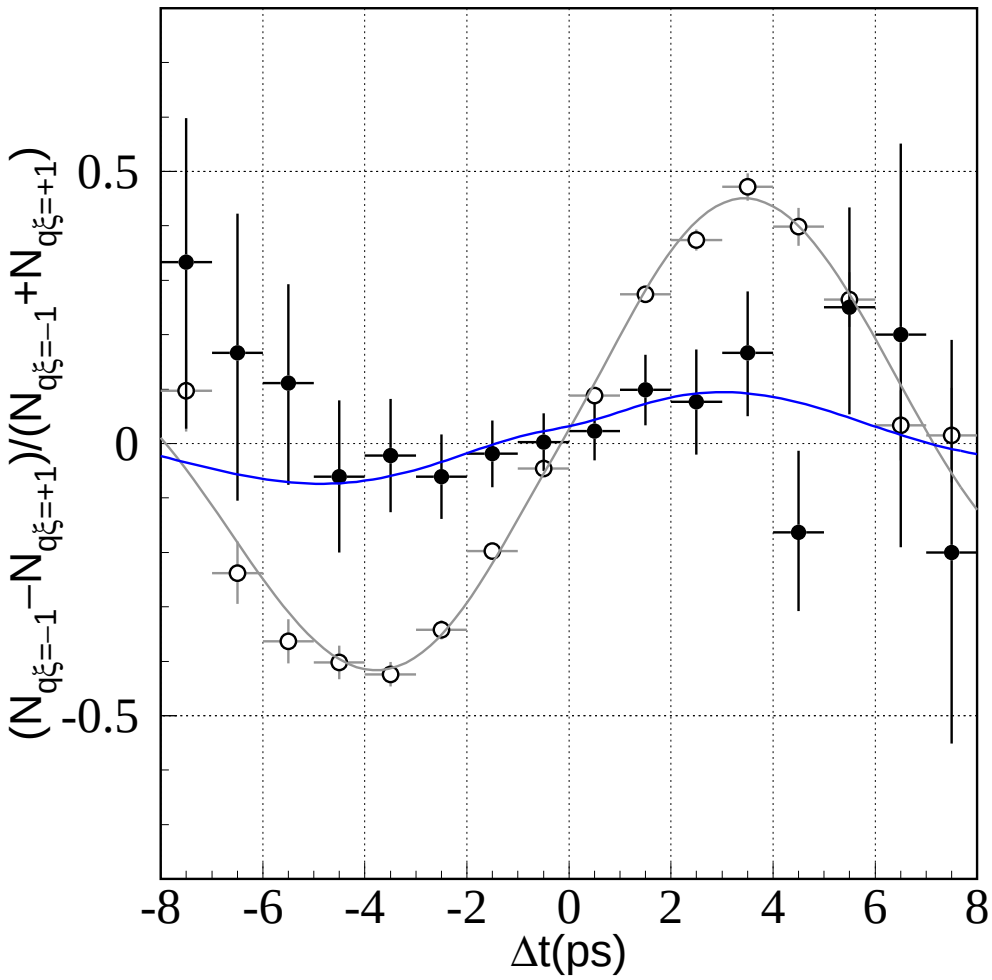

Figure 4.10: Raw asymmetries for $B^0 \to \phi K^0_S$ and $B^0 \to J/\psi K^0_S$ at 5 ab^{-1}. Input values are $\mathcal{S}_{\phi K^0_S} = +0.24$ and $\mathcal{A}_{\phi K^0_S} = +0.07$, which are the HFAG average for the $b \to s$ transition as of LP03 [17].

The above studies aim at providing estimates of the possible deviation within the SM based on some models of QCD. A different approach has recently been proposed by Y. Grossman, Z. Ligeti, Y. Nir and H. Quinn [34]. They do not rely on specific QCD models but instead use SU(3) relations to estimate or bound the contributions to these amplitudes proportional to $V_{ub}^* V_{us}$, which induce a non-zero $\mathcal{S}$ value within the SM. At present, the power of the method is limited by the uncertainties on branching fractions of charmless two-body decays. As a result, they conclude that $\Delta\mathcal{S}(\phi K_S^0) < 0.25$, $\Delta\mathcal{S}(K^+K^-K_S^0) \sim 0.13$ and $\Delta\mathcal{S}(\eta' K_S^0) < 0.36$. As data improve, these bounds could become significantly stronger. Taking these theoretical considerations into account, we conclude that SuperKEKB can provide precision measurements of $\Delta\mathcal{S}$ up to the limit of hadronic uncertainties, which will be a few percent level.

4.3 $b \to s\gamma$ and $b \to s\ell^+\ell^-$

4.3.1 Introduction

In this section, we discuss the radiative and electroweak processes $b \to s(d)\gamma$ and $b \to s(d)\ell^+\ell^-$. The corresponding exclusive decays are $B \to K^*(\rho)\gamma$ and $B \to K^{(*)}\ell^+\ell^-$. Due to the GIM mechanism, the radiative process $b \to s\gamma$ starts at one-loop order, but still has a large branching fraction because of the non-decoupling effect of the top quark loop and the large CKM factor $V_{tb}V_{ts}^*$. The other processes, $b \to s\ell^+\ell^-$ and $b \to d\gamma$ are suppressed with respect to $b \to s\gamma$ by two orders of magnitude mainly due to additional $\alpha_{\rm em}$ and $|V_{td}/V_{ts}|^2$ factors, respectively; $b \to d\ell^+\ell^-$ is suppressed by four orders of magnitude due to both of them. These decay processes are sensitive to new physics effects that are predicted in extensions to the Standard Model. Moreover, new physics effects from flavor changing neutral interaction contribute to $b \to s(d)\gamma$ and to $b \to s(d)\ell^+\ell^-$ in a different way. Typically in the former case new physics effects always appear at one-loop or higher orders, while in the latter process new physics effects may arise at tree-level, *i.e.*, violations of the GIM mechanism. Therefore, even if no new physics effect is found in $b \to s\gamma$, there could be a significant effect in $b \to s(d)\ell^+\ell^-$.

The $b \to s\gamma$ process was first observed by CLEO a decade ago and has been extensively studied since then. The $b \to s\ell^+\ell^-$ process has recently been measured by the B factories. The measured branching fractions are consistent with Standard Model predictions. No $b \to d\gamma$ process has been measured yet, but it is expected to be observed sooner or later. With one or two orders of magnitude more B decay data, it will become possible to measure various distributions and asymmetries accurately enough to observe possible deviations from the Standard Model, in addition to significant improvements in branching fraction measurements. Various properties of $b \to d$ transitions can also be measured. These measurements will be essential in order to understand the parity, chirality and Lorentz structures that may differ from the Standard Model, before, and especially after the discovery of new physics beyond the Standard Model, elsewhere if not in these decays.

The major targets of Super-KEKB for these decays are as follows.

1. Precision test of the Standard Model with improved accuracy,
2. Search for a deviation from the Standard Model in various distributions, *e.g.* in the forward-backward asymmetry of $B \to K^*\ell^+\ell^-$,
3. Search for a lepton flavor dependence of $b \to s\ell^+\ell^-$,
4. Measurement of mixing induced CP asymmetry in $b \to s\gamma$,
5. Search for direct CP violation in $B \to K^*\gamma$, and
6. Study of flavor changing transitions in the $b \to d$ sector, *i.e.* $B \to \rho\gamma$, and hopefully an exclusive $b \to d\ell^+\ell^-$ processes such as $B \to \pi\ell^+\ell^-$.

Both exclusive and inclusive modes are useful to test the strong interation in weak decays. In the past decade, perturbative QCD corrections to the radiative and electroweak B decays were computed beyond the leading order which leads to the predictions with higher accuracy [35]. The theoretical errors from this part are reduced to a few percent level coming from the renormalization point dependence and charm quark mass uncertainty. To include non-perturbative effects for inclusive decays, we may apply the heavy quark expansion. The photon energy spectrum $d\Gamma/dE_\gamma$ in $b \to s\gamma$ is sensitive to the non-pertubative effects, *e.g.* Fermi-motion

effects which are encoded in the structure function of B mesons. Such non-perturbative effects can be determined by measuring the moments of the photon energy spectrum. Because the structure function is process independent, we can apply the one determined in $b \to s\gamma$ to other inclusive modes such as $B \to X_s\ell^+\ell^-$ [36]. As for the exclusive processes, there remain large uncertainties from the form factors of the hadronic matrix elements; these form factors have usually been calculated using QCD sum rules, for which no clear idea on how to reduce their errors is available. The situation might improve by using a new approach with lattice QCD. It is usually thought that a large fraction of uncertainty is canceled by measuring ratio or asymmetry of two decay rates. Experimental information is essential to check the various theoretical models, to evaluate the size of the errors especially for cases where the uncertainty are thought to cancel.

Factorization, pertubative QCD (PQCD), light-front QCD, lattice QCD and other models predictions for exclusive rare B decays can be compared with the experimental data. This certainly improves understanding of the weak decays of B mesons. Interestingly, a complete understanding of the long-distance effects in $B \to X_s\ell^+\ell^-$ is not available yet. This effect comes from the the decay chains $B \to J/\psi(\psi')X_s \to \ell^+\ell^-X_s$ [37]. By measuring the dilepton mass squared distribution near the charmonuum resonances, we may study the long-diatance effects experimentally.

In order to search for or constrain so many predictions from extensions to the Standard Model described above, a model independent study is a useful approach. New physics effects may appear as modification to the short-distance couplings, which can be expressed as modifications to the Wilson coefficients. The $b \to s\gamma$ transition is sensitive to the coefficient C_7 for the $bs\gamma$ coupling and to a lesser extent to C_8 for the bsg coupling through higher order corrections; the $b \to s\ell^+\ell^-$ transition is sensitive to C_9 and C_{10} for the vector and axial-vector $bs\ell^+\ell^-$ coupling in addition.

One can further generalize this approach [38,39]. New physics effects that may affect $b \to s\gamma$ can be parametrized by four types of interactions, which include two types of $b \to sg$ interactions and two types of $b \to s\gamma$ transitions. In addition to these, there are four fermi-interactions with the form of the bilinear products of $\bar{b}s$ and $\ell^+\ell^-$. They can be parametrized by 12 types of interactions in $B \to X_s\ell^+\ell^-$ [38]. With the data at Super-KEKB, we can improve the situation and may pinpoint the new physics effect in a model independent way, which covers a wider class of models than the present analysis.

Among the various interesting aspects of these decay channels, we select the following channels as benchmark modes that will be tested with Super-KEKB. They are: the $B \to X_s\gamma$ inclusive branching fraction, the forward-backward asymmetry of $B \to K^*\ell^+\ell^-$, the ratio of $B \to K\mu^+\mu^-$ to $B \to Ke^+e^-$, the mixing induced CP asymmetry in $B \to K^*\gamma$, and the direct CP asymmetry in $B \to X_s\gamma$.

4.3.2 $B \to X_s\gamma$ branching fraction

The excellent agreement of the measured $B \to X_s\gamma$ branching fraction with the theory prediction, within about 10% accuracy both for the measurement and theory, has constrained various new physics scenarios; for example, the charged Higgs constructively interferes with the SM amplitude, and its mass must be above 3.5 TeV if no other new physics contribution cancels the enhancement. It is not expected to be easy to reduce neither the measurement or theory errors, and therefore probably one can not expect to measure a significant deviation in the near future. Nevertheless, improved measurements of $B \to X_s\gamma$ are extremely important to fix the magnitude of the Wilson coefficient C_7 and the photon energy spectrum for other measurements.

The theory error, which is now determined by the accuracy of the next-to-leading-order

corrections, is expected to be reduced down to 5% when all next-to-next-to-leading-order corrections are included. The work is on-going, and is expected to be completed within a few years.

There have been two techniques to measure $B \to X_s\gamma$: a fully inclusive method just to tag the photon in which the background subtraction is the main issue, and a method of summing up exclusive modes, in which the extrapolation to the un-measured modes is the key issue. The former method has several options, to clean up the events by either requiring a lepton-tag or a full-reconstruction tag for the other side B, if it is not statistically limited. The latter method gives more constraints, but is seriously affected by the hadronization model uncertainty that makes it unsuitable for a precision measurement.

The measurements are currently systematics limited, with a minimum photon energy requirement typically at 2.0 GeV. One can in principle reduce the systematic error below 5% by reducing the minimum photon energy close to 1.5 GeV. This is not a straightforward task, since the background increases rapidly in the lower photon energy range while the signal decreases, as shown in Fig. 4.11. Typically, twice as much data is required to decrease the minimum photon energy by 0.1 GeV while keeping the same statistical error. Therefore, $B \to X_s\gamma$ is a suitable measurement at SuperKEKB; scaling from the currently available results, about 5 ab^{-1} on- plus 0.5 ab^{-1} off-resonance data will be needed to decrease the photon energy requirement down to 1.5 GeV and to reduce the statistical error by half at the same time, so that the total error becomes around 5%. The dominant background is from continuum background, which can be reliably subtracted using an off-resonance sample. The second largest background is from $B \to \pi^0 X$ (and ηX), which can be also subtracted using a photon energy spectrum inferred from the measured π^0 momentum distribution. The problematic part will be the background from neutral hadrons (K^0_L, n and anti-n), for which control samples of $e^+e^- \to \phi\gamma$, $\phi \to K^0_S K^0_L$ and inclusive Λ ($\overline{\Lambda}$) tagged events have to be studied.

4.3.3 $B \to K^*\ell^+\ell^-$ forward-backward asymmetry

The forward-backward asymmetry in $B \to K^*\ell^+\ell^-$, defined as

$$\overline{A}_{\rm FB}(q^2) = \frac{N(q^2;\, \theta_{B\ell^+} > \theta_{B\ell^-}) - N(q^2;\, \theta_{B\ell^+} < \theta_{B\ell^-})}{N(q^2;\, \theta_{B\ell^+} > \theta_{B\ell^-}) + N(q^2;\, \theta_{B\ell^+} < \theta_{B\ell^-})}$$

is an ideal quantity to disentangle the Wilson coefficients C_9, C_{10} together with the sign of C_7.

In a SUSY scenario, the sign of the $b \to s\gamma$ amplitude (C_7) can be opposite to the Standard Model prediction, while the transition rate may be the same as in the Standard Model. This case can be discriminated by measuring the forward-backward asymmetry of $B \to X_s\ell^+\ell^-$ or $B \to K^*\ell^+\ell^-$. Within the Standard Model, there is a zero crossing point of the forward-backward asymmetry in the low dilepton invariant mass region, while the crossing point may disappear in some SUSY scenarios. Another important new physics effect can be searched for by using the $B \to K^*\ell^+\ell^-$ forward-backward asymmetry. In a model with $SU(2)$ singlet down type quarks, tree-level Z flavor-changing-neutral-currents are induced. In this case, the axial-vector coupling (C_{10}) to the dilepton is affected more than the vector coupling (C_9). Because the forward-backward asymmetry is proportional to the axial vector coupling, the sign of the asymmetry can be opposite to the Standard Model. The same new physics effect is also effective for $B^0 \to \phi K^0_S$ where anomalous mixing induced CP violation may have been observed. A correlation is expected between $b \to s\ell^+\ell^-$ and $b \to s\bar{s}s$.

The forward-backward asymmetry is roughly proportional to $C_{10}(2C_7 + C_9\hat{s})$. In the SM, C_7 is about -0.3 and C_9 is about 4, so this function crosses zero around $\hat{s} \sim 0.15$, or $q^2 \sim$

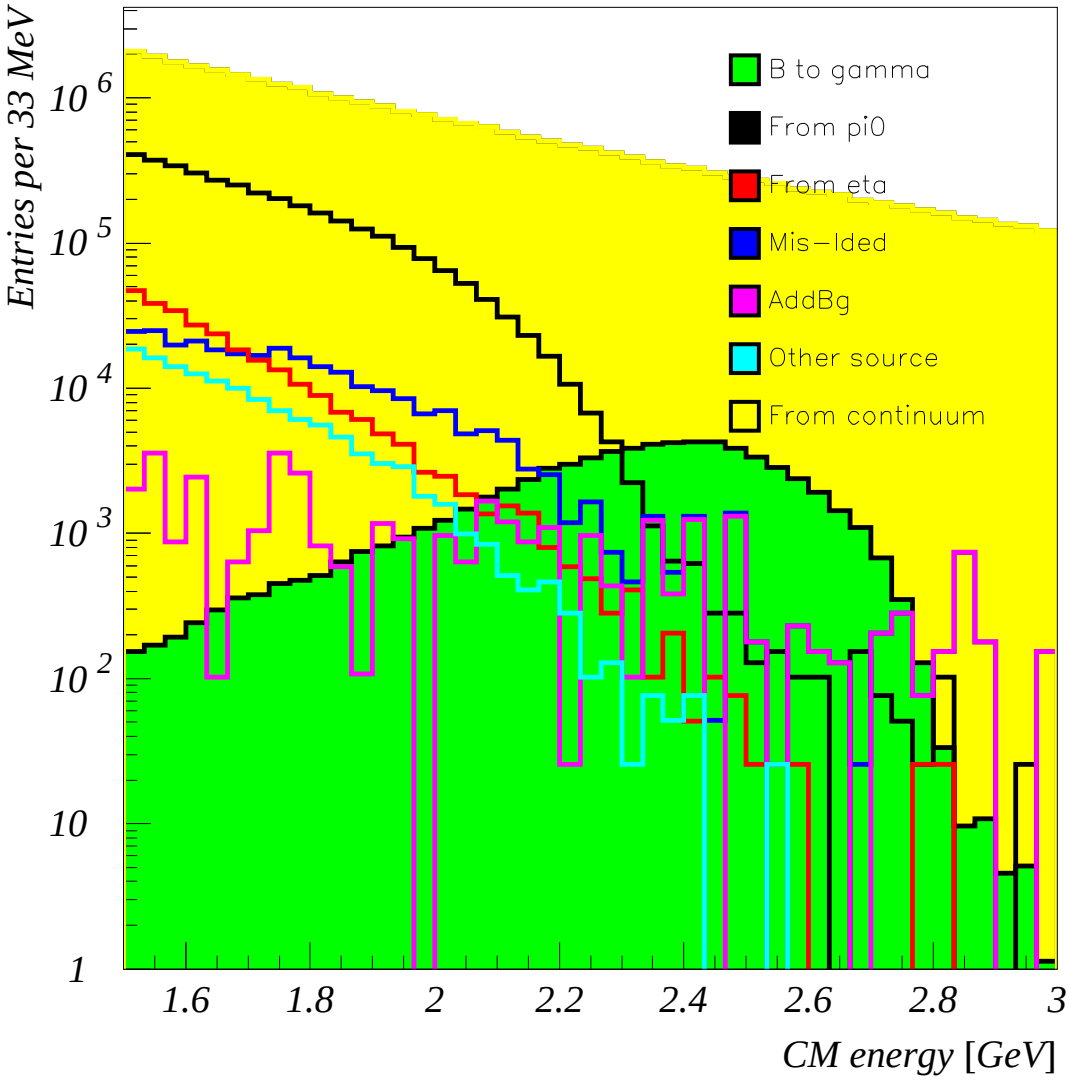

Figure 4.11: Photon energy spectrum (MC) for 140 fb^{-1}.

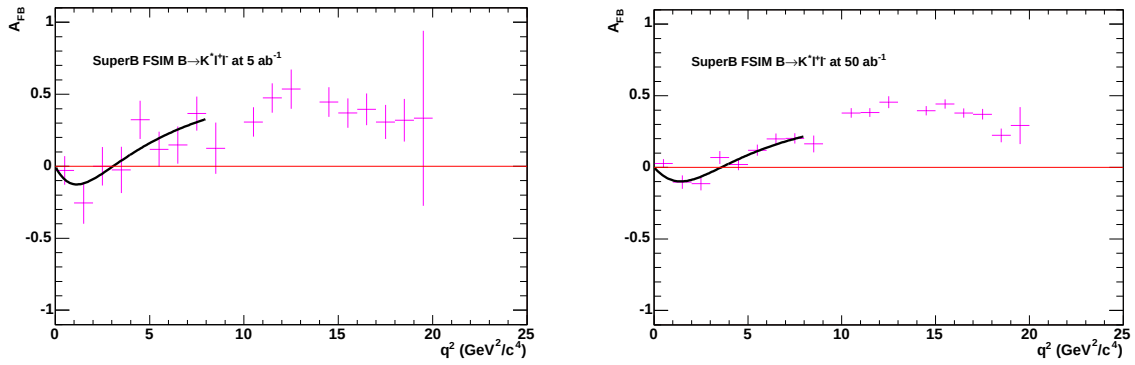

Figure 4.12: Forward-backward asymmetry in $B \to K^* \ell^+ \ell^-$ at 5 ab^{-1} (left) and 50 ab^{-1} (right).

3.5 GeV/c^2. Fig. 4.12 shows the expected $\overline{A}_{\rm FB}$ at 5 and 50 ab^{-1}. It can be seen that this crossing pattern of the forward-backward asymmetry will be already visible at 5 ab^{-1}, and is clearly observed at 50 ab^{-1}. The fitted curves in Fig. 4.12 are empirical functional forms that are proportional to $C_{10}(2C_7 + C_9\hat{s})$. From these fits, it is possible to disentangle C_{10} and C_9, if the size of C_7 is fixed using $b \to s\gamma$. From a fit to the 50 ab^{-1} sample, we obtained $\delta C_9 = 0.43$ and $\delta C_{10} = 0.59$, or roughly 10% and 14% errors, respectively. The uncertainty due to C_7 is small. It has to be noted that a more realistic fitting function that includes all next-to-next-to-leading order corrections and form factors is needed. The result will be improved by combining it with a $B \to X_s \ell^+ \ell^-$ branching fraction measurement and q^2 fit results, which is only possible at e^+e^- B-factories.

4.3.4 $B \to K\mu^+\mu^-$ versus $B \to Ke^+e^-$

Branching fractions for the exclusive decays $B \to K^{(*)}\ell^+\ell^-$ have already been measured to be consistent with SM predictions. The measurement error is already smaller than that for the theory. Theory predictions suffer from large model dependent and irreducible uncertainties in the form-factors of at least $\pm 30\%$, and the currently available predictions vary by a factor of two or more. However, one can still utilize the measurements in such a way as to cancel the theory uncertainties.

In new physics models with different Higgs sector from that the Standard Model, scalar and pseudo-scalar type of interactions may arise in $b \to s\ell^+\ell^-$. Depending on the lepton flavor $\ell = e$ and $\ell = \mu$, the new physics effects can differ. By measuring $R_{K^{(*)}} = \mathcal{B}(B \to K^{(*)}\mu^+\mu^-)/\mathcal{B}(B \to K^{(*)}e^+e^-)$, such new physics effects can be searched for. A particular example can be found in a minimal supergravity model [39, 40].

In the SM, the branching fractions for $B \to Ke^+e^-$ and $B \to K\mu^+\mu^-$ are predicted to be equal except for a tiny phase space difference due to the lepton masses. For $B \to K^*\ell^+\ell^-$ modes, the branching fraction for $B \to K^*e^+e^-$ is larger than $B \to K^*\mu^+\mu^-$ for small dilepton masses, due to a larger interference contribution from $B \to K^*\gamma$ in $B \to K^*e^+e^-$. However, this situation may be modified in the models mentioned above, in which a neutral SUSY Higgs contribution can significantly enhance only the $B \to K^{(*)}\mu^+\mu^-$ channel if $\tan\beta$ is large. Therefore, the ratio $R_K = \mathcal{B}(B \to K\mu^+\mu^-)/\mathcal{B}(B \to Ke^+e^-)$ is an observable that is sensitive to new physics if it is larger than unity.

From current Belle results on the branching fractions, we obtain $R_K = 1.0 \pm 0.4$ or $R_K < 1.7$ (90% CL). The error on R_K is currently dominated by the statistical error, and the error will

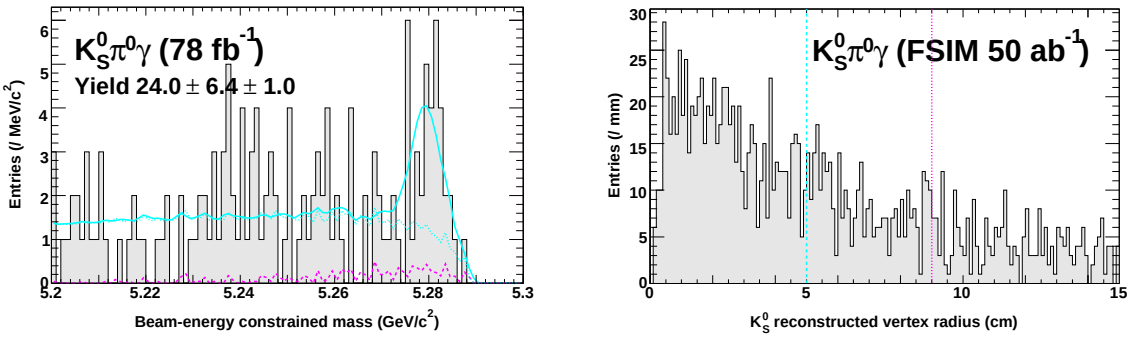

Figure 4.13: $B^0 \to K^{*0}\gamma$, $K^{*0} \to K^0_S\pi^0$ signal with 78 fb^{-1} (left) and the radial K^0_S decay vertex distribution (right).

simply scale with the luminosity even at 50 ab^{-1}. The expected error is

$$\begin{aligned} \delta R_K &= 0.07 \text{ (at 5 ab}^{-1}\text{)} \\ \delta R_K &= 0.02 \text{ (at 50 ab}^{-1}\text{)}. \end{aligned} \tag{4.10}$$

The systematic error in the ratio is dominated by the error on the lepton identification efficiency, which will still be much smaller than the statistical error even at 50 ab^{-1}.

Since the $b \to s\ell^+\ell^-$ transition diagram is equivalent with $B_s \to \mu^+\mu^-$, there already is a bound from the CDF's limit, which corresponds to $R_K < 1.6$. However, this limit is model dependent unless $B_s \to e^+e^-$ is observed, which is very unlikely.

4.3.5 Mixing induced CP asymmetry in $B \to K^*\gamma$

Mixing induced CP asymmetry in $b \to s\gamma$ is a good window to study the new phase that may also be observed in the hadronic transition $b \to s\bar{s}s$. The CP asymmetry parameter $\mathcal{S}_{K^*\gamma}$ is expected to be $\mathcal{O}(m_s/m_b)$ in the SM within an error of a few percent, and any deviation would be a sign of new physics.

For example, the existance of neutrino mass suggests that left-right symmetry is restored at higher energy, while parity is spontaneously broken at low energy. In left-right symmetric models, the helicity of the photon from $b \to s\gamma$ can be a mixed state of two possible photon helicities, while the left-handed photon is dominant in the Standard Model. This case can be tested by using the mixing induced CP asymmetry in $b \to s\gamma$. It can also be checked by measuring the azumuthal angle distribution of $B \to K^*\ell^+\ell^-$ [41].

In order to measure the mixing induced CP asymmetry, a suitable CP final state is needed. The final state $B^0 \to K^{*0}\gamma$, $K^{*0} \to K^0_S\pi^0$ is such a CP eigenstate, and the technique for the $\sin 2\phi_1$ measurement is applicable. This mode was previously considered to be technically challenging due to the detached K^0_S decay vertex; however, it is now found to be feasible from recent studies of $B \to K^0_S\pi^0$, if one requires hits for the $K^0_S \to \pi^+\pi^-$ tracks in the silicon vertex detector.

Although the branching fraction for $B^0 \to K^{*0}\gamma$ is rather high ($\sim 4 \times 10^{-5}$), the number of events in the $K^0_S\pi^0\gamma$ final state is rather limited due to its small sub-decay branching fraction and low efficiency. The signal is clearly observed already at 78 fb^{-1} as shown in Fig. 4.13-a.

The efficiency for the current data is about 1%. Assuming that the efficiency is unchanged for SuperKEKB, one expect about 2×10^3 (2×10^4) events at 5 (50) ab^{-1}. The useful events with at least two hits in the current SVD must have the decay vertex within about 5 cm radius,

which corresponds to half of the total, as shown in Fig. 4.13-b. This will increase to about 70% for a SVD radius of 9 cm. Using the result of $B \to \eta' K^0_S$, which has a similar signal-to-noise ratio, and a better Δt resolution that would be compensated by the expected better SVD for SuperKEKB, the anticipated error of the S term is

$$\begin{array}{c} \delta S_{K^*\gamma} = 0.14 \text{ (at 5 ab}^{-1}\text{)} \\ \delta S_{K^*\gamma} = 0.04 \text{ (at 50 ab}^{-1}\text{)}. \end{array} \tag{4.11}$$

There are other exclusive decay channels for the mixing induced CP asymmetry study that have no difficulty in the vertex reconstruction. One possible channel is $B^0 \to K^0_S \phi\gamma$ for which a 3σ signal is already obsreved (5σ signal is observed for the corresponding charged decay $B^+ \to K^+\phi\gamma$). Since $K^0_S\phi\gamma$ is not a CP eigenstate, one has to perform an angular analysis. From past experience with $B \to J/\psi K^{*0}$, we obtained an error of 0.63 with 89 events. At 5 (50) ab^{-1}, we expect 150 (1500) $K^0_S\phi\gamma$ events that will lead to an error of 0.5 (0.15) in the S term, and it therefore becomes interesting with 50 ab^{-1} or more. The other possibility is to use higher resonances, namely $B \to K_1(1270)^0\gamma$, $K_1(1270) \to K^0_S\rho^0$. However, this is now considered to be difficult, because these modes have not been observed yet and one has to disentangle them from $K_1(1270) \to K^{*+}\pi^-$ that has the same $K^0_S\pi^+\pi^-$ final state.

4.3.6 $B \to X_s\gamma$ direct CP asymmetry

The direct CP asymmetry for $B \to X_s\gamma$ is one of the most precisely calculated quantities to which is not matched by the experimental sensitivity. The predicted SM CP asymmetry is $A_{CP} = 0.0042^{+0.0017}_{-0.0012}$ [42], while its magnitude could be above 10% in many extensions to the SM. Therefore, a large space remains to be explored.

The sensitivity at Super-B can be obtained by extrapolating the latest Belle results, $A_{CP}(B \to X_s\gamma) = -0.004 \pm 0.051(\text{stat}) \pm 0.038(\text{syst})$. This measurement was performed by summing up exclusive modes, $B \to Kn(\pi)$ ($n = 1$ to 4) and $B \to KK^+K^-(\pi)$, where K is a $K^\pm$ or K^0_S and most one π^0 is allowed. This method has the advantage of suppressing the $B \to X_d\gamma$ contribution to a negligible level. Another method that uses the inclusive photon and tags the charge by an additional lepton, cannot distinguish the $B \to X_d\gamma$ contribution; however it is an another interesting subject because of the partial sensitivity to the $B \to X_d\gamma$ channel.

Although the systematic error is not much smaller than the statistical error, most of the systematic errors are limited by the statistics of the control samples and hence can be reduced with a larger dataset. Note that systematic errors in the tracking efficiency and particle identification cancel in the asymmetry. The breakdown of the errors at 140 fb^{-1} are, from the signal shape (~ 0.008) partly due to the uncertainty in the $M(X_s)$ spectrum and partly due to the multiplicity distribution, from the possible A_{CP} in the charmless B decay background (0.02), and from charge asymmetry in the background suppression requirements (0.029). The $M(X_s)$ shape and charmless contributions will be better known with more data, and other errors just scale with the statistics. The irriducible model error of the first error is about 0.003, giving the expected errors at 5 ab^{-1} and 50 ab^{-1} of

$$\begin{array}{lcl} \delta A_{CP}(\text{at 5 ab}^{-1}) & = & \pm 0.009(\text{stat}) \pm 0.006(\text{syst}) \\ \delta A_{CP}(\text{at 50 ab}^{-1}) & = & \pm 0.003(\text{stat}) \pm 0.002(\text{syst}) \pm 0.003(\text{model}) \end{array} \tag{4.12}$$

Therefore, at 50 ab^{-1}, the measurement is more or less systematics limited, but it is still insufficient to measure the predicted SM asymmetry beyond a 1σ significance.

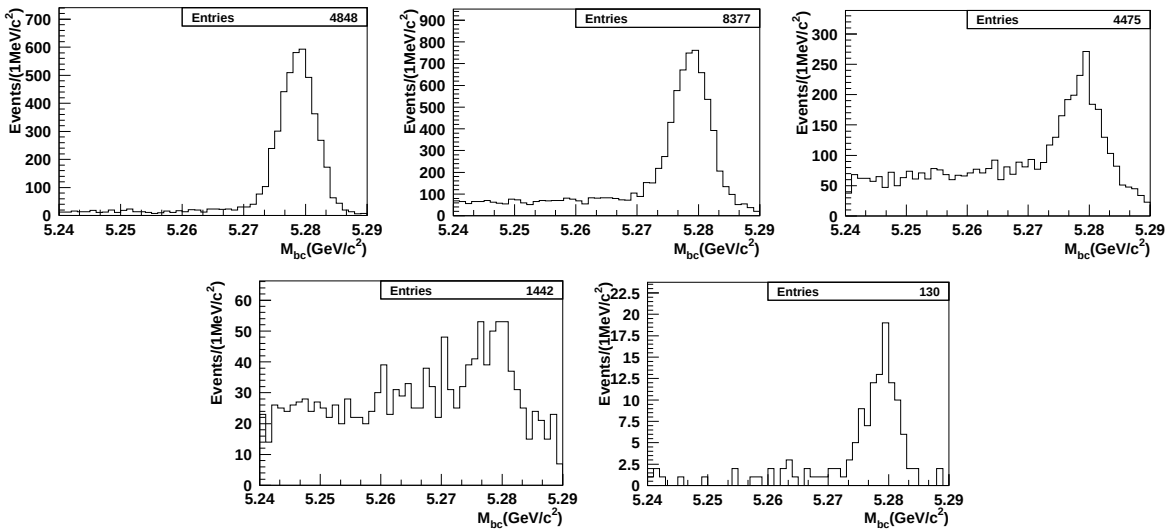

Figure 4.14: Breakdown of the expected $B \to X_s\gamma$ exclusive modes: $K\pi\gamma$ other than $B \to K^*\gamma$, $K\pi\pi\gamma$, $K\pi\pi\pi\gamma$, $K\pi\pi\pi\pi\gamma$, and $KK^+K^-\gamma$ from left-top to right-bottom.

Table 4.6: Summary of the expected errors for $b \to s(d)\gamma$ and $b \to s\ell^+\ell^-$ at SuperKEKB.

mode	5 ab^{-1}	50 ab^{-1}
$\mathcal{B}(B \to X_s\gamma)$	5%	5%
$A_{CP}(B \to X_s\gamma)$	$0.009 \oplus 0.006$	$0.003 \oplus 0.002 \oplus 0.003$
Mixing induced $S_{K^*\gamma}$	0.14	0.04
$R_K(B \to K\ell^+\ell^-)$	0.07	0.02
$\overline{A}_{\rm FB}(B \to K\ell^+\ell^-)$		
C_9 from $\overline{A}_{\rm FB}(B \to K^*\ell^+\ell^-)$	32%	10%
C_{10} from $\overline{A}_{\rm FB}(B \to K^*\ell^+\ell^-)$	44%	14%

4.3.7 $b \to d\gamma$ and $b \to d\ell^+\ell^-$

Finding new physics effects in a $b \to d$ transition may be easier than in a $b \to s$ transition because the Standard Model amplitude is suppressed in the $b \to d$ transition. Therefore, measurement of the decay rates of $B \to \rho\gamma$ will be a good test of the Standard Model. By combining $|V_{td}V_{tb}^*|$ measured in B_d^0-$\overline{B}_d^0$ mixing, we can search for new physics effects in the $b \to d\gamma$ transition [43]. Since the Standard Model prediction for the $B \to \rho\gamma$ branching fraction suffers from a large model-dependent uncertainty, ideally it is necessary to measure the inclusive rate for $B \to X_d\gamma$.

Although it has yet to be measured, the $b \to d\gamma$ process will provide various interesting new physics probes.

4.3.8 Summary

We have discussed various decay channels of $b \to s(d)\gamma$ and $b \to s\ell^+\ell^-$ that are good probes of new physics effects. The sensitivity results are summarized in Table 4.6.

Decay	SM Prediction	BELLE (60 fb^{-1})	BABAR (81 fb^{-1})
$B^{\pm} \to e^{\pm}\nu$	9.2×10^{-12}	$\leq 5.4 \times 10^{-6}$	
$B^{\pm} \to \mu^{\pm}\nu$	3.9×10^{-7}	$\leq 6.8 \times 10^{-6}$	$\leq 6.6 \times 10^{-6}$
$B^{\pm} \to \tau^{\pm}\nu$	8.7×10^{-5}		$\leq 4.1 \times 10^{-4}$

Table 4.7: SM predictions and current experimental limits from BELLE/BABAR.

4.4 More than one neutrino I: $B \to K^{(*)}\nu\bar{\nu}$ and $B \to \tau\nu$

4.4.1 Introduction

In the Standard Model the rare FCNC decay $b \to s\nu\bar{\nu}$ proceeds at the one-loop level through penguin and box diagrams.Additional new physics heavy particles may therefore contribute to this decay mode, leading to significant enhancements of the branching fraction. Since the final state leptons do not have electric charge, this mode is not affected by long distance effects from vector resonances (ρ, J/ψ, ψ' *etc.*) and its theoretical prediction is cleaner than $b \to sl^+l^-$. The inclusive branching fraction is estimated to be 4×10^{-5} [44, 45] for the sum of three neutrino flavors, whereas the exclusive branching fractions are predicted to be $Br(B^- \to K^-\nu\bar{\nu}) \approx 4 \times 10^{-6}$ [46].

However, the experimental measurement of $b \to s\nu\bar{\nu}$ is quite challenging due to the presence of two unobserved neutrinos. The best inclusive limit to date is from ALEPH $Br(b \to s\nu\bar{\nu}) < 6.4 \times 10^{-4}$ [47], and a limit of $< 2.4 \times 10^{-4}$ at 90% confidence level on the exclusive branching fraction of $B \to K\nu\bar{\nu}$ was set by CLEO [48]. BABAR has recently reported a preliminary upper limit $Br(B \to K\nu\bar{\nu}) < 7.0 \times 10^{-5}$ [49]. At Super-KEKB, measurements of these decay branching fractions will become possible, as millions of fully reconstructed B samples will be accumulated.

The purely leptonic decays $B^{\pm} \to l^{\pm}\nu$ in the SM proceed via annihilation to a $W^{\pm}$ and are proportional to the square of the B meson decay constant (f_B). In models beyond the SM there can be additional tree-level contributions such as a $H^{\pm}$ (s-channel) [50], [51] or sfermions (s, t-channels) in R parity violating SUSY models [52]. The SM predictions and the current experimental upper limits are shown in Table 4.7, where we take $f_B = 200$ MeV. Observation of such decays would provide the first direct measurement of f_B or even evidence for new physics. In particular, the sensitivity of the $\tau^{\pm}\nu$ and $\mu^{\pm}\nu$ channels to any $H^{\pm}$ contribution is complementary and competitive with that of the exclusive semi–leptonic decay $B \to \overline{D}\tau^{\pm}\nu$. The tree–level partial width (including only $W^{\pm}$ and $H^{\pm}$ contributions) is as follows [50]:

$$\Gamma(B^{\pm} \to \ell^{\pm}\nu) = \frac{G_F^2 m_B m_l^2 f_B^2}{8\pi} |V_{ub}|^2 \left(1 - \frac{m_l^2}{m_B^2}\right)^2 \times r_H \tag{4.13}$$

where r_H is independent of the lepton flavour and is given by

$$r_H = \left(1 - \frac{\tan^2\beta}{1 + \tilde{\epsilon}_0 \tan\beta} \frac{m_B^2}{m_{H^{\pm}}^2}\right)^2 \tag{4.14}$$

The overall factor of m_l^2 arises from helicity suppression for $W^{\pm}$ and Yukawa suppression for $H^{\pm}$. The parameter $\tilde{\epsilon}_0$ encodes the effects of large SUSY corrections to the b quark Yukawa coupling, and is typically constrained $|\tilde{\epsilon}_0| \leq 0.01$. In Fig. 4.15 we plot r_H as a function of $\tan\beta/m_{H^{\pm}}$ for several values of $\tilde{\epsilon}_0(m_{H^{\pm}}/100\,GeV)$. The current experimental limits from Table 4.7 constrain $r_H < 4.7$ and $r_H < 17.4$ from the $\tau^{\pm}\nu$ and $\mu^{\pm}\nu$ channels, respectively. Sensitivity

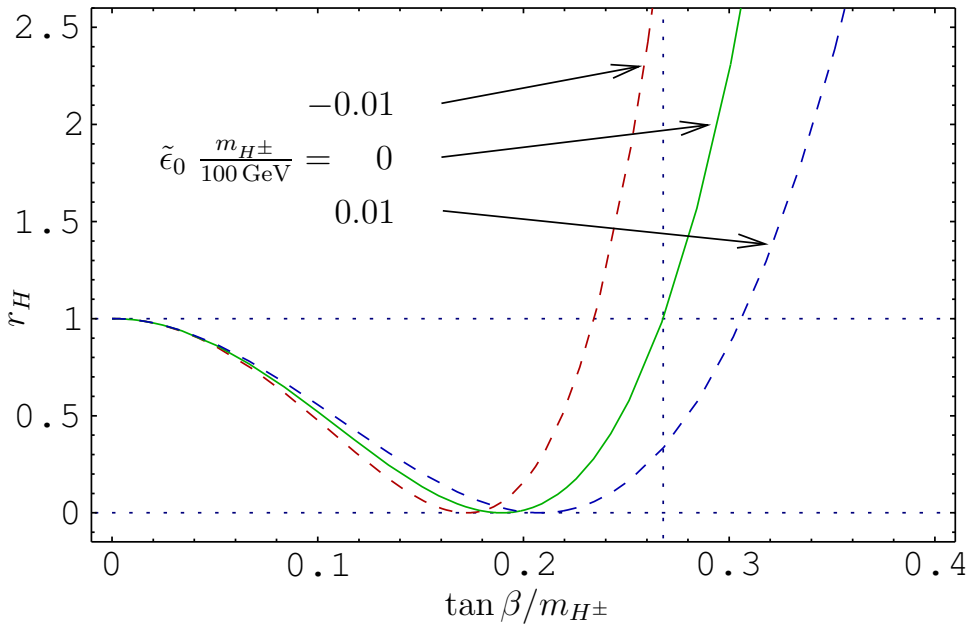

Figure 4.15: r_H as a function of $\tan\beta/m_{H^\pm}$. We show curves for $\tilde{\epsilon}_0 \frac{m_{H^\pm}}{100\,\mathrm{GeV}} = 0, \pm 0.01$.

to the SM rate ($r_H = 1$) is expected in both channels with data samples of a few ab^{-1}, so that Super-KEKB might actually be able to measure r_H. One can see that $r_H = 1$ is obtained for $\tan\beta/m_{H^\pm} = 0.27 \pm 0.03\,\mathrm{GeV}^{-1}$, while complete cancellation can occur around $\tan\beta/m_{H^\pm} = 0.2\,\mathrm{GeV}^{-1}$. Importantly, any signal of a $H^\pm$ in the decay $B \to \overline{D}\tau^\pm\nu$ (which is sensitive to $\tan\beta/m_{H^\pm} > 0.14$ with 5 ab^{-1}) would also manifest itself in both $B^\pm \to \tau^\pm\nu$ and $B^\pm \to \mu^\pm\nu$.

An additional observable in which f_B cancels out is the ratio $R_{\tau\mu}$ defined by:

$$R_{\tau\mu} = \frac{BR(B^\pm \to \tau^\pm\nu)}{BR(B^\pm \to \mu^\pm\nu)} \tag{4.15}$$

Assuming only $W^\pm$ and $H^\pm$ contributions, r_H would also cancel out, and thus $R_{\tau\mu} \sim m_\tau^2/m_\mu^2$. However, sizeable deviations of $R_{\tau\mu}$ from this value are possible in R parity violating SUSY models, since r_H is in general no longer independent of the lepton flavour. In addition, in such models the decay $B^\pm \to e^\pm\nu$ may be enhanced to experimental observability.

4.4.2 Estimation of signal and background

To estimate the sensitivity for these decays, we start with the decay mode, $B^- \to K^-\nu\bar{\nu}$, taking a nominal full reconstruction efficiency of 0.2% for B^+using high quality hadronic tags, with an integrated luminosity of 50 ab^{-1}. Although the physics is different, the B decay to $\tau\nu$ has the same topology when one prong τ decay modes are used to observe the signal. Thus, in the following the $B \to \tau\nu$ decay will be analyzed as well.

The signature of a $B^- \to K^-\nu\bar{\nu}$ decay is a single kaon and nothing else recoiling against the reconstructed B meson. In order to estimate backgrounds for this decay, we first identify other B decay modes that have only one charged particle in the final state, using the QQ generator. We find that examples of such decays are: semi-leptonic B decays, $B \to D^{(*)}\ell\nu$ in which the D decays to $K_L\pi^0$, $B \to D\rho$, $D\pi$ with $D \to K_L\pi^0$; charmless B decays such as $B^+ \to \rho^+\pi^0$.

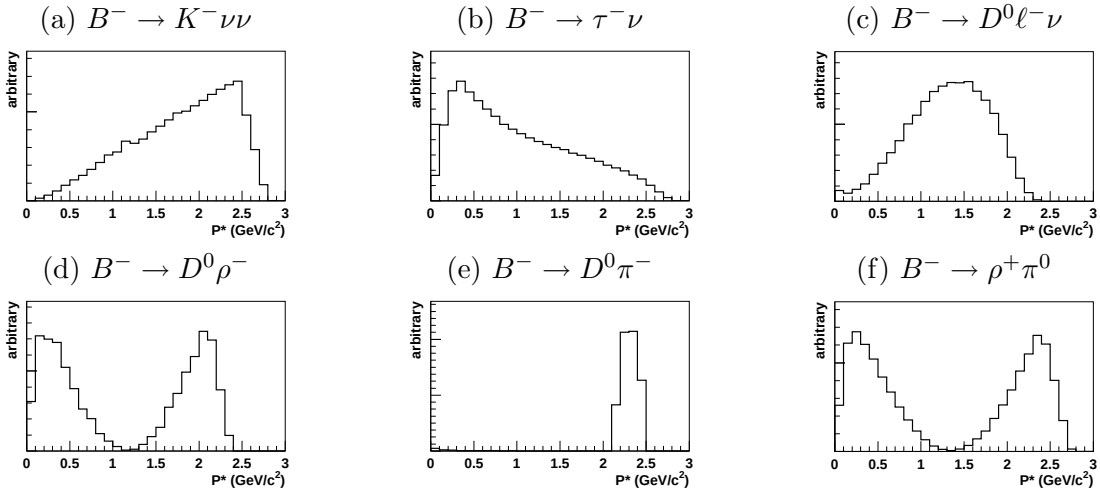

Figure 4.16: Momentum distributions of the only charged particle for various B decays.

Figure 4.16 shows the momentum distributions of the charged particle in these decays as well as in the signal modes. A three body phase space decay for $B \to K\nu\bar{\nu}$ is assumed.

We then estimate the amount of signal and background assuming 50 ab^{-1} using a full simulation program based on GEANT3 for the Belle experiment. We assume that the full reconstruction is perfect and its efficiency is 0.2%. Figure 4.17 shows the total energy deposited in the electro-magnetic calorimeter by the signal side "B" meson decay, unmatched hadronic interactions and beam related backgrounds. We select events in which only one charged track is observed with a momentum cut; $|\vec{p}^*| > 0.7$ GeV/c. Particle identification cuts are not applied on the charged particle. These criteria are rather similar to the recent analyses. It is obvious that we need tighter selection criteria to observe signals.

We optimize the momentum selection to 2.0 GeV/$c < |\vec{p}^*| < 2.7$ GeV/c using Fig. 4.16. We also apply tight KID requirements. Figure 4.18 shows the total energy distribution after applying these selection criteria. If we define the signal region to be $E < 0.5$ GeV, the number of $B \to K\nu\bar{\nu}$ events is estimated to be 43.0±1.1, while the contribution from the background, 29.3±3.4 events. This corresponds to a significance of 5.1σ. Table 4.8 summarizes the background contribution for each decay mode. Large contributions from semi-leptonic decays are reduced by applying tight kaon identification selection.

4.4.3 Discussion

Further improvements for this analysis are expected. The efficiency for the full reconstruction tagging technique can be improved. Optimisation of the tag side efficiency and background can be studied separately for the discovery of the decay and setting upper limit. Likelihood methods can be used for the tag side as well as information on the signal single charged track and energy deposits in the calorimeter. Better solid angle coverage will improve both tagging efficiency and signal efficiency. Much better kaon identification and rejection of other spieces will reduce the backgrounds. More effective rejection of the events that contain K_L's can be studied. On the other hand, the environment may become much harsher as luminosity goes up and beam related backgrounds will certainly increase if the detector performance remains the same, reducing the tagging efficiency and giving more energy deposits in the calorimeter. So far we are not able to estimate such effects quantitatively, but are hoping to continue to study this important decay

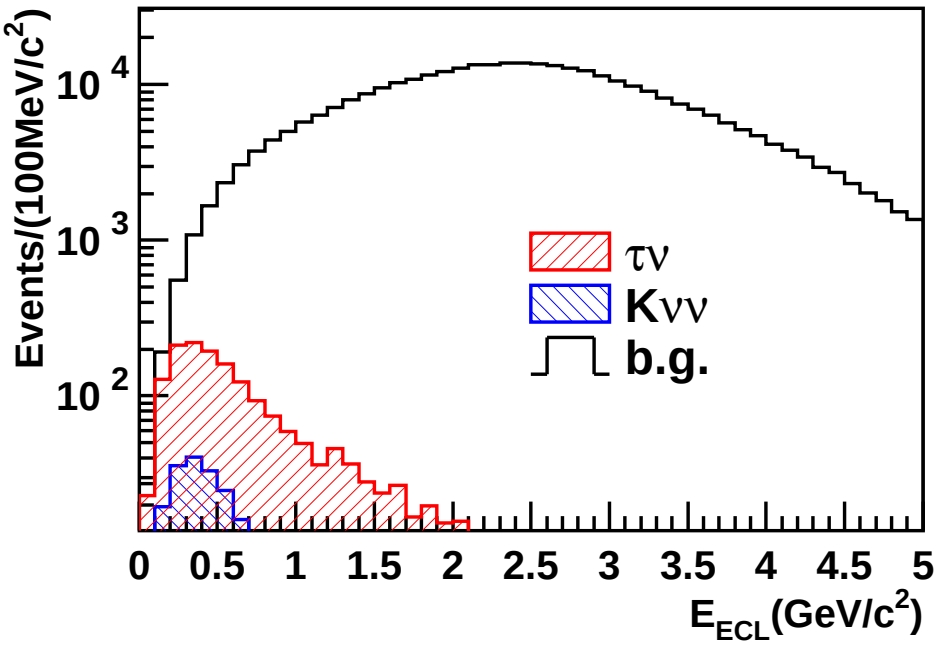

Figure 4.17: ECL energy distribution for $B \to K\nu\bar{\nu}$, $B \to \tau\nu$ and background MC (log scale). The only requirement applied to the charged particle is$|\vec{p}^*| > 0.7$ GeV/c.

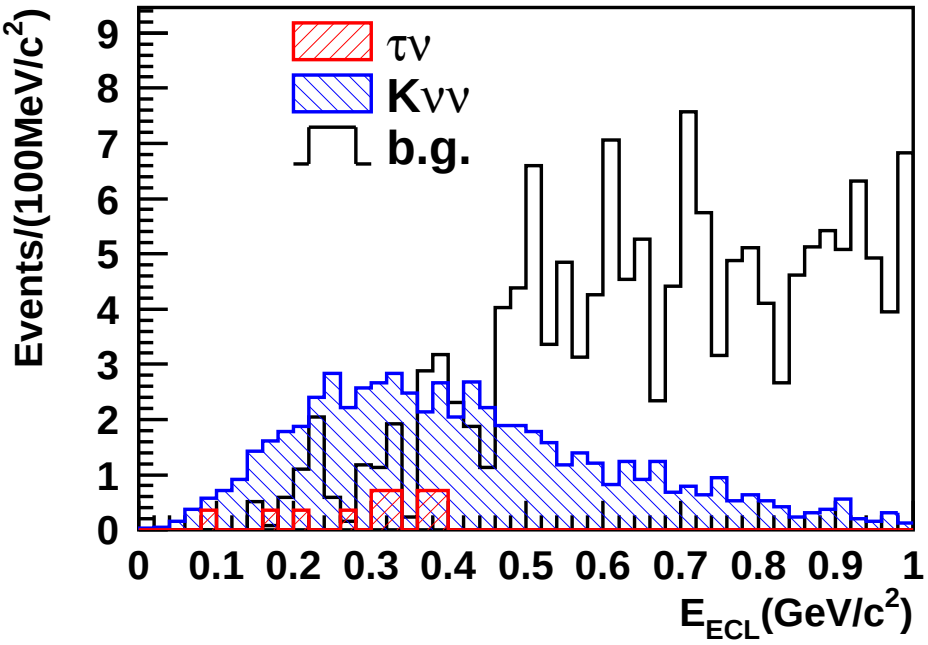

Figure 4.18: ECL energy distribution for $B \to K\nu\bar{\nu}$, $B \to \tau\nu$ and background MC, with 2.0 GeV/$c < |\vec{p}^*| <$ 2.7 GeV/c and a tight KID requirement applied to the charged particle.

Table 4.8: Backgrounds in the $B \to K\nu\bar{\nu}$

Mode	$E < 1.0$ GeV	$E < 1.0$ GeV with KID	$E < 0.5$ GeV with KID
$B^- \to D^{*0}\mu^-\bar{\nu}$	265.7 ± 11.7	8.2 ± 2.1	2.1 ± 1.0
$B^- \to D^0\pi^-$	199.0 ± 10.1	7.7 ± 2.0	3.1 ± 1.3
$B^- \to D^{*0}e^-\bar{\nu}$	181.1 ± 9.6	8.7 ± 2.1	2.1 ± 1.0
$B^- \to D^0\mu^-\bar{\nu}$	131.3 ± 8.2	25.1 ± 3.6	5.1 ± 1.6
$B^- \to D^{*0}\pi^-$	110.3 ± 7.5	3.6 ± 1.4	0.0 ± 0.0
$B^- \to D^0\rho^-$	95.9 ± 7.0	6.2 ± 1.8	1.0 ± 0.7
$B^- \to D^0e^-\bar{\nu}$	85.7 ± 6.6	19.5 ± 3.2	4.1 ± 1.5
$B^- \to D^{*0}\rho^-$	43.6 ± 4.7	3.6 ± 1.4	0.5 ± 0.5
$B^- \to D^0K^-$	13.3 ± 2.6	8.7 ± 2.1	2.1 ± 1.0
$B^- \to D^{*0}K^-$	5.6 ± 1.7	4.6 ± 1.5	0.5 ± 0.5
Other $b \to c$ decays	29.8 ± 3.9	3.1 ± 1.3	1.0 ± 0.7
$b \to c$ decays total	1161.4 ± 24.4	99.0 ± 7.1	21.5 ± 3.3
$B^- \to K^{*-}\pi^-\pi^+$	28.0 ± 1.5	0.8 ± 0.2	0.2 ± 0.1
$B^- \to \pi^-\bar{K}^0$	22.8 ± 1.3	0.5 ± 0.2	0.0 ± 0.0
$B^- \to \rho^+\pi^0$	21.1 ± 1.3	0.4 ± 0.2	0.0 ± 0.0
$B^- \to K^-f_2'(1525)$	19.1 ± 1.2	12.5 ± 1.0	1.1 ± 0.3
$B^- \to K^-\pi^0$	18.5 ± 1.2	12.7 ± 1.0	3.3 ± 0.5
$B^- \to K^{*-}\rho^0$	13.6 ± 1.0	0.2 ± 0.1	0.1 ± 0.1
$B^- \to K^{*-}f_2(1270)$	10.9 ± 0.9	0.4 ± 0.2	0.0 ± 0.0
$B^- \to K^{*-}f_2'(1525)$	10.7 ± 0.9	8.2 ± 0.8	1.3 ± 0.3
$B^- \to \pi^-\pi^0$	9.3 ± 0.8	0.4 ± 0.2	0.2 ± 0.1
$B^- \to K^{*-}\gamma$	7.9 ± 0.8	0.0 ± 0.0	0.0 ± 0.0
$B^- \to \rho^+K^0$	7.1 ± 0.7	0.1 ± 0.1	0.0 ± 0.0
$B^- \to \pi^-K^{*0}$	6.0 ± 0.7	0.1 ± 0.1	0.0 ± 0.0
$B^- \to K^-\eta'$	4.5 ± 0.6	3.2 ± 0.5	0.2 ± 0.1
$B^- \to K^-f_0(1370)$	4.0 ± 0.6	2.2 ± 0.4	0.2 ± 0.1
$B^- \to K^-\eta$	3.9 ± 0.5	2.7 ± 0.5	0.5 ± 0.2
$B^- \to K^-f_2(1270)$	3.5 ± 0.5	2.4 ± 0.4	0.2 ± 0.1
$B^- \to \bar{K}_0^*(1430)^0\pi^-$	2.8 ± 0.5	0.2 ± 0.1	0.1 ± 0.1
$B^- \to \rho^-\eta$	2.8 ± 0.5	0.0 ± 0.0	0.0 ± 0.0
$B^- \to K^-K^0$	2.5 ± 0.4	1.7 ± 0.4	0.4 ± 0.2
Other rare B decays	16.7 ± 1.1	3.2 ± 0.5	0.2 ± 0.1
Rare B decays total	215.6 ± 4.1	51.6 ± 2.0	7.8 ± 0.8
Total	1377.0 ± 24.7	150.6 ± 7.3	29.3 ± 3.4

mode.

4.5 More than one neutrino II: $B \to \bar{D}\tau^+\nu_\tau$

The decay of $B \to \bar{D}\tau^+\nu_\tau$ is sensitive to the existence of charged Higgs bosons, which are introduced in the Minimal Supersymmetric Standard Model (MSSM). A large branching fraction of $B \to \bar{D}\tau^+\nu_\tau$ is expected (8×10^{-3}) in the SM. However, much more data is needed to be employed to measure the branching fraction because of the presence of two or more neutrinos in the decay final state. This mode consequently requires the tagging of other side B, for which reconstruction efficiency is estimated to be 0.2%, that has been discussed in subsection 4.1.2. Therefore, study of the MSSM Higgs through this decay mode is only possible with the statistical power of SuperKEKB.

4.5.1 Introduction

In the MSSM, the couplings of the charged Higgs bosons, $H^\pm$, to quarks and leptons are given by

$$\begin{aligned} \mathcal{L}_H &= (2\sqrt{2}G_F)^{1/2} \times \left[\tan\beta\,(\bar{u}_L V_{KM} M_d d_R + \bar{\nu}_L M_\ell \ell_R) + \frac{\bar{u}_R V_{KM} M_u d_L}{\tan\beta} \right] H^\pm \\ &\quad + h.c., \end{aligned} \tag{4.16}$$

where M_u and M_d are the quark mass matrices, M_ℓ is the lepton ($\ell = e$, μ, or τ) mass matrix, V_{KM} is the Cabbibo-Kobayashi-Maskawa matrix, and $\tan\beta = v_2/v_1$ is a ratio of the vacuum expectation values of the Higgs fields. Therefore, the decay amplitude of $B \to \bar{D}\tau^+\nu_\tau$ that is mediated by $\bar{b} \to c\tau^+\nu$ transition has the term proportional to $M_b M_\tau \tan^2\beta$ [53]. The large τ mass is an advantage of this decay in measuring the charged Higgs mass compared to other semi-leptonic decays.

Figure 4.19 (left) shows the ratio B:

$$B = \frac{\Gamma(B \to \bar{D}\tau^+\nu_\tau)}{\Gamma(B \to \bar{D}\mu^+\nu_\mu)_{\rm SM}} \tag{4.17}$$

as a function of the charged Higgs mass with several $\tan\beta$ values. The width of each band is due to uncertainty in the hadron form factor. The form factor can be modeled as a function of the momentum transfer, q^2, and is parameterized by a slope parameter, ρ_1^2 [54]. The dominant uncertainty in the form factor is from the uncertainty in ρ_1^2. The Belle collaboration has determined $\rho_1^2 = 1.33 \pm 0.22$ [55].

Figure 4.19 (right) shows the $\delta B/B|_{\rm exp}$ distribution as a function of $\delta\rho_1^2/\rho_1^2|_{\rm exp}$. In the figure we show several curves with varying $R \equiv M_W \tan\beta/M_H^\pm$.

4.5.2 $B \to \bar{D}\tau^+\nu_\tau$ Reconstruction

Final states for the $B \to \bar{D}\tau^+\nu_\tau$ decay includes two τ-neutrinos after taking into account the sub-decay of the τ; one additional neutrino exists when τ decays into a leptonic mode. Because of the presence of two or more invisible particles, the decay of $B \to \bar{D}\tau^+\nu_\tau$ has few kinematic constraints. To reduce the number of combinations of the reconstructed D and τ, we first remove particles originating from the other B ($B_{\rm ful}$), which does not decay into $B \to \bar{D}\tau^+\nu_\tau$ ($B_{\rm sig}$). We then reconstruct D and τ candidates using the remaining particles. Finally, we apply kinematic selection requirements on the reconstructed D and τ combination to reduce background.

In the following paragraphs we describe the reconstruction of $B \to \bar{D}\tau^+\nu_\tau$. A detailed description of the full reconstruction of $B_{\rm ful}$ mesons is given in subsection 4.1.2.

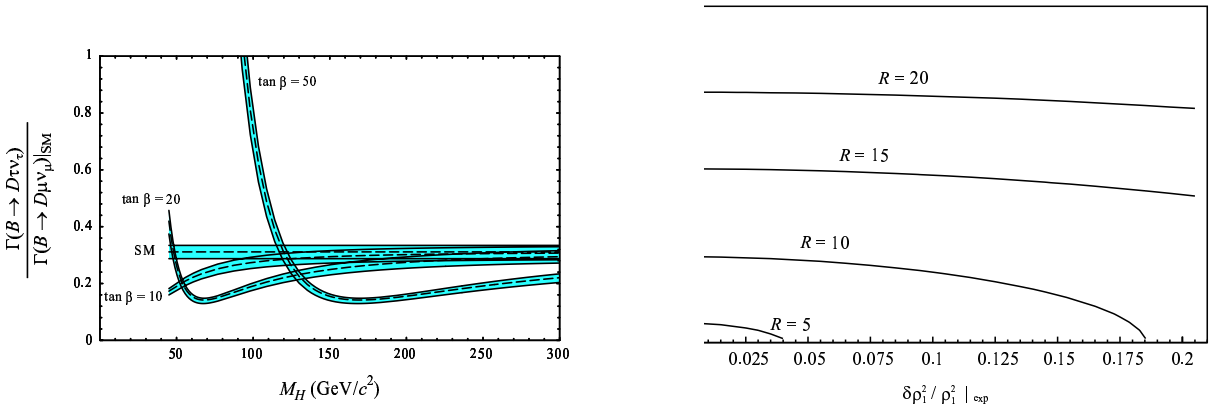

Figure 4.19: The left figure shows the ratio of $\Gamma(B \to \bar{D}\tau^+\nu_\tau)$ to $\Gamma(B \to \bar{D}\mu^+\nu_\mu)$. The flat band is the prediction of the Standard Model; also shown is the charged Higgs contribution, which is a function of the charged Higgs mass with several $\tan\beta$ values. The width of each band is due to uncertainty in the form factor. The right figure shows the $\delta B/B|_{\rm exp}$ distribution as a function of $\delta\rho_1^2/\rho_1^2|_{\rm exp}$ with varying $R \equiv M_W \tan\beta/M_H^\pm$.

Light Meson Reconstructions The K_S^0 mesons are reconstructed from a pair of oppositely charged π tracks. The invariant mass of the π pair should be within $|M_{\pi\pi} - M_{K_S^0}| < 15{\rm GeV}/c^2$. The position of closest approach of the π tracks should be displaced from the interaction point in the plane perpendicular to the beam axis. The selection criteria for the track position (dr) depends on the total momentum of the K_S^0 ($|p_{K_S^0}|$): $dr > 0.5$ mm, $dr > 0.3$ mm, and $dr > 0.2$ mm for $|p_{K_S^0}| < 0.5$ GeV/c^2, $0.5 \le |p_{K_S^0}| < 1.5$ GeV/c^2, and $1.5 \le |p_{K_S^0}|$ GeV/c^2, respectively.

Neutral pions are reconstructed from a pair of two photons. The π^0 invariant mass is required to be within $|M_{\gamma\gamma} - M_{\pi^0}| < 16$ MeV/c^2. We require the photon energy deposit in the calorimeter to be greater than 50 MeV.

Charmed Meson Reconstructions We reconstruct D mesons from $\bar{D}^0 \to K^+\pi^-(\pi^0)$, $K^+\pi^+\pi^-\pi^-(\pi^0)$, $K_S^0\pi^+\pi^-(\pi^0)$, and $K_S^0\pi^0$ [56], where (π^0) indicates zero or one neutral pion. These channels cover 35% of the total $\bar{D}^0$ decay width. The charged D meson is reconstructed from $D^+ \to K^-\pi^+\pi^+(\pi^0)$ and $K_S^0\pi^+$, covering 16% of the total D^+ decay width.

We construct kaon ($\mathcal{L}(K)$) and pion ($\mathcal{L}(\pi)$) likelihoods to identify the particle species of each charged particle by combining the dE/dx in the drift chamber, the hit in the time of flight counter and the ring imaging Cherenkov counter. The charged particle is identified as a kaon if $\mathcal{L}(K)/[\mathcal{L}(\pi) + \mathcal{L}(K)]$ exceeds 0.4; otherwise it is a pion.

The reconstructed D^0 or D^+ should have invariant mass within $|M_{Kn\pi} - M_D| < 30$ MeV/c^2.

If more than one D meson is reconstructed, the D meson that has the closest invariant mass to the world average value is taken [57].

B Meson Reconstructions The $B \to \bar{D}\tau^+\nu_\tau$ decay is reconstructed from $B^0 \to D^-\tau^+\nu_\tau$ and $B^+ \to \bar{D}^0\tau^+\nu_\tau$, where the τ^+ is identified in one of four following sub-decays: $\tau^+ \to \pi^+\nu_\tau$, $\rho^+(\pi^+\pi^0)\nu_\tau$, $e^+\nu_\tau\bar{\nu}_e$, and $\mu^+\nu_\tau\bar{\nu}_\mu$.

The $B \to \bar{D}\tau^+\nu_\tau$ candidate is reconstructed by adding one charged particle, which is assumed to originate from the τ^+ decay, to the reconstructed D meson. Positively identified protons are rejected.

If the additional charged particle is consistent with the electron or muon hypothesis, the τ^+ decay is treated as a leptonic mode ($\tau^+ \to \ell^+\nu_\tau\bar{\nu}_\ell$) [58]; otherwise the τ^+ decay is considered as a hadronic mode ($\tau^+ \to \pi^+\nu_\tau$).

In the case of $\tau^+ \to \pi^+\nu_\tau$ decay, one neutral pion (if it exists) that is associated to neither $B_{\rm ful}$ nor D decay is added to the $\pi^+\nu_\tau$ final state to reconstruct $\tau^+ \to \rho^+(\pi^+\pi^0)\nu_\tau$ mode. In this case, the $\pi^+\pi^0$ invariant mass should be within $|M_{\pi^+\pi^0} - M_{\rho^+}| < 300$ MeV/c^2.

To reject $B \to \bar{D}^*\tau\nu_\tau$ events, we reconstruct D^*'s by adding a π^0 to the reconstructed D. When $|(M_{Kn\pi\pi^0} - M_{Kn\pi}) - \Delta M_{D^*-D}| < 10$ MeV/c^2, we discard the event.

If any charged particle and/or K^0_L candidate remains after the reconstructions of $B_{\rm ful}$ and $B_{\rm sig}$, the event is rejected.

4.5.3 Kinematic Event Selection

We use three kinematic parameters to select the $B \to \bar{D}\tau^+\nu_\tau$ signal events from the reconstructed candidates.

The first is the residual cluster energy in the calorimeter ($E_{\rm res}$). We require $E_{\rm res} < 100$ MeV.

The second is the missing-mass squared defined by

$$|MM|^2 \equiv |p_{B_{\rm sig}} - p_D - p_{X^+}|^2, \tag{4.18}$$

where p_{X^+} is the charged particle momentum originating from the τ^+ decay. The momentum $p_{B_{\rm sig}}$ is given by $p_{B_{\rm sig}} = p_{\Upsilon(4S)} - p_{B_{\rm ful}}$.

The last is the cosine of the angle between the momenta of the two τ-neutrinos ($\cos\theta$) in the frame where $\vec{p}_{B_{\rm sig}} = \vec{p}_D$. This parameter can only be defined for $\tau^+ \to h^+\bar{\nu}_\tau$ sub-decay. Energy-momentum conservation for the $B_{\rm sig} \to D\tau^+(h^+\bar{\nu}_\tau)\nu_\tau$ decay is expressed by

$$p_{B_{\rm sig}} = p_D + p_{h^+} + p_{\bar{\nu}_\tau} + p_{\nu_\tau}. \tag{4.19}$$

The τ^+ and neutrino masses are given by

$$(p_{h^+} + p_{\bar{\nu}_\tau})^2 = m_\tau^2, \tag{4.20}$$

$$p_{\bar{\nu}_\tau}^2 = p_{\nu_\tau}^2 = 0. \tag{4.21}$$

We then boost the system to the frame where

$$\vec{p}_{B_{\rm sig}} = \vec{p}_D. \tag{4.22}$$

Using Eq. (4.19)-(4.22), we have

$$(E_{B_{\rm sig}} - E_D)^2 - 2E_{\nu_\tau}(E_{B_{\rm sig}} - E_D) = m_\tau^2. \tag{4.23}$$

Then, the energies of the two neutrinos can be expressed in terms of measurable parameters as

$$E_{\nu_\tau} = \frac{(E_{B_{\rm sig}} - E_D)^2 - m_\tau^2}{2(E_{B_{\rm sig}} - E_D)}, \qquad E_{\bar{\nu}_\tau} = E_{B_{\rm sig}} - E_D - E_{h^+} - E_{\nu_\tau}. \tag{4.24}$$

Finally, we can measure $\cos\theta$ using the following equation:

$$\begin{aligned} (\vec{p}_{B_{\rm sig}} - \vec{p}_D - \vec{p}_{h^+})^2 &= (\vec{p}_{\bar{\nu}_\tau} + \vec{p}_{\nu_\tau})^2 \\ &= 2\vec{p}_{\bar{\nu}_\tau} \cdot \vec{p}_{\nu_\tau} \\ &= 2E_{\bar{\nu}_\tau}E_{\nu_\tau}\cos\theta. \end{aligned} \tag{4.25}$$

Table 4.9: Summary of the reconstruction efficiencies. The numbers of reconstructed signal ($N_{\rm sig}$) and the background events ($N_{\rm bkg}$) in generic B decay MC samples are also shown, where $Br(B \to \bar{D}\tau^+\nu_\tau) = 8 \times 10^{-3}$ is assumed.

Decay mode	efficiency (%)	Br	$N_{\rm sig}$	$N_{\rm bkg}$
$\bar{D}^0\tau^+(\ell^+\bar{\nu}_\tau\nu_\ell)\nu_\tau$	4.9 ± 0.3	13.5×10^{-4}	213	293
$\bar{D}^0\tau^+(h^+\bar{\nu}_\tau)\nu_\tau$	10.9 ± 0.5	13.6×10^{-4}	476	2085
$D^-\tau^+(\ell^+\bar{\nu}_\tau\nu_\ell)\nu_\tau$	0.7 ± 0.2	6.2×10^{-4}	15	22
$D^-\tau^+(h^+\bar{\nu}_\tau)\nu_\tau$	3.3 ± 0.4	6.4×10^{-4}	68	194

The $\cos\theta$ of the signal events is limited from -1 to $+1$, while that of the background events is unrestricted.

The background contamination is studied by using generic B decay MC samples. We generate samples of 3.2×10^6 fast simulated MC events for generic charged and neutral B decays. In this case, 8×10^{-3} is taken as the branching fraction of $B \to \bar{D}\tau^+\nu_\tau$ decay for both charged and neutral B. To increase statistics, the $B_{\rm ful}$ is pseudo-reconstructed using generator information, i.e.: the $B_{\rm ful}$ is fully reconstructed with perfect efficiency and purity.

Figure 4.20 shows the distribution of the reconstructed $B^+ \to \bar{D}^0\tau^+(h^+\bar{\nu}_\tau)\nu_\tau$ candidates in the $|MM|^2$-$\cos\theta$ plane. The left column figures show the signal events only and the right ones show the background distribution (gray points) with superimposed signal distribution (black points). We determine the optimal signal region to be $|MM|^2 > 0.1$ (GeV/c^2)^2 and $-1.0 < \cos\theta < 0.8$, irrespectively of the $\tau^+ \to \pi^+\bar{\nu}_\tau$ or $\tau^+ \to \rho^+\bar{\nu}_\tau$ by maximizing $S/\sqrt{S+B}$ (FOM), where S and B are the numbers of reconstructed signal and background events, respectively.

Figure 4.21 shows the $|MM|^2$ distribution of the reconstructed candidates of $B^+ \to \bar{D}^0\tau^+(\ell^+\bar{\nu}_\tau\nu_\ell)\nu_\tau$. For that decay irrespectively of the lepton flavor from the τ decay, we determine the selection criteria $|MM|^2 > 1.2$ (GeV/c^2)^2 by maximizing the FOM.

We find that $|MM|^2$ and $\cos\theta$ for the neutral B decay have similar distributions in both signal and background as the charged B decay. Therefore, the selection criteria determined by charged B decays are also applied to neutral B decays.

Table 4.9 summarizes the reconstruction efficiency. The numbers of reconstructed signal and the background events in the generic B decay MC samples are also shown.

4.5.4 Background Components

The dominant background source in the $B^+ \to \bar{D}^0\tau^+(h^+\bar{\nu}_\tau)\nu_\tau$ signal region is the decay $B^+ \to D^{*-}\ell^+\nu_\ell\pi^+$, due mainly to the missing ℓ^+ and slow pion from the D^{*-}. The next largest background modes are $B^+ \to \bar{D}^{*0}\ell^+\nu_\ell$ with a missing γ or π^0 from the $\bar{D}^{*0}$ and misidentification of ℓ^+ as π^+, and the $B^+ \to \bar{D}^{*0}\tau^+\nu_\tau$ with a missing slow pion. In this study the $B^+ \to \bar{D}^0\tau^+(\ell^+\bar{\nu}_\tau\nu_\ell)\nu_\tau$ decay is considered as a background for the $B^+ \to D^-\tau^+(h^+\bar{\nu}_\tau)\nu_\tau$ analysis; they contribute to the signal region due mostly to misidentification of the ℓ^+ from the τ^+ decay as π^+. The sum of the background modes listed above are $\sim 45\%$ of the total background. The contribution from D_s inclusive decays is $\sim 8\%$ of the total.

The largest contribution to the $B^+ \to \bar{D}^-\tau^+(\ell^+\bar{\nu}_\tau\nu_\ell)\nu_\tau$ signal region comes from $B^+ \to \bar{D}^{*-}\ell^+\nu_\ell\pi^+$ where both pions from B^+ and $\bar{D}^{*-}$ are missed. The next largest background components are $B^+ \to \bar{D}^{*0}\ell^+\nu_\ell$ and $B^+ \to \bar{D}^{*0}\tau^+\nu_\tau$ when the γ or π^0 from the $\bar{D}^{*0}$ are missed.

The dominant background mode in the $B^0 \to D^-\tau^+(h^+\bar{\nu}_\tau)\nu_\tau$ signal region is $B^0 \to D^-\tau^+\nu_\tau$

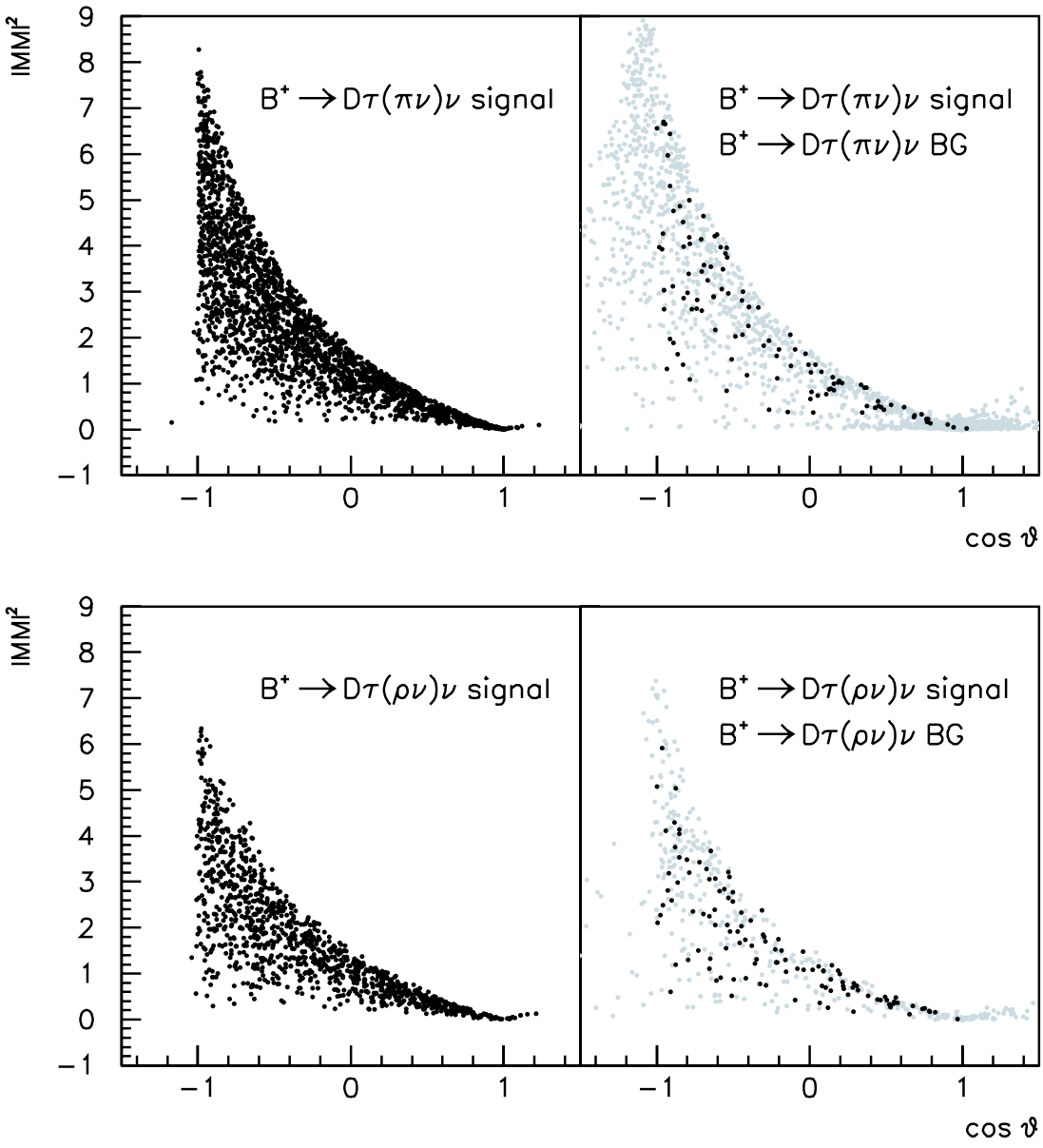

Figure 4.20: A scatter plot of the reconstructed $B^+ \to \bar{D}^0\tau^+(h^+\bar{\nu}_\tau)\nu_\tau$ candidates in the $|MM|^2$-$\cos\theta$ plane. The upper two figures are obtained in the $\tau^+ \to \pi^+\bar{\nu}_\tau$ decay, and the lower two figures are obtained in the $\tau^+ \to \rho^+(\pi^+\pi^0)\bar{\nu}_\tau$ decay. The left figures show the distributions obtained from signal MC. In the right figures, the background distributions are shown by gray points and the signal distributions are shown by black points.

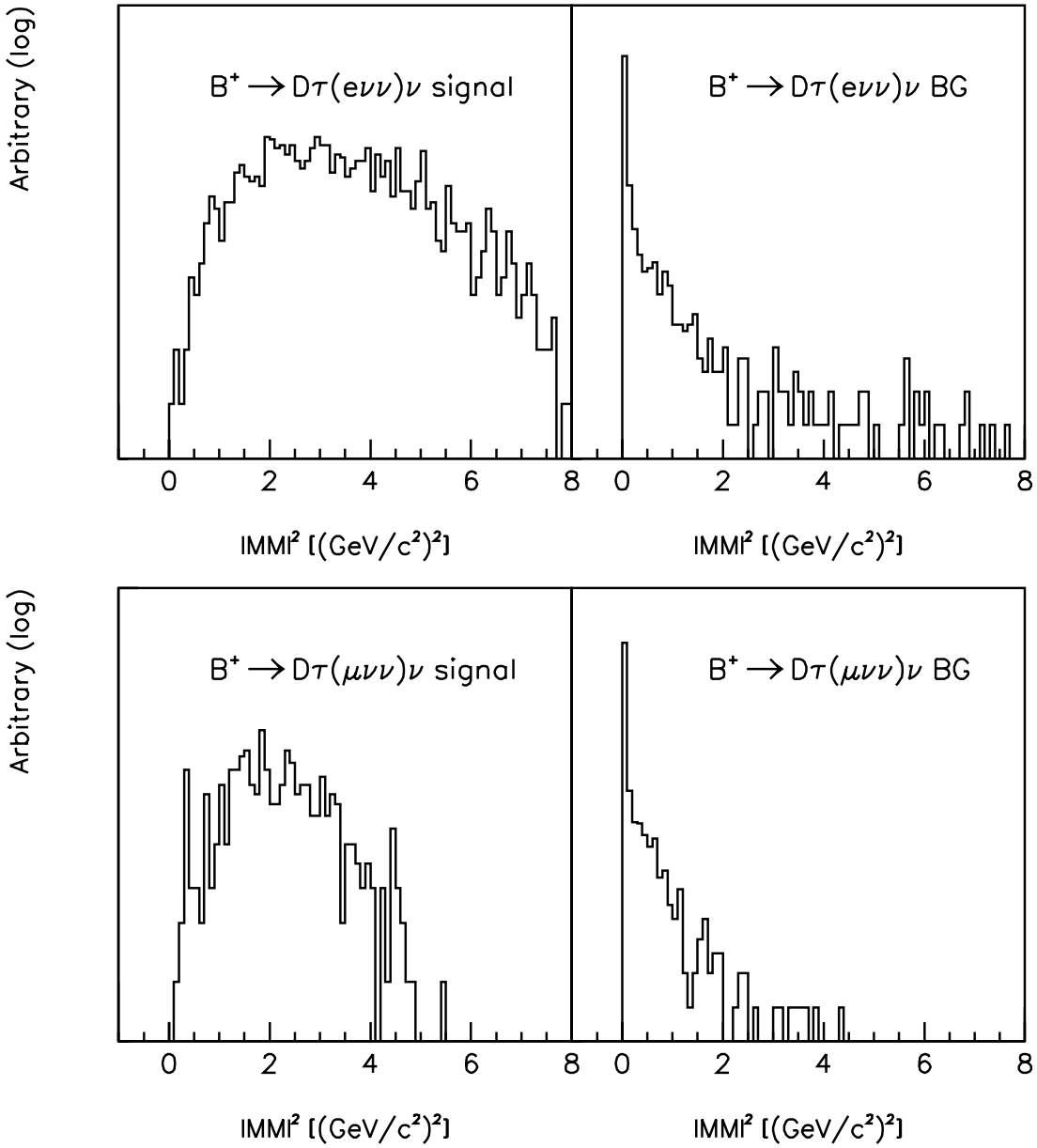

Figure 4.21: The $|MM|^2$ distribution for reconstructed $B^+ \to \bar{D}^0\tau^+(e^+\bar{\nu}_\tau\nu_e)\nu_\tau$ candidates (upper) and $B^+ \to \bar{D}^0\tau^+(\mu^+\bar{\nu}_\tau\nu_\mu)\nu_\tau$ candidates (lower). The left figures show the distributions obtained from signal MC, and the right figures show the background.

Table 4.10: The expected signal yields and backgrounds at integrated luminosities of 5 and 50 ab^{-1}, assuming $Br(B \to \bar{D}\tau^+\nu_\tau) = 8 \times 10^{-3}$. The expected uncertainties in the measured branching fraction ($\delta(Br)/Br$) are also shown.

Decay mode	5 ab^{-1}			50 ab^{-1}		
	$N_{\rm sig}$	$N_{\rm bkg}$	$\delta(Br)/Br$	$N_{\rm sig}$	$N_{\rm bkg}$	$\delta(Br)/Br$
$\bar{D}^0\tau^+(\ell^+\bar{\nu}_\tau\nu_\ell)\nu_\tau$	280 ± 20	550 ± 20	7.9%	2800 ± 50	5500 ± 70	2.5%
$\bar{D}^0\tau^+(h^+\bar{\nu}_\tau)\nu_\tau$	620 ± 20	3600 ± 60		6200 ± 80	36000 ± 200	
$D^-\tau^+(\ell^+\bar{\nu}_\tau\nu_\ell)\nu_\tau$	10 ± 3	21 ± 5	28.5%	98 ± 10	210 ± 10	9.0%
$D^-\tau^+(h^+\bar{\nu}_\tau)\nu_\tau$	45 ± 7	170 ± 10		450 ± 20	1700 ± 40	

with a mis-reconstructed τ^+; the next largest is $B^0 \to D^{*-}\mu^+\nu_\mu$, although it is only $\sim 20\%$ of the total. No other background modes make significant contributions in the signal region.

For the $B^0 \to D^-\tau^+(\ell^+\bar{\nu}_\tau\nu_\ell)\nu_\tau$ mode, because of the small MC statistics, we cannot yet evaluate the background.

4.5.5 Statistical Significance

As described in subsection 4.1.2, the full reconstruction efficiencies for charged and neutral B mesons are estimated to be 0.2% and 0.1%, respectively. The estimated purity is 80%.

Table 4.10 lists the expected signal yields and backgrounds at integrated luminosities of 5 and 50 ab^{-1}. The values include a correction for the purity of $B_{\rm ful}$ reconstruction. We assume $Br(B \to \bar{D}\tau^+\nu_\tau) = 8 \times 10^{-3}$ in the table. The values listed are obtained by scaling the results in Table 4.9 according to the integrated luminosity. The expected uncertainties in the measured branching fraction ($\delta(Br)/Br$) are also shown.

The branching fraction for $B^+ \to \bar{D}^0\tau^+\nu_\tau$ is expected to be determined with 12σ statistical significance at an integrated luminosity of 5 ab^{-1}. The branching fractions of the neutral B modes can also be measured at 50 ab^{-1} with 11σ significance.

4.5.6 Systematic Uncertainty

Major sources of systematic uncertainty in the branching fraction measurement in $B \to \bar{D}\tau^+\nu_\tau$ decay are expected to be $B_{\rm ful}$ reconstruction efficiency and purity, particle identification efficiency and purity, and the slow pion detection efficiency.

4.5.7 Constraints on the Charged Higgs Mass

Figure 4.22 (left) shows the maximum R value constrained by the branching fraction measurement of $B^+ \to \bar{D}^0\tau^+\nu_\tau$ as a function of the integrated luminosity for several $\delta\rho_1^2/\rho_1^2|_{\rm exp}$. The right figure shows for the case assuming a doubled uncertainty of the measured branching fraction. The systematic uncertainty in the branching fraction measurement is not considered. We ignore the uncertainty in $\delta B/B|_{\rm exp}$ that comes from the uncertainty in the $B^+ \to \bar{D}^0\mu^+\nu_\mu$ branching fraction because it can be determined much precisely than that of $\bar{D}^0\tau^+\nu_\tau$. We can expect

$$M_H > \frac{M_W \tan\beta}{11}$$

at an integrated luminosity of 5 ab^{-1}, assuming that the current ρ_1^2 precision is unchanged.

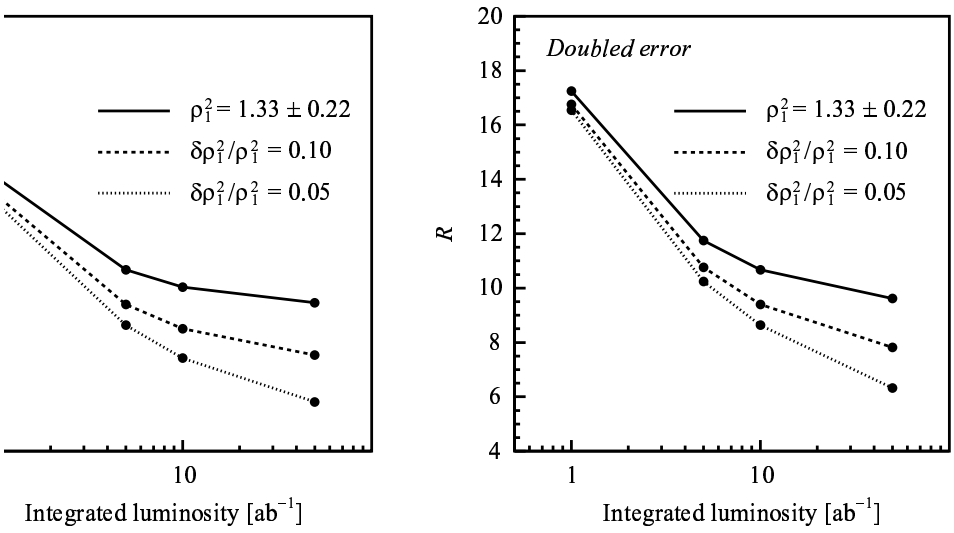

Figure 4.22: The left figure shows the maximum R constrained by the $B^+ \to \bar{D}^0\tau^+\nu_\tau$ branching fraction measurement as a function of the integrated luminosity for several values of $\delta\rho_1^2/\rho_1^2|_{\rm exp}$. The right figure shows the same plot for the case with double the uncertainty in the measured branching fraction

4.5.8 Summary

The $B \to \bar{D}\tau^+\nu_\tau$ decay is a sensitive mode to probe the charged Higgs in the MSSM. Using this decay mode we expect that the charged Higgs mass will be constrained by $M_H > M_W \tan\beta/11$ at an integrated luminosity of 5 ab^{-1}.

4.6 $\sin 2\phi_1$

Very precise measurements of $\sin 2\phi_1$, or $\mathcal{S}_{J/\psi K^0_S}$, will remain important at Super-KEKB. There are two major reasons. One is to search for a new CP-violating phase from the SM in CP violation in $b \to s$ transitions by testing whether $\mathcal{S}_{\phi K^0_S} = \mathcal{S}_{J/\psi K^0_S}$. The other is to check the consistency of the Unitarity Triangle. As explained in Section 2.4.1, $\sin 2\phi_1$ is determined using the $B^0 \to J/\psi K^0_S$ mode with very small hadronic uncertainties. It is also insensitive to effects beyond the SM. Thus it serves as a reliable reference point for the SM.

The present world average value for $\sin 2\phi_1$ is obtained with the modes $B^0 \to J/\psi K^0_L$, $J/\psi K^{*0}$, $\psi(2S)K^0_S$, $\chi_{c1}K^0_S$ and $\eta_c K^0_S$ in addition to the $B^0 \to J/\psi K^0_S$ decay. This is to reduce statistical uncertainties. With an integrated luminosity of 5 ab^{-1}, however, the systematic uncertainties will be dominant. Therefore, in this study we use only the gold-plated mode $B^0 \to J/\psi(\to \ell^+\ell^-)K^0_S(\pi^+\pi^-)$ to minimize systematic uncertainties. We perform MC pseudo-experiments assuming that the performance of the detector at Super-KEKB is identical to that of the present Belle detector. The analysis procedure for the measurements of time-dependent CP asymmetries at Belle is described in Section 4.1.2. In addition to the standard 2-parameter fit, we also test a 1-parameter fit with $\sin 2\phi_1$ as the free parameter assuming $\mathcal{A}_{J/\psi K^0_S} = 0$. Because of the additional assumption, the error on $\sin 2\phi_1$ is slightly smaller than that for $\mathcal{S}_{J/\psi K^0_S}$. In the following we treat these two cases separately. An example of a fit to a Δt distribution for $B^0 \to J/\psi K^0_S$ candidates in a MC pseudo-experiment at 5 ab^{-1} is shown in Fig. 4.23.

Sources of systematic error include uncertainties in the flavor tagging, in the vertex reconstruction, in the background fractions and Δt distributions, in the resolution function, in Δm_d and τ_{B^0}, a possible bias in the fit, and the effect of interference [59] in the $f_{\rm tag}$ final state. Some of these uncertainties are evaluated from control samples, which have large but finite statistics. As the integrated luminosity increases, this part of the systematic error will decrease. In order to estimate the expected systematic error at 5 ab^{-1}, we therefore need to separate such *reducible* systematic errors from the other part, which is *irreducible*. In this study, we conservatively assume that uncertainties that do not arise from statistics of control samples are irreducible, and use estimates obtained for the 140 fb^{-1} data for any integrated luminosity. Further studies on these "*irreducible*" errors will probably find a way to reduce them. Table 4.11 and 4.12 summarize the sources of systematic errors for $\sin 2\phi_1$ (1-parameter fit) and $\mathcal{S}$ and $\mathcal{A}$ (2-parameter fit), respectively. All the values are evaluated at 140 fb^{-1}. The total irreducible systematic error for

Source	Irreducible	Error of $\sin 2\phi_1$
Wrong tag		0.007
Physics parameteres		0.002
Vertexing	$\surd$	0.012
Background fraction		0.006
Background $\lvert\Delta t\rvert$ shape		0.001
Resolution function		0.005
Resolution parameterization	$\surd$	0.006
Tag-side interference	$\surd$	0.001
Possible fit bias		0.008
Total		0.019

Table 4.11: Systematic errors for $\sin 2\phi_1$ measured with the $J/\psi K_S$ mode at 140 fb^{-1}.

$\mathcal{S}$ is estimated to be 0.014 (0.013) for $\mathcal{S}_{J/\psi K^0_S}$ ($\sin 2\phi_1$). The dominant sources of the irreducible

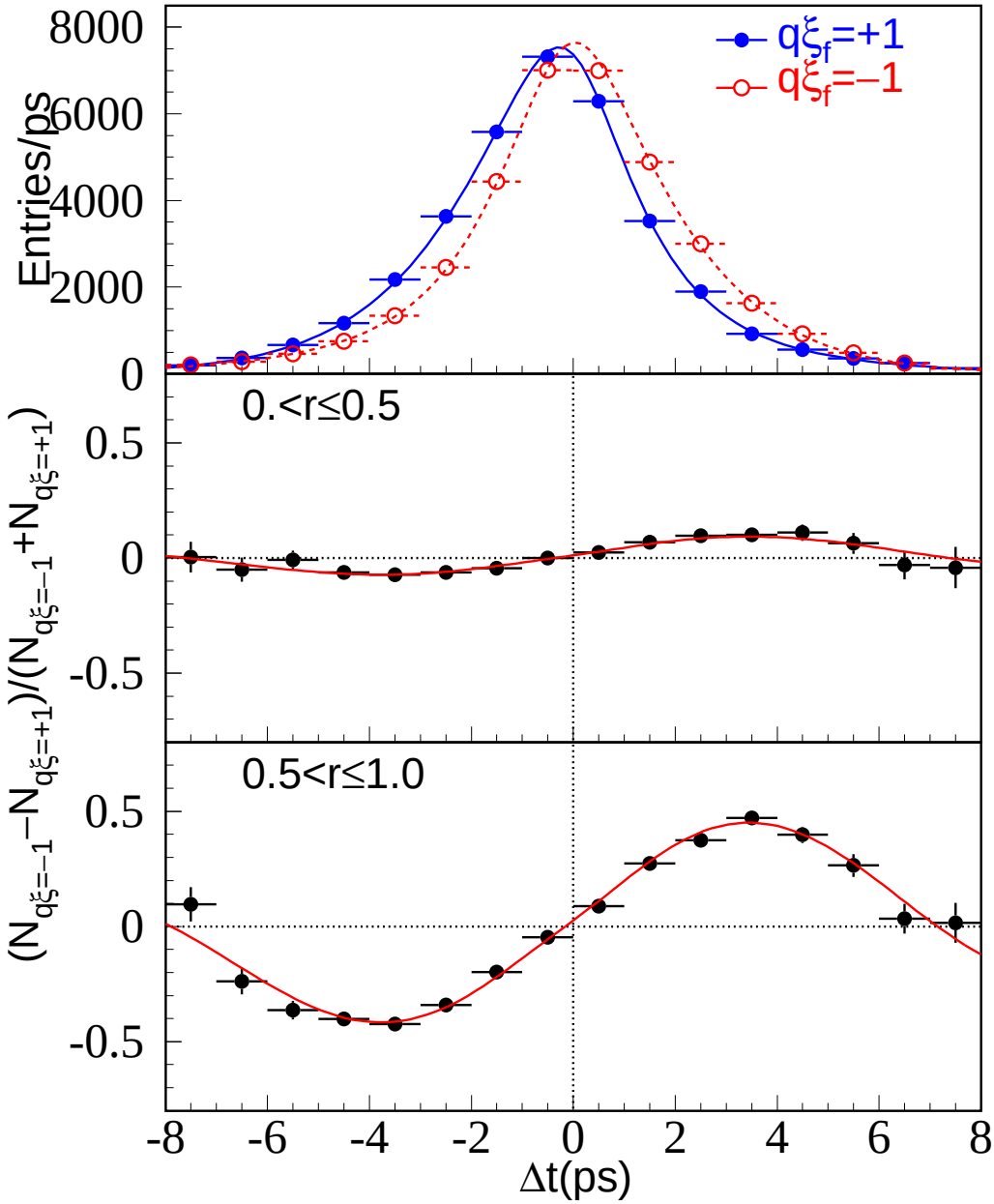

Figure 4.23: An example of a fit to a MC pseudo-experiment at 5 ab^{-1}.

Source	Irreducible	Error of $\mathcal{S}$	Error of $\mathcal{A}$
Wrong tag		0.007	0.008
Physics parameteres		0.002	0.001
Vertexing	$\surd$	0.012	0.026
Background fraction		0.006	0.012
Background $\lvert\Delta t\rvert$ shape		0.001	0.000
Resolution function		0.005	0.007
Resolution parameterization	$\surd$	0.006	0.002
Tag-side interference	$\surd$	0.001	0.027
Possible fit bias		0.008	0.006
Total		0.019	0.041

Table 4.12: Systematic errors on $\mathcal{A}$ and $\mathcal{S}$ measured with the $J/\psi K_S$ mode at 140 fb^{-1}.

systematic error are the effect of detector misalignment (0.008) and uncertainties in the resolution function determination (0.007). The systematic error for $\mathcal{A}$ is dominated by the tag-side interference. As mentioned above, there will be a possibility to reduce these "*irreducible*" errors from dedicated studies. Table 4.13 lists the expected errors at 140 fb^{-1}, 5 ab^{-1} and 50 ab^{-1}. The total error for $\mathcal{S}_{J/\psi K^0_S}$, $\sigma_{\rm tot}(\mathcal{S}_{J/\psi K^0_S})$, is obtained from

		Statistical	Systematic		Total
			reducible	irreducible	
$\sin 2\phi_1$	(140 fb^{-1})	0.080	0.014		0.082
	(5 ab^{-1})	0.013	0.002	0.013	0.019
	(50 ab^{-1})	0.004	0.001		0.014
$\mathcal{S}_{J/\psi K^0_S}$	(140 fb^{-1})	0.080	0.014		0.082
	(5 ab^{-1})	0.013	0.002	0.014	0.019
	(50 ab^{-1})	0.004	0.001		0.015
$\mathcal{A}_{J/\psi K^0_S}$	(140 fb^{-1})	0.056	0.017		0.070
	(5 ab^{-1})	0.009	0.003	0.038	0.039
	(50 ab^{-1})	0.003	0.001		0.038

Table 4.13: Expected errors at 140 fb^{-1}, 5 ab^{-1} and 50 ab^{-1}.

$$\sigma_{\rm tot}(\mathcal{S}_{J/\psi K^0_S}) = \sqrt{0.080^2 \times 0.14/\mathcal{L}_{\rm int} + 0.014^2 \times 0.14/\mathcal{L}_{\rm int} + 0.014^2}, \tag{4.26}$$

where $\mathcal{L}_{\rm int}$ is the integrated luminosity in the unit of ab^{-1}. We obtain $\sigma_{\rm tot}(\mathcal{S}_{J/\psi K^0_S}) = 0.019$ at $\mathcal{L}_{\rm int} = 5$ ab^{-1}, which is much smaller than the statistical uncertainties for $\mathcal{S}_{\phi K^0_S}$ and $\mathcal{S}_{\eta' K^0_S}$.

	central value WA from [17]	error at 140 fb^{-1}	error at 500 fb^{-1}	error at 5 ab^{-1}	error at 50 ab^{-1}
$BR(\pi^+\pi^-)$	4.55±0.44	0.50	0.25	0.082	0.026
$BR(\pi^+\pi^0)$	5.27±0.79	0.88	0.47	0.15	0.47
$BR(\pi^0\pi^0)$	1.90±0.47	0.65	0.34	0.11	0.034
$\mathcal{S}_{\pi\pi}$	-0.58 ± 0.20	0.23	0.12	0.039	0.012
$\mathcal{A}_{\pi\pi}$	$+0.38 \pm 0.16$	0.19	0.10	0.031	0.010
$\mathcal{A}_{\pi^0\pi^0}$	0.0	1.00	0.53	0.17	0.053

Table 4.14: Estimated errors for the $\pi\pi$ branching ratios and asymmetries.

4.7 ϕ_2

The CKM angle ϕ_2 can be measured using multi-pion final states coming from the quark-level decay $b \to u\bar{u}d$. As discussed in Section 2.4 the determination through the time-dependent asymmetry of $B^0 \to \pi^+\pi^-$ suffers from large penguin contributions. Here we consider two methods to eliminate an effect of the penguin amplitude: an isospin analysis of $B \to \pi\pi$ [60], and Dalitz analysis of $B \to \rho\pi$ [61].

4.7.1 Status of the $B^0 \to \pi^+\pi^-$ analysis

The time-dependent asymmetry defined in (2.40) for $B^0 \to \pi^+\pi^-$ has already been measured by the Belle [62] and BaBar [63] collaborations. Based on 85×10^6 [62] and 88×10^6 [63] $B\bar{B}$ pairs, they obtained

$$\mathcal{A}_{\pi\pi} = +0.77 \pm 0.27 \pm 0.08,\ \mathcal{S}_{\pi\pi} = -1.23 \pm 0.41^{+0.08}_{-0.07} \quad [62], \tag{4.27}$$

$$\mathcal{A}_{\pi\pi} = +0.30 \pm 0.25 \pm 0.04,\ \mathcal{S}_{\pi\pi} = -0.02 \pm 0.34 \pm 0.05 \quad [63]. \tag{4.28}$$

The first and the second errors are statistical and systematic errors, respectively. The world average is then $\mathcal{A}_{\pi\pi} = +0.38 \pm 0.16$ and $\mathcal{S}_{\pi\pi} = -0.58 \pm 0.20$ [17].

From the Belle result [62], the case that CP symmetry is conserved, $\mathcal{A}_{\pi\pi} = \mathcal{S}_{\pi\pi} = 0$, is ruled out at the 99.93% confidence level (CL), and the 95.5% CL region of $\mathcal{A}_{\pi\pi}$ and $\mathcal{S}_{\pi\pi}$ gives $78^\circ \leq \phi_2 \leq 152^\circ$ with a modest assumption for $|P_{\pi\pi}/T_{\pi\pi}|$. From the theoretical side, QCD factorization gives $-6 \pm 12\%$ for the direct CP asymmetry $\mathcal{A}_{\pi\pi}$ [64], while perturbative QCD (pQCD) suggests a larger direct asymmetry in the range (16−30%) [65].

4.7.2 Isospin analysis for $B \to \pi\pi$

Here we describe the expected sensitivity for the determination of ϕ_2 at the Super-KEKB using the $\pi\pi$ isospin analysis.

Estimated errors for the branching ratios and asymmetries at the target luminosities are shown in Table 4.14. We assume the current world average [17] for the central values, and also assume that the direct CP violation is absent for $B^0 \to \pi^0\pi^0$ decay *i.e.*, $\mathcal{A}_{\pi^0\pi^0} = 0.0$. In the following analysis we use the CKMfitter program [66].

From the $\pi^+\pi^-$ time-dependent asymmetry we may extract the parameters $\mathcal{S}_{\pi\pi}$ and $\mathcal{A}_{\pi\pi}$. The phase of the parameter $\lambda_{\pi\pi} = (q/p)(\bar{A}_{\pi\pi}/A_{\pi\pi})$ is extracted as

$$\sin 2\phi_{2\text{eff}} = \frac{\mathcal{S}_{\pi\pi}}{\sqrt{1 + \mathcal{A}^2_{\pi\pi}}}, \tag{4.29}$$

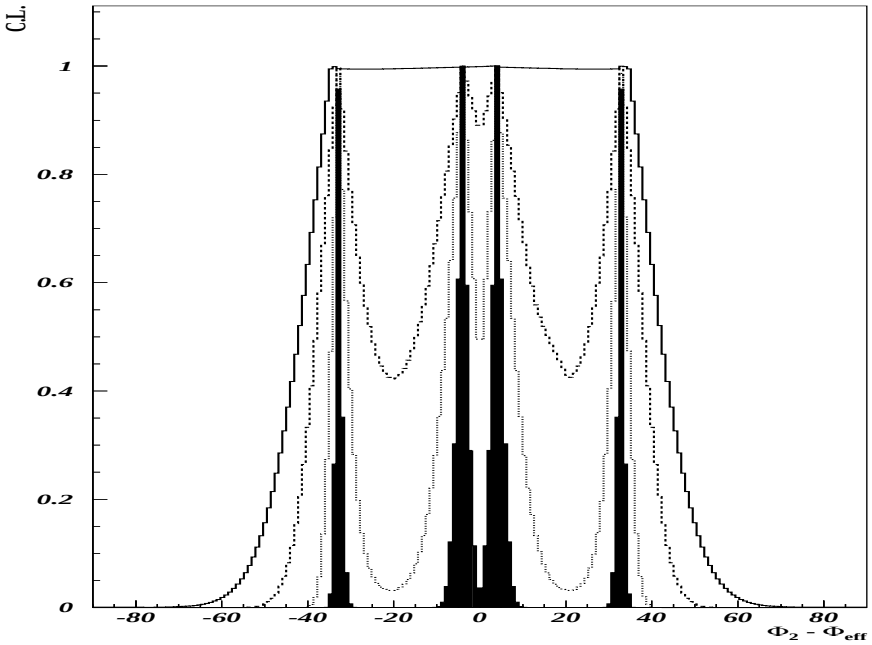

Figure 4.24: CL versus $\phi_2 - \phi_{2\text{eff}}$ (deg) for the inputs given in Table 4.14 at 140 fb^{-1} (solid curve), 500 fb^{-1} (dashed curve), 5 ab^{-1} (dotted curve), and 50 ab^{-1} (shaded area).

which is equal to $\sin 2\phi_2$ if the decay is dominated by the tree amplitude. In the presence of a penguin contribution, we have to subtract the penguin amplitude using isospin relations (2.53) and (2.54).

The results for $\phi_2 - \phi_{2\text{eff}}$ and ϕ_2 are plotted in Figures 4.24 and 4.25, respectively. In those figures the confidence level is plotted at target luminosities up to 50 ab^{-1}. The absence of direct CP violation for $B^0 \to \pi^0\pi^0$ decay leads to the symmetric solutions shown in the figures.

When flavor tagging for $B^0 \to \pi^0\pi^0$ is missing as in the 140 fb^{-1} case, only the outer borders of the curves can be obtained. By knowing the flavor of $B^0 \to \pi^0\pi^0$ the inner structure shows up, and $\phi_2 - \phi_{2\text{eff}}$ is determined up to a four-fold ambiguity and ϕ_2 is determined up to an eight-fold ambiguity in the range $(0°, 180°)$.

Figure 4.26 shows CL as a function of ϕ_2 at 50 ab^{-1} for several values of $\mathcal{A}_{\pi^0\pi^0}$. The best ϕ_2 resolution ($0.8° \sim 1.4°$) is expected at $\mathcal{A}_{\pi^0\pi^0} = -0.13$, for which the angle between A^{+0} and A^{+-} is the same as the angle between $\bar{A}^{+0}$ and $\bar{A}^{+-}$. At $\mathcal{A}_{\pi^0\pi^0} = -0.86$ and $+0.35$, on the other hand, one isospin triangle is squashed, and the expected ϕ_2 resolution is about 2.6° except for the region where two solutions overlap.

Since the decay $B^+ \to \pi^+\pi^0$ has no strong penguin contribution, the occurrence of the direct CP violation in this decay mode would imply an electroweak penguin contribution. The effect of the electroweak penguin to $\pi\pi$ amplitudes is estimated in Table 4.15 using the perturbative QCD calculation with and without the electroweak penguin (EWP) amplitude [67]. This calculation suggests that the effect on $\pi^+\pi^-$ and $\pi^\pm\pi^0$ is negligible, while the effect on $\pi^0\pi^0$ is of order of several percent.

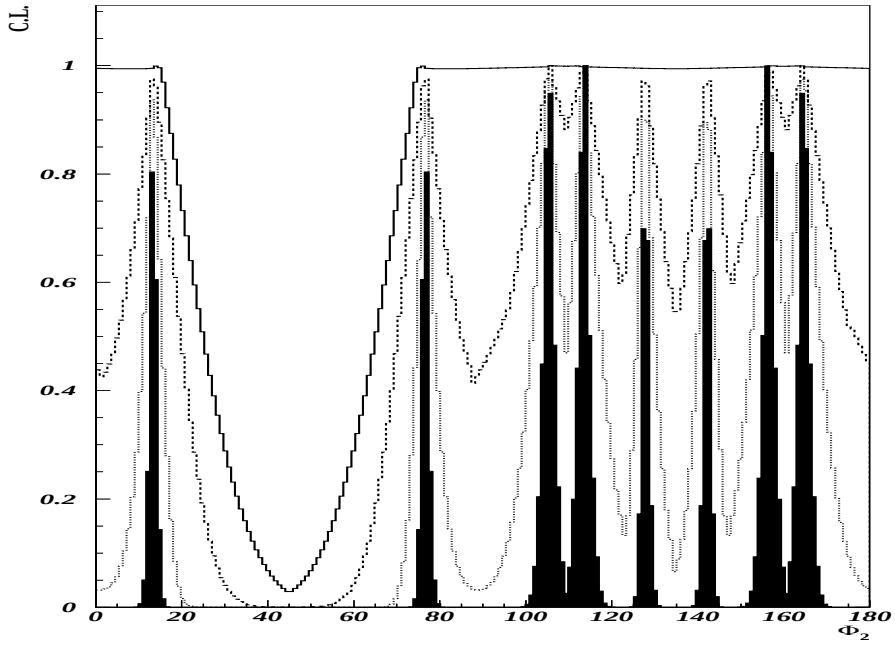

Figure 4.25: CL versus ϕ_2 (deg) for the inputs given in Table 4.14 at 140 fb^{-1} (solid curve), 500 fb^{-1} (dashed curve), 5 ab^{-1} (dotted curve), and 50 ab^{-1} (shaded area).

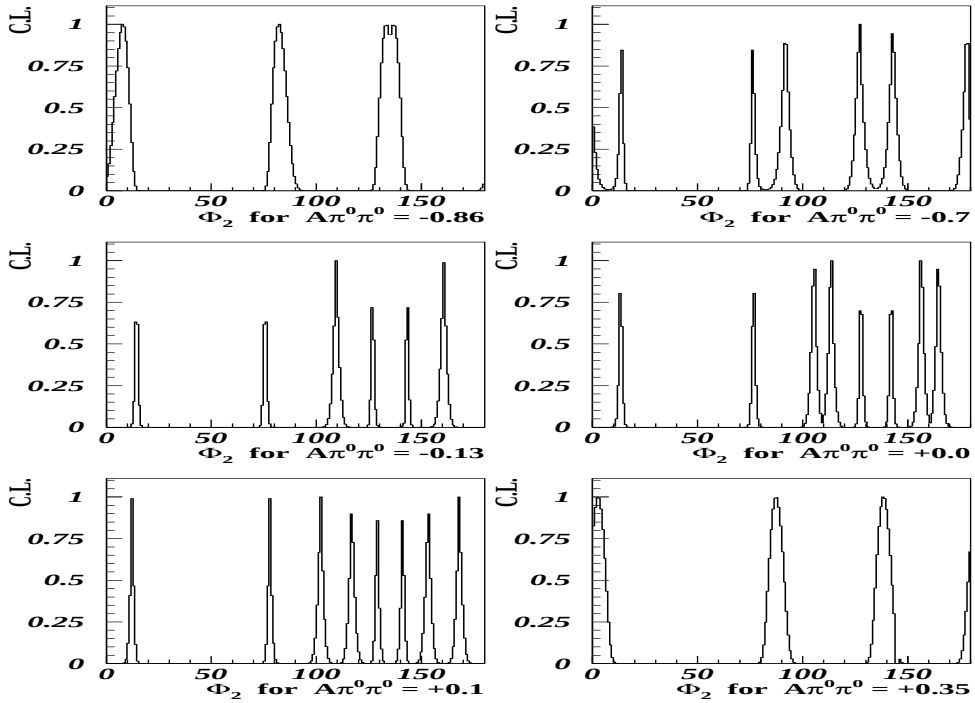

Figure 4.26: CL versus ϕ_2 (deg) at 50 ab^{-1} for $\mathcal{A}_{\pi^0\pi^0} = -0.86$ (top left), -0.7 (top right), -0.13 (middle left), 0.0 (middle right), $+0.1$ (bottom left), and $+0.35$ (bottom right).

amplitudes	$\lvert A^{+0}\rvert$ ($\times 10^{-4}$)	$\lvert A^{+-}\rvert$ ($\times 10^{-4}$)	$\lvert A^{00}\rvert$ ($\times 10^{-4}$)
with EWP	1.68	2.30	0.82
w/o EWP	1.69	2.31	0.87
difference	0.5%	0.5%	6.5%
amplitudes	$\lvert \bar{A}^{+0}\rvert$ ($\times 10^{-4}$)	$\lvert \bar{A}^{+-}\rvert$ ($\times 10^{-4}$)	$\lvert \bar{A}^{00}\rvert$ ($\times 10^{-4}$)
with EWP	1.68	2.90	0.96
w/o EWP	1.69	2.90	1.01
difference	0.5%	0.0%	5.5%

Table 4.15: A perturbative QCD calculation of the $B \to \pi\pi$ amplitudes with and without electroweak penguin contributions [67].

4.7.3 Status of the $B^0 \to \rho\pi$ analysis

In principle, the CKM angle ϕ_2 can be measured even in the presence of penguin contributions, using a full Dalitz plot analysis of the final state. However, there are difficulties from combinatorics and the lower efficiency in a three-body topology with a π^0 as well as large backgrounds from mis-reconstructed signal events and other decays. In order to extract ϕ_2 cleanly, data with large statistics are then required.

Unlike the $B^0 \to \pi^+\pi^-$ decay, $B^0 \to \rho^\pm\pi^\mp$ is not a CP eigenstate. In $B^0 \to \rho^\pm\pi^\mp$ decay, four different flavor decays ($B^0(\bar{B}^0) \to \rho^\pm\pi^\mp$) must be considered. Following a quasi-two-body approach, the current analysis by the BaBar collaboration [68] is restricted to the two regions of the $\pi^\pm\pi^0 h^\pm$ Dalitz plot ($h = \pi$ or K) that are dominated by $\rho^\pm h^\mp$. The decay rate is given by

$$f_q^{\rho^\pm h^\mp}(\Delta t) = (1 \pm A_{CP}^{\rho h}) \frac{e^{-|\Delta t|/\tau_{B^0}}}{4\tau_{B^0}} \times [1 + q\cdot\{(S_{\rho h} \pm \Delta S_{\rho h})\sin(\Delta m_d \Delta t) - (C_{\rho h} \pm \Delta C_{\rho h})\cos(\Delta m_d \Delta t)\}], \tag{4.30}$$

where $\Delta t = t_{\rho h} - t_{\rm tag}$ is the time interval between the decay of $B^0_{\rho h}$ and that of the other B^0 meson. One finds a relation

$$S_{\rho\pi} \pm \Delta S_{\rho\pi} = \sqrt{1 - (C_{\rho\pi} \pm \Delta C_{\rho\pi})^2}\,\sin(2\phi_{\rm 2eff}^\pm \pm \delta), \tag{4.31}$$

where $2\phi_{\rm 2eff}^\pm = \arg[(q/p)(\bar{A}_{\rho\pi}^\pm / A_{\rho\pi}^\mp)]$ and $\delta = \arg[A_{\rho\pi}^- / A_{\rho\pi}^+]$. $\arg[q/p]$ is the $B^0 - \bar{B}^0$ mixing phase, and $A_{\rho\pi}^+(\bar{A}_{\rho\pi}^+)$ and $A_{\rho\pi}^-(\bar{A}_{\rho\pi}^-)$ are the transition amplitudes for the processes $B^0(\bar{B}^0) \to \rho^+\pi^-$ and $B^0(\bar{B}^0) \to \rho^-\pi^+$, respectively. The angles $\phi_{\rm 2eff}^\pm$ are equal to ϕ_2 if contributions from penguin amplitudes are absent.

With a data sample of 89×10^6 $B\bar{B}$ pairs the BaBar Collaboration obtained [68]

$$A_{CP}^{\rho\pi} = -0.18 \pm 0.08 \pm 0.03, \tag{4.32}$$

$$C_{\rho\pi} = +0.36 \pm 0.18 \pm 0.04, \quad S_{\rho\pi} = +0.19 \pm 0.24 \pm 0.03, \tag{4.33}$$

$$\Delta C_{\rho\pi} = +0.28 \pm 0.19 \pm 0.04, \quad \Delta S_{\rho\pi} = +0.15 \pm 0.25 \pm 0.03. \tag{4.34}$$

4.7.4 Dalitz plot analysis of $B^0 \to \rho\pi$

A measurement of ϕ_2 using isospin relations among $B \to \pi\pi$ decays has a four-fold ambiguity as we mentioned in Section 2.4. This ambiguity can be avoided with a full Dalitz plot analysis of the $B^0 \to \rho\pi \to \pi^+\pi^-\pi^0$ decay [61].

Using the notation of [69] the decay amplitudes of $B \to \rho\pi$ are expressed as

$$\begin{aligned}
\sqrt{2}A(B^+ \to \rho^+\pi^0)(\equiv S_1) &= T^{+0} + 2P_1, && (4.35)\\
\sqrt{2}A(B^+ \to \rho^0\pi^+)(\equiv S_2) &= T^{0+} - 2P_1, && (4.36)\\
A(B^0 \to \rho^+\pi^-)(\equiv S_3) &= T^{+-} + P_1 + P_0, && (4.37)\\
A(B^0 \to \rho^-\pi^+)(\equiv S_4) &= T^{-+} - P_1 + P_0, && (4.38)\\
A(B^0 \to \rho^0\pi^0)(\equiv S_5) &= T^{+0} + T^{0+} - T^{+-} - T^{-+} - 2P_0. && (4.39)
\end{aligned}$$

Here T^{ij} (i, $j = +$, $-$, or 0) are the tree amplitudes, and P_0 and P_1 are the penguin amplitudes for $I = 0$ and 1 final states, respectively. Similarly, for the CP-conjugate channels, we define the amplitudes $\bar{S}$, $\bar{T}^{ij}$, and $\bar{P}_i$ which differ from the original amplitudes only in the sign of the weak phase of each term. From isospin constraints, the following relation is hold for the above parameters

$$\begin{aligned}
S_1 + S_2 &= S_3 + S_4 + S_5, && (4.40)\\
\bar{S}_1 + \bar{S}_2 &= \bar{S}_3 + \bar{S}_4 + \bar{S}_5. && (4.41)
\end{aligned}$$

In the full Dalitz plot analysis for the $\pi^+\pi^-\pi^0$ final states, we do not specify which intermediate state the $\pi^+\pi^-\pi^0$ final state comes from. Thus, we can see the quantum interference. The amplitude of $B^0 \to \pi^+\pi^-\pi^0$ decay is expressed as

$$A(f) = f^+ S_3 + f^- S_4 + f^0 S_5/2, \tag{4.42}$$

while the amplitude of the CP-conjugate channel is given by

$$\bar{A}(f) = f^- \bar{S}_3 + f^+ \bar{S}_4 + f^0 \bar{S}_5/2. \tag{4.43}$$

f^i is the Breit-Wigner kinematical distribution function for $\rho^{\pm,0}$

$$f(m,\theta) = \frac{\cos\theta\,\Gamma_\rho/2}{m_\rho - m - i\Gamma_\rho/2}, \tag{4.44}$$

where m_ρ and Γ_ρ are the mass and width of ρ meson, respectively. The decay rate is given as a function of Δt, invariant mass m_i and helicity angle θ_i of ρ by

$$\begin{aligned}
\mathcal{P}_{sig}(\Delta t, m_+, m_-, m_0, \theta_+, \theta_-, \theta_0) = \frac{e^{-|\Delta t|/\tau_{B^0}}}{4\tau_{B^0}} \Bigg[&(|\bar{A}|^2 + |A|^2) \\
&+ q\left((|\bar{A}|^2 - |A|^2)\cos(\Delta m \Delta t) + 2\mathrm{Im}(\frac{\bar{A}}{A})\sin(\Delta m \Delta t) \right) \Bigg] \qquad (4.45)
\end{aligned}$$

where $q = 1$ for $B_{tag} = B^0$ and $q = -1$ for $B_{tag} = \bar{B}^0$. To clarify fit parameters, we denote T^{ij} and P_0 as follows:

$$\begin{aligned}
T &= T^{+0} + T^{0+} = |T| e^{i\phi_3} e^{i\delta_T}, && (4.46)\\
\bar{T} &= \bar{T}^{+0} + \bar{T}^{0+} = |T| e^{-i\phi_3} e^{i\delta_T}, && (4.47)\\
T^{+-} &= |T^{+-}| e^{i\phi_3} e^{i\delta_{+-}},\ \bar{T}^{+-} = |T^{+-}| e^{-i\phi_3} e^{i\delta_{+-}}, && (4.48)\\
T^{-+} &= |T^{-+}| e^{i\phi_3} e^{i\delta_{-+}},\ \bar{T}^{-+} = |T^{-+}| e^{-i\phi_3} e^{i\delta_{-+}}, && (4.49)\\
P_0 &= |P_0| e^{-i\phi_1} e^{i\delta_0},\ \bar{P}^0 = |P_0| e^{i\phi_1} e^{i\delta_0}, && (4.50)\\
P_1 &= |P_1| e^{-i\phi_1} e^{i\delta_1},\ \bar{P}^1 = |P_1| e^{i\phi_1} e^{i\delta_1}. && (4.51)
\end{aligned}$$

ϕ_2	1.57 (90 deg)		
$\|T\|$	1.59	δ_T	-0.65
$\|T^{+-}\|$	1	$\delta_{T_{+-}}$	0
$\|T^{-+}\|$	0.78	$\delta_{T_{-+}}$	-2.91
$\|P_0\|$	0.19	δ_{P_0}	-0.61
$\|P_1\|$	0.19	δ_{P_1}	1.04

Table 4.16: Input parameters for a full Dalitz plot analysis of $B^0 \to \pi^+\pi^-\pi^0$ decay.

We have 9 fit parameters

$$\phi_2,\ |T|,\ \delta_T,\ |T^{-+}|,\ \delta_{-+},\ |P_0|,\ \delta_0,\ |P_1|,\ \delta_1 \tag{4.52}$$

and set $|T^{+-}| = 1$ and $\delta_{+-} = 0$.

We use ensembles of the Monte Carlo (MC) pseudo-experiments for this study. Each pseudo-experiment consists of events generated with the nominal probability density functions (PDFs). At present, the only background is continuum. Assuming $BR(B^0 \to \rho\pi) = 25 \times 10^{-6}$ and the detection efficiency is 15%, we generate 10080 candidate events equivalent to a 300fb^{-1} data sample. There are about 1240 signal event in this sample. We parametrize the continuum background as

$$\mathcal{P}_{q\bar{q}} = \frac{1}{2}\mathcal{M}(m_+, m_-, m_0, \theta_+, \theta_-, \theta_0)\Big\{f_\tau \frac{e^{-|\Delta t|/\tau_{\rm bkg}}}{2\tau_{\rm bkg}} + (1 - f_\tau)\delta(\Delta t)\Big\}, \tag{4.53}$$

where f_τ is the fraction of the background with effective lifetime $\tau_{\rm bkg}$, and $\mathcal{M}$ is a PDF in the Dalitz plane for continuum background. We define the likelihood value for each event as a function of the 9 parameters:

$$\begin{aligned} P_i(\Delta t_i, m_+, m_-, m_0, \theta_+, \theta_-, \theta_0) &= (1 - f_{ol}) \int_{-\infty}^{+\infty} d\Delta t' \\ &\{f_{sig}\mathcal{P}_{sig}(\Delta t', q, w_l) + f_{q\bar{q}}\mathcal{P}_{q\bar{q}}(\Delta t') \cdot R_{q\bar{q}}(\Delta t_i - \Delta t')\} + f_{ol}\mathcal{P}_{ol}(\Delta t_i), \end{aligned} \tag{4.54}$$

where f_{sig} and $f_{q\bar{q}}$ are the probability functions for signal events and continuum background, respectively. They are determined on an event-by-event basis. The signal fraction is estimated using the data at the Belle experiment up to the summer of 2002. For signal events, we use the same values of resolution parameters as those used for $\sin 2\phi_1$ analysis. We estimate the parameters for continuum background using sideband data.

The input values of the fit parameters used here are listed in Table 4.16 [70]. The result is shown in Figure 4.27. We obtain an error for ϕ_2 of $\delta\phi_2 = 11.4^\circ$ at 300 fb^{-1} and $\delta\phi_2 = 3.5^\circ$ at 3 ab^{-1}. From these results, the error of ϕ_2 is expected to be 2.9° at 5 ab^{-1} and 0.9° at 50ab^{-1}.

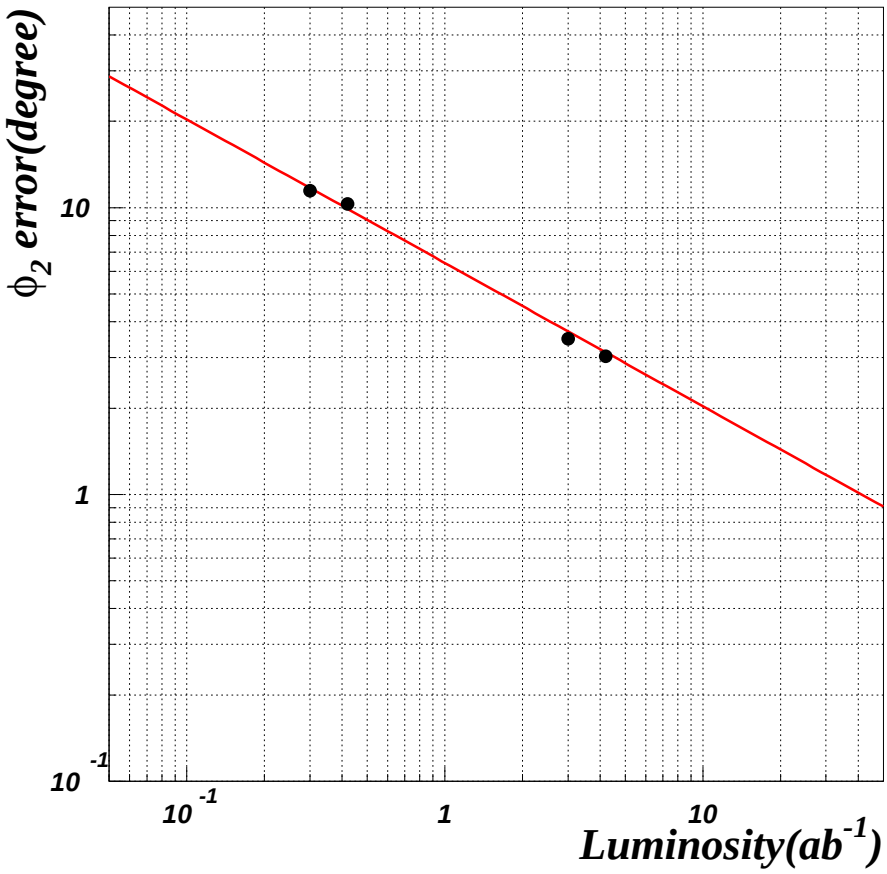

Figure 4.27: ϕ_2 error as a function of luminosity. Dots are the results from the MC psuedo-experiments and the line is a linear fit to these dots.

4.8 ϕ_3

4.8.1 Introduction

The angle ϕ_3 is defined as

$$\phi_3 \equiv -\arg\left[\frac{V_{ud}V_{ub}^*}{V_{cd}V_{cb}^*}\right], \tag{4.55}$$

which is independent of the quark phase convention. In the standard phase convention, all elements of the CKM matrix except for V_{ub} and V_{td} are nearly real, and in particular both V_{ud} and $-V_{cd}V_{cb}^*$ are (nearly) real and positive, and we have

$$\phi_3 \equiv \arg V_{ub}^* . \quad \text{(standard phase convention)} \tag{4.56}$$

There are several decay channels that can be used to extract information on ϕ_3, and each has distinct merits and drawbacks. Here, we will investigate the following channels:

$D^{(*)-}\pi^+$ **modes** The flavor-tagged time-dependent measurement of $D^{(*)-}\pi^+$ and its charge-conjugate mode. This mode measures $2\phi_1 + \phi_3$ and is affected by a strong phase. There is, however, no penguin contribution. One could fully reconstruct the $D^-\pi^+$ and $D^{*-}\pi^+$ final states, or one could use a partial-reconstruction technique where $\bar{D}^0$ of the decay $D^{*-} \to \bar{D}^0\pi^+$ is not explicitly detected. The latter has more statistics but with more background. In both cases, the value of r, the ratio of Cabibbo-favored amplitude to the Cabibbo-suppressed amplitude, needs to be input externally.

$B^+ \to DK^{(*)+}$ **(ADS method)** $B^+ \to DK^{(*)+}$, $D \to PP$, where D is D^0 or $\bar{D}^0$, and their charge-conjugate modes. Even though there are strong phases involved, ϕ_3 can be extracted in a theoretically-clean manner if one uses more than one kind of D decays. The required statistics, however, is quite large. The value of the relevant amplitude ratio r can be obtained by the fit. If it is known, one can improve the statistical power significantly.

$B^\pm \to DK^\pm$ **(Dalitz analysis)** $B^+ \to DK^+$, $D \to PPP$, where D is D^0 or $\bar{D}^0$, and their charge-conjugate modes. This mode takes advantage of the interferences that occur in the Dalitz plot of the $D \to PPP$ decay to extract ϕ_3 as well as the strong phase. The value of the amplitude ratio r is also obtained in the fit. This analysis has a good statistical power; it requires, however, a detailed understanding of the structure of the Dalitz plot.

More on the theoretical frameworks for each mode as well as the sensitivities are covered in later subsections.

4.8.2 $D^{(*)-}\pi^+$ modes

For the final state $D^{(*)-}\pi^+$, the amplitudes of diagrams shown in Figure 4.8.2 interfere. The two diagrams contributing to the amplitude a (or $\bar{b}$) have the same CKM factors, and information on ϕ_3 is contained in

$$\rho \equiv \frac{q\bar{b}}{pa} = -r\exp(\delta - \phi_w), \quad \phi_w \equiv 2\phi_1 - \phi_3 , \tag{4.57}$$

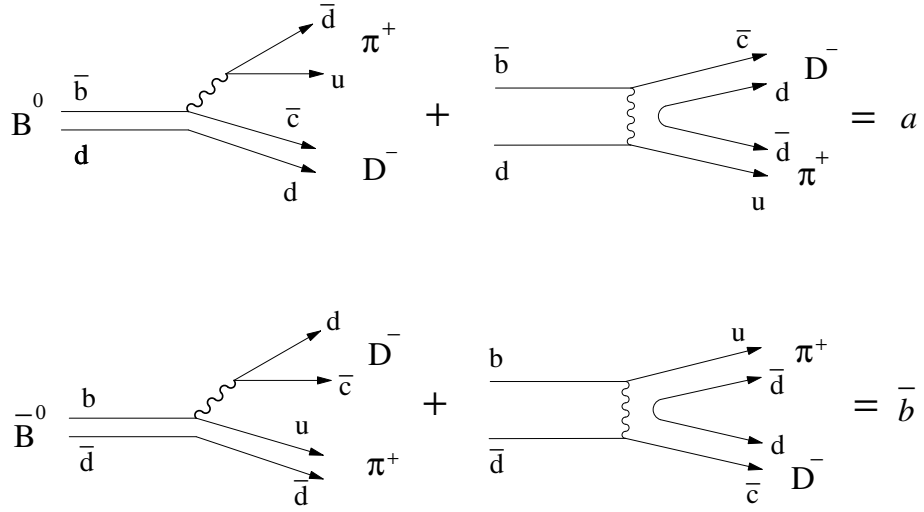

Figure 4.28: Diagrams for $B^0, \bar{B}^0 \to D^-\pi^+$.

where $B_H = pB^0 - q\bar{B}^0$, $r \equiv |\rho|$ and δ is the relative strong phase between $\bar{b}$ and a. The time-dependent distributions are then given by

$$\begin{aligned}
\Gamma_{\ell^-,D^-\pi^+}(\Delta t) &= Ne^{-\gamma|\Delta t|}\left[(1+r^2)+(1-r^2)\cos\delta m\Delta t - 2r\sin(\phi_w-\delta)\,\sin\delta m\Delta t\right] \\
\Gamma_{\ell^+,D^+\pi^-}(\Delta t) &= Ne^{-\gamma|\Delta t|}\left[(1+r^2)+(1-r^2)\cos\delta m\Delta t + 2r\sin(\phi_w+\delta)\,\sin\delta m\Delta t\right] \\
\Gamma_{\ell^-,D^+\pi^-}(\Delta t) &= Ne^{-\gamma|\Delta t|}\left[(1+r^2)-(1-r^2)\cos\delta m\Delta t - 2r\sin(\phi_w+\delta)\,\sin\delta m\Delta t\right] \\
\Gamma_{\ell^+,D^-\pi^+}(\Delta t) &= Ne^{-\gamma|\Delta t|}\left[(1+r^2)-(1-r^2)\cos\delta m\Delta t + 2r\sin(\phi_w-\delta)\,\sin\delta m\Delta t\right]
\end{aligned} \quad . \quad (4.58)$$

where $\Gamma_{\ell^-,D^-\pi^+}(\Delta t)$ is the distribution of $\Delta t \equiv t_{D\pi} - t_{\rm tag}$ when the tag-side is $\bar{B}^0$, etc., and $D\pi$ can also be $D^*\pi$ in which case r and δ will be replaced by r^* and δ^*, respectively. The two relevant observables are $r\sin(\phi_w+\delta)$ and $r\sin(\phi_w-\delta)$. The value of r cannot be obtained by the fit itself, while the expected value of $r^{(*)}$ is roughly 0.02. One way to obtain r^* experimentally is to use the $SU(3)$-related modes $B^0 \to D_s^{(*)-}\pi^+$. However, there will be uncertainty associated with the validity of $SU(3)$ and the size of the exchange diagram which is missing for $D_s^{(*)-}\pi^+$.

The distributions are plotted in Figure 4.29 where the value of r is artificially enhanced to 0.1 in order to show the CP violating effects clearly. The top two of (4.58) can be called unmixed modes and the bottom two mixed modes. As may be noticeable in the figure, most of information on CP violation is in the mixed modes where CP violation appears as the height asymmetry of $\Delta t > 0$ vs $\Delta t < 0$ and the shift of the minimum from $\Delta t = 0$. Note that $r\sin(\phi_w+\delta)$ can be obtained from the third distribution alone and $r\sin(\phi_w-\delta)$ from the fourth alone. The final state $D^{*-}\pi^+$ can be detected by full recontruction using the standard technique, it or can also

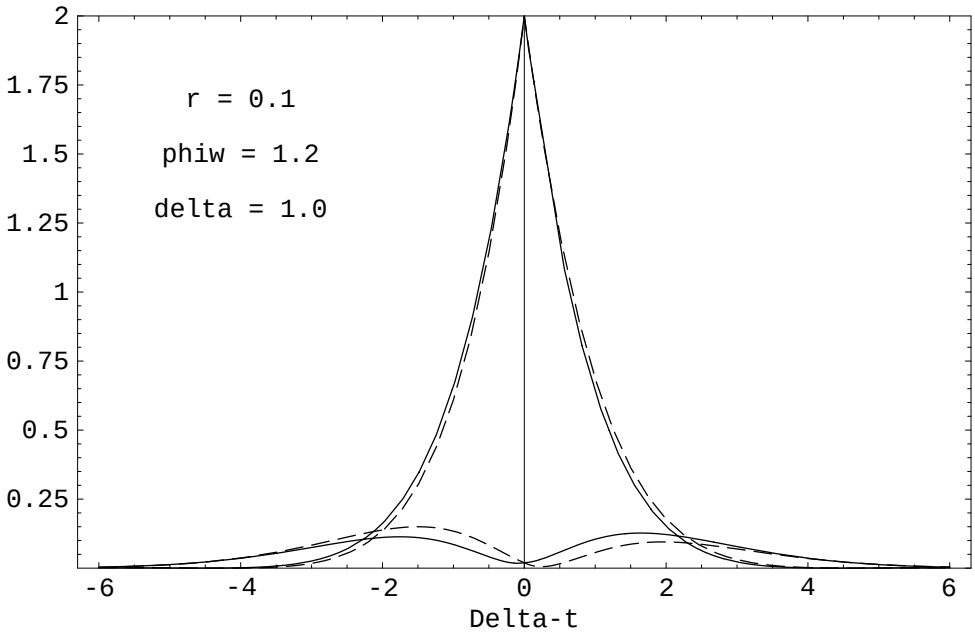

Figure 4.29: The Δt distributions of the flavor-tagged $D\pi$ modes for $r = 0.1$, $\phi_w = 1.2$ radian, and $\delta = 1.0$ radian. The solid lines are for $D^-\pi^+$ final state and dashed lines are for $D^+\pi^-$ final states. The mixing parameter x is taken to be 0.71.

be reconstructed by a partial reconstruction method where the $\bar{D}^0$ meson in $D^{*-} \to \bar{D}^0\pi^-$ is not explicitely reocnstructed. Note that the $D^{(*)-}\pi^+$ methods works even when there are sizable exchange diagrams while the value of $r^{(*)}$ needs to be supplied externally.

The distributions of Δt for $\bar{B}^0$-tagged $D^{*+}\pi^-$ and $D^{*+}\pi^-$ are shown in Figure 4.30 for events with good tagging quality. The analysis was performed on $140 fb^{-1}$ of data. The full-reconstruction anaysis gave the following preliminary results:

$$\begin{aligned} 2r^* \sin(\phi_w + \delta^*) &= 0.109 \pm 0.057 \pm 0.019 \\ 2r^* \sin(\phi_w - \delta^*) &= 0.011 \pm 0.057 \pm 0.019 \\ 2r \sin(\phi_w + \delta) &= 0.087 \pm 0.054 \pm 0.019 \\ 2r \sin(\phi_w - \delta) &= 0.037 \pm 0.052 \pm 0.019\,. \end{aligned} \tag{4.59}$$

For 5 ab^{-1} and 50 ab^{-1} of data, the statistical errors will be

$$\delta\, 2r^* \sin(\phi_w + \delta^*) \sim \delta\, 2r \sin(\phi_w + \delta) \sim \left\{ \begin{array}{ll} 0.009 & (5 \text{ ab}^{-1}) \\ 0.003 & (50 \text{ ab}^{-1}) \end{array} \right. . \tag{4.60}$$

We note that the value of $r^{(*)}$ is approximately 0.02; thus, the above errors correspond to the errors on $\sin(\phi_w \pm \delta^{(*)})$ of 0.23 and 0.07, respectively. If the value of $r^{(*)}$ is known, $\phi_w = 2\phi_1 + \phi_3$ (and $\delta^{(*)}$) can be extracted from $\sin(\phi_w \pm \delta^{(*)})$. At this time, determining the value of $r^{(*)}$ to 23% seems reasonably possible while 7% seems quite challenging. On the other hand, our knowledge on $r^{(*)}$ will improve significantly by the time 50 ab^{-1} of data is taken. It is possible that the systematic error on ϕ_3 due to $r^{(*)}$ is not overwhelming even with 50 ab^{-1} of data.

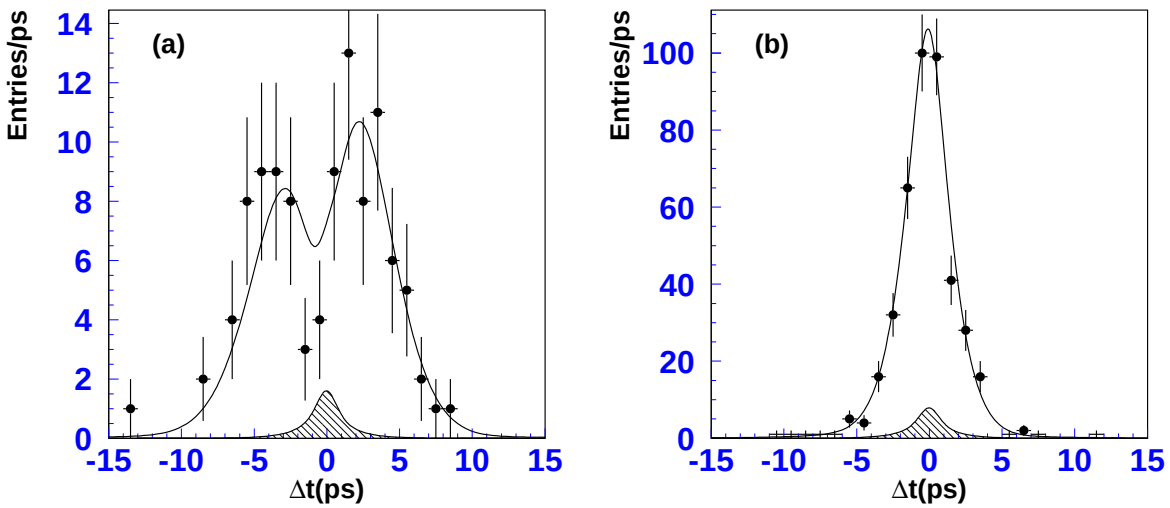

Figure 4.30: The distributions of Δt for $\bar{B}^0$-tagged $D^{*+}\pi^-$ (a) and $D^{*+}\pi^-$ (b). For fully-reconstructed events with good-quality tags. ($140 fb^{-1}$)

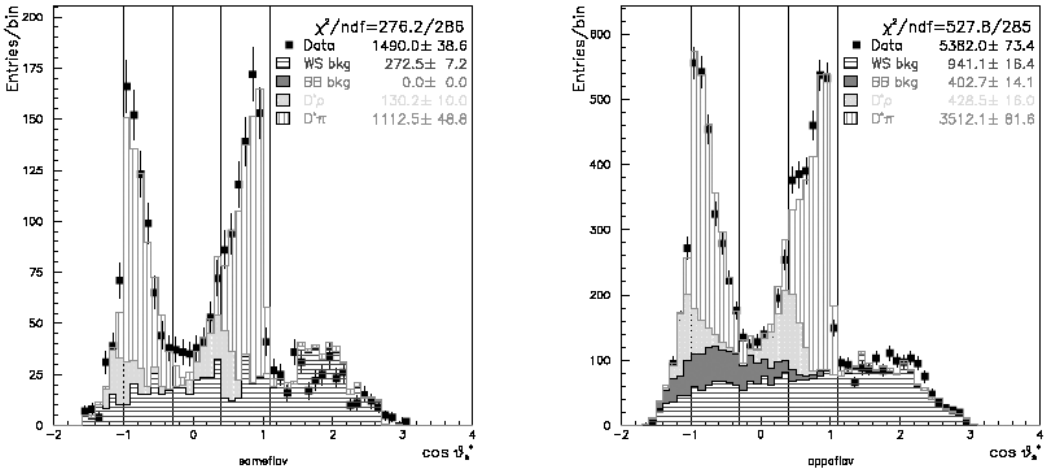

Figure 4.31: The partial reconstruction of $D^*\pi$. The distributions of $\cos\theta^*$ for two lepton tagged samples, same-flavor and opposite-flavor tags. Based on 78 fb^{-1} of data.

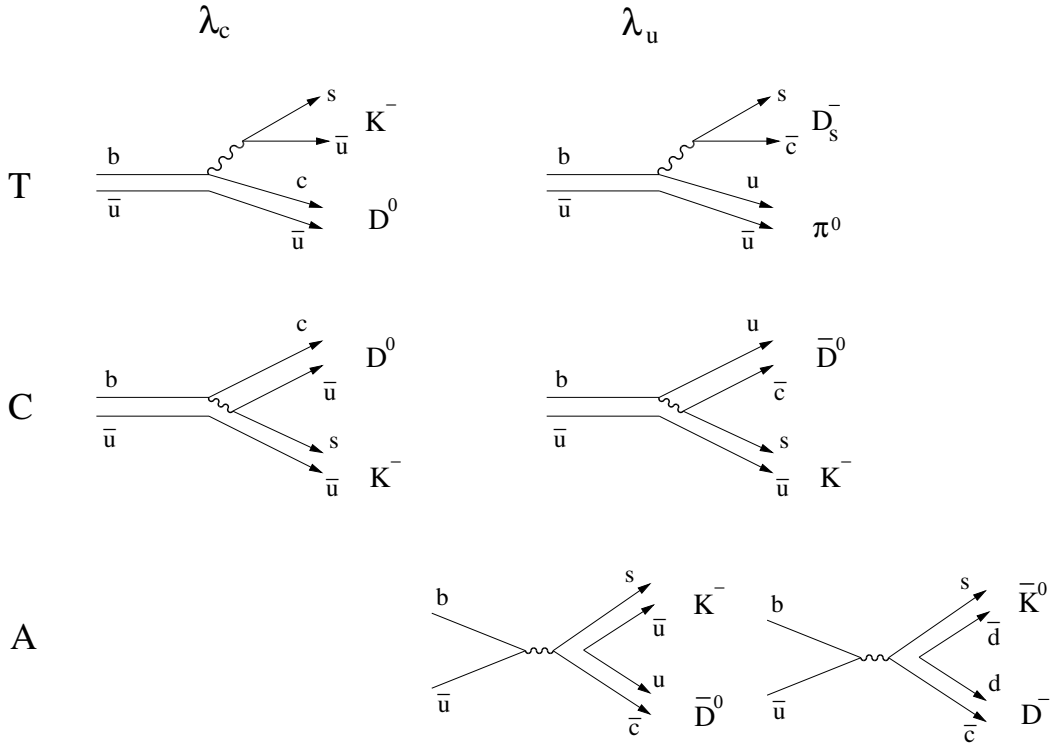

Figure 4.32: Diagrams contributing to $B^{\pm} \to DK^{\pm}$ and related modes.

The statistical situation with the partially-reconstructed $D^{*+}\pi^-$ is substantially better. The helicity of D^{*+} in the B rest frame is 0 due to conservation of angular momentum. Thus, the decay angle θ^* of the decay $D^{*+} \to D^0\pi^+$ should have the $\cos^2\theta^*$ shape. One can reconstruct $\cos\theta^*$ without explicitly detecting D^0, and the distributions based on 78 fb^{-1} of data are shown in Figure 4.31 separately for the two lepton-tagged datasets. There are 1110 ± 50 signal events in the same-flavor sample and 3510 ± 80 signal events in the opposite-flavor sample. As a result of Δt fit, the error on $2r^* \sin(\phi_w \pm \delta^*)$ was found to be 0.029. The statistical errors extrapolated to 5 ab^{-1} and 50 ab^{-1} of data are

$$\delta\, 2r^* \sin(\phi_w + \delta^*) \sim \left\{ \begin{array}{ll} 0.005 & (\ 5\ \text{ab}^{-1}\ ) \\ 0.0015 & (50\ \text{ab}^{-1}\ ) \end{array} \right. \quad \text{(partial rec.)}\,. \tag{4.61}$$

The background is about 30% and comes mainly from B decays such as $D^*\rho$ and $D^{**}\pi$. The accuracy of these background estiamtions is likely to improve with statistics. The uncertainty of r^*, however, may become a limitting systematics.

4.8.3 $B^{\pm} \to DK^{*\pm}$ (ADS method)

In $B^{\pm} \to DK^{\pm}$, the number of c or $\bar{c}$ quark in the final state is one, and as a result the penguin processes $b \to s/d$ cannot contribute. When the neutral D meson is detected in a final state that can come from D^0 and $\bar{D}^0$, the two processes $B^- \to D^0K^-$ and $B^- \to \bar{D}^0K^-$ interfere. Diagrams contributing to $B^{\pm} \to DK^{\pm}$ and related modes are shown in Figure 4.32. They are categorized in terms of the CKM factors involved ($\lambda_c = V_{cb}V_{us}^*$ and $\lambda_u = V_{ub}V_{cs}^*$) and type of

process (T: color-favored tree, C: color-suppressed tree, A: annihilation). $B^- \to D^0 K^-$ receives contributions from T and C both with the CKM factor λ_c, while $B^- \to \bar{D}^0 K^-$ can proceed by C and A both with the CKM factor λ_u. Thus,

$$\arg \frac{Amp(B^- \to \bar{D}^0 K^-)}{Amp(B^- \to D^0 K^-)} = \delta_B - \phi_3 \,, \quad \arg \frac{Amp(B^+ \to D^0 K^-)}{Amp(B^+ \to \bar{D}^0 K^-)} = \delta_B + \phi_3 \,, \tag{4.62}$$

where δ_B is the strong phase. We have noted

$$\arg \frac{\lambda_u}{\lambda_c} = \arg \frac{V_{ub} V_{cs}^*}{V_{cb} V_{us}^*} = -\phi_3 \,, \quad \text{(standard phase convention)} \tag{4.63}$$

and that when charge conjugate decay is taken, the weak phase changes sign while the strong phase does not. On the other hand, the absolute size of $Amp(B^- \to \bar{D}^0 K^-)$ or $Amp(B^- \to D^0 K^-)$ is the same for charge conjugate decays.

$$|Amp(B^- \to \bar{D}^0 K^-)| = |Amp(B^+ \to D^0 K^+)| \equiv B \tag{4.64}$$

$$|Amp(B^- \to D^0 K^-)| = |Amp(B^+ \to \bar{D}^0 K^+)| \equiv A \tag{4.65}$$

If D^0 and $\bar{D}^0$ are detected in a CP eigenstate such as $K^- K^+$ (which is $CP+$; i.e. $D_1 = (D^0 + \bar{D}^0)/\sqrt{2}$), the decay rates of $B^\pm$ are, up to an overall constants of 1/2,

$$\Gamma(B^- \to D_1 K^-) = \left| A + B e^{i(\delta_B - \phi_3)} \right|^2 = A^2 + B^2 + 2AB \cos(\delta_B - \phi_3) \tag{4.66}$$

$$\Gamma(B^+ \to D_1 K^+) = \left| A + B e^{i(\delta_B + \phi_3)} \right|^2 = A^2 + B^2 + 2AB \cos(\delta_B + \phi_3) \tag{4.67}$$

then, there can be decay rate asymmetry [71, 72] between $B^- \to D_1 K^-$ and $B^+ \to D_1 K^+$:

$$A_1 \equiv \frac{\Gamma_{D_1 K^-} - \Gamma_{D_1 D^+}}{\Gamma_{D_1 K^-} + \Gamma_{D_1 K^+}} = \frac{-2r \sin\delta_B \sin\phi_3}{1 + r^2 + 2r \cos\delta_B \cos\phi_3} \,, \tag{4.68}$$

with

$$r \equiv \frac{B}{A} \,. \tag{4.69}$$

The value of this r is expected to be around 0.1 to 0.2. For a $CP-$ final states (such as $K_S \pi^0$; i.e. $D_2 = (D^0 - \bar{D}^0)/\sqrt{2}$), the asymmetry becomes

$$A_2 \equiv \frac{\Gamma_{D_2 K^-} - \Gamma_{D_2 K^+}}{\Gamma_{D_2 K^-} + \Gamma_{D_2 K^+}} = \frac{2r \sin\delta_B \sin\phi_3}{1 + r^2 + 2r \cos\delta_B \cos\phi_3} \,. \tag{4.70}$$

Thus, once the value of r is given, the measurements of A_1 and A_2 can give δ_B and ϕ_3 (2 equations and 2 unknowns). In practice, however, it is difficult to measure the value of r because of the doubly-Cabibbo-suppressed decays of D^0 [73, 74]. It was pointed out, however, that by taking more than one final states that D^0 can $\bar{D}^0$ can both decay to, one can solve for r and δ_B (the ADS method [73, 74]).

The authors of [73, 74] used $B^- \to D K^{*-}$ and assumed the D decay modes listed in Table 4.17. The strong phase δ_i includes that for the B decay as well as that for the D decay. The table also shows the number of events expected for 10^8 $B^\pm$ or roughly 0.1 ab^{-1}, where the detection efficiencies for each DK^{*-} are taken to be the same as the branching fraction of $D \to i$ where i is the D decay mode shown. Namely, the detection efficiency of K^{*-} and those of the D decay final states shown are assumed to be unity. Under these assumptions, the estimated sensitibity on ϕ_3 is 9°. The scale factor includes 2/3 per track, 1/2 per π^0, and relevant branching

mode	#event	scale factor	strong phase δ_i
$K^+\pi^-$	83	1	10°
$K_s\pi^0$	791	0.34	20°
$K^+\rho^-$	224	0.5	30°
K^+a_1-	791	0.22	49°
$K_s\rho^0$	362	0.30	200°
$K^{*+}\pi^-$	65	0.33	50°

Table 4.17: The D decay modes used for the sensitibity study of $B^- \to DK^{*-}$ mode and the strong phases assumed. The number of events are for 10^8 $B^\pm$ when the DK^{*+} detection efficiency is assumed to be $Br(D \to i)$. The scale factors are realative to the $K^+\pi^-$ mode for realistic detection efficiencies described in the text.

fractions where K^{*+} is assumed to be detected as $K^-\pi^0$ and $K_S\pi^-$. The value of ϕ_3 is taken to be 60° and r to be 0.1. Figure 4.33 shows the ΔE distribution for $B^- \to DK^-$, $D \to K^+\pi^-$ using 78 fb^{-1} of data. The detection efficiency was estimated by MC to be 0.27. With the measured background and the expected signal yield, S/N is estimated to be 1/7. Combining all the above, the required integrated luminosity for $\delta\phi_3$ of 9° becomes 31 ab^{-1}, or equivalently

$$\delta\phi_3 = \left\{ \begin{array}{cc} 22^\circ & (5\text{ ab}^{-1}) \\ 7^\circ & (50\text{ ab}^{-1}) \end{array} \right. \qquad (DK^*)\,. \tag{4.71}$$

If the value of r is larger than 0.1, the sensitivities will be better. This analysis is theoretically clean and will probably be limitted by statistics even for 50 ab^{-1} of data. Approximately the same sensitivity is expected from DK^- mode and the conbined sensitivities will be $1/\sqrt{2}$ times those shown above; namely,

$$\delta\phi_3 = \left\{ \begin{array}{cc} 16^\circ & (5\text{ ab}^{-1}) \\ 5^\circ & (50\text{ ab}^{-1}) \end{array} \right. \qquad (DK^* + DK)\,. \tag{4.72}$$

If the value of r is known, then one can use CP eigen states of D decay such as K^+K^- ($CP+$) and $K_s\pi^0$ ($CP-$) to extract ϕ_3 as well as the strong phase δ_B. This method is statistically more powerful than the ADS method described above; the value of r, however, is not known well at this time and seems to be more difficult than the value of r for the $D^{(*)}\pi$ modes. It should be noted, however, that the value of r measured in the Dalitz analysis of the following section may be used for this analysis.

4.8.4 $B^\pm \to DK^\pm$ (Dalitz analysis)

Use of the Daitz plot of D decay in $B^\pm DK^\pm$ has been suggested in [73,74] and recently by [75]. In this analyis, the D meson is detected in the final state $K_S\pi^+\pi^-$. If the amplitude of D^0 decaying to a point in the Dalitz plot, $m^2(K_S\pi^+) = m_+^2$ and $m^2(K_S\pi^-) = m_-^2$, is given by $f(m_+^2, m_-^2)$, then that of $\bar{D}^0$ decaying to the same final state can be written as $f(m_-^2, m_+^2)$ where the two arguments are simply exchanged. This is due to the approximate CP conservation of the D decay. Explicitly,

$$\begin{aligned} Amp(D^0)(m_{K_S\pi^+} = m_+, m_{K_S\pi^-} = m_-) &\equiv f(m_+^2, m_-^2) \\ Amp(\bar{D}^0)(m_{K_S\pi^+} = m_+, m_{K_S\pi^-} = m_-) &\equiv f(m_-^2, m_+^2) \end{aligned} \tag{4.73}$$

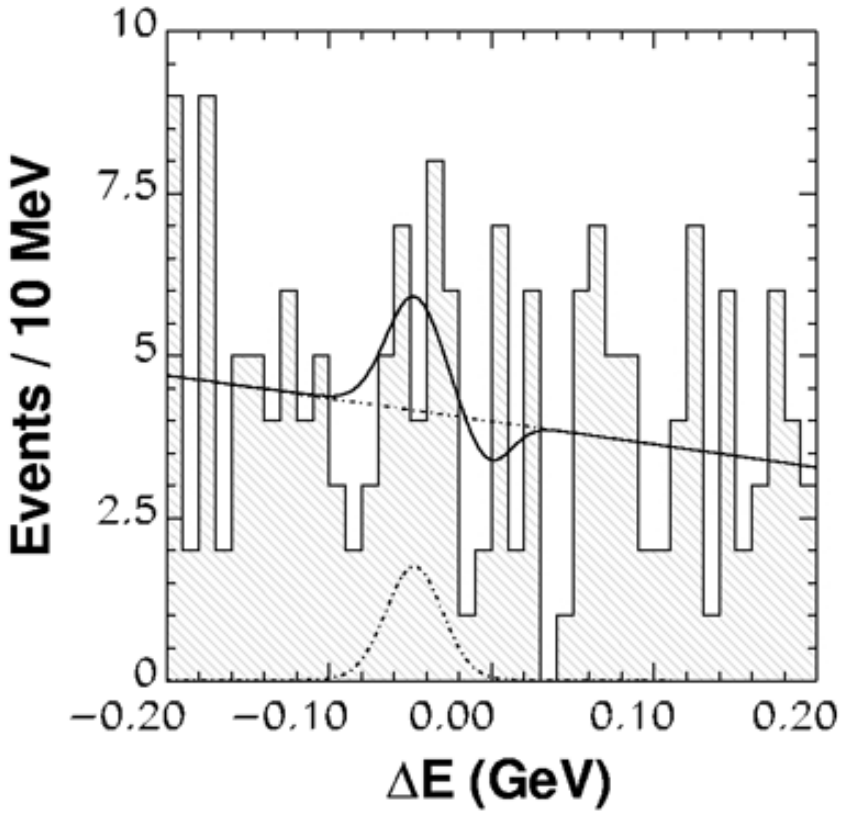

Figure 4.33: Search for $B^- \to DK^-$, $D \to K^+\pi^-$. The data is 78 fb^{-1}.

The total decay amplitude for $B^- \to DK^-$, $D \to K_S\pi^+\pi^-$ is then

$$\begin{aligned} M_- &= Amp(D^0_{\to K_S\pi^+\pi^-}K^-) + Amp(\bar{D}^0_{\to K_S\pi^+\pi^-}K^-) \\ &= A[f(m_+^2, m_-^2) + re^{i(\delta_B-\phi_3)}f(m_-^2, m_+^2)]\,, \end{aligned} \tag{4.74}$$

where A, r, δ_B are as defined in the previous section. The total decay amplitude for $B^+ \to DK^+$, $D \to K_S\pi^+\pi^-$ where $m^2(K_S\pi^+) = m_+^2$ and $m^2(K_S\pi^-) = m_-^2$ is similaly

$$\begin{aligned} M_+ &= Amp(\bar{D}^0_{\to K_S\pi^+\pi^-}K^+) + Amp(D^0_{\to K_S\pi^+\pi^-}K^+) \\ &= A[f(m_-^2, m_+^2) + re^{i(\delta_B+\phi_3)}f(m_+^2, m_-^2)]\,, \end{aligned} \tag{4.75}$$

where the sign of ϕ_3 has flipped while the strong phase δ_B stayed the same.

The Dalitz plot for $D^0 \to K_S\pi^+\pi^-$ based on the CLEO measurement [76] is shown in Figure 4.34. As can be seen from the Dalitz plot, the distribution is highly asymmetric under the exchange of $m_{K_S\pi^+}$ and $m_{K_S\pi^-}$ which indicates that the interference in the Dalitz plot has a good sensitivity on the phase between the two terms of (4.74) and (4.75). The phase angles $\delta_B - \phi_3$ and $\delta_B + \phi_3$ are obtained from the separate fits of B^- and B^+ decays and ϕ_3 can be extracted therefrom.

Figure 4.35 shows the ΔE and M_B distributions for $B^\pm \to DK^\pm$, $D \to K_S\pi^+\pi^-$, based on 140 fb^{-1} of data, and the dalitz plots of the D decays are shown in Figure 4.36 separately for B^+ and B^- [77]. The results of a unbinned maximum likelihood fit for the parameters $r(= a)$, $\delta_B(= \delta)$, and ϕ_3 are shown in Figure 4.37. For ϕ_3 and δ_B, one obtained

$$\begin{aligned} \phi_3 &= 95^{+25}_{-20} \pm 13 \pm 10\,(^\circ) \\ \delta_B &= 162^{+20}_{-25} \pm 12 \pm 24\,(^\circ) \end{aligned} \tag{4.76}$$

where the first systematic error is experimental, such as background shapes and efficiency shapes, and the second systematic error is due to the D decay model dependence. With 5 ab^{-1} and 50 ab^{-1} of data, the statistical errors will be

$$\delta\phi_3 = \left\{ \begin{array}{ll} 4^\circ & (5\text{ ab}^{-1}) \\ 1.2^\circ & (50\text{ ab}^{-1}) \end{array} \right. . \tag{4.77}$$

With more statistics, the Dalitz distribution of $D^0 \to K_S\pi^+\pi^-$ will be measured more accurately using $D^{*+} \to D^0\pi^+$. Even though it is not clear at present if the systematic uncertainty due to the D decay modeling can be reduced to one degree level, it is quite possible that the measurement is not overwhelmed by systematics at 5 ab^{-1}. Furthermore, the value of r measured in this mode can be used in the $B^\pm \to DK^\pm$ modes.

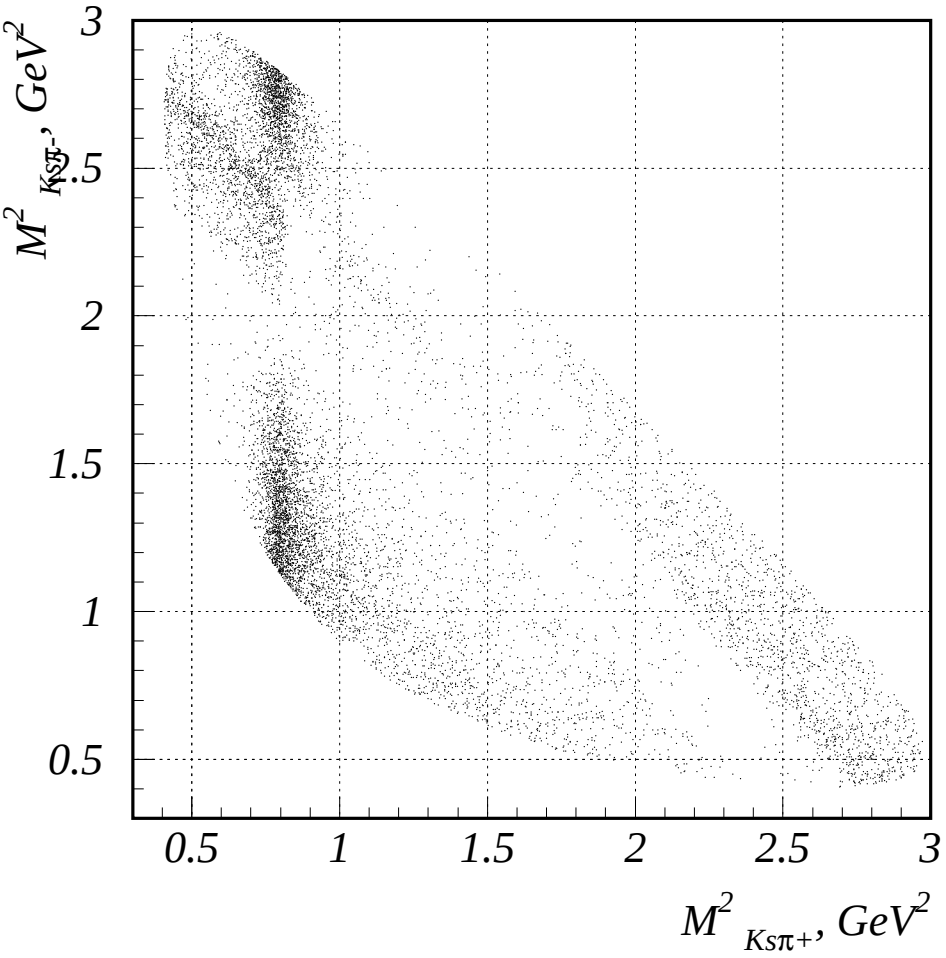

Figure 4.34: The Dalitz plot for $D^0 \to K_S\pi^+\pi^-$ based on the CLEO measurement.

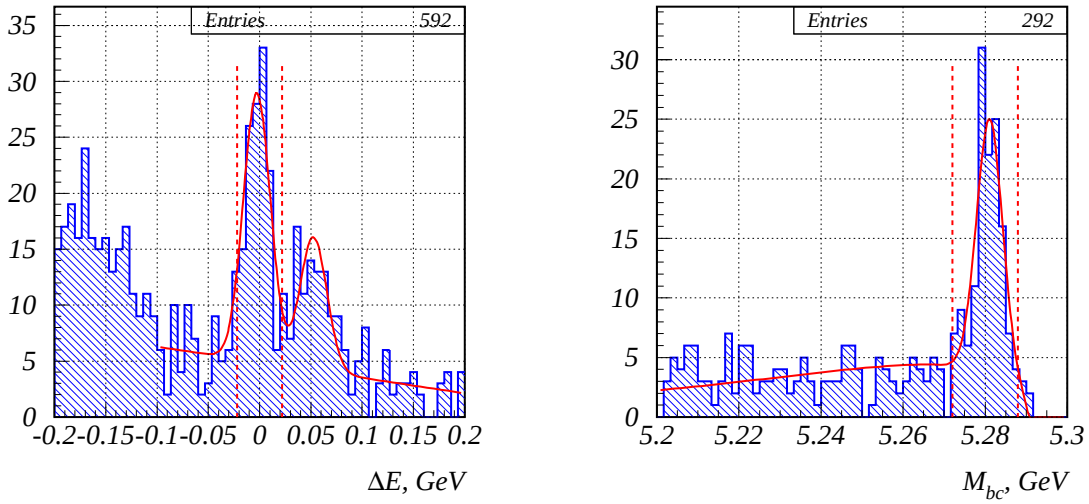

Figure 4.35: The ΔE and M_B distributions for $B^{\pm} \to DK^{\pm}$, $D \to K_S\pi^+\pi^-$, based on 140 fb^{1} of data.

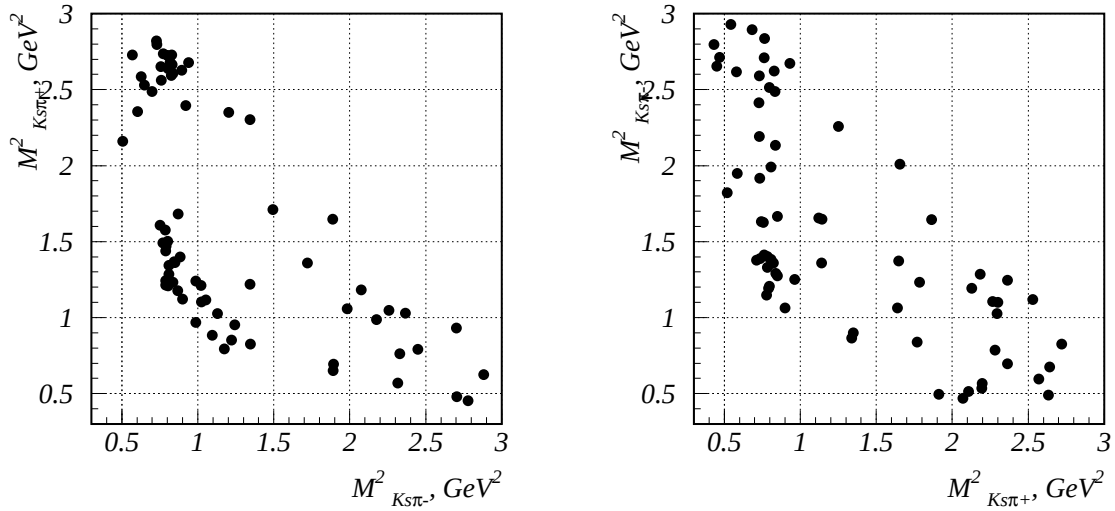

Figure 4.36: The Dalitz distributions for $B^+ \to DK^+$ (left) and $B^- \to DK^-$ (right), where $D \to K_S\pi^+\pi^-$ based on 140 fb^{1} of data.

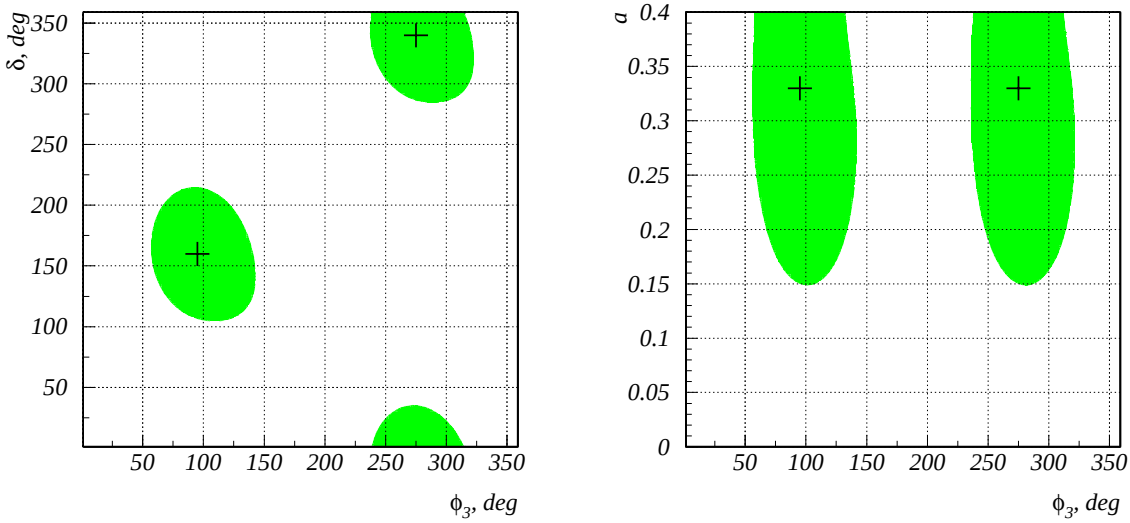

Figure 4.37: The results of the fit for $r(= a)$, $\delta_B(= \delta)$, and ϕ_3.

4.9 $|V_{ub}|$

4.9.1 Introduction

Precise determination of the magnitude of the Cabibbo-Kobayashi-Maskawa matrix element V_{ub} is of fundamental importance in overconstraining the unitarity triangle, and thereby finding effects of physics beyond the Standard Model. Such a serious examination would require precision of a few %. A high luminosity SuperKEKB/Belle experiment will provide such a unique opportunity.

In principle, $|V_{ub}|$ can be determined using data for semileptonic $B \to X_u \ell\nu$ decays, where X_u denotes a hadronic system containing a u-quark. Both inclusive and exclusive measurements are useful. However, the present error in $|V_{ub}|$ determination is about $\pm 20\%$ [78], and limited by both experimental and theoretical systematic errors. The high luminosity at the Super-KEKB will enable us to perform high statistics measurements of $B \to X_u \ell\nu$ decays with "B tagging". This will lead to rate measurements with significantly reduced experimental systematic errors and also to $|V_{ub}|$ extraction much less biased by theoretical ambiguities. These features are unqiue at a high luminosity e^+e^- B-factory, and cannot be achieved at e^+e^- machines with the luminosity available so far nor at present or future hadron machines.

In this section, we discuss strategy and prospects for determination of $|V_{ub}|$ at the SuperKEKB/Belle experiment using both inclusive and exclusive semileptonic $B \to X_u \ell\nu$ decays.

4.9.2 Theoretical formalisms for the semileptonic B decays

Inclusive decays

The amplitude for $B \to X_u l\nu$ inclusive decay can be computed in perturbative QCD using the Operator Product Expansion (OPE). Since the b quark inside the B meson has momentum $(m_b v + k)^\mu$, where k is the residual momentum of $O(\Lambda_{QCD})$, the OPE is carried out by expanding the quark propagator as

$$\frac{1}{(m_b v + k - q)^2} = \frac{1}{(m_b v - q)^2}\left[1 - \frac{(m_b v - q)\cdot k}{(m_b v - q)^2} - \frac{k^2}{(m_b v - q)^2} + \cdots\right]. \tag{4.78}$$

Denoting the invariant mass and the energy of the hadron state X_u as m_X and E_X, the first term is of order $E_X \Lambda_{QCD}/m_X^2$ while the second term is of order Λ_{QCD}^2/m_X^2.

The phase space can be divided into the following three regions (see Figure 4.38): (i) a generic region where Λ_{QCD}/m_X, $(E_X \Lambda_{QCD})/m_X^2 \ll 1$. In this region, the differential decay rate can be successfully expanded by the OPE; (ii) a shape function region (or collinear region) where $\Lambda_{QCD}/m_X \ll 1$ and $(E_X \Lambda_{QCD})/m_X^2 \sim 1$. In this region, a class of $\Lambda_{QCD} E/m_X^2$ terms must be resummed, which can be described by the shape function of the B meson [79–81] and its higher twist corrections; (iii) a resonance region where $\Lambda_{QCD}/m_X \sim 1$. In this region, the differential decay rate is dominated by a few exclusive states so that neither the OPE nor the twist expansion work.

Since the $B \to X_u l\nu$ decay suffers from $B \to X_c l\nu$ decay background one has to introduce the cut of the following kinds:

- lepton energy cut : $E_l > (m_B^2 - m_D^2)/(2m_B)$.
- hadron invariant mass cut : $m_X^2 < m_D^2$.
- lepton mass cut : $q^2 < (m_B - m_D)^2$.

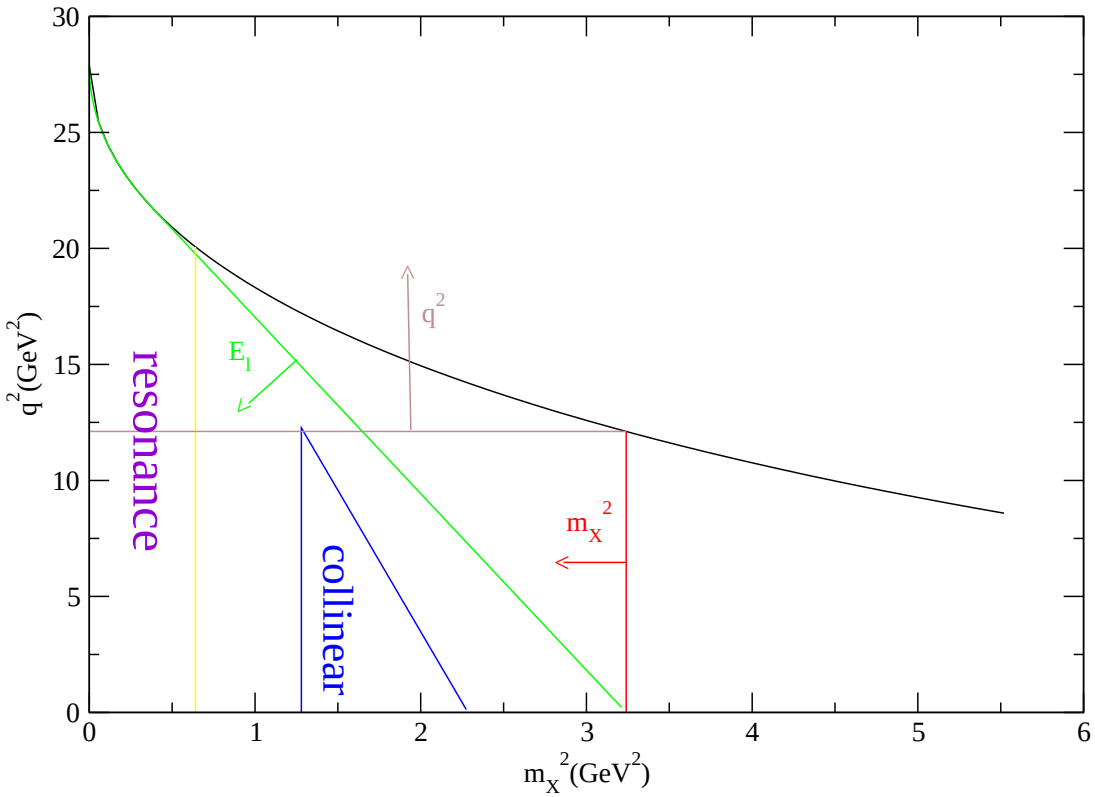

Figure 4.38: Phase space for $B \to X_u l\nu$ decay.

- combined (q^2, m_X^2) cut.

For the E_l cut, only 10% of the rate is available, which is dominated by the shape function region. In this region, the lepton energy spectrum at the leading order is given by

$$\frac{d\Gamma}{dE_l} = \frac{G_F^2 |V_{ub}|^2 m_b^4}{96\pi^3} \int d\omega \theta(m_b - 2E_l - \omega) f(\omega), \tag{4.79}$$

where $f(\omega)$ is the shape function define by

$$f(\omega) = \frac{1}{2m_B} \langle B | \bar{h} \delta(in \cdot D + \omega) | B \rangle. \tag{4.80}$$

Since this function is a universal quantity of the B meson, it can be measured experimentally through other processes. For example, the photon spectrum of $B \to X_s\gamma$ decay is given by [82]

$$\frac{d\Gamma}{dE_\gamma} = \frac{G_F^2 |V_{tb} V_{ts}^*|^2 \alpha_{QED} m_b^5}{32\pi^4} f(\omega). \tag{4.81}$$

Therefore, the extraction of $|V_{ub}|$ can be done without the theoretical uncertainty of the shape function, if one considers a ratio of weighted integrals over the endpoint regions of $B \to X_u l\nu$ decays and the photon spectrum in $B \to X_s\gamma$ decays as [83, 84]

$$\left| \frac{V_{ub}}{V_{tb} V_{ts}^*} \right|^2 = \frac{3\alpha_{QED}}{\pi} K_{pert}(E_0) \frac{\Gamma_u(E_0)}{\Gamma_s(E_0)} + \mathcal{O}(\Lambda/M_B), \tag{4.82}$$

where

$$\Gamma_u(E_0) = \int_{E_0}^{M_B/2} dE_l \frac{d\Gamma(B \to X_u l\nu)}{dE_l}, \tag{4.83}$$

$$\Gamma_s(E_0) = \frac{2}{M_B} \int_{E_0}^{M_B/2} dE_\gamma (E_\gamma - E_0) \frac{d\Gamma(B \to X_s\gamma)}{dE_\gamma}. \tag{4.84}$$

The coefficient $K_{pert}(E_0)$ is a factor from short-distance effect which can be calculated in perturbative QCD. There are two major sources of uncertainties. The first is the unknown higher twist corrections to the shape function $1/m_b$ [85–88]. Based on model calculations this higher twist correction is expected to be of order 15% for $E_l^{cut} = 2.3$ GeV. The second is the weak annihilation contribution of $O(1/m_b^2)$, which is estimated as 10% for $E_l^{cut} = 2.3$ GeV [89, 90]. These two uncertainties can be reduced below 10% by lowering the lepton energy cut by combining with other cuts.

For the m_X^2 cut [91–95], 80% of the kinematic range is available but still the results are sensitive to the shape function. This cut also suffers from the singularity due to the bremsstrahlung diagram when the partonic invariant mass $s = (m_b - v)^2$ is zero.

For the pure q^2 cut, 20% of the rate is available and the decay rate is not sensitive to the shape function [96]. However, the kinematic range is sensitive to the resonance region and the convergence of the OPE as well as the convergence in the perturbative expansion in α_s are slower. The largest error comes from the weak annihilation contribution of $O(1/m_b^3)$. The rate with q^2 is also sensitive to the uncertainty of m_b [97] as can be seen from the m_b dependence of the partial decay rate parametrized as $\Gamma(q^2 > q_{cut}^2) \propto m_b^{\Delta(q_{cut}^2)}$, where $\Delta(q_{cut}^2) \sim 10 + \dfrac{q_{cut}^2 - (m_B - m_D)^2}{1\text{GeV}^2}$.

To summarize, possible sources of errors are (1) perturbative error from unknown two-loop corrections, (2) shape function contributions and bremsstrahlung, (3) uncertainties in m_b, and

Cuts on $(q^2,\, m_X^2)$	$G(q^2_{\rm cut}, m_{\rm cut})$	$\Delta_{\rm struct}G$	$\Delta_{\rm pert}G$	$\Delta_{m_b}G$ $\pm 80/30\,{\rm MeV}$	$\Delta_{1/m^3}G$	ΔG
Combined cuts						
$6\,{\rm GeV}^2, 1.86\,{\rm GeV}$	0.38	-4%	4%	13%/5%	6%	15%/9%
$8\,{\rm GeV}^2, 1.7\,{\rm GeV}$	0.27	-6%	6%	15%/6%	8%	18%/12%
$11\,{\rm GeV}^2, 1.5\,{\rm GeV}$	0.15	-7%	13%	18%/7%	16%	27%/22%
Pure q^2 cuts						
$(m_B - m_D)^2, m_D$	0.14	$--$	15%	19%/7%	18%	30%/24%
$(m_B - m_{D^*})^2, m_{D^*}$	0.17	$--$	13%	17%/7%	14%	26%/20%

Table 4.18: $G(q^2_{\rm cut}, m_{\rm cut})$ and its errors for different choices of $(q^2_{\rm cut}, m_{\rm cut})$. $\Delta_{\rm struct}G$ gives the fractional effect of the structure function $f(k_+)$ in the simple model which is not included in the error estimate. The total error is obtained by adding each error in quadrature. The two values correspond to $\Delta m_b^{1S} = \pm 80\,{\rm MeV}$ and $\pm 30\,{\rm MeV}$. Table is from [98].

(4) $O(1/m_b^3)$ power corrections. The optimized method would be obtained by combining the q^2 and m_X^2 cuts [98]. The kinematical constraints $m_X < m_D$ and $q^2_{cut} > m_B m_b - (m_X^{cut})^2$ reduce the charm background. If we raise q^2_{cut} the errors (3) and (4) gets larger while if we lower q^2_{cut} the errors (2) gets larger and (1) is small in the intermediate q^2 region. Thus it is important to find the best cut that minimizes the sum of these errors.

In Table 4.18, we give results of [98] for the errors of the partial decay rate normalized by the total tree level parton decay rate defined as

$$\frac{G_F^2 |V_{ub}|^2 m_b^5}{192\pi^3} G(q^2_{\rm cut}, m_{\rm cut}) \equiv \int_{\hat{q}^2_{\rm cut}}^1 {\rm d}\hat{q}^2 \int_0^{\hat{s}_0} {\rm d}\hat{s}\, \frac{{\rm d}\Gamma}{{\rm d}\hat{q}^2 {\rm d}\hat{s}}. \tag{4.85}$$

In order to achieve the $|V_{ub}|$ determination with a few percent accuracy, q^2_{cut}=6 GeV^2 (and $m^2_{X\,cut} = m_D^2$) is the optimal choice. The dominant error in this case is the uncertainty in m_b. It is therefore important to determine the bottom quark mass to 30 MeV accuracy.

Exclusive decays

The exclusive semileptonic decay $B \to \pi l \nu$ determines the CKM matrix element $|V_{ub}|$ through the following formula,

$$\frac{d\Gamma}{dq^2} = \frac{G_F^2}{24\pi^3} |(v\cdot k_\pi)^2 - m_\pi^2|^{3/2} |V_{ub}|^2 |f^+(q^2)|^2, \tag{4.86}$$

where the form factor f^+ is defined as

$$\langle \pi(k)|\bar{q}\gamma^\mu b|B(p)\rangle = f^+(q^2)\left[(p+k)^\mu - \frac{m_B^2 - m_\pi^2}{q^2} q^\mu\right] + f^0(q^2)\frac{m_B^2 - m_\pi^2}{q^2} q^\mu, \tag{4.87}$$

with p and k the B and π meson momenta. $q = p - k$ is the momentum transfer and $q^2 = m_B^2 + m_\pi^2 - 2m_B v\cdot k$, where v is the velocity of the B meson. Since the most promising approach in which systematic improvement based on first principle calculations is possible is lattice QCD, we focus on the lattice computation of the form factors.

Lattice calculation suffers from three major limitations. One is the discretization error from the large energy of the initial and final hadrons. In order to avoid such error, spatial momenta

method	stat.	disc.	$1/M$ extrap.	pert.
NRQCD (JLQCD)	10%	16%	–	4%
extrap. (APE)	10%	5%	15%	–
NRQCD (future)	$< 5\%$	4-10%	–	4%
extrap.+ HQET (future)	$< 5\%$	5%	5%	–

Table 4.19: Typical errors of the form factor $f^+(q^2)$ for $q^2 > 16$ GeV^2 at present and future prospects. "stat.", "disc.", "$1/M$ extrap", and "pert." stand for statistical, discretizations, $1/M$ extrapolation, and perturbative errors.

must be much smaller than the cutoff, *i.e.* $|\vec{p}_B|$, $|\vec{k}_\pi| < 1$ GeV. This means that the form factors can be computed reliably only in the range of $v \cdot k \equiv E_\pi < 1$ GeV or equivalently $q^2 > 18$ GeV^2. Another limitation is the fact that due to the limited computer power the light quark mass range for practical simulations is $m_s/3 \leq m_q \leq m_s$ or $m_\pi = 0.4 \sim 0.8$ GeV. In order to obtain physical results chiral extrapolation in the light quark masses is necessary. The last limitation is the large discretization error from the b-quark mass. In the present simulations, the lattice cutoff is limited to $a^{-1} = 2 - 3$ GeV, so that the b-quark mass in lattice unit is larger than unity. This makes the discretization error of $O(am_b)$ completely out of control. In order to avoid this error, one either carry out simulations around charm quark mass region and extrapolate the result in the inverse heavy quark mass $1/m_Q$ (extrapolation method), or use heavy quark effective theory, such as NRQCD action or Fermilab action (HQET). In both cases, extrapolation or interpolation of the form factors in $1/m_Q$ may be performed using the HQET motivated form factors $f_1(v \cdot k)$ and $f_2(v \cdot k)$ [99]

$$\langle \pi(k)|\bar{q}\gamma^\mu b|B(p)\rangle = 2\left[f_1(v\cdot k)v^\mu + f_2(v\cdot k)\frac{k^\mu}{v\cdot k}\right]. \tag{4.88}$$

With this choice the heavy quark scaling law is explicit, and the form factors are simply expanded in terms of $1/m_Q$.

So far all lattice calculations of the form factors have been performed only in the quenched approximation, in which the sea quark effects are neglected. The systematic error due to quenching is hard to estimate but typical errors in many quantities such as light hadron masses and decay constants are expected to be at 10-15% level.

Recently five lattice collaborations have carried out quenched QCD calculations of $B \to \pi l\nu$ form factors using extrapolation method [100, 101], the Fermilab action [102], and the NRQCD action [103, 104] for the heavy quark. Figure 4.9.2 shows the result by different lattice groups. $f^+(q^2)$ agrees within systematic errors, while $f^0(q^2)$ shows deviations among different methods. The reason for the discrepancies in $f^0(q^2)$ can be attributed to the systematic error in the chiral extrapolation and heavy quark mass extrapolation (interpolation) error. The error of the form factors in the present calculations is around 20%. In addition to the quenching error and the chiral extrapolation error, the major errors are the statistical error, the discretization error and the $1/M$ extrapolation error.

Table 4.19 shows the errors by and the JLQCD collaboration (NRQCD) and the APE collaboration (extrapolation method). We also list expected errors in unquenched lattice calculations with $a^{-1} = 2^3$ GeV in the near future. The present NRQCD method (JLQCD) has a large discretization error since $a^{-1} = 1.6$ GeV. It would be possible to carry out simulations with $a^{-1} = 2 - 3$ GeV, so that the error of $O((ak)^2)$ are reduced to 4-10%. The discretization error in the extrapolation method appear in the lattice results for the charm quark region them-

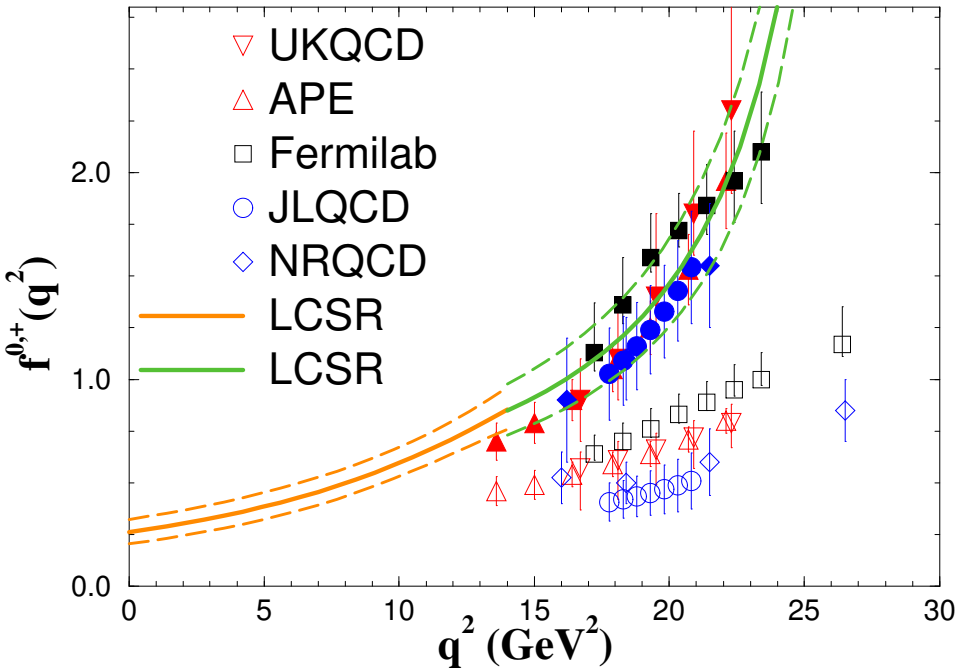

Figure 4.39: $B \to \pi l \nu$ form factors by different lattice groups. Filled symbols represent $f^+(q^2)$ and open symbols are $f^0(q^2)$.

selves which is propagated through the final result by extrapolation in $1/M$. Since the present quenched calculation is carried out with $a^{-1} = 2.7$ GeV, they will remain to be of the same order.

There are several proposals to improve the form factor determination.

The quenching error can be resolved only by performing the unquenched calculations. Recently, the JLQCD collaboration has accumulated $n_f = 2$ unquenched lattice configurations with $O(a)$-improved Wilson fermions [105], and $n_f = 2+1$ unquenched configurations with improved staggered fermions have been produced by the MILC collaboration [106]. These unquenched QCD data should be applied to form factor calculations.

Using the heavy quark symmetry is another way of improvement. Since the CLEO-c experiment can measure form factors for $D \to \pi l\nu$ to a few percent accuracy, their results will be a good approximation for the $B \to \pi l\nu$ form factors. Then the task for lattice QCD is to provide the $1/m_Q$ dependence of the form factors. The B to D ratio $\dfrac{d\Gamma(B \to \pi l\nu)/d(v \cdot k_\pi)}{d\Gamma(D \to \pi l\nu)/d(v \cdot k_\pi)}$ with the same recoil energy $v \cdot k_\pi$ would be a nice quantity to measure on the lattice, since a large part of the statistical error, the perturbative error and the chiral extrapolation errors are expected to cancel in this ratio.

Model independent bounds for the whole q^2 range can be obtained with dispersion relation, perturbative QCD, and lattice QCD data [107]. Reducing the lattice errors or having other inputs would significantly improve the results. More elaborate studies along this line would be important.

Recently, the UKQCD collaboration [108] and the SPQcdR collaboration [109] performed studies of $B \to \rho l\nu$ form factors. Both collaborations use $O(a)$-improved Wilson action for the heavy quark and extrapolate the numerical results of $m_Q \sim m_c$ toward the physical b quark mass. UKQCD obtained the partially integrated decay rate in the region $12.7\,\mathrm{GeV}^2 < q^2 < 18.2\,\mathrm{GeV}^2$ as $\Gamma = (4.9^{+12+\ 0}_{-10-14}) \times 10^{12} s^{-1} |V_{ub}|^2$.

4.9.3 Measurement of inclusive $b \to u$ semileptonic decays

Measurement of the inclusive rate for $B \to X_u \ell\nu$ decays is the most straightforward approach to determine $|V_{ub}|$. OPE provides a firm theoretical basis to convert the measured rate to $|V_{ub}|$. However, this is true only when the total rate can be measured with a small enough error. Experimentally, however, we have to introduce cuts on kinematical variables, such as E_ℓ, m_X and q^2, to reduce the huge $B \to X_c \ell\nu$ background, and only a limited phase space is available in a practical measurement. This complicates the situation, and the cut has to be chosen carefully to minimize the theoretical uncertainties. As discussed in the above section, one of the best strategies is to apply a combined cut on (q^2, m_X).

In $\Upsilon(4S)$ experiments, a correct measurement of (q^2, m_X) is possible when the accompanying B decays are fully reconstructed. This technique, referred to as "full reconstruction tagging", allows us to isolate tracks from the signal B decays for correct reconstruction of m_X, and also to determine the momentum vector of the signal-side B meson. The latter helps to improve reconstruction of the missing neutrino, leading to correct reconstruction of q^2 and better discrimination of $B \to X_c \ell\nu$ background leaking into the signal phase space. Full reconstruction tagging also allows us to determine the flavor and charge of the signal-side B. It helps to identify the signal lepton using the correlation between the B flavor and lepton charge, and also to measure the decay rate separately for neutral and charged B mesons. However, this ultimate measurement requires a large accumulation of $B\overline{B}$ data because of the relatively small efficiency in the full reconstruction of the accompanying B's (a few times 0.1%). Therefore, the high lu-

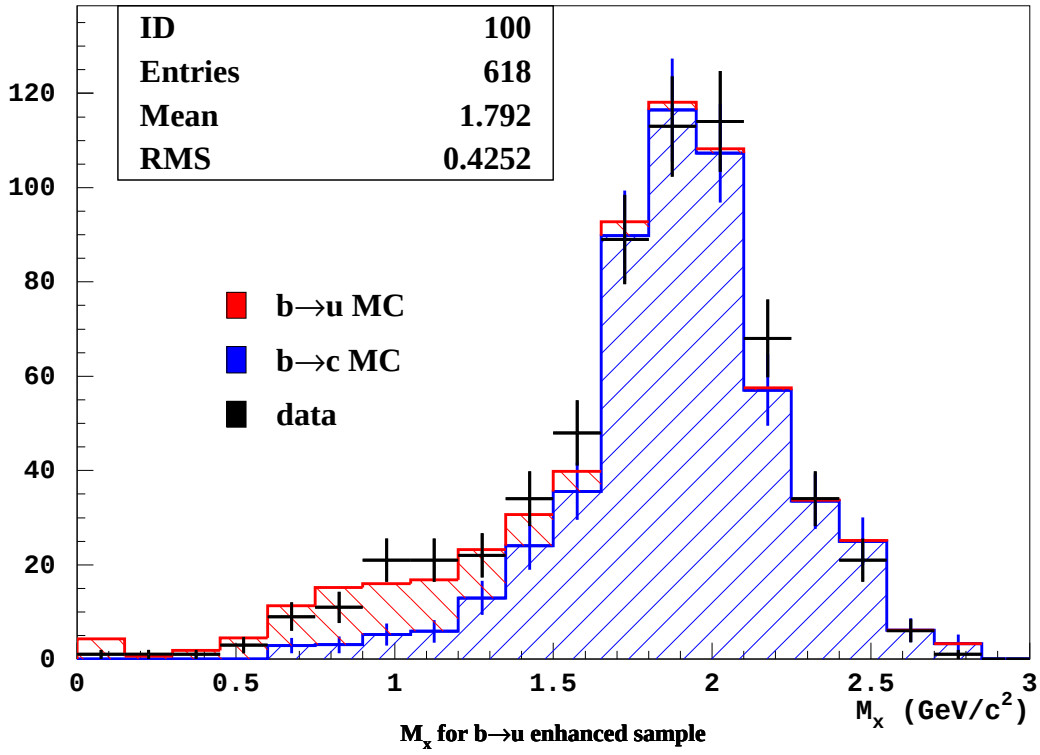

Figure 4.40: Distribution of reconstructed m_X with a full reconstruction analysis using 141 fb^{-1} of data.

minosity of the SuperKEKB provides an unique opportunity to perform this measurement with high statistics.

Such analysis with the full reconstruction tagging is being performed with the present Belle data, although with limited statistics. Figure 4.9.3 shows the distribution of reconstructed m_X for the q^2 region above 6 GeV^2, based on 141 fb^{-1} of data accumulated by Summer 2003. In this data sample, the number of fully reconstructed events is about 1.4×10^5 (9.1×10^4 of B^+ and 4.7×10^4 of B^0 events), and it corresponds to the full reconstruction efficiency (ϵ_{frecon}) of 0.1%. In the low m_X region, one can see a clear enhancement of the $B \to X_u \ell\nu$ signal over the expected $B \to X_c \ell\nu$ background. In the region $m_X < 1.5$ GeV/c^2, for example, the observed signal (S) is 68 with a predicted background (B) of 56, resulting in a signal-to-background ratio (S/B) of 1.2. Table 4.20 summarize the efficiency to detect the $B \to X_u \ell\nu$ signal once the accompanying B's fully reconstructed ($\epsilon_{b\to u}$) and the signal-to-background ratio (S/B). Here, values are shown for three m_X cuts, $m_X < 1.5, 1.7$ and 1.86 GeV/c^2, with the q^2 cut fixed at 6 GeV^2. We note here that a similar analysis by the BaBar collaboration has better S/B by a factor of 2 [110].

Based on extrapolation of the present Belle results and realistic assumptions for the improvement in ϵ_{frec} and S/B, we have estimated the $|V_{ub}|$ precision at a SuperKEKB/Belle experiment. We consider here the statistical, experimental systematic and theoretical errors, and estimate them as follows.

Statistical error The statistical error (Δ_{stat}) is simply scaled with the integrated luminosity

Quantity	m_{Xcut}		
	1.5 GeV/c^2	1.7 GeV/c^2	1.86 GeV/c^2
$\epsilon_{b\to u}$	0.14	0.17	0.17
S/B	1.21	0.61	0.32

Table 4.20: Efficiencies to detect the $B \to X_u \ell\nu$ signal for the fully reconstructed events ($\epsilon_{b\to u}$) and the signal-to-background ratio (S/B) for three different cut values.

(L),

$$\Delta_{stat} = \frac{1}{2} \times \sqrt{\frac{1 + (S/B \times f_{S/B})^{-1}}{n_0 \times f_{frec} \times \epsilon_{b\to u} \times L}} \quad , \tag{4.89}$$

where n_0 is the rate of $B \to X_u \ell\nu$ decays after full reconstruction, estimated as $68/(0.14 \times 141) = 3.2/\text{fb}^{-1}$. The factor f_{frec} accounts for the improvement in ϵ_{frec}, that is $2.2 \times 10^5/1.4 \times 10^5 = 1.6$ (see Table 4.3). The factor $f_{S/B}$ accounts for a possible improvement in S/B from the results in Table 4.20, and is assumed to be $f_{S/B} = 2$ based on the above mentioned BaBar result.

Experimental systematic error The major source of experimental systematic error (Δ_{syst}) will be associated with the background subtraction, and largely depend on the signal-to-background ratio. For instance, the (q^2, m_X) measurement by Belle using an advanced neutrino reconstruction technique [111] has $S/B = 0.18$ and the total experimental systematic error (in $Br(B \to X_u \ell\nu)$) of 18.1%, dominated by the $B\overline{B}$ background subtraction error of 16.8%. Relying on this result and assuming a naive scaling of the background subtraction error with $(S/B)^{-1}$, Δ_{syst} is estimated as,

$$\Delta_{syst} = \frac{1}{2} \times [0.168 \times \frac{0.18}{S/B \times f_{S/B}} \oplus 0.03] \quad . \tag{4.90}$$

Here, we add in quadrature a 3% error associated with the signal detection efficiency. The estimation then gives $\Delta_{syst} = 2.8\%$ in $|V_{ub}|$.

Theoretical error As discussed in Section 4.9.2, the theoretical error (Δ_{theo}) is minimum at a choice of $(q^2_{cut}, m_{Xcut}) = (6\text{GeV}^2, 1.86\text{GeV}/c^2)$. The dominant error in this case is the uncertainty in the b-quark mass. Based on a combined fit to recent experimental data of B semileptonic decays, Bauer, Ligeti, Luke and Manohar have deduced $m_b^{1S} = 4.74 \pm 0.10\,\text{GeV}$, where the error is dominated by experimental uncertainties [112]. If the experimental uncertainties are eliminated in the future, the present 100 MeV error shrinks to 30 MeV. Then $\Delta_{theo} = 1/2 \times 9 = 4.5\%$ in $|V_{ub}|$, according to Table 4.18.

Adding the above three error sources in quadrature, Figure 4.41 demonstrates the expected improvement of $|V_{ub}|$ error as a function of the integrated luminosity L, with the optimal choice of $(q^2_{cut}, m_{Xcut}) = (6\text{GeV}^2, 1.86\text{GeV}/c^2)$. In conclusion, with a precise determination of the b-quark mass, a $|V_{ub}|$ error of less than 5% is achievable at $L = 5\ \text{ab}^{-1}$.

4.9.4 Mesurement of exclusive $b \to u$ semileptonic decays

The measurement of the inclusive $B \to X_u \ell\nu$ decay is insensitive to theoretical ambiguities, but experimentally challenging because of the large background from $B \to X_c \ell\nu$ decays. Complementary to this, the measurement of exclusive decays, such as $B \to \pi\ell\nu$ and $B \to \rho\ell\nu$, provides

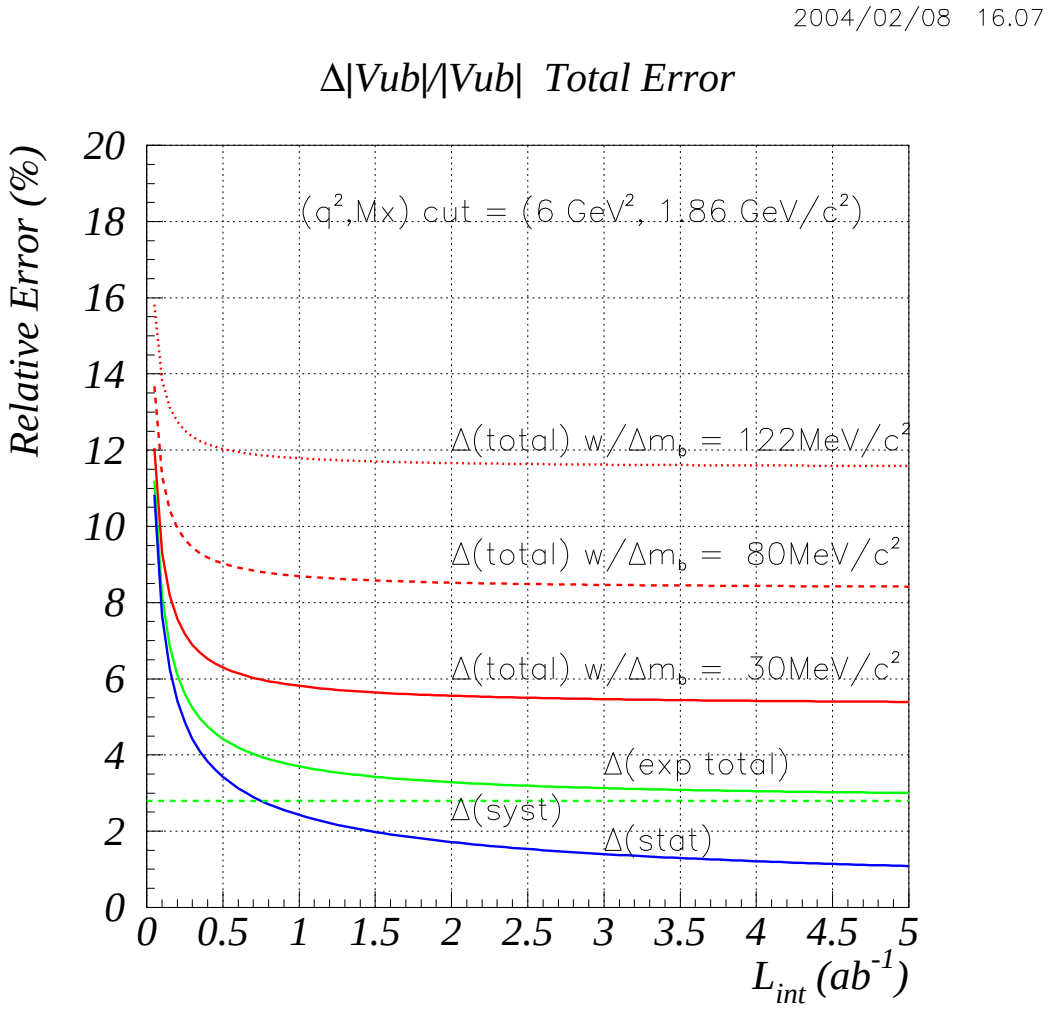

Figure 4.41: Expected improvement of $|V_{ub}|$ error as a function of L.

experimentally cleaner information, but is subject to large theoretical uncertainties in the form factors. On the experimental side, it is essential to provide precise data for the differential rates $d\Gamma/dq^2$ of each exclusive channel. This is because $d\Gamma/dq^2$ varies depending on theory models, and such data helps to test the model. Precise data in the high q^2 region is especially important, since lattice-QCD calculations, the most promising tool for reliable model-independent determination of $|V_{ub}|$, are possible only in the region $q^2 > 18\text{GeV}^2$, as discussed in Section 4.9.2. While there have been several exclusive measurements in the literature [113–118], these data lack information on the q^2 distribution or, even if they include such information, suffer from poor statistics and from relatively large systematic errors. A high luminosity SuperKEKB/Belle experiment will enable us to measure the q^2 distributions with high statistics and less systematic uncertainties. Combined with improvements in lattice QCD with unquenched calculations in future, this will lead to useful determinations of $|V_{ub}|$.

One of experimental key issues in measuring the exclusive $B \to \pi\ell^+\nu/\rho\ell^+\nu$ decays is the

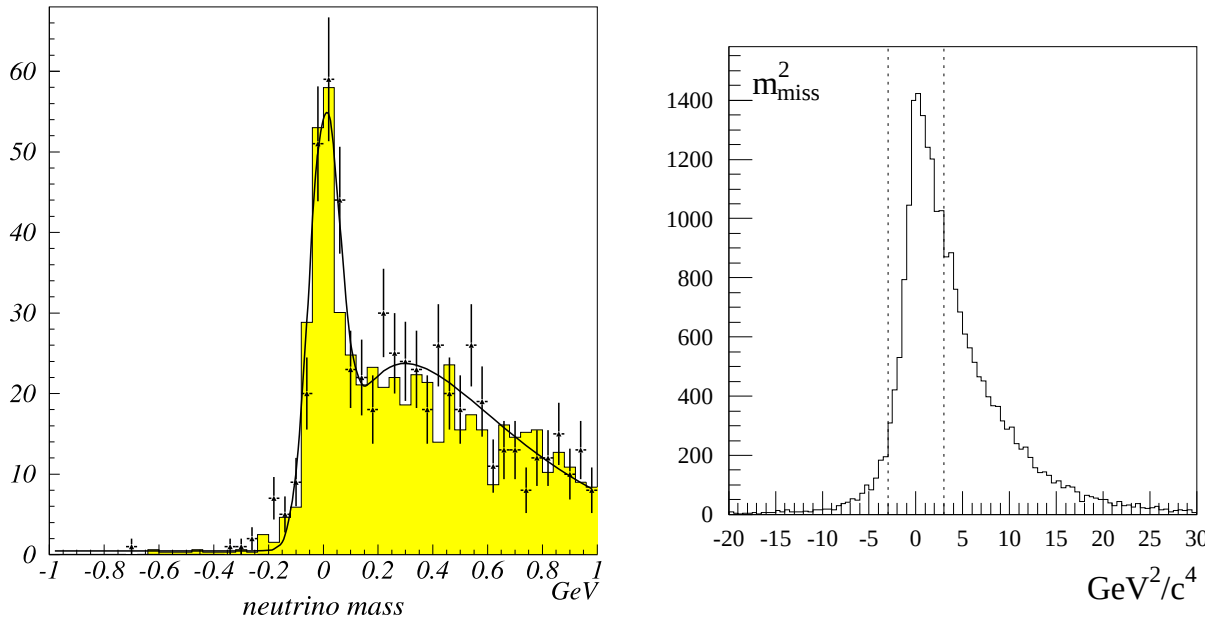

Figure 4.42: Missing mass resolution in (left) a full reconstruction analysis and (right) a classical neutrino reconstruction analysis.

reconstruction of the undetected neutrino in the final state. Information on missing energy and momentum of the event have been used to infer information about the missing neutrino ("neutrino reconstruction"). This method, originally developed by CLEO, has been applied in existing measurements and exploits the known kinematics of the $e^+e^- \to \Upsilon(4S)$ reaction and near 4π coverage ("*hermeticity*") of the detector. In reality, however, hermeticity of a detector is never complete. This lack of hermeticity allows background from both $B\overline{B}$ and cross-feed (*e.g.*, $\pi\ell\nu \leftrightarrow \rho\ell\nu$) to contribute, where the latter is serious especially in the high q^2 region. For instance, the recent CLEO measurement [116] provides $Br(B \to \pi\ell\nu)$ with a statistical error of 13.5(36.0)% and an experimental systematic error of 8.6(18.3)% for the whole q^2 ($q^2(> 16\text{GeV}^2)$ region. The experimental systematic errors are mainly associated with the neutrino reconstruction; 6.8% in the whole q^2 region and 17.2% in the $q^2 > 16\text{GeV}^2$ region. The CLEO result has been obtained with event sample of only ~ 10 fb^{-1}, and we can quickly improve the statistical error to a few %. However, the systematic error arising mainly from the neutrino reconstruction will soon limit the experimental uncertainties.

As in the case of the inclusive measurement, discussed in the previous section, analyses with full reconstruction tagging improve the situation substantially, and make best use of the high luminosity at SuperKEKB/Belle. Figure 4.42 compares the missing mass resolution for (a) full reconstruction tagging (for $B \to D^0\ell^+\nu$ with 78 fb^{-1}), and (b) classical ν reconstruction (for $B \to \omega\ell^+\nu$ with 78 fb^{-1}) in the present Belle analyses. An improvement in the FWHM by almost a factor of 50 is seen for the full reconstruction analysis. We can also consider semileptonic tagging, where one tags more abundant $B \to D^{(*)}\ell^+\nu$ decays in the accompanying B decays. This technique provides about 4 times more statistics by sacrificing purity and q^2 resolution. Belle has presented a preliminary inclusive analysis using this method [119]. An exclusive analysis using this method is also in progress.

Figure 4.43 shows the expected improvement of the experimental error in $|V_{ub}|$ as a function of the integrated luminosity L, for the whole q^2 and the high q^2 regions. Here, the errors

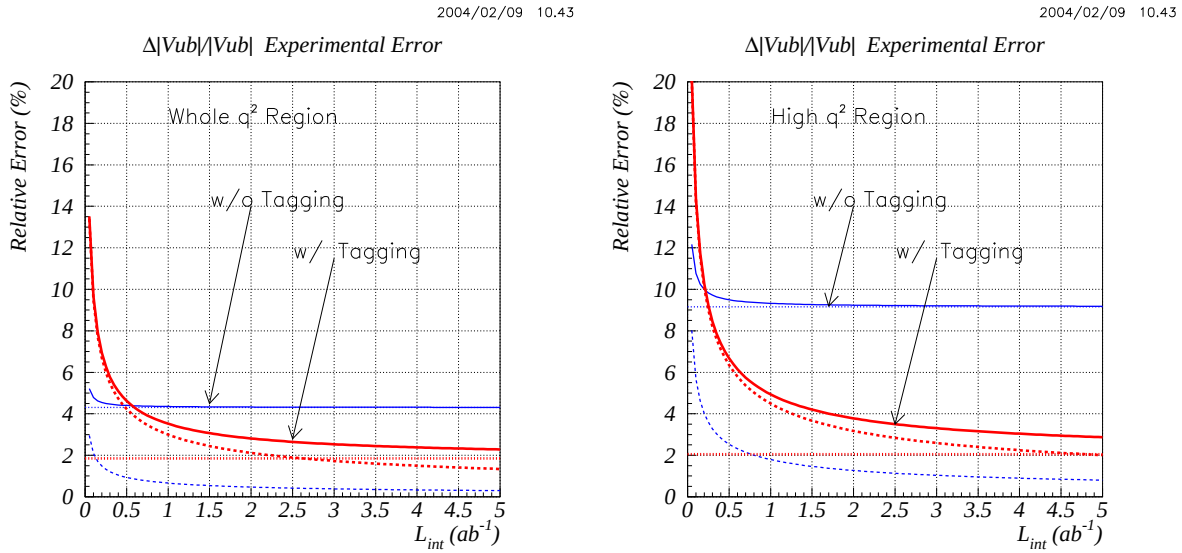

Figure 4.43: Expected improvement of the experimental error in $|V_{ub}|$ as a function of the integrated luminosity L, (left) for the whole q^2 and (right) the high q^2 regions.

are estimated by extrapolating the present Belle analysis using semileptonic tagging, and are compared with the classical neutrino reconstruction. One can see that the classical neutrino reconstruction will soon hit the systematic limit. At a few times 100 fb^{-1}, the tagging analysis will provide more precise results. The experimental precisions in $|V_{ub}|$ expected at 5 and 50 ab^{-1} are 2.3% and 1.9%, respectively, for the whole q^2 region, and 2.9% and 2.1%, respectively, for the $q^2 > 16\text{GeV}^2$ region.

4.10 Tau decays

4.10.1 Introduction

The τ lepton is the only charged lepton that is heavy enough to decay hadronically. Its variety of pure-leptonic and semi-leptonic decay modes makes it possible to study various physics issues. With an anticipated luminosity of 5×10^{35} cm^{-2}sec^{-1}, SuperKEKB is expected to deliver a sample of 1.5×10^{10} tau-pairs in three years of data taking. This huge data sample allows us to attain a single event sensitivity of 3×10^{-10} for branching fractions under assuming a 10% detection efficiency with no backgrounds. Research making the best use of such a large data sample can be divided into two categories: the sensitivity frontier and the precision frontier. The sensitivity frontier involves searches for new physics phenomena in rare or forbidden decays, while on the precision frontier one searches for a small inconsistency with the SM in a high precision measurement. Among many possible subjects at the sensitivity frontier, here we discuss the search for Lepton Flavor Violation (LFV) phenomena at SuperKEKB.

A theoretical overview of lepton-flavor-violating process beyond the Standard Model is given in Section 3.5.

4.10.2 Present experimental status

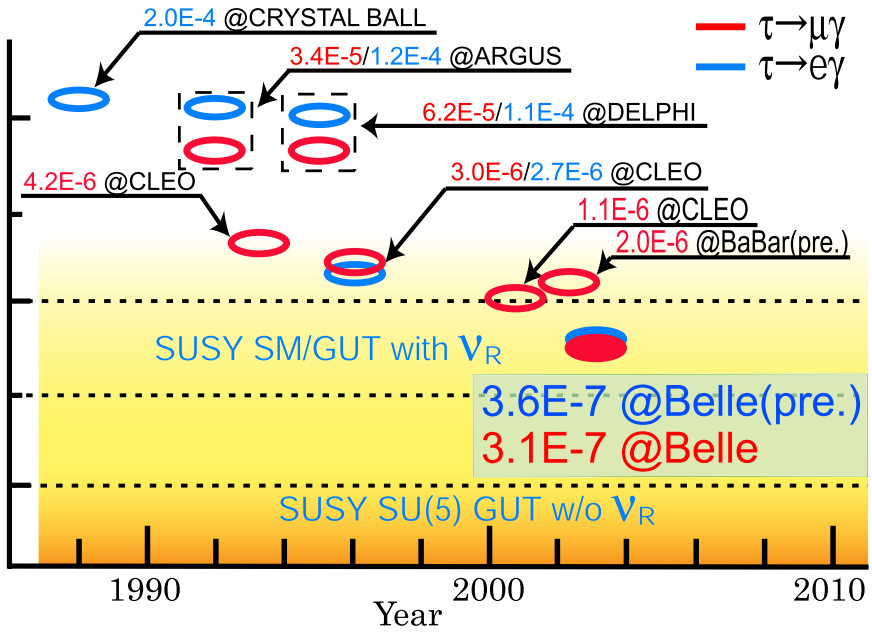

Figure 4.44: Experimental status of the LFV search.

So far, tau physics has been carried out mostly at electron-positron collider facilities. Samples of $e^+e^- \to \tau^+\tau^-$ reactions are selected based on characteristic properties, such as low multiplicity with a well collimated back-to-back jet-like pattern and missing momentum(energy) due to missing neutrinos. While these requirements will remove $B\bar{B}$ and a large portion of continuum reactions, an appreciable amount of Bhabha, muon-pair and two-photon processes remain and constitute severe backgrounds. Since τ decays always include neutrinos, the τ cannot be exclusively reconstructed and therefore background contamination cannot be totally avoided. The

LFV processes discussed here are exclusive decays and much higher sensitivity than for other decay modes could be attained.

Belle has so far analyzed 86 fb^{-1} of data for $\tau \to \mu^-(e^-)\gamma$, 83 fb^{-1} of data for $\tau^- \to \mu^-(e^-)h^0$ (where h^0 denotes either $h^0 = \eta, \eta'$ or π^0), and 87 fb^{-1} of data for $\tau^- \to l^-l^+l^-$. The current experimental status is summarized in Table 4.21 and the history of $\tau^- \to \mu^-(e^-)\gamma$ searches is shown in Figure 4.44. It is seen that the older data, mostly collected by CLEO, are no longer competitive with the best limits from the Belle collaboration. Branching fractions attained go down to the 10^{-7} level and the searches are approaching the sensitivities required for new physics.

In this section, we discuss the experience in τ physics research that we have acquired during the analysis of the current Belle data.

While the signal side τ is exclusively reconstructed for every LFV process, the tag side is required to be composed of a single charged track and any number of photons with neutrinos. The mode $\tau^- \to \mu^-(e^-)\gamma$ has the fewest constraints, so that a certain amount of background inevitably remains. The $\tau^- \to \mu^-(e^-)h$ mode includes extra constraints that provide additional background-rejection power, although there is some decrease of the detection efficiency due to the higher multiplicity. Together with the kinematic constraints for the signal, particle identification, especially for muon and electron, play an essential role for event selection. The Belle detector provides a μ-id efficiency of 90% and an e-id efficiency of 97-98%: the event selection power is strong and then background contamination is little at the electron accompanying processes. The contamination due to the inefficiency of μ-id is 28% for $\tau^- \to \mu^-\gamma$, while the rate due to the inefficiency of e-id is 6% in $\tau^- \to e^-\gamma$.

We have introduced a new requirement on the relation between the missing momentum and the missing mass-squared in $\tau^- \to \mu^-(e^-)\gamma$, in addition to the conventional requirements. It is quite effective: 98% of generic tau-pairs and 80-90% of radiative Bhabhas, muon-pairs and continuum are removed, while 76% of the signal is retained (See Figure 4.45).

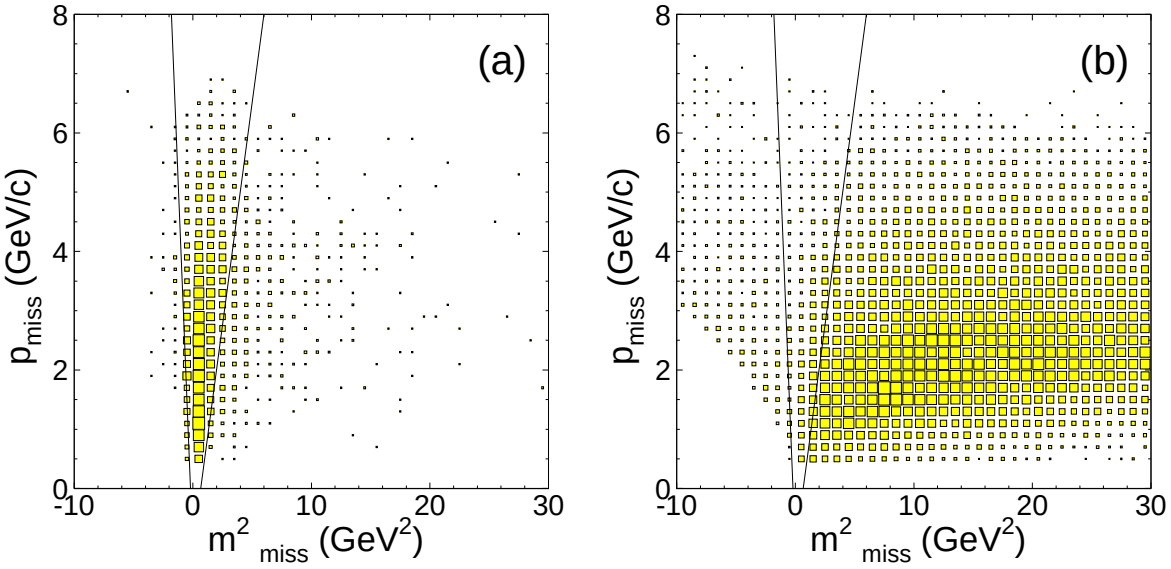

Figure 4.45: A newly introduced selection requirement regarding the missing quantities, $p_{\rm miss}$ vs $m^2_{\rm miss}$. (a) For signal-MC events, and (b) for generic tau-pair MC. The selected region is the area between the lines.

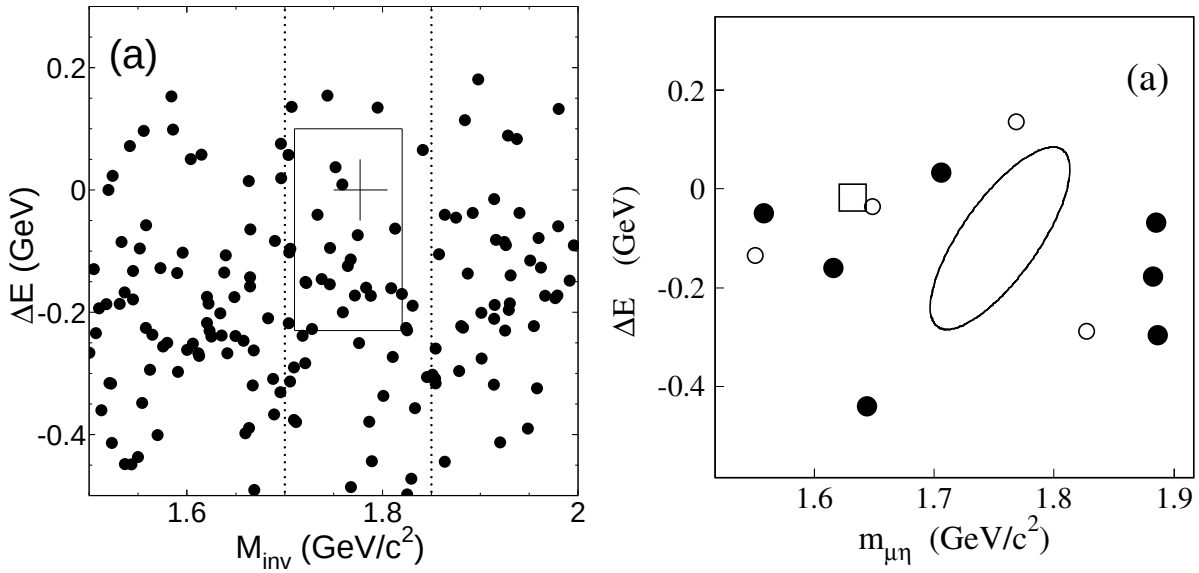

Figure 4.46: Distributions of events after all selection requirements. (a) $\tau \to \mu(e)\gamma$ with 86 fb^{-1}, (b) $\tau \to \mu\eta$ with 83 fb^{-1}.

Within the data analyzed, no signal candidates are found in the signal regions for $\tau^- \to \mu^-(e^-)h^0$ and $\tau^- \to l^-l^+l^-$. On the other hand, $\tau^- \to \mu^-(e^-)\gamma$ suffers from backgrounds as seen in Figure 4.46 (a). The principal background remaining after the selections for $\tau^- \to \mu^-(e^-)\gamma$ is originates from $\tau^+\tau^-$. In particular, the radiative tau-pair process ($e^-e^- \to \tau^+\tau^-\gamma$) dominates. One of τ's decays semi-leptonically from which the lepton and the radiated photon composes a tau candidate, while the other tau decays leaving one charged track in the detector with a different lepton flavor. Multi-photon radiative muon-pair (and Bhabha) yields the second largest background: one of leptons and a radiated photon forms a tau candidate, and the other lepton is mis-identified. These backgrounds cannot be discriminated from the true signal.

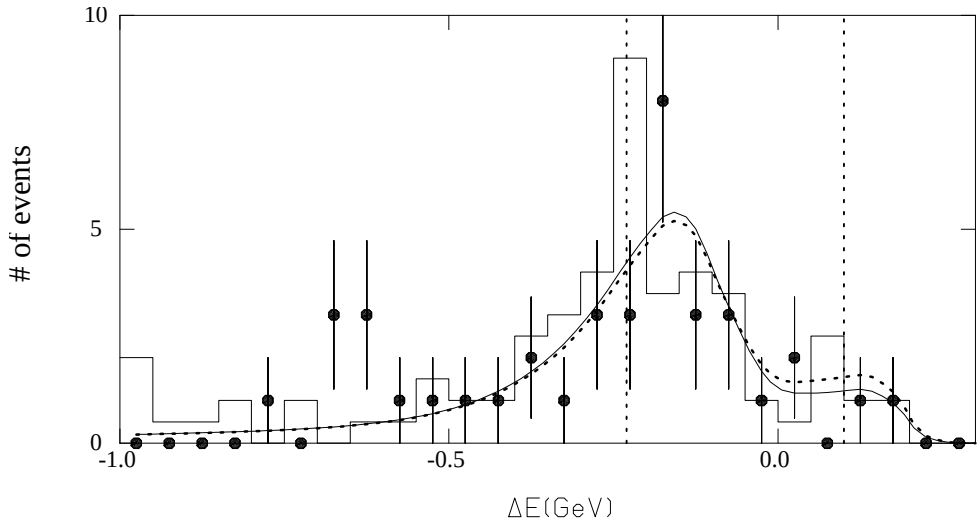

Figure 4.47: Expected background distribution for $\tau^- \to \mu^-\gamma$.

For $\tau^- \to \mu^-(e^-)\eta, \mu^-(e^-)\eta', \mu^-(e^-)\pi^0$ and $\tau^- \to l^-l^+l^-$, we evaluated the expected backgrounds in the signal region from the sidebands and extract the number of signal candidates. No candidates are found. The upper limits are calculated according to a Baysian approach. For $\tau^- \to \mu^-(\mathrm{e}^-)\gamma$ the background distribution was intensively studied using actual data and MC simulations, as is seen in Figure 4.47. A thorough understanding of the background's origin and properties was obtained. Finally, the number of signal events was obtained by means of an unbinned extended maximum likelihood method.

Mode	Limit	Luminosity (fb^{-1})	Refs.	Limit in PDG2000
$\tau^- \to \mu^-\gamma$	$< 3.1 \times 10^{-7}$	86	[120]	$< 11 \times 10^{-7}$
$\tau^- \to e^-\gamma$	$< 3.6 \times 10^{-7}$	86		$< 27 \times 10^{-7}$
$\tau^- \to \mu^-\eta$	$< 3.4 \times 10^{-7}$	83	[121]	$< 96 \times 10^{-7}$
$\tau^- \to e^-\eta$	$< 6.9 \times 10^{-7}$	83		$< 82 \times 10^{-7}$
$\tau^- \to e^-e^+e^-$	$< 3.5 \times 10^{-7}$	87	[122]	$< 29 \times 10^{-7}$
$\tau^- \to e^-e^+\mu^-$	$< 1.9 \times 10^{-7}$	87	[122]	$< 17 \times 10^{-7}$
$\tau^- \to e^-\mu^+e^-$	$< 1.9 \times 10^{-7}$	87	[122]	$< 15 \times 10^{-7}$
$\tau^- \to e^-\mu^+\mu^-$	$< 2.0 \times 10^{-7}$	87	[122]	$< 18 \times 10^{-7}$
$\tau^- \to \mu^-e^+\mu^-$	$< 2.0 \times 10^{-7}$	87	[122]	$< 15 \times 10^{-7}$
$\tau^- \to \mu^-\mu^+\mu^-$	$< 2.0 \times 10^{-7}$	87	[122]	$< 19 \times 10^{-7}$

Table 4.21: Limits on lepton-flavor-violating decay modes(90% confidence level) obtained so far from Belle data. The last column shows the previous limits from the PDG 2000 compilation.

4.10.3 Achievable sensitivity at SuperKEKB and physics reaches

Figures 4.48 shows the sensitivities anticipated at SuperKEKB. The sensitivities shown by the trianglar symbols are the expected sensitivities obtained by assuming some signal-to-background conditions and applying the unbinned extended maximum likelihood method at SuperKEKB. The lower-solid line are obtained by assuming no candidate events in the signal-region.

The former case corresponds to $\tau^- \to \mu^-(\mathrm{e}^-)\gamma$. In the latter case, the upper limit decreases inversely proportional to the total luminosity, Br $\propto 1/N_{\tau^+\tau^-}$. The $\tau^- \to \mu^-(e^-)\eta, \mu^-(e^-)\eta', \mu^-(e^-)\pi^0$ and $\tau^- \to l^-l^+l^-$ modes would follow a $\propto 1/N_{\tau^+\tau^-}$ behavior for a short time as up-to a luminosity of a few 100 fb^{-1} and then gradually change to a $\propto 1/\sqrt{N_{\tau^+\tau^-}}$ dependence as candidates begin to appear. Therefore, if the current signal-to-background condition is still maintained, the ultimate goal at 5,000 fb^{-1} could be a branching fraction sensitivity of several $\times 10^{-9}$ for $\tau^- \to \mu^-(e^-)\eta, \mu^-(e^-)\eta', \mu^-(e^-)\pi^0$ and $\tau^- \to l^-l^+l^-$. The $\tau^- \to \mu^-(\mathrm{e}^-)\gamma$ mode could be with a brantiong fraction sensitivity of of a few $\times 10^{-8}$.

Can we improve the sensitivity more? Experimental sensitivity is in general determined by the three key elements: statistics, resolution, and signal-to-background ratio; and its experimental reliability depends on how well the systematic uncertainty of these aspects is controlled. We discuss here possible measures for improvements, based on experience from the Belle $\tau^- \to \mu^-(\mathrm{e}^-)\gamma$ analysis.

Statistics Besides accumulating higher luminosity, it is important to the detection efficiency in-

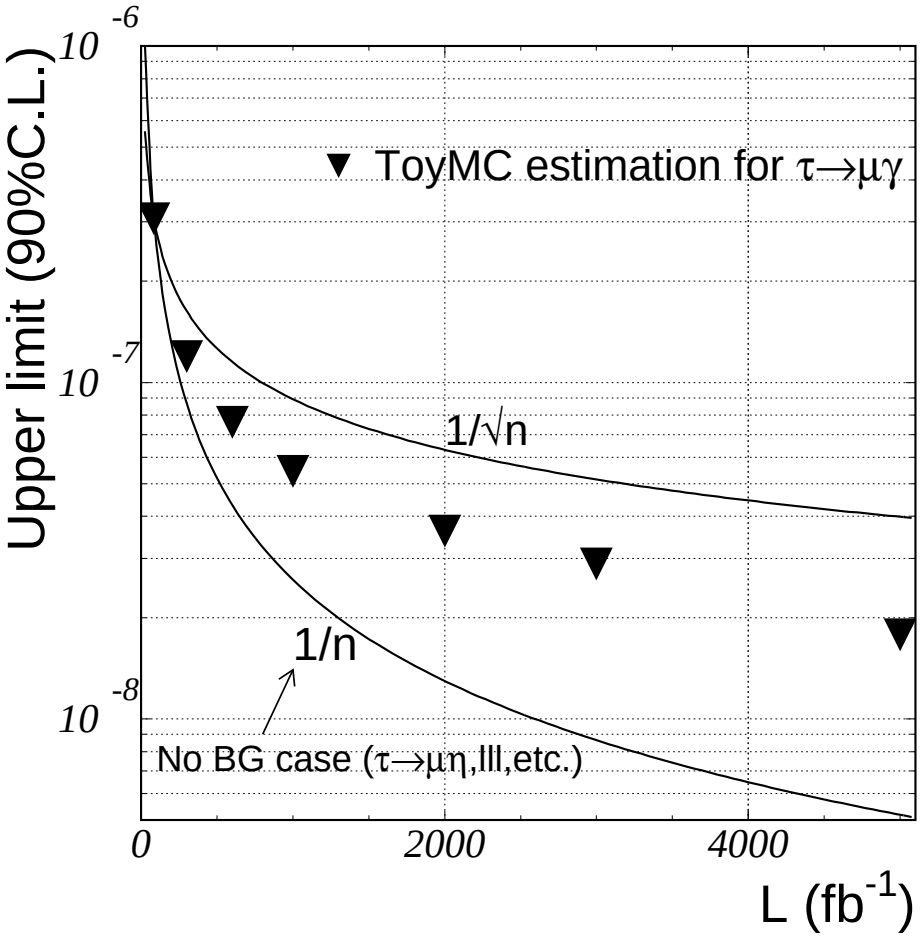

Figure 4.48: Achievable upper limits for LFV decays at SuperKEKB.

cluding trigger performance. However, at a SuperKEKB. the selection criteria will become tighter and efficiencies will be lower than the current sizes. There is no way to increase the detection efficiency.

Resolution Improvement of the momentum and energy resolution reduces the size of the signal region. The signal-to-background ratio, the sensitivity, is enhanced because the background distributes uniformly for a narrow ΔE vs. M_{inv} region. As is seen in Figure 4.49, energy leakage in the calorimeter and initial state radiation yields a long low-energy tail, so that our signal region is defined to be quite large to include a sufficient portion of the signal, say, more than 90%. While the effect of initial state radiation cannot be controlled, the effect of the calorimeter leakage can be improved, for instance, by using a crystal with a longer radiation length and containing less lateral energy leakage in the analysis procedure.

Improvement of particle identification ability is essential for all decay modes. The efficiency of e-id is already 98% so that further improvement would be not practical. On the other hand, the μ-id efficiency is now 90% so that the increase efficiency may reduce background contamination, for example, $(\mu\gamma)$+not$-\mu$ events in the $\tau^- \to \mu^-\gamma$ search, and the sensitivity will increase. A KLM counter with finer segmentation in the radial direction might provide a better muon identification. K/π separation is also important in searches for decays into 3 hadrons. The Time-Of-Propagation counter being studied by the Nagoya group could be a very good candidate for improvement here.

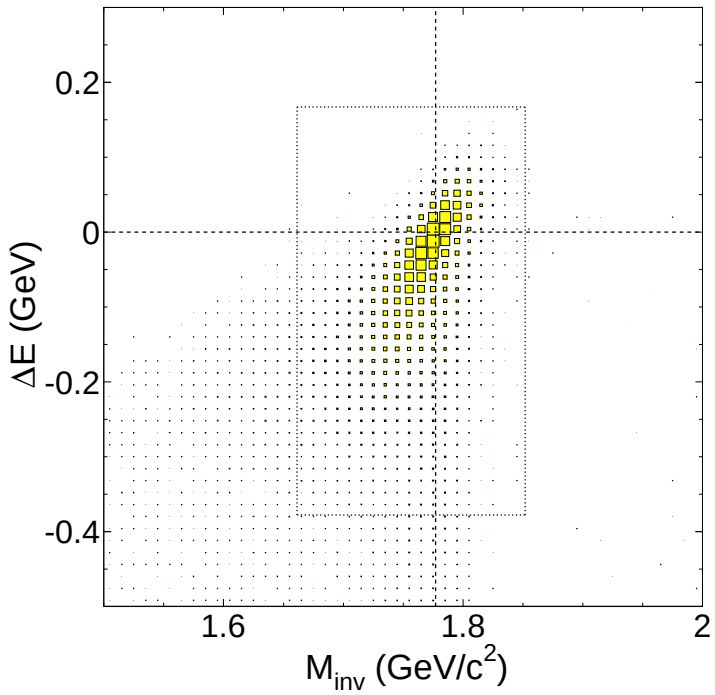

Figure 4.49: ΔE vs. M_{inv} distribution for $\tau^- \to \mu^-\gamma$ decay.

Signal-to-background A newly introduced requirement for the missing quantities, $p_{miss} - M^2_{miss}$, plays an important rule for background as seen in Figure 4.45. It makes it possible

to achieve a sensitivity higher than that of the CLEO experiment. We also apply a new selection for $\tau^- \to e^-\gamma$, using the opening angle between the tagged track and missing particle direction; this criterion quite effectively removes the radiative Bhabha background.

We have to create this kind of new criteria for future analysis.

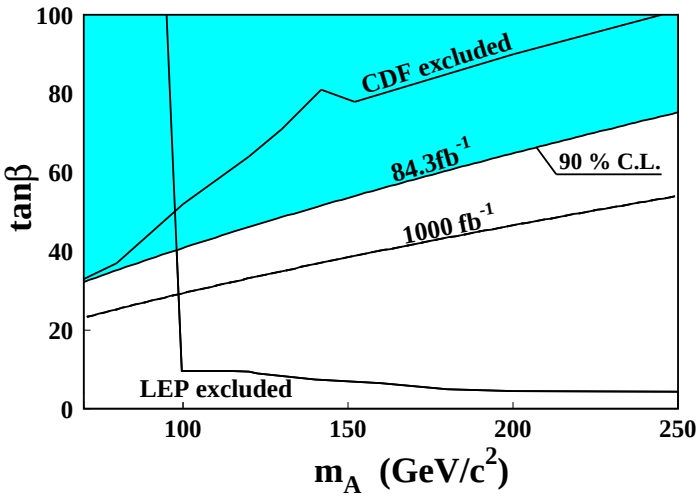

Figure 4.50: Physics reach in $m_A - \tan\beta$ parameter space at 1000fb^{-1} for the $\tau^- \to \mu^-\eta$ decay, together with the regions excluded by direct searches at LEP and in Tevatron experiments [123, 124]. Here, m_A is the pseudo-scalar Higgs mass in the Higgs mediated model.

Figures 4.50 and 4.51 show the τ physics reach with 1,000 fb^{-1}.
i) Fig. 4.50 shows a possible exclusion region in the $m_A - \tan\beta$ parameter space from $\tau^- \to \mu^-\eta$. The region allowed by the current upper-bound from the Belle experiment($< 3.4 \times 10^{-7}$) and the one from non-observation with the 1000fb^{-1} are shown. The boundary is evaluated by multiplying a factor 8.4 to the formula given by Eq.(3.13), *i.e.*

$$\mathcal{B}(\tau^- \to \mu^-\eta) = 3.2 \times 10^{-6} \times |\delta^L_{\tau\mu}|^2 \times \left(\frac{\tan\beta}{60}\right)^6 \times \left(\frac{M_A}{100GeV}\right)^{-4}.$$

where $|\delta^L_{\tau\mu}| = 1$ is assumed for the evaluation of the boundary [2]. It is worth mentioning that we already have achieved a sensitivity similar to that obtained by FNAL-Tevatron experiments for the $\tan\beta$ vs. m_A relation.

ii) Fig. 4.51 shows a possible exclusion region in $m_{SUSY} - \tan\beta$ parameter space for $\tau^- \to \mu^-\gamma$. The excluded regions are from Belle's current upper-bound ($< 3.1 \times 10^{-7}$) and from non-observation at 1000fb^{-1}. In this evaluation, we use the branching fraction for $\tau^- \to \mu^-\gamma$ provided from Eqs.(3.3)-(3.7). Assuming also $|\delta^R_{\tau\mu}| = 1$ and $|\delta^L_{\tau\mu}| = 1$, the approximate formula for $Br(\tau^- \to \mu^-\gamma)$ is given as

$$\mathcal{B}(\tau^- \to \mu^-\gamma) = 3.0 \times 10^{-6} \times \left(\frac{\tan\beta}{60}\right)^2 \times \left(\frac{M_{SUSY}}{1TeV}\right)^{-4}.$$

[2]This mean we are assuming the maximum branching fraction.

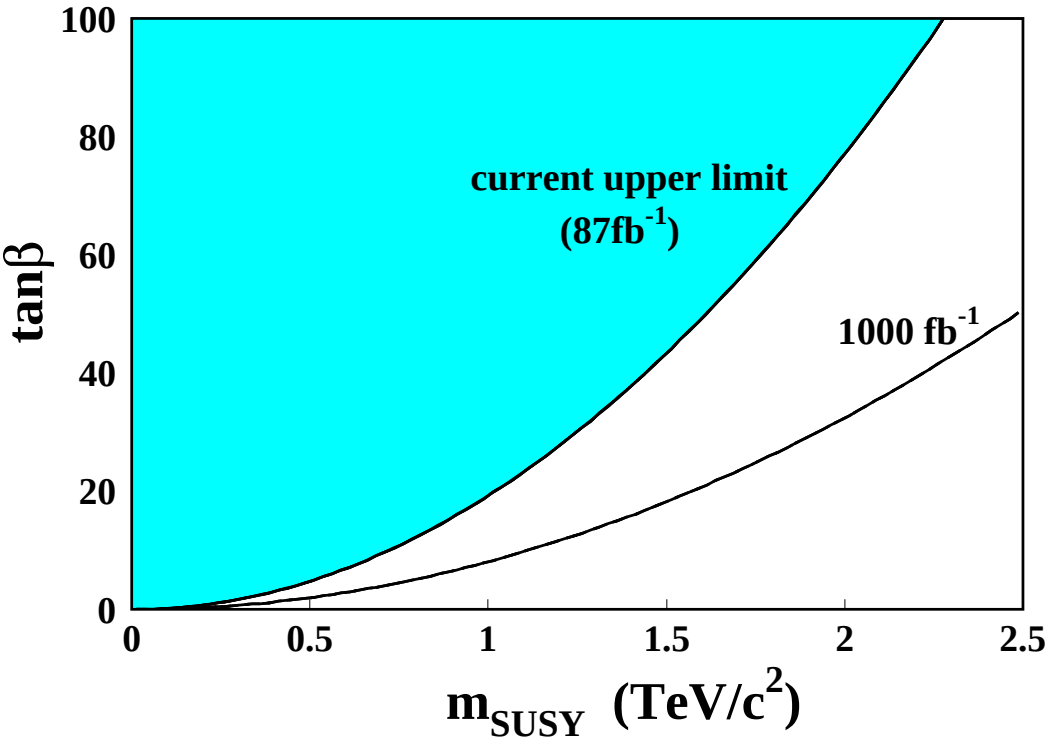

Figure 4.51: Physics reach in $m_{SUSY} - \tan\beta$ parameter space from Belle's current upper-bound and at 1000fb^{-1} luminosity for $\tau^- \to \mu^-\gamma$. The maximum branching fraction is obtained by taking $|\delta^R_{\tau\mu}| = |\delta^L_{\tau\mu}| = 1$ in Eq.(3.4)-(3.5).

4.10.4 Summary

Higgs and SUSY particles must exist, nevertheless there is no evidence for them yet. Many possible mechanisms for LFV decays are possible and a very wide range of the relevant parameter spaces are allowed now. Accordingly, many different models have been proposed as discussed in Section 3.5. Some predict relatively large branching fractions while others give extremely small values. Systematic and extensive investigation of various τ decay modes would provide a powerful means to select models, restrict their parameter space, and possiblly discover new phenomena beyond the Standard Model. The τ lepton is the most suitable charged lepton and a SuperKEKB is the facility best suited to carry out this frontier research.

4.11 Diversity of physics at Super-KEKB–other possibilities

4.11.1 Charm physics

At a B factory, a large number of charm mesons are produced from the $q\bar{q}$ continuum and also from decay products of B mesons. For example, with 11.1 fb^{-1} Belle reconstructs 10^5 D^0 ($\bar{D}^0$), 8×10^3 $D^\pm$ and 6×10^3 $D_s^\pm$ mesons in low multiplicity decay modes. We can expect data samples a hundred times larger with a luminosity of $10^{35}\,\mathrm{cm}^{-2}\mathrm{s}^{-1}$.

Due to the effectiveness of the GIM mechanism, flavor-changing neutral current (FCNC) decays, $D^0-\bar{D}^0$ mixing and CP violation are small in the charm sector. This is in sharp contrast with K and B FCNC processes, which are enhanced by the presence of top quarks in loops. In many cases, extensions of the Standard Model (SM) upset this suppression and give contributions sometimes orders of magnitude larger than the SM. As a result, rare charm processes are an excellent place to look for new physics.

The strength of $D^0-\bar{D}^0$ mixing is characterized by two parameters $x=\Delta M/\Gamma$ and $y=\Delta\Gamma/2\Gamma$. According to the conventional expectation of the SM, $x,y\leq10^{-3}$. However, in a recent treatment by Falk *et al.*, the possibility of y (and perhaps x) $\sim10^{-2}$ within the SM is raised [128]. The current experimental limits are at the level of a few times 10^{-2}.

Experimental searches for $D^0-\bar{D}^0$ mixing usually involve hadronic decay modes such as $D^0\to K^+\pi^-$. For such modes, there are contributions from both mixing and doubly Cabibbo suppressed decays (DCSD), which can be distinguished by their time dependences. In the CP conserving limit, the rate for wrong sign decays is

$$r_{WS}(t)=[R_D+\sqrt{R_D}y't+1/4(x'^2+y'^2)t^2]e^{-t},$$

where R_D is the DCSD rate, and $y'=y\cos\delta-x\sin\delta$ and $x'=x\cos\delta+y\sin\delta$ are the mixing parameters y and x rotated by δ, the relative strong phase between $D^0\to K^+\pi^-$ and $\bar{D}^0\to K^+\pi^-$. In the absence of interference, mixing has a t^2e^{-t} dependence which peaks at 2 D^0 lifetimes, whereas DCSD follows the usual e^{-t} dependence. The interference term is proportional to te^{-t} and dominates the sensitivity to mixing, since $(x'^2+y'^2)=(x^2+y^2)\ll R_D$. Since the measurement of y' and x' requires that these three terms be distinguished from each other, decay-time resolution is crucial: improved vertexing at the Belle upgrade, together with the very large D^0 samples available at $10^{35}\,\mathrm{cm}^{-2}\mathrm{s}^{-1}$, will lead to an improvement in sensitivity over previous experiments [129] and the existing B-factories.

Interpretation of $D^0\to K^+\pi^-$ and other hadronic-decay mixing analyses is complicated by the strong phase difference δ, which may be large [130], [131]: it is important to obtain constraints on this quantity. At a tau-charm facility, δ can be determined by using quantum correlations with two fully reconstructed D decays [132]. At a high luminosity B factory, δ can be determined by measuring related DCSD modes, including modes with K_L mesons [133].

If CP is violated in the D system, then additional $D^0-\bar{D}^0$ mixing signals may be seen. CP violation in the interference of D^0 decays with and without $D^0-\bar{D}^0$ mixing is parameterized by the phase $\phi_D=\arg(q/p)$: the SM expectation is $\mathcal{O}(10^{-3}-10^{-2})$, whereas in new physics scenarios it can be $\mathcal{O}(1)$. This is in contrast with direct CP violation, which occurs in Cabibbo suppressed decays such as $D\to\rho\pi$ at the 10^{-3} level in the SM: new physics scenarios are unlikely to change this expectation.

A time dependent asymmetry

$$\Gamma(D^0(t)-\bar{D}^0(t))\propto x\sin\phi_D\Gamma te^{-\Gamma t}$$

may be measured by comparing $D^0\to K^+\pi^-$ and $\bar{D}^0\to K^-\pi^+$ decays [134], and would (unlike CP-conserving mixing) be a clear signal of new physics. The corresponding asymmetry between

D^0 and $\bar{D^0}$ decay rates to K^+K^-, where the D^0 flavor is tagged by the pion from $D^{*+} \to D^0\pi^+$, allows an especially clean measurement since the final state is identical in both cases, and is only singly Cabibbo suppressed. The analysis of this mode is similar to that used for time dependent CP violation in B decay.

There are several classes of rare D decays where the large data samples available at high luminosity will allow improved measurements. Two body decay modes such as $D^0 \to \gamma\gamma, \mu^+\mu^-$ and $\mu^\pm e^\mp$ are strongly suppressed in the Standard Model: expectations are 10^{-8} for $D^0 \to \gamma\gamma$, 10^{-13} for $D^0 \to \mu^+\mu^-$ and 0 for $D^0 \to \mu e$. In new physics scenarios, the rates can be orders of magnitude larger [135]. For example, in both R-parity violating and leptoquark models, the branching fraction for $D^0 \to \mu^+\mu^-$ can be as large as 3×10^{-6} while that for $D^0 \to \mu^\pm e^\mp$ could be 5×10^{-7}. The current experimental bounds for $D^0 \to \mu^+\mu^-$ and $D^0 \to \mu^\pm e^\mp$ are 3.3×10^{-6} and 8.1×10^{-6}, respectively. For 3-body final states such as $\rho\ell^+\ell^-$, where SM expectations are similar, orders of magnitude enhancements are expected at low $\ell^+\ell^-$ invariant masses in some new physics models. In the case of radiative decays such as $D^0 \to K^*\gamma, \rho\gamma$, which are long-distance dominated, measurement at Super KEKB could constrain long-distance effects in the corresponding modes in the B sector.

By the time Super KEKB begins taking data, the tau-charm facility at Cornell will also be operating. Although the design luminosity is relatively low ($5 \times 10^{32}\,\mathrm{cm^2 s^{-1}}$), correlated D meson pairs are produced at threshold from the ψ'' resonance. For measurements where kinematic constraints from production at threshold are essential, such as f_D and D absolute branching fractions, the Cornell facility will remain competitive; and a sensitivity to $D^0 - \bar{D^0}$ mixing at the 10^{-4} level is claimed [132]. Super KEKB will have the advantage of precision vertexing for measurement of time-dependent decay distributions—especially important if CP violation is associated with mixing—and very large D meson samples. Other facilities in the world such as ATLAS/CMS/CDF/D0 cannot do charm physics. LHC-B and BTeV may record large charm data samples if they modify their trigger configurations, which are optimized for B physics. However, these experiments cannot efficiently reconstruct final states with neutrals or K_L mesons.

4.11.2 Electroweak physics

The standard-electro weak model has two fundamental parameters, which are directly related to measurable quantities: the parameter $\rho = M_W^2/(M_Z^2 \sin^2\Theta_W)$, which is unity in the standard model and the Weinberg angle Θ_W, which determines the relative contributions of electromagnetic and weak forces. Both parameters have been measured at the e^+e^- colliders PETRA and TRISTAN before the high precision measurements at the Z-Pole became available from LEP.

Recently a growing interest is being observed to revisit this type of physics and repeat $\sin^2\Theta_W$ and ρ measurements with high precision. There are two aspects to this renewed interest in a precision determination of the fundamental electro-weak parameters. One is related to a measurement of the NuTeV collaboration at Fermilab [136], who observe values of ρ and $\sin^2\Theta_W$, which are not in agreement with the standard model. The second motivation is that the scale dependence of gauge couplings has been observed for the strong coupling constant α_s and the electromagnetic coupling α, however, not yet for the coupling constant of the weak isospin group SU(2).

The quantity $\sin^2\Theta_W$ is related to the coupling parameters of two gauge groups, U(1) for the electromagnetic part and SU(2) for the weak isospin part of the standard electro weak model. Both couplings have a different scale dependence resulting in a scale dependence of a more

complicated nature for $\sin^2\Theta_W$ [137] as shown in Fig. 1. To test the scale dependence, data below the Z-pole with an accuracy of a few 10^{-4} will serve the purpose.

Two experiments are being proposed to measure $\sin^2\Theta_W$ at center of mass energies below 1 GeV, QWEAK at the Jefferson Lab in Virginia and one at SLAC, E-158. The QWEAK experiment will deduce $\sin^2\Theta_W$ from elastic scattering of polarised electrons off protons, while the SLAC experiment measures Moller scattering of polarised electrons.

The NuTeV Detector at Fermilab consists of an 18 m long, 690 ton active steel-scintillator target with drift chambers as tracking devices followed by an iron-toroid spectrometer. High purity ν_μ and $\overline{\nu_\mu}$ beams resulting from interactions of 800 GeV protons in a BeO target can be directed onto the detector.

In principle $\sin^2\Theta_W$ can be derived from a measurement of the ratio between neutral current (NC) and charged current interactions (CC) in a nuclear target for just one neutrino species. This aproach is, however, subject to large QCD corrections. The corrections can be minimized by a determination of the ratio R^- with

$$R^- = \frac{\sigma(\nu_\mu N \to \nu_\mu X) - \sigma(\overline{\nu_\mu} N \to \overline{\nu_\mu} X)}{\sigma(\nu_\mu N \to \mu^- X) - \sigma(\overline{\nu_\mu} N \to \mu^+ X)}$$

NuTeV obtains with this method $\sin^2\Theta_W = 0.2277 \pm 0.0013 \pm 0.0009$, a value which is 3σ above the value expected for the standard electro weak model. From a two parameter fit to ρ and $\sin^2\Theta_W$ they conclude that one of the quantities, but not both of them can be made to agree with the standard model value. Their result is sensitive to new physics in the W and Z sector and suggests a smaller left-handed NC coupling to light quarks than expected. But this result also depends on hadronic corrections and nuclear structure functions, which is the main criticism with respect to an interpretation in terms of deviations from the standard model.

In the electro-weak process $e^+e^- \to \mu^+\mu^-$ the values for $\sin^2\Theta_W$ and ρ are derived from a fit to the angular distribution (Θ^*) of μ pairs with respect to the axis of the incoming positron in the e^+e^- center of mass system [139].

$$\frac{d\sigma}{d\Omega} = \frac{\alpha^2}{4s}(C_1(1+\cos^2\Theta^*) + C_2\cos\Theta^*)$$

with the following definitions:

$$C_1 = 1 + 2v_e v_\mu \chi + (v_e^2 + a_e^2)(v_\mu^2 + a_\mu^2)\chi^2$$

$$C_2 = -4a_e a_\mu \chi + 8 v_e a_e a_\mu \chi^2$$

$$v_{e,\mu} = -1 + 4\sin^2\Theta_W \qquad a_{e,\mu} = -1$$

The quantity χ may be written in two different ways, as a function of $\sin^2\Theta_W$ or as a function of ρ

$$\chi = \frac{1}{16\sin^2\Theta_W\cos^2\Theta_W}\frac{s}{(s - M_Z^2)}$$

or

$$\chi = \frac{\rho G_F M_Z^2}{8\pi\alpha\sqrt{2}}\frac{s}{(s - M_Z^2)}$$

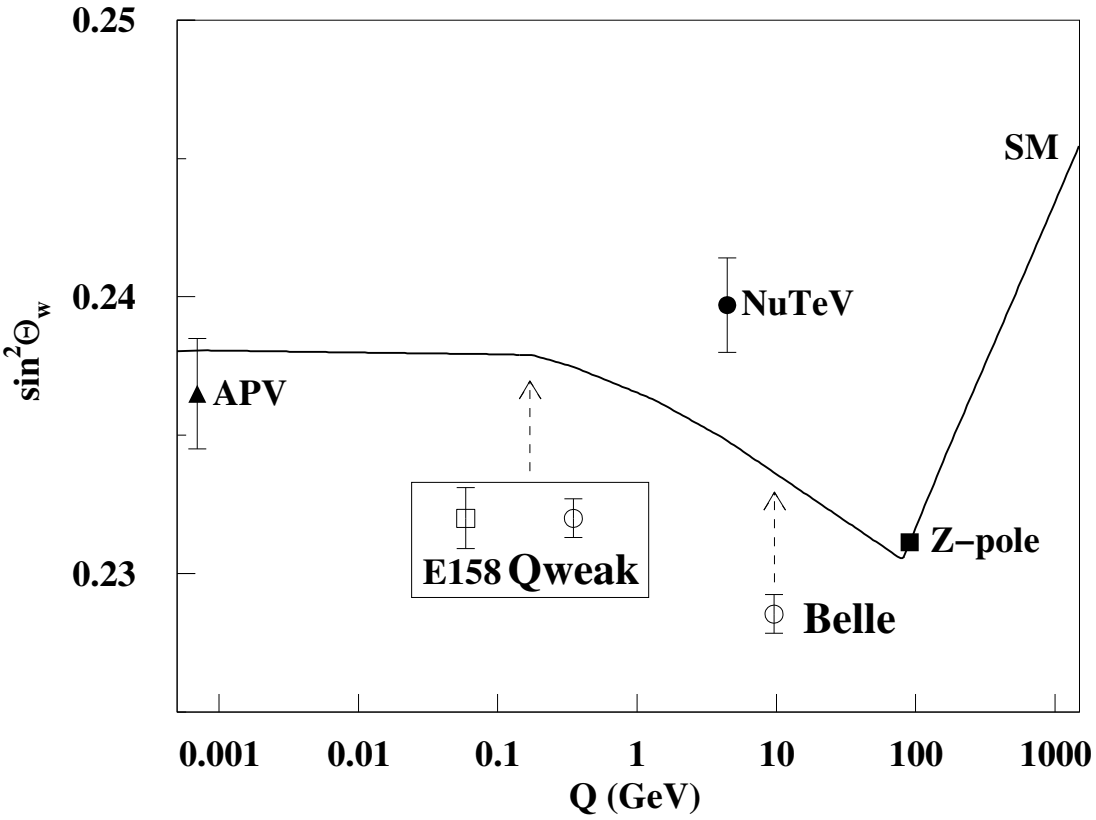

Figure 4.52: Scale dependence of $\sin^2\Theta_W$. The full symbols show the current situation, while the open symbols with error bars for the proposed experiments QWEAK, SLAC E-158 and Belle are placed at the correct cm energy with arbitrarily chosen vertical positions. The previous measurements are determinations from atomic parity violation (AVP) [138], deep inelastic neutrino scattering (NuTeV), and from Z-pole asymmetries (LEP/SLC).

where s is the square of the center of mass energy and $G_F = 1.17 \times 10^{-5}$ GeV^{-2} is the Fermi coupling constant.

For the purpose of estimating statistical errors and significance levels it is sufficient to consider the forward-backward charge asymmetry integrated over all angles, while in an actual experiment, one would fit the angular distribution.

$$A_{FB} = \frac{3C_2}{8C_1} = 1.5\chi$$

A guidline for estimating the significance of a measurement at $\sqrt{s} = 10$ GeV would be the capability of distinguishing the value of $\sin^2\Theta_W$ at the Z-pole from a value it would assume if it were running according to the predictions of the standard model.

With the Z-pole value of $\sin^2\Theta_W = 0.232$ the forward-backward asymmetry assumes a value of $A_{FB}(\sqrt{s} = 10\ GeV) = 6.34 \times 10^{-3}$.

For $\sin^2\Theta_W$ running according to the standard model, the asymmetry is $A_{FB}(\sqrt{s} = 10\ GeV) = 6.38 \times 10^{-3}$.

The charge asymmetries for a running and a constant coupling coupling constant thus differ by $\delta(A_{FB}) = 4 \times 10^{-5}$.

At 10 GeV center of mass energy, the statistical error on $\sin^2\Theta_W$ is 30 times larger than the error on the forward-backward asymmetry:

$$\sigma(\sin^2\Theta_W) = 30\ \sigma(A_{FB})$$

With a statistical error of $\sigma(A_{FB}) = \pm 1 \times 10^{-5}$ on the charge asymmetry the corresponding error on $\sin^2\Theta_W$ is $\sigma(\sin^2\Theta_W) = 3 \times 10^{-4}$.

The number of events required to achieve this accuracy is certainly smaller than 10^{10} events, because when fitting an angular distribution much more efficient use is being made of the experimental data and, thus for an accumulated luminosity of 1 ab^{-1} with 10^9 events a statistically significant measurement can be made, which is compatible with that of the two dedicated experiments as may be inferred from Fig.1.

The μ-pairs from the decay of the Υ(4S) will have a different asymmetry from those of the continuum, as with Υ as an intermediate state the Z-boson couples to b-quarks and the relative weight between γ and Z-exchange is altered with respect to the continuum. However the branching fraction of BR(Υ(4S)$\rightarrow \mu^+\mu^-$) $= 3 \times 10^{-5}$ is, however so small that corrections to the angular dependence will become less important and they can be calculated with sufficient accuracy, as all couplings and weak charges are known. The experiment is thus a continuum experiment.

Radiative corrections are small and can be calculated with sufficient accuracy. Also bin to bin migrations are expected to be small. A potential source of systematic errors are radiative returns of the Υ(1S) resonance. These events can be removed by a mass cut on the invariant two lepton mass.

The angular distribution of electron pairs is known with high accuracy and therefore electron pairs can be used to check the charge symmetry of the detector and other systematic errors like those, which may be related to the fact that the muon momenta in the forward and backward hemispheres are different due to the asymmetric energies of the colliding electron and positron beams.

Muon identification need not be very restrictive, because there are only very few reactions, which could fake muon pairs, if collinearity of the two tracks is requested. Tau pairs will be

rejected by collinearity cuts and invariant mass cuts, the cross section for pion pairs is too small to present a serious background and electron pairs are easily identified by their unique signature in the CsI crystals. As a first guess, a loosely identified muon track would be sufficient for one track, while the second collinear particle need not be identified as a muon, it should be compatible with a muon and incompatible with an electron.

The presence of SU(2) breaking forces could result in a different phonomenological pattern for reactions, where quarks are present or only leptons are involved. Leptoquarks as an example could alter the result of a $\sin^2\Theta_W$ measurement in neutrino-nucleon scattering without a measurable impact on the charge asymmetry of muon pairs in e^+e^- annihilation. Therefore one could imagine to face a situation, where purely leptonic experiments do agree with the standard model, while reactions involving nucleons don't. In this case one could extend the program at SuperKEKB to a determination of the charge asymmetry of jets. This is a very ambitious measurement, which needs extensive Mt. Carlo studies beforehand to investigate the feasebility of such an experiment.

The Super-KEKB will be capable of performing a statistically significant measurement of the Weinberg angle $\sin^2\Theta_W$ in order to prove the running of the U(1)/SU(2) couplings of the standard electroweak model and set limits on new weak isospin breaking interactions. In order to achieve this, data corresponding to about $1ab^{-1}$ are needed.

4.11.3 Charmonium physics

In the history of physics, many new and important insights have derived from detailed studies of "well understood" systems: precise measurements of the motion of planets in the solar system led to the discovery of an anomalous precession of the perihelion of Mercury's orbit, which provided an important impetus for General relativity; high resolution measurements of atomic spectra were the key to the discovery of fermion spin.

In hadronic physics, the most "well understood" systems are the quarkonium mesons, i.e, $c\bar{c}$ or $b\bar{b}$ mesons. Here, because the quarks are massive, they are nearly non-relativistic and ordinary quantum mechanics is applicable. Moreover, lattice calculations are particularly well suited to heavy quark systems. As these improve we can expect reliable first-principle calculations of quarkonium properties with good precision.

In B meson decays, the $b \to c\bar{c}s$ subprocess is CKM-favored and, thus, final states containing charmonium particles are common. A super-B factory would provide *superb* opportunities for precision, high sensitivity measurements of the charmonium system.

Even right at the $\Upsilon(4S)$ peak, the cross-section for the continuum production of $c\bar{c}$ quark pairs is higher than that for $b\bar{b}$ pairs. Thus, a "super-B" factory is also a "super-charm" factory that will support a variety of interesting studies of charmed particle and charmonium physics.

New results on charmonium from Belle/KEKB

There are still a few undiscovered charmonium states that are predicted to have masses below the relevant threshold for open charm production and are, thus, expected to be narrow. These include the $n = 1$ singlet P state, the h_c, and possibly the $n = 1$ singlet and triplet spin-2 D states, i.e. the 1^1D_{c2} and 1^3D_{c2}. The discovery of these states and the measurements of their properties is important for a number of reasons, including:

- Measurements of the masses of these states will pin down unknown parameters of the charmonium model, such as the strength of the fine and hyperfine terms in the inter-quark potential.

- The properties of these states are highly constrained by theory. Measured variances from theoretical predictions could indicate new and unexpected phenomena.

In Belle, modest efforts of studying charmonium production in B decays and continuum e^+e^- processes have produced interesting examples of both of these cases.

- The η_c' discovery
  In 2002, with a 42 fb^{-1} data sample, Belle discovered the η_c' via its $K_SK\pi$ decay mode in exclusive $B^- \to K^-K_SK\pi$ decays [140] (see Fig. 4.53). This observation was subsequently confirmed by other Belle measurements [141] as well as CLEO [142] and BaBar [143]. Although nobody ever doubted the existence of the η_c', it had evaded detection for nearly thirty years. A "candidate" η_c', reported by the Crystal Ball in 1982 [144], indicated an ψ'-η_c' mass splitting (92 ± 7 MeV) that is above the range of theoretical expectations ($43 \sim 75$ MeV) [145]. The Belle measurement of the η_c' mass indicates that mass splitting (32 ± 10 MeV) is, in fact, at the lower end of the theoretically preferred range and has helped pin down the strength of the hyperfine splitting terms in the charmonium potential.

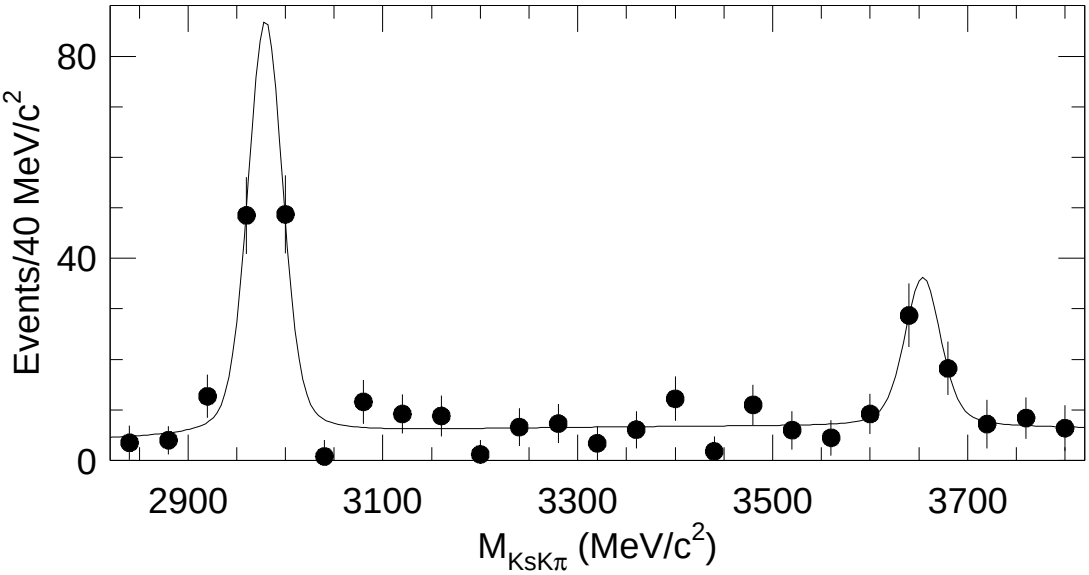

Figure 4.53: The $K_SK\pi$ invariant mass distribution for $B^- \to K^-K_SK\pi$ decays. The large peak near 2980 MeV is the η_c; the smaller peak near 3650 MeV is attributed to the η_c'.

- The $X(3872)$ discovery
  In 2003, with a nearly four-times larger data sample, Belle discovered a narrow charmonium-like $\pi^+\pi^-J/\psi$ state with a mass of 3872 MeV in exclusive $B \to K\pi\pi J/\psi$ decays [146] (see Fig. 4.54). This state, called the $X(3872)$, was originally considered to be the $^3D_{c2}$, however a closer examination of its properties indicated problems with this interpretation: the 3872 MeV mass is substantially above model expectations of ~ 3815 MeV; the decay rate to $\gamma\chi_{c1}$ is too small; the shape of the $M(\pi\pi)$ distribution is too peaked at high $\pi\pi$ masses; and the inferred exclusive branching ratio for $B \to K(^3D_{c2})$ is too large. As a result, a number of theorists have speculated that this particle may not be a $c\bar{c}$ charmonium state, but, instead, a new type of four-quark meson [147]. Either the standard charmonium model has to be modified, or the $X(3872)$ is a first example of an altogether new type of particle. More data will help sort this out.

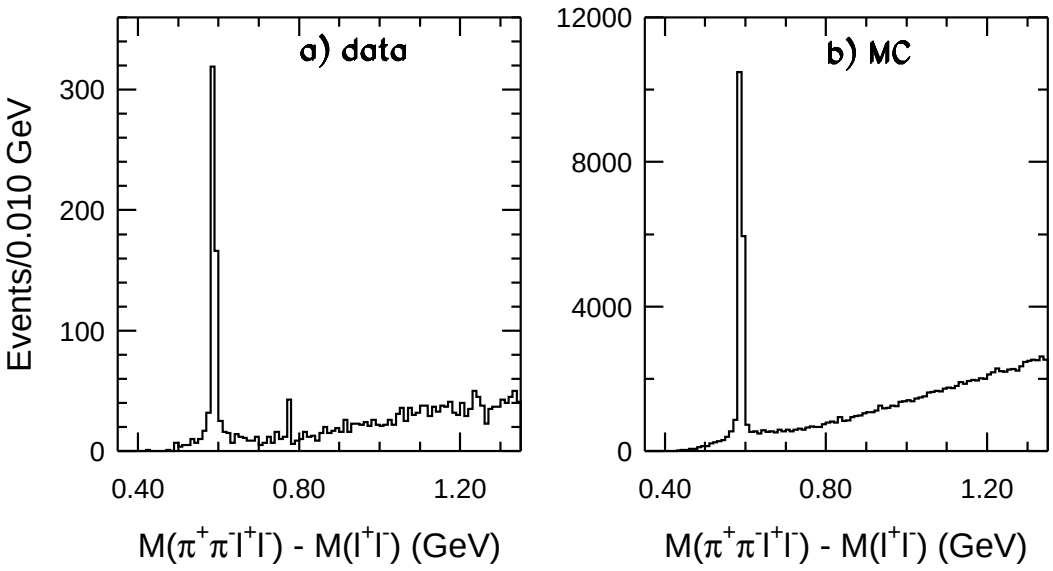

Figure 4.54: Distribution of $M(\pi^+\pi^-\ell^+\ell^-) - M(\ell^+\ell^-)$ for selected events in the ΔE-$M_{\rm bc}$ signal region for **(a)** Belle data and **(b)** generic $B\bar{B}$ MC events.

- The discovery of the large rate for the continuum process $e^+e^- \to c\bar{c}c\bar{c}$
  A major problem for QCD are calculations of the production of physical hadrons. This is because the long-range, low-q^2 processes that are involved, can not be dealt with perturbatively. Charmonium is an exception. Since charmonium is formed at relatively short distances, perturbation theory should be applicable. An elegant effective theory called Nonrelativistic QCD (NRQCD) has been developed to deal with various aspects of charmonium production [148]. In Belle, studies of J/ψ production in continuum e^+e^- annihilation processes were started as a way to test the predictions of NRQCD. This led to the remarkable, and totally unexpected discovery that continuum-produced J/ψs are almost always accompanied by another $c\bar{c}$ system; As can be seen in Fig. 4.55, the recoil system appears to be totally saturated by either other charmonium states such as η_c, χ_{c0} or η_c', or by pairs of charmed particles [141]. There is no evidence in the spectrum for low recoil masses that NRQCD predicts should dominate; the measured cross-sections for exclusive and inclusive $e^+e^- \to c\bar{c}c\bar{c}$ processes are an order-of-magnitude larger than NRQCD predictions. Theorists have not been able to modify the model to accommodate the Belle experimental results. NRQCD specialist Bodwin has said that explaining these results "either requires the invention of charmonium production mechanisms within the standard model that have not yet been recognized, or physics beyond the standard model" [149].

Strategies for a Super-B factory

These examples demonstrate that when data samples containing a significantly larger number of B mesons becomes available, we can reasonably expect that, as a bonus, charmonium studies might produce important new discoveries. As the $X(3872)$ and continuum $e^+e^- \to c\bar{c}c\bar{c}$ discoveries demonstrate, these could provide new insights into hadronic physics.

The e^+e^- environment is well suited for these investigations. The $X(3872) \to \pi^+\pi^- J/\psi$ has an especially distinct signature that makes it observable at hadron colliders [150]. However,

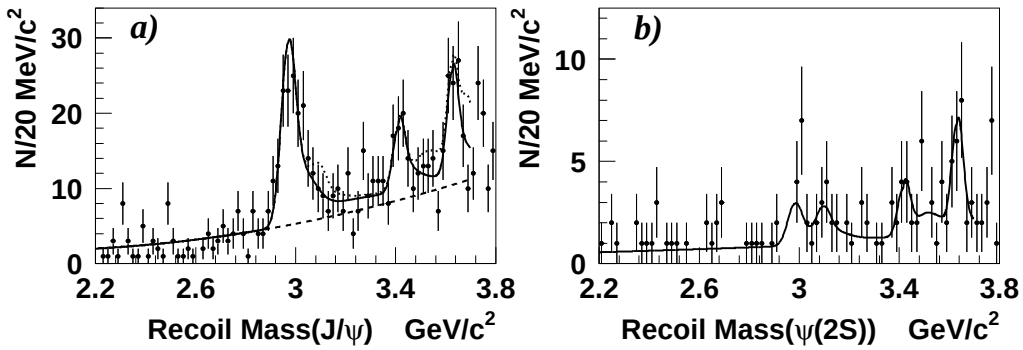

Figure 4.55: Distribution of recoil masses from inclusive **(a)** J/ψ and **(b)** $\psi(2S)$ mesons produced in continuum e^+e^- annihilation processes near $\sqrt{s} = 10.6$ GeV. The three peaks in the J/ψ recoil mass spectrum are the η_c, the χ_{c0} and the η_c'. There is no evidence for events with recoil masses below the η_c; there the observed level of events is consistent with background.

understanding the nature of the particle requires sensitivity to other, less distinct modes such as $\gamma\chi_{c1}$, and also $\pi^0\pi^0 J/\psi$, $\pi^+\pi^-\pi^0 J/\psi$ and $D^0\bar{D}^0\pi^0$ [151]; these are only accessible in the e^+e^- environment. Likewise, the recoil-mass technique that was used to discover $e^+e^- \to c\bar{c}c\bar{c}$ is also only possible in the e^+e^- environment.

- Search for the h_c
  The h_c has proven to be the most elusive of the low-lying charmonium states. A signal for an h_c candidate in E760 at Fermilab [152] was not reproduced in the subsequent experiment E835 [153]. The h_c is expected to decay predominantly into final states that include an η_c; these are experimentally not very distinct. Searches in B meson decays are also hampered by the fact that the exclusive decay process $B \to Kh_c$, which violates factorization, is expected to be small. Using a technique based on a suggestion by Suzuki [154], Belle is looking for the h_c via the $B \to Kh_c$: $h_c \to \gamma\eta_c$ decay chain. Here the hope is that the large expected decay branching ratio for $h_c \to \gamma\eta - c$ ($\sim 60\%$) might compensate for the small, factorization-suppressed rate for $B \to Kh_c$.

  So far, no signal is seen, but the branching ratio limit (of $\sim 1\times10^{-4}$) is not very restrictive. This is because of the low efficiency for reconstructing the η_c in low-background channels. Future searches at higher luminosity will improve this limit, but only by a factor that goes as the square-root of the increase in luminosity.

  The process process $e^+e^- \to \eta_c h_c$ is allowed by C-parity conservation. Thus, another approach for h_c searches would be to use experimentally distinct η_c decay final states, such as $p\bar{p}$ and $4K$ modes, to study states recoiling against continuum η_cs in $e^+e^- \to c\bar{c}c\bar{c}$ processes. Since the useful η_c modes have branching fractions ($\sim 10^{-3}$) that are $\sim 10^{-2}$ smaller than those for the J/ψ this method will require a large data sample. If we assume that the $\sigma(e^+e^- \to \eta_c h_c) \simeq \sigma(e^+e^- \to J/\psi\chi_{c0})$, about 10 ab^{-1} of data would be needed to uncover the h_c by this method.

- Search for the $^3D_{c2}$
  Since it looks more-and-more unlikely that the $X(3872)$ is the $^3D_{c2}$, the discovery of the

$^3D_{c2}$ remains an open experimental question. Since the exclusive decay $B \to K^3D_{c2}$ is expected to by strongly suppressed by factorization, here also searches in exclusive decays are not promising. Since the $\gamma\chi_{c1}$ and $\pi^+\pi^- J/\psi$ modes are expected to be strong and are experimentally distinct, inclusive searches are feasible. (Belle has reported a strong signal for the inclusive process $B \to \chi_{c2}X$ [155], even though no evidence has been seen for it in exclusive two-body decays.)

Summary

A super-B factory will provide opportunities for unprecendented studies of the properties of charmonium systems and to search for the missing charmonium states. These measurements will provide stringient tests of hadronic models where they are supposed to be most reliable.

Taking history as our guide, we are confident that new and surprising discoveries will be made.

Observable	Belle 2003	SuperKEKB		LHCb
	(0.14ab^{-1})	($5\ \text{ab}^{-1}$)	($50\ \text{ab}^{-1}$)	(0.002ab^{-1})
$\Delta\mathcal{S}_{\phi K^0_S}$	0.51	0.079	0.031	0.2 [156]
$\Delta\mathcal{S}_{K^+K^-K^0_S}$	$^{+0.32}_{-0.26}$	0.056	0.026	
$\Delta\mathcal{S}_{\eta' K^0_S}$	0.27	0.049	0.024	$\times$
$\Delta\mathcal{S}_{K^0_S K^0_S K^0_S}$	NA	0.14	0.04	$\times$
$\Delta\mathcal{S}_{\pi^0 K^0_S}$	NA	0.10	0.03	$\times$
$\sin 2\chi$ ($B_s \to J/\psi\phi$)	$\times$	$\times$	$\times$	0.058
$\mathcal{S}_{K^{*0}\gamma}$	NA	0.14	0.04	$\times$
$\mathcal{B}(B \to X_s\gamma)$	26% ($5.8\ \text{fb}^{-1}$)	5%	5%	$\times$
$A_{CP}(B \to X_s\gamma)$	0.064	0.011	5×10^{-3}	$\times$
C_9 from $\overline{A}_{\rm FB}(B \to K^*\ell^+\ell^-)$	NA	32%	10%	
C_{10} from $\overline{A}_{\rm FB}(B \to K^*\ell^+\ell^-)$	NA	44%	14%	
$\mathcal{B}(B_s \to \mu^+\mu^-)$	$\times$	$\times$	$\times$	4σ (3 years) [158]
$\mathcal{B}(B^+ \to K^+\nu\nu)$	NA		5.1σ	$\times$
$\mathcal{B}(B^+ \to D\tau\nu)$	NA	12.7σ	40.3σ	$\times$
$\mathcal{B}(B^0 \to D\tau\nu)$	NA	3.5σ	11.0σ	$\times$
$\sin 2\phi_1$	0.06	0.019	0.014	0.022
ϕ_2 ($\pi\pi$ isospin)	NA	3.9°	1.2°	$\times$
ϕ_2 ($\rho\pi$)	NA	2.9°	0.9°	$\times$
ϕ_3 ($DK^{(*)}$)	20°	4°	1.2°	8°
ϕ_3 ($B_s \to KK$)	$\times$	$\times$	$\times$	5°
ϕ_3 ($B_s \to D_sK$)	$\times$	$\times$	$\times$	14°
$\lvert V_{ub}\rvert$ (inclusive)	16%	5.8%	4.4%	$\times$
$\mathcal{B}(\tau \to \mu\gamma)$	$< 3.1 \times 10^{-7}$	$< 1.8 \times 10^{-8}$		
$\mathcal{B}(\tau \to \mu(e)\eta)$	$< 3.4(6.9) \times 10^{-7}$	$< 5 \times 10^{-9}$		
$\mathcal{B}(\tau \to \ell\ell\ell)$	$< 1.4\text{-}3.1\times10^{-7}$	$< 5 \times 10^{-9}$		

Table 4.22: Summary of sensitivity studies. Values for LHCb are taken from [157] unless otherwise stated.

4.12 Summary

Table 4.22 summarizes the sensitivities for some of key observables described in the previous sections. As a comparison, we also list expected sensitivities at LHCb whenever available. It is seen that most of key observables are accessible only at the e^+e^- B factories. The advantage of the clean environment at SuperKEKB is thus clear. Note that the B physics program at hadron colliders has its own unique measurements that are not accessible at e^+e^- B factories. Examples include rare B_s decays such as $B_s \to \mu^+\mu^-$. Thus B physics programs at hadron colliders also help scrutinize the rich phenomenologies of B meson decays.

References

[1] A. B. Carter and A. I. Sanda, Phys. Rev. D **23**, 1567 (1981); I. I. Bigi and A. I. Sanda, Nucl. Phys. **B193**, 85 (1981).

[2] Belle Collaboration, K. Abe *et al.*, Phys. Rev. D **66**, 071102 (2002).

[3] H. Tajima *et al.*, hep-ex/0301026.

[4] T. Matsumoto, "Tagging with fully reconstructed B's in B-factory experiments," ACAT03 conference, Dec. 1-5, 2003, KEK, Japan.

[5] BaBar Collaboration, "Measurement of the Inclusive Charmless Semileptonic Branching Ratio of B Mesons and Determination of $|V_{ub}|$," Submitted to Phys. Rev. Lett. [arXiv:hep-ex/0307062]

[6] del Re, Daniele, "Measurement of V_{ub} studying inclusive semileptonic decays on the recoil of fully reconstructed B's with the BaBar experiment Ph.D. thesis, Dec. 5, 2002.

[7] A. Sugiyama, "$B \to X_u l\nu$ measurement using the pseudo full reconstruction of $\Upsilon(4s)$ at BELLE," Belle Note No. 509.

[8] BaBar Collaboration, "A Search for $B^+ \to K^+\nu\bar{\nu}$," [arXiv:hep-ex/0207069]

[9] BaBar Collaboration, "A Search for $B^+ \to \tau^+\nu_\tau$ Recoiling Against $B^- \to D^0 l^- \bar{\nu}_l X$", [arXiv:hep-ex/0303034]

[10] For a recent review, see Y. Nir, hep-ph/0208080.

[11] T. Moroi, Phys. Lett. B **493**, 366 (2000); S. Baek, T. Goto, Y. Okada and K. Okumura, Phys. Rev. D **63**, 051701, 2001; D. Chang, A. Masiero and H. Murayama, hep-ph/0205111.

[12] For a recent review, see W. Bernreuther, hep-ph/0205279.

[13] Y. Grossman and M. P. Worah, Phys. Lett. B **395**, 241 (1997);

[14] A. B. Carter and A. I. Sanda, Phys. Rev. D **23**, 1567 (1981); I. I. Bigi and A. I. Sanda, Nucl. Phys. **B193**, 85 (1981).

[15] Belle Collaboration, K. Abe *et al.*, Phys. Rev. D **67**, 031102 (2003); Belle Collaboration, K. Abe *et al.*, Phys. Rev. Lett. **91**, 261602 (2003).

[16] BaBar Collaboration, H. Monchenault, talk given at 2003 Rencontres de Moriond; Babar Collaboration, results given by T. Browder at the XXI International Symposium on Lepton and Photon Interactions at High Energies, Aug.11-16, 2003, Fermilab, Illinois, U.S.A. w

[17] Heavy Flavor Averaging Group, http://www.slac.stanford.edu/xorg/hfag/.

[18] T. E. Browder, `hep-ex/0312024`; B. Aubert *et al.* (BaBar Collaboration), BABAR-PLOT-0053; A. Farbin (BaBar Collaboration), poster presented at Lepton Photon 2003.

[19] T. Gershon and M. Hazumi, hep-ex/0402097.

[20] A. Garmash, *et al.* (Belle Collaboration), `hep-ex/0307082`, to appear in Phys. Rev. D.

[21] M. Ciuchini *et al.*, Phys. Rev. Lett. **79**, 978 (1997).

[22] Y. Chao, K. Suzuki, Y. Unno *et al.* (Belle Collaboration), hep-ex/0311061, to appear in Phys. Rev. D.

[23] M. Hazumi, Phys. Lett. B **583**, 285 (2004).

[24] Particle Data Group, K. Hagiwara *et al.*, Phys. Rev. D **66**, 010001 (2002).

[25] Belle Collaboration, F. Fang, T. Hojo *et al.*, Phys. Rev. Lett. **90**, 071801 (2003).

[26] Belle Collaboration, H.-C. Huang *et al.*, Phys. Rev. Lett. **91**, 241802 (2003).

[27] N. G. Deshpande and J. Trampetic, Phys. Lett. B **339**, 270 (1994); M. Gourdin, Y. Y. Keum and X. Y. Pham, Phys. Rev. D **51**, 3510 (1995); M. R. Ahmady and E. Kou, Eur. Phys. J. C **1**, 243 (1998).

[28] G. Eilam, M. Gronau and R. R. Mendel, Phys. Rev. Lett. **74**, 4984 (1995).

[29] In this study we take $M = 2980$ MeV/c^2 and $\Gamma = 29$ MeV, which are the values from the recent measurements by the Belle collaboration [25].

[30] A. Abashian *et al.* (Belle Collab.), Nucl. Instr. and Meth. A **479**, 117 (2002).

[31] Belle Collaboration, J. Kaneko *et al.*, Phys. Rev. Lett. **90**, 021801 (2003).

[32] Y. Grossman, G. Isidori and M. P. Worah, Phys. Rev. D **58** 057504 (1998).

[33] D. London and A. Soni, Phys. Lett. B **407**, 61 (1997).

[34] Y. Grossman, Z. Ligeti, Y. Nir and H. Quinn, Phys. Rev. D **68**, 015004 (2003).

[35] H. M. Asatrian, K. Bieri, C. Greub and A. Hovhannisyan, "NNLL corrections to the angular distribution and to the forward-backward asymmetries in $b \to X_s l^+ l^-$," Phys. Rev. D **66**, 094013 (2002) [arXiv:hep-ph/0209006].

[36] A. Ali, G. Hiller, L. T. Handoko and T. Morozumi, "Power corrections in the decay rate and distributions in $B \to X_s l^+ l^-$ in the standard model," Phys. Rev. D **55**, 4105 (1997) [arXiv:hep-ph/9609449].

[37] C. S. Lim, T. Morozumi and A. I. Sanda, "A Prediction For $d\Gamma(B \to s l\bar{l})/dQ^2$ Including The Long Distance Effects," Phys. Lett. B **218**, 343 (1989).

[38] S. Fukae, C. S. Kim, T. Morozumi and T. Yoshikawa, "A model independent analysis of the rare B decay $B \to X_s l^+ l^-$," Phys. Rev. D **59**, 074013 (1999) [arXiv:hep-ph/9807254].

[39] G. Hiller and F. Kruger, "More model-independent analysis of $b \to s$ processes," arXiv:hep-ph/0310219.

[40] Y. Wang and D. Atwood, "Rate difference between $b \to s\mu^+\mu^-$ and $b \to se^+e^-$ in SUSY with large $\tan\beta$," Phys. Rev. D **68**, 094016 (2003) [arXiv:hep-ph/0304248].

[41] C. S. Kim, Y. G. Kim, C. D. Lu and T. Morozumi, "Azimuthal angle distribution in $B \to K^*(\to K\pi) l^+ l^-$ at low invariant $m_{l^+l^-}$ region," Phys. Rev. D **62**, 034013 (2000) [arXiv:hep-ph/0001151].

[42] T. Hurth, E. Lunghi and W. Porod, "Untagged $B \to X_s\gamma$ CP asymmetry as a probe for new physics," arXiv:hep-ph/0312260.

[43] L. T. Handoko and T. Morozumi, "$b \to s(d)\gamma$ with a vector - like quark as fourth generation," Mod. Phys. Lett. A **10**, 309 (1995) [Erratum-ibid. A **10**, 1733 (1995)] [arXiv:hep-ph/9409240].

[44] G. Buchalla and A. J. Buras, "QCD corrections to rare K and B decays for arbitrary top quark mass," Nucl. Phys. B **400**, 225 (1993).

[45] Y. Grossman, Z. Ligeti and E. Nardi, "First limit on inclusive $B \to X_s\nu\bar{\nu}$ decay and constraints on new physics," Nucl. Phys. B **465**, 369 (1996) [Erratum-ibid. B **480**, 753 (1996)] [arXiv:hep-ph/9510378].

[46] P. Colangelo, F. De Fazio, P. Santorelli and E. Scrimieri, "Rare $B \to K^{(*)}\nu\bar{\nu}$ decays at B factories," Phys. Lett. B **395**, 339 (1997) [arXiv:hep-ph/9610297].

[47] R. Barate *et al.* [ALEPH Collaboration], "Measurements of $BR(b \to \tau^-\bar{\nu}_\tau X)$ and $BR(b \to \tau - \bar{\nu}_\tau D^{*\pm} X)$ and upper limits on $BR(B^- \to \tau^-\bar{\nu}_\tau)$ and $BR(b \to s\nu\bar{n}u)$," Eur. Phys. J. C **19**, 213 (2001) [arXiv:hep-ex/0010022].

[48] T. E. Browder *et al.* [CLEO Collaboration], Phys. Rev. Lett. **86**, 2950 (2001) [arXiv:hep-ex/0007057].

[49] B. Aubert *et al.* [BABAR Collaboration], "A Search for the decay $B^- \to K^-\nu\bar{\nu}$," arXiv:hep-ex/0304020.

[50] W. S. Hou, Phys. Rev. D **48**, 2342 (1993)

[51] A. G. Akeroyd and S. Recksiegel, J. Phys. G **29**, 2311 (2003)

[52] D. Guetta and E. Nardi, Phys. Rev. D **58**, 012001 (1998) S. Baek and Y. G. Kim, Phys. Rev. D **60**, 077701 (1999) A. G. Akeroyd and S. Recksiegel, Phys. Lett. B **541**, 121 (2002)

[53] M. Tanaka, Z. Phys. C**67**, 321 (1995).

[54] I. Caprini, L. Lellouch and M. Neubert, Nucl. Phys. B **530**, 153 (1998).

[55] K. Abe *et al.* [Belle Collaboration], BELLE-CONF-0121 (2001).

[56] Charge conjugate modes are implicitly included throughout this report.

[57] K. Hagiwara *et al.*, Phys. Rev. D**66**, 010001 (2002).

[58] Throughout this report, the symbol ℓ indicates leptons except τ unless otherwise specified .

[59] O. Long, M. Baak, R. N. Cahn and D. Kirkby, Phys. Rev. D **68**, 034010 (2003).

[60] M. Gronau and D. London, "Isospin Analysis Of CP Asymmetries In B Decays," Phys. Rev. Lett. **65**, 3381 (1990).

[61] A. E. Snyder and H. R. Quinn, "Measuring CP asymmetry in $B \to \rho\pi$ decays without ambiguities," Phys. Rev. D **48**, 2139 (1993).

[62] K. Abe *et al.* [Belle Collaboration], "Evidence for CP-violating asymmetries $B^0 \to \pi^+\pi^-$ decays and constraints on the CKM angle ϕ_2," Phys. Rev. D **68**, 012001 (2003) [arXiv:hep-ex/0301032].

[63] B. Aubert *et al.* [BABAR Collaboration], "Measurements of branching fractions and CP-violating asymmetries in $B0 \to \pi^+\pi^-$, $K^+\pi^-$, K^+K^- decays. ((B))," Phys. Rev. Lett. **89**, 281802 (2002) [arXiv:hep-ex/0207055].

[64] M. Beneke, G. Buchalla, M. Neubert and C. T. Sachrajda, "QCD factorization in $B \to \pi K$, $\pi\pi$ decays and extraction of Wolfenstein parameters," Nucl. Phys. B **606**, 245 (2001) [arXiv:hep-ph/0104110].

[65] Y. Y. Keum and A. I. Sanda, "Possible large direct CP violations in charmless B decays: Summary report on the pQCD method. ((U))," Phys. Rev. D **67**, 054009 (2003) [arXiv:hep-ph/0209014]; Y.-Y. Keum, private communication.

[66] The CKMfitter site on the web: http://ckmfitter.in2p3.fr/.

[67] Y.-Y. Keum, private communication.

[68] B. Aubert *et al.* [BABAR Collaboration], "Measurements of branching fractions and CP-violating asymmetries in $B0 \to \rho^\pm h^\mp$ decays," Phys. Rev. Lett. **91**, 201802 (2003) [arXiv:hep-ex/0306030].

[69] H. J. Lipkin, Y. Nir, H. R. Quinn and A. Snyder, "Penguin trapping with isospin analysis and CP asymmetries in B decays," Phys. Rev. D **44**, 1454 (1991).

[70] J. Stark, "$B0 \to \pi^+\pi^-\pi^0$ feasibility studies," eConf **C0304052**, WG423 (2003) [arXiv:hep-ph/0307032].

[71] M. Gronau and D. London., "How To Determine All The Angles Of The Unitarity Triangle From $B^0_d \to DK_S$ And $B^0_s \to D^0$," Phys. Lett. B **253**, 483 (1991).

[72] M. Gronau and D. Wyler, "On determining a weak phase from CP asymmetries in charged B decays," Phys. Lett. B **265**, 172 (1991).

[73] D. Atwood, I. Dunietz and A. Soni, "Enhanced CP violation with $B \to KD^0(\bar{D}^0)$ modes and extraction of the CKM angle γ," Phys. Rev. Lett. **78**, 3257 (1997) [arXiv:hep-ph/9612433].

[74] D. Atwood, I. Dunietz and A. Soni, "Improved methods for observing CP violation in $B^\pm \to KD$ and measuring the CKM phase γ," Phys. Rev. D **63**, 036005 (2001) [arXiv:hep-ph/0008090].

[75] A. Giri, Y. Grossman, A. Soffer and J. Zupan, "Determining γ using $B^\pm \to DK^\pm$ with multibody D decays," Phys. Rev. D **68**, 054018 (2003) [arXiv:hep-ph/0303187].

[76] H. Muramatsu *et al.* [CLEO Collaboration], "Dalitz analysis of $D^0 \to K^0_S\pi^+\pi^-$. ((B))," Phys. Rev. Lett. **89**, 251802 (2002) [Erratum-ibid. **90**, 059901 (2003)] [arXiv:hep-ex/0207067].

[77] K. Abe *et al.* [Belle Collaboration], "Measurement of the angle ϕ_3 with Dalitz analysis of three-body D^0 decay from $B \to D^0K$ process," arXiv:hep-ex/0308043.

[78] K. Hagiwara *et al.* [Particle Data Group Collaboration], "Review Of Particle Physics," Phys. Rev. D **66**, 010001 (2002).

[79] M. Neubert, "QCD based interpretation of the lepton spectrum in inclusive $\bar{B} \to X_u l \bar{\nu}$ decays," Phys. Rev. D **49**, 3392 (1994) [arXiv:hep-ph/9311325].

[80] T. Mannel and M. Neubert, "Resummation of nonperturbative corrections to the lepton spectrum in inclusive $B \to X l \bar{\nu}$ decays," Phys. Rev. D **50**, 2037 (1994) [arXiv:hep-ph/9402288].

[81] I. I. Y. Bigi, M. A. Shifman, N. G. Uraltsev and A. I. Vainshtein, "On the motion of heavy quarks inside hadrons: Universal distributions and inclusive decays," Int. J. Mod. Phys. A **9**, 2467 (1994) [arXiv:hep-ph/9312359].

[82] M. Neubert, "Analysis of the photon spectrum in inclusive $B \to X_s \gamma$ decays," Phys. Rev. D **49**, 4623 (1994) [arXiv:hep-ph/9312311].

[83] A. K. Leibovich, I. Low and I. Z. Rothstein, "Extracting V_{ub} without recourse to structure functions," Phys. Rev. D **61**, 053006 (2000) [arXiv:hep-ph/9909404].

[84] M. Neubert, "Note on the extraction of $|V_{ub}|$ using radiative B decays," Phys. Lett. B **513**, 88 (2001) [arXiv:hep-ph/0104280].

[85] C. W. Bauer, M. E. Luke and T. Mannel, "Light-cone distribution functions for B decays at subleading order in $1/m_b$," Phys. Rev. D **68**, 094001 (2003) [arXiv:hep-ph/0102089].

[86] C. W. Bauer, M. Luke and T. Mannel, "Subleading shape functions in $B \to X_u l n \bar{u}$ and the determination of $|V_{ub}|$," Phys. Lett. B **543**, 261 (2002) [arXiv:hep-ph/0205150].

[87] A. K. Leibovich, Z. Ligeti and M. B. Wise, "Enhanced subleading structure functions in semileptonic B decay," Phys. Lett. B **539**, 242 (2002) [arXiv:hep-ph/0205148].

[88] M. Neubert, "Subleading shape functions and the determination of $|V_{ub}|$," Phys. Lett. B **543**, 269 (2002) [arXiv:hep-ph/0207002].

[89] I. I. Y. Bigi and N. G. Uraltsev, "Weak annihilation and the endpoint spectrum in semileptonic B decays," Nucl. Phys. B **423**, 33 (1994) [arXiv:hep-ph/9310285].

[90] M. B. Voloshin, "Nonfactorization effects in heavy mesons and determination of $|V_{ub}|$ from inclusive semileptonic B decays," Phys. Lett. B **515**, 74 (2001) [arXiv:hep-ph/0106040].

[91] A. F. Falk, Z. Ligeti and M. B. Wise, "V_{ub} from the hadronic invariant mass spectrum in semileptonic B decay," Phys. Lett. B **406**, 225 (1997) [arXiv:hep-ph/9705235].

[92] R. D. Dikeman and N. G. Uraltsev, "Key distributions for charmless semileptonic B decay," Nucl. Phys. B **509**, 378 (1998) [arXiv:hep-ph/9703437].

[93] I. I. Y. Bigi, R. D. Dikeman and N. Uraltsev, "The hadronic recoil mass spectrum in semileptonic B decays and extracting $|V_{ub}|$ in a model-insensitive way," Eur. Phys. J. C **4**, 453 (1998) [arXiv:hep-ph/9706520].

[94] A. K. Leibovich, I. Low and I. Z. Rothstein, "On the resummed hadronic spectra of inclusive B decays," Phys. Rev. D **62**, 014010 (2000) [arXiv:hep-ph/0001028].

[95] A. K. Leibovich, I. Low and I. Z. Rothstein, "Extracting $|V_{ub}|$ from the hadronic mass spectrum of inclusive B decays," Phys. Lett. B **486**, 86 (2000) [arXiv:hep-ph/0005124].

[96] C. W. Bauer, Z. Ligeti and M. E. Luke, "A model independent determination of $|V_{ub}|$," Phys. Lett. B **479**, 395 (2000) [arXiv:hep-ph/0002161].

[97] M. Neubert, "On the inclusive determination of $|V_{ub}|$ from the lepton invariant mass spectrum," JHEP **0007**, 022 (2000) [arXiv:hep-ph/0006068].

[98] C. W. Bauer, Z. Ligeti and M. E. Luke, "Precision determination of $|V_{ub}|$ from inclusive decays," Phys. Rev. D **64**, 113004 (2001) [arXiv:hep-ph/0107074].

[99] G. Burdman, Z. Ligeti, M. Neubert and Y. Nir, "The Decay $B \to \pi l \nu$ in heavy quark effective theory," Phys. Rev. D **49**, 2331 (1994) [arXiv:hep-ph/9309272].

[100] K. C. Bowler *et al.* [UKQCD Collaboration], "Improved $B \to \pi l \nu_l$ form factors from the lattice," Phys. Lett. B **486**, 111 (2000) [arXiv:hep-lat/9911011].

[101] A. Abada, D. Becirevic, P. Boucaud, J. P. Leroy, V. Lubicz and F. Mescia, "Heavy $\to$ light semileptonic decays of pseudoscalar mesons from lattice QCD," Nucl. Phys. B **619**, 565 (2001) [arXiv:hep-lat/0011065].

[102] A. X. El-Khadra, A. S. Kronfeld, P. B. Mackenzie, S. M. Ryan and J. N. Simone, "The semileptonic decays $B \to \pi l \nu$ and $D \to \pi l \nu$ from lattice QCD," Phys. Rev. D **64**, 014502 (2001) [arXiv:hep-ph/0101023].

[103] S. Aoki *et al.* [JLQCD Collaboration], "Differential decay rate of $B \to \pi l \nu$ semileptonic decay with lattice NRQCD," Phys. Rev. D **64**, 114505 (2001) [arXiv:hep-lat/0106024].

[104] J. Shigemitsu, S. Collins, C. T. H. Davies, J. Hein, R. R. Horgan and G. P. Lepage, "Semileptonic B decays from an NRQCD/D234 action," Phys. Rev. D **66**, 074506 (2002) [arXiv:hep-lat/0207011].

[105] S. Aoki *et al.* [JLQCD Collaboration], "Light hadron spectroscopy with two flavors of $O(a)$-improved dynamical quarks," Phys. Rev. D **68**, 054502 (2003) [arXiv:hep-lat/0212039].

[106] C. T. H. Davies *et al.* [HPQCD Collaboration], "High-precision lattice QCD confronts experiment," Phys. Rev. Lett. **92**, 022001 (2004) [arXiv:hep-lat/0304004].

[107] L. Lellouch, "Lattice-Constrained Unitarity Bounds for $\bar{B}^0 \to \pi^+ \ell^- \bar{\nu}_\ell$ Decays," Nucl. Phys. B **479**, 353 (1996) [arXiv:hep-ph/9509358].

[108] K. C. Bowler, J. F. Gill, C. M. Maynard and J. M. Flynn, "$B \to \rho l \nu$ form factors in lattice QCD," arXiv:hep-lat/0402023.

[109] A. Abada, D. Becirevic, P. Boucaud, . M. Flynn, . P. Leroy, V. Lubicz and F. Mescia [SPQcdR collaboration], "Heavy to light vector meson semileptonic decays," Nucl. Phys. Proc. Suppl. **119**, 625 (2003) [arXiv:hep-lat/0209116].

[110] B. Aubert *et al.* [BABAR Collaboration], "Measurement of the inclusive charmless semileptonic branching ratio of B mesons and determination of $|V_{ub}|$," Phys. Rev. Lett. **92**, 071802 (2004) [arXiv:hep-ex/0307062].

[111] H. Kakuno *et al.* [BELLE Collaboration], "Measurement of $|V_{ub}|$ using inclusive $B \to X_u l\nu$ decays with a novel X/u reconstruction method," arXiv:hep-ex/0311048.

[112] C. W. Bauer, Z. Ligeti, M. Luke and A. V. Manohar, "B decay shape variables and the precision determination of $|V_{cb}|$ and m_b," Phys. Rev. D **67**, 054012 (2003) [arXiv:hep-ph/0210027].

[113] J. P. Alexander *et al.* [CLEO Collaboration], "First measurement of the $B \to \pi l\nu$ and $B \to \rho(\omega) l\nu$ branching fractions," Phys. Rev. Lett. **77**, 5000 (1996).

[114] B. H. Behrens *et al.* [CLEO Collaboration], "Measurement of $B \to \rho l\nu$ decay and $|V_{ub}|$," Phys. Rev. D **61**, 052001 (2000) [arXiv:hep-ex/9905056].

[115] B. Aubert *et al.* [BABAR Collaboration], "Measurement of the CKM matrix element $|V_{ub}|$ with $B \to \rho e\nu$ decays. ((B))," Phys. Rev. Lett. **90**, 181801 (2003) [arXiv:hep-ex/0301001].

[116] S. B. Athar *et al.* [CLEO Collaboration], Phys. Rev. D **68**, 072003 (2003) [arXiv:hep-ex/0304019].

[117] C. Schwanda [BELLE Collaboration], "Evidence for $B^+ \to \omega l^+\nu$," eConf **C0304052**, WG116 (2003) [arXiv:hep-ex/0306059].

[118] K. Abe *et al.* [Belle Collaboration], "Evidence for $B^+ \to \omega l^+\nu$," arXiv:hep-ex/0307075.

[119] A. Sugiyama [BELLE Collaboration], "Measurements of $|V_{ub}|$ at BELLE," arXiv:hep-ex/0306020.

[120] Belle Collaboration, K. Inami *et al.*,"An upper bound on the decay $\tau \to \mu\gamma$ from Belle", hep-ex/0310029, submitted to PRL.

[121] Belle Collaboration, Y. Enari," Search for the lepton-flavor-violating $\tau^- \to \mu^-\eta$ decay at Belle", Contributed paper for 2003 summer conference, BELLE-CONF-0330.

[122] Y. Yusa, "Search for neutrinoless decays $\tau \to 3l$ ", Nucl. Phys. B(Proc. Suppl.) **123**, 95 (2003).

[123] K. Hagiwara *et al.*, Phys. Rev. D**66**, 010001 (2002), LEP Higgs Working Group, http://lephiggs.web.cern/LEPHIGGS/papers/Note2001-04.

[124] T. Affolder *et al.*, CDF Collaboration, Phys. Rev. Lett. **86**, 4472 (2001).

[125] Y. Grossman, J. R. Peláez, M. P. Worah, Phys. Rev. D **58**, 096009 (1998).

[126] I. Dunietz, Eur. Phys. J. C **7**, 197 (1999).

[127] A. F. Falk and A. A. Petrov, Phys. Rev. Lett. **85**, 252 (2000).

[128] A. Falk *et al.*, [arXiv:hep-ph/0110317].

[129] R. Godang *et al.*, Phys. Rev. Lett. **84**, 5038 (2000), [arXiv:hep-ex/0001060].

[130] S. Bergmann *et al.*, Phys. Lett. B **486**, 418 (2000), [arXiv: hep-ph/0005181].

[131] G. Blaylock et al., Phys. Lett. B **355**, 555 (1995), [arXiv:hep-ph/9504306].

[132] M. Gronau, Y. Grossman and J. Rosner, Phys. Lett. B **508**, 37 (2001), [arXiv:hep-ph/0103110].

[133] E. Golowich and S. Pakvasa, Phys. Lett. B **505**, 94 (2001),[arXiv:hep-ph/0102068].

[134] L. Wolfenstein, Phys. Rev. Lett. **75**, 2460 (1995), [arXiv:hep-ph/9505285].

[135] G. Burdman, E. Golowich, J. Hewett and S. Pakvasa, [arXiv:hep-ph0112235].

[136] G.P. Zeller et al., hep-ex/0110059 v3 March 2003 and PRL 88 (2002) 091802

[137] M.J. Ramsey-Musof, Phys. Rev. C60 (1999) 015501

[138] C.S. Wood et al., Science 275 (1997) 1759

[139] W. Bartel et.al., Z.Phys. C43 (1989), 607
R.Marshall, Z. Phys. C43 (1989), 607 (Review article)

[140] S.K. Choi *et al.* (Belle Collaboration), Phys. Rev. Lett. **89**, 102001 (2002).

[141] K. Abe *et al.* (Belle Collaboration), Phys. Rev. Lett. **89**, 142001 (2002) and hep-ex/0306015.

[142] D.M. Asner *et al.* (CLEO Collaboration), hep-ex/0312058, submitted to Phys. Rev. Lett.

[143] B. Aubert *et al.* (BaBar Collaboration), hep-ex/0311038.

[144] C. Edwards *et al.* (Crystal Ball Collaboration), Phys. Rev. Lett. **48**, 70 (1982).

[145] W. Buchmüller and S.H.H. Tye, Phys. Rev. **D24**, 132 (1981); T.A. Lähde and D.O. Riska, Nucl. Phys. **A707**, 425 (2002).

[146] S.K. Choi *et al.* (Belle Collaboration), Phys. Rev. Lett. **91**, 262001 (2003).

[147] See, for example, M.B. Voloshin and L.B. Okun, JETP Lett. **23**, 333 (1976); A. De Rujula, H. Georgi and S.L. Glashow, Phys. Rev. Lett. **38**, 317 (1977); and N. Tornqvist, .Z. Physik **C61**, 525 (1994).

[148] V.V. Kiselev, A.K. Likhoded, M.V. Shevlyagin, Phys. Lett. **B332**, 441 (1994); G.T. Bodwin, J. Lee, E. Braaten, Phys. Rev. **D67**, 054023 (2003).

[149] Geoffrey T. Bodwin, hep-ph/0312173.

[150] D. Acosta *et al.* (CDF II Collaboration), hep-ex/0312021, submitted to Phys. Rev. Lett.

[151] See, for example, M.B. Voloshin, hep-ph/0309307 and E.S. Swanson, hep-ph/0311229.

[152] T.A. Armstrong *et al.* (E760 Collaboration), Phys. Rev. Lett. **69**, 2337 (1992).

[153] A. Tomaradze, Talk presented at Hadron 2001, Prodvino, Russia, Aug. 25 - Sept. 1, 2001.

[154] M. Suzuki, Phys. Rev. **D66**, 037503 (2002).

[155] K. Abe *et al.* (Belle Collaboration), Phys. Rev. Lett. **89**, 011803 (2002).

[156] Round table discussions at 19th International Workshop on Weak Interactions and Neutrinos (WIN03), Oct. 6-11, 2003, Lake Geneva, Wisconsin, USA, http://conferences.fnal.gov/win03/Talks/CKM/SecIX+X/ROUNDTABLE.doc.

[157] T. Nakada, talk given at the 5th workshop on higher luminosity B factory, Sep. 24-26, 2003, Izu, Japan, http://belle.kek.jp/superb/workshop/2003/HL05/slide/H/Nakada.ppt.

[158] R. Forty, talk given at Eighth workshop on high energy physics phenomenology (WHEPP-8), January 5-16, 2004, Bombay, India, http://lhcb-doc.web.cern.ch/lhcb-doc/presentations/conferencetalks/postscript/2004presentations/FortyBombay04.ppt.

Chapter 5

Study of New Physics Scenarios at SuperKEKB

5.1 New Physics Case Study

As discussed in the previous sections, there are a number of processes in which one may find observable effects of physics beyond the Standard Model (BSM). In particular, processes induced by loop diagrams can be sensitive to new particles at the TeV energy scale, as the Standard Model contribution is relatively suppressed. Such processes include $\mathcal{S}_{\phi K^0_S}$, $A^{\rm dir}_{CP}(b \to s\gamma)$, $A^{\rm mix}_{CP}(b \to s\gamma)$, $Br(b \to s\ell^+\ell^-)$, $A_{FB}(b \to s\ell^+\ell^-)$, and $Br(\tau \to \mu\gamma)$. In this section we consider some specific new physics models in the context of supersymmetry and investigate how their effects could be seen in these processes.

The hierarchy problem of the Higgs mass suggests that the physics beyond the Standard Model most likely exists at the TeV energy scale, and hence the LHC has a good chance of discovering some new particles. However, the flavor structure of BSM will still remain to be investigated, as hadron collider experiments are largely insensitive to flavor-violating processes. In SUSY models, for example, flavor physics is the key to investigating the mechanism of SUSY breaking, which is expected to lie at a higher energy scale.

As discussed in Section 3.3, even in the minimal supersymmetric extension of the SM (MSSM) most of the parameter space is already excluded by the present FCNC constraints, and hence one has to consider some structure in the soft SUSY breaking terms such that the FCNC processes are naturally suppressed. In this study we consider the following three models according to refs. [1, 2].

- *Minimal supergravity model (mSUGRA)*
  In this model one assumes that supersymmetry is broken in some invisible (hidden) sector and its effect is mediated to the visible (observable) world only through the gravitational interaction. Since gravity is insensitive to flavor, the induced soft breaking terms are flavor blind at the scale where they are generated. Namely, all sfermions have degenerate mass m_0^2; trilinear couplings of scalars are proportional to Yukawa couplings; all gauginos are degenerate with mass $M_{1/2}$. Even though the soft breaking terms are flavor blind, they could induce flavor violation as they evolve from the SUSY breaking scale (assumed here to be $M_X \simeq 2 \times 10^{16}$ GeV for simplicity) to the electroweak scale by the renormalization group equations, since the Yukawa couplings are flavor dependent. In general, FCNC effects are small for this model.

- *$SU(5)$ SUSY GUT with right-handed neutrinos*
  Grand Unification (GUT) is one of the motivations to consider supersymmetric models, as they naturally lead to the unification of the gauge couplings. Since, in GUT models quarks and leptons belong to the same multiplet at the GUT scale, the flavor mixings of the quark and lepton sectors are related to each other. In particular, large neutrino mixing can induce large squark mixing for right-handed down-type squarks [3–8]. In this class of models we consider two cases where the masses of the right-handed neutrinos are *degenerate* or *non-degenerate*. Because of the large neutrino mixing, the bulk of the parameter space is excluded in the degenerate case due to the $\mathcal{B}(\mu \to e\gamma)$ constraint, and as a result the effect on other FCNC processes is limited. On the other hand, for the non-degenerate case one can expect larger FCNC effects.

- *$U(2)$ flavor symmetry*
  The family structure of the quarks and leptons could be explained by some flavor symmetry among generations. Although $U(3)$ is a natural candidate for such a symmetry, it is badly broken by the top quark Yukawa coupling. Therefore, here we consider a $U(2)$ flavor symmetry among the first two generations in the context of SUSY. We assume some breaking structure of the $U(2)$ symmetry for the Yukawa couplings, squark mass matrices, and the scalar trilinear couplings.

These models still contain many parameters. We randomly choose a number of points from the multi-dimensional parameter space, while fixing the gluino mass at 600 GeV and $\tan\beta = 30$. Among these points, those that are already excluded from existing mass bounds and FCNC constraints, such as ϵ_K, $b \to s\gamma$ branching fraction, and $\mu \to e\gamma$ branching ratio, are eliminated. The results for several quantities are then shown in the following scatterplots.

First of all, the expectations from these models for two interesting FCNC processes $\mathcal{S}_{\phi K^0_S}$ and $A_{CP}^{\rm mix}(b \to s\gamma)$ are shown in Fig. 5.1, together with the expected sensitivity at SuperKEKB. Each dot in the plots shows a randomly chosen parameter point of the model. One can observe a significant deviation from the SM for the $SU(5)$ SUSY GUT with a right-handed neutrino (non-degenarate case) while the mSUGRA model gives comparatively small deviations from the SM for these FCNC processes. We emphasize that these different models could have almost an identical mass spectrum of SUSY particles as shown on the bottom panels in the figure. This means that the flavor structure of BSM models is barely probed by measurements at high energy collider experiments.

Predictions for other interesting FCNC processes are shown in Figs. 5.2–5.6 for the above four SUSY models.

5.2 Model Independent Approaches

In the SuperKEKB experiment there are a number of processes from which we can measure the fundamental parameters of the Standard Model (SM), *i.e.* quark mixing angles and phases. In this chapter we discuss how these measurements at SuperKEKB may be used to gain insight into the flavor structure of BSM without assuming some particular model.

Fitting the CKM parameters using the available data is a common practice. One draws the constraints obtained from several measurements in the parameter space of $(\bar{\rho}, \bar{\eta})$, which are the least known parameters in the usual parametrization of the CKM matrix. If one found an inconsistency among the different input quantities, it would indicates the existence of a BSM effect for some quantities. We investigate how SuperKEKB can contribute to narrowing down the allowed region from each measurement.

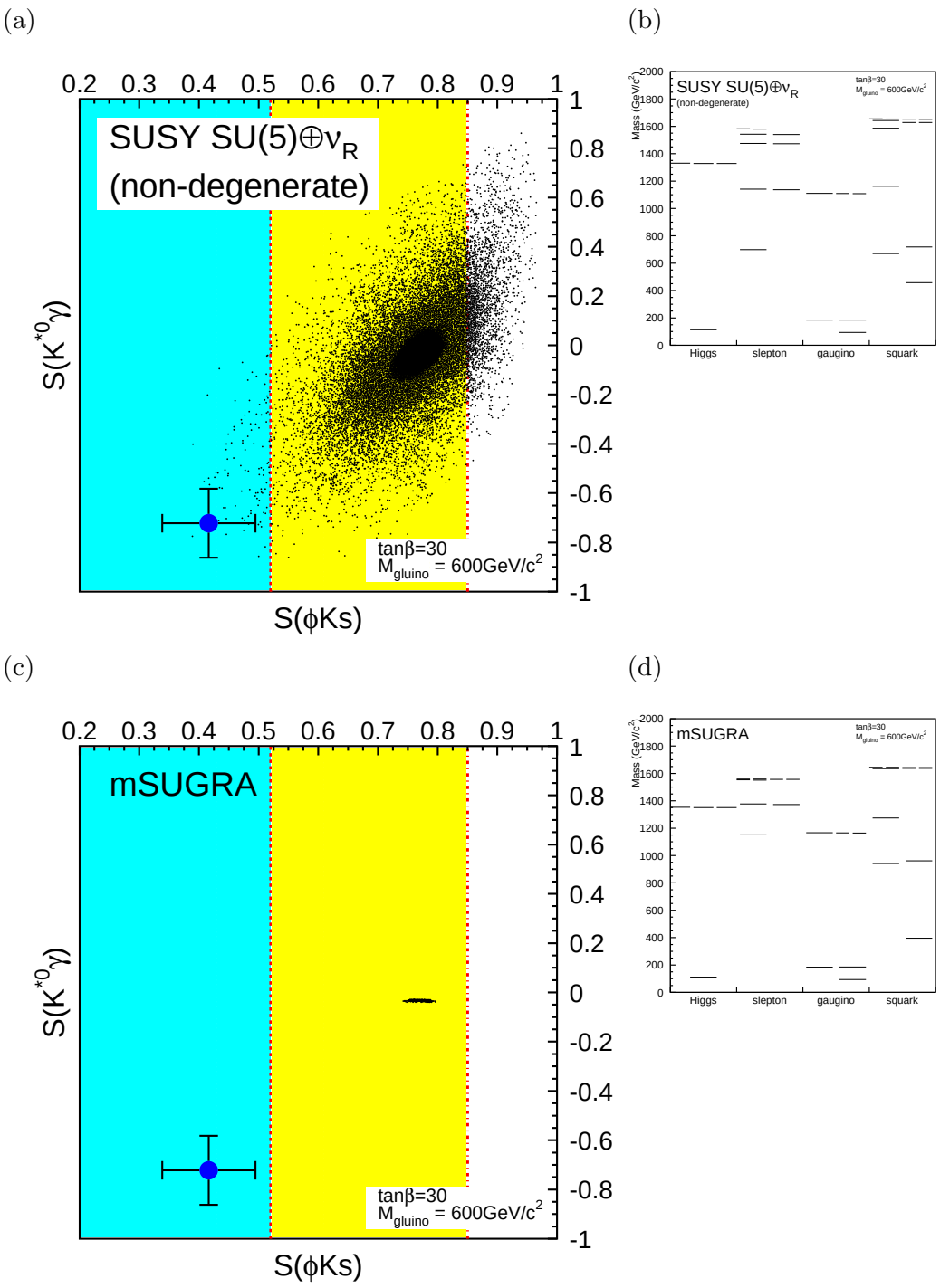

Figure 5.1: $\mathcal{S}_{K^{*0}\gamma}$ and $\mathcal{S}_{\phi K^0_S}$ for various parameters in (a) SUSY $SU(5)$ with right-handed neutrinos (the non-degenerate case), and (c) mSUGRA. Circles with error bars indicate an expected result from a certain parameter set in the $SU(5)$ SUSY GUT, where the errors are obtained at 5 ab^{-1}. A present experimental bound at 2σ (3σ) level is also shown by the dashed (dot-dashed) vertical line. Associated small figures show examples of mass spectra of SUSY particles for (b) the SUSY $SU(5)$ and (d) mSUGRA.

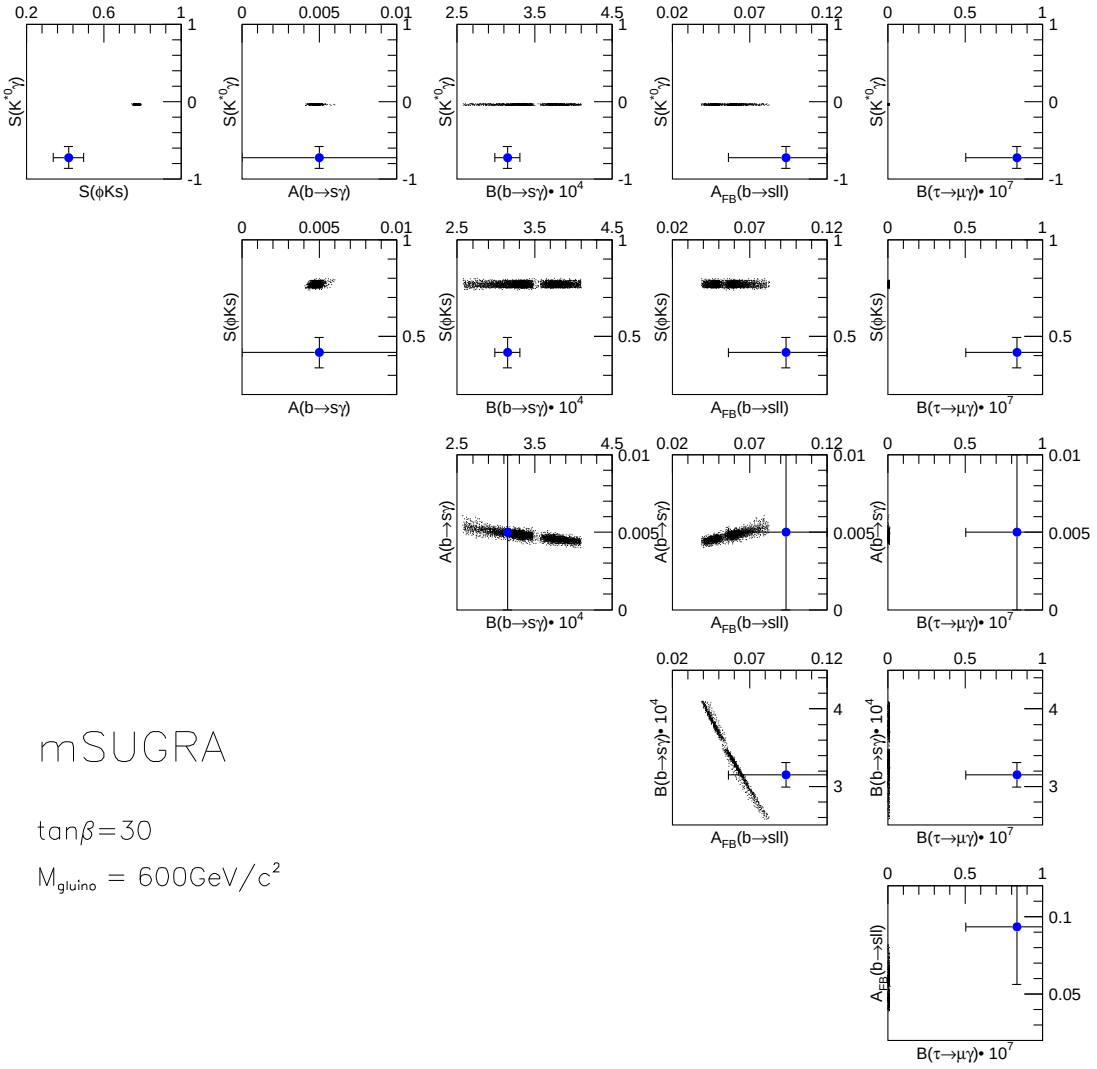

Figure 5.2: Correlations between key observables in the case of mSUGRA. Dots show the possible range in mSUGRA. The circles correspond to a certain parameter set of non-degenerate SUSY SU(5) GUT model with ν_R. Expected errors with an integrated luminosity of 5 ab^{-1} are shown by bars associated with the circles.

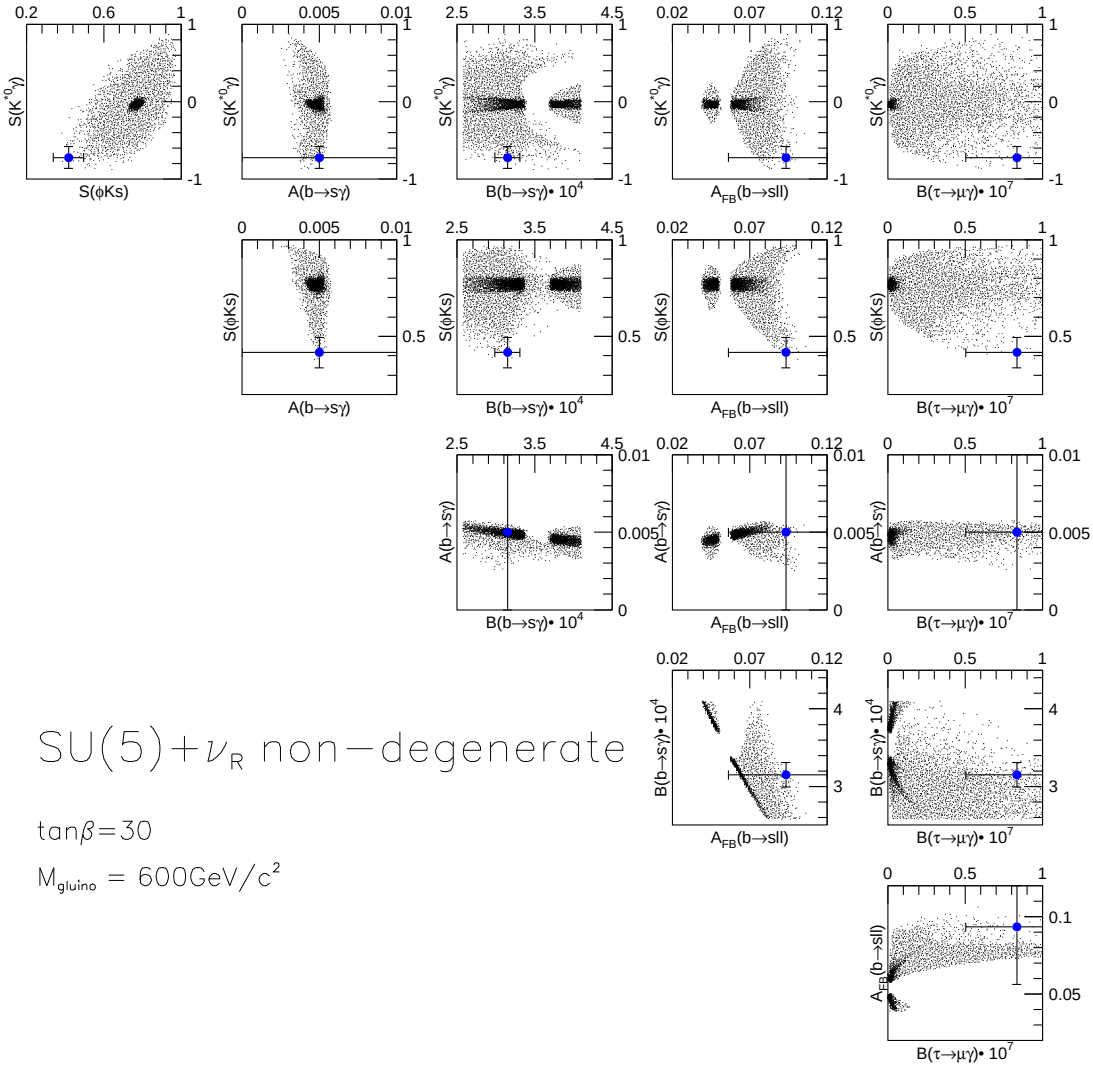

Figure 5.3: Correlations between key observables in the case of the non-degenerate SUSY SU(5) GUT model with ν_R. Dots show the possible range in the model. The circles correspond to a certain parameter set in this model. Expected errors with an integrated luminosity of 5 ab^{-1} are shown by bars associated with the circles.

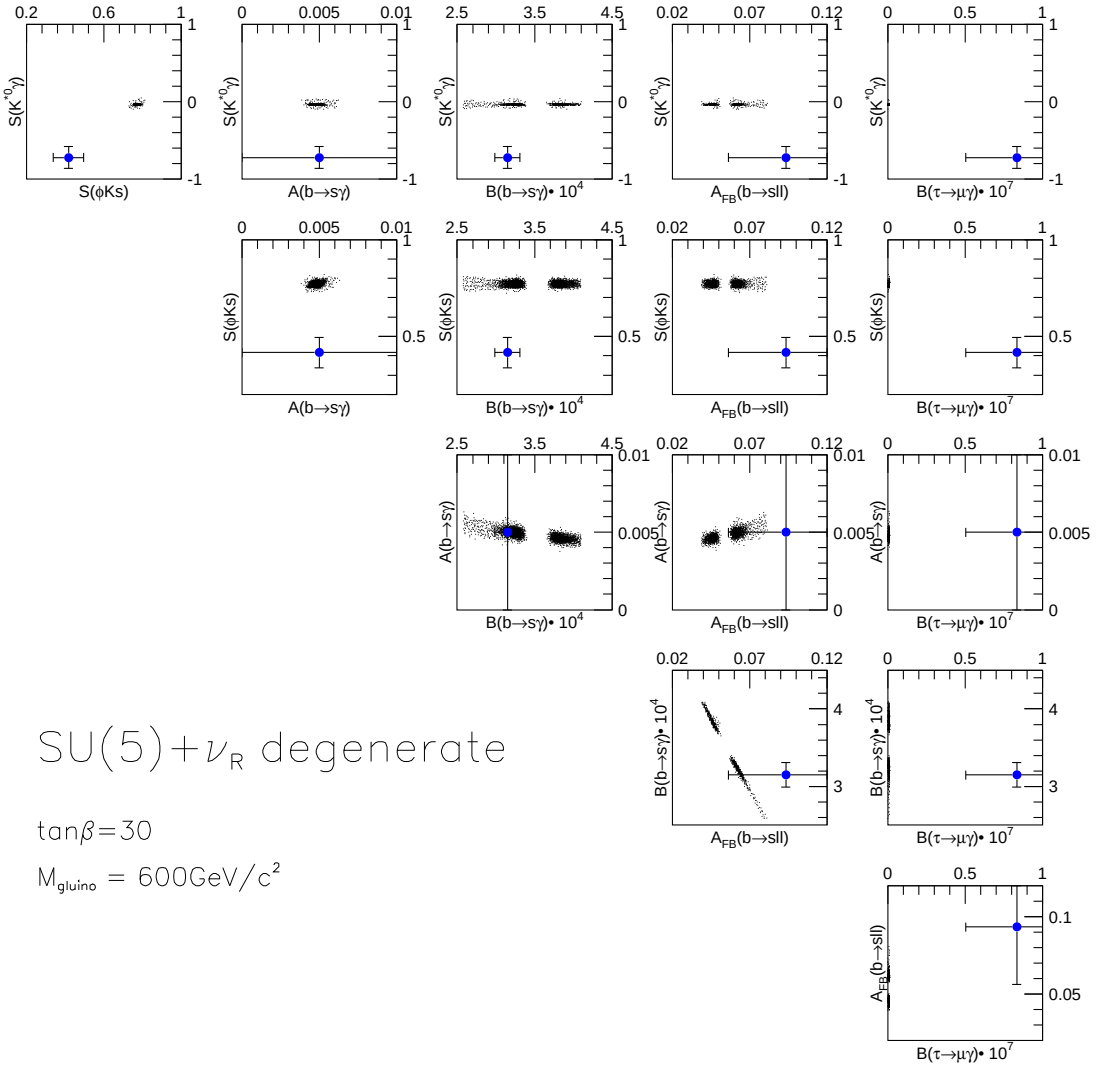

Figure 5.4: Correlations between key observables in the case of the degenerate SUSY SU(5) GUT model. Dots show the possible range in the model. The circles correspond to a certain parameter set of the non-degenerate SUSY SU(5) GUT model with ν_R. Expected errors with an integrated luminosity of 5 ab^{-1} are shown by bars associated with the circles.

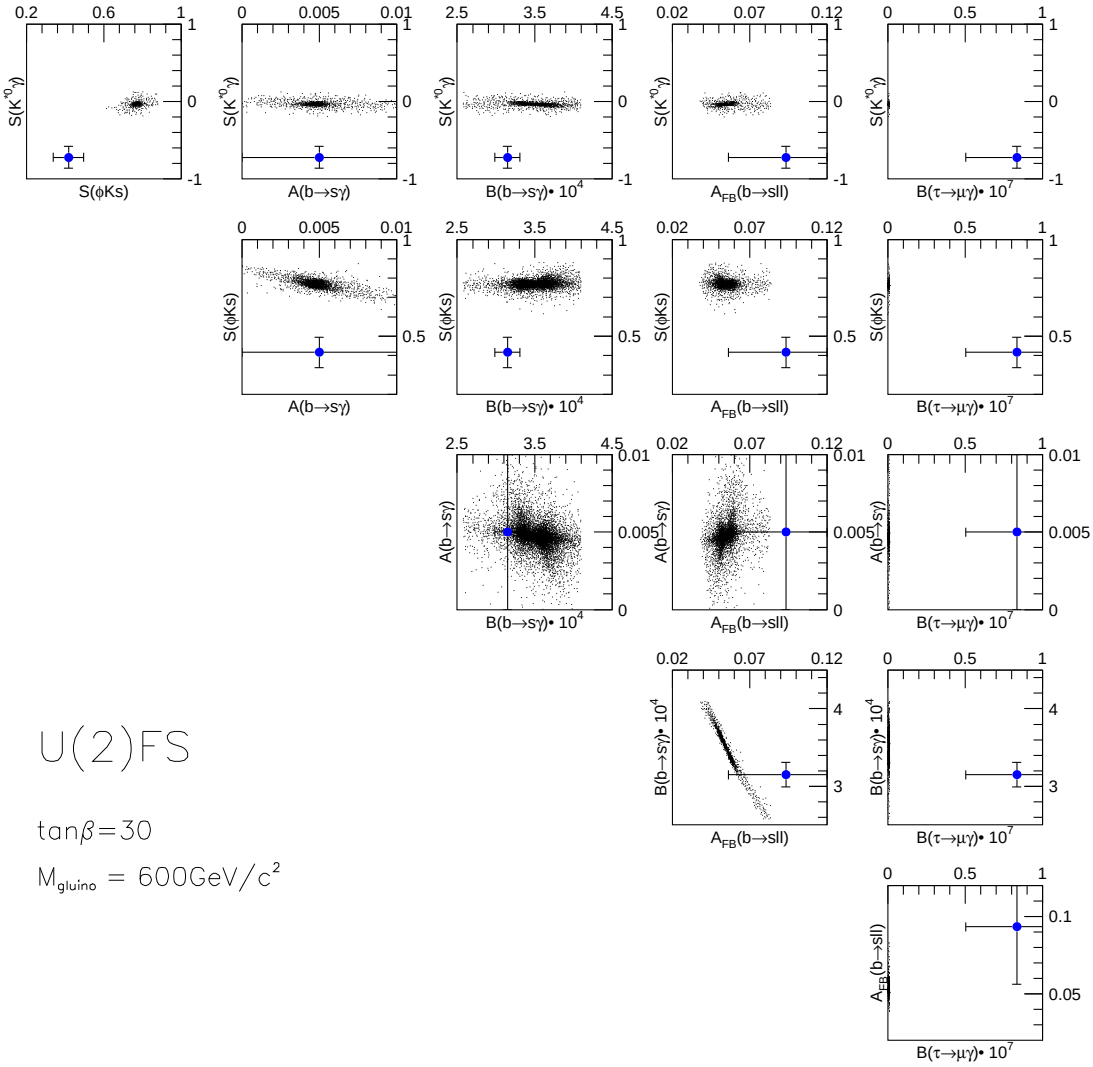

Figure 5.5: Correlations between key observables in the case of the U(2) flavor symmetry model. Dots show the possible range in the model. The circles correspond to a certain parameter set of the non-degenerate SUSY SU(5) GUT model with ν_R. Expected errors with an integrated luminosity of 5 ab^{-1} are shown by bars associated with the circles.

Figure 5.6: Correlations between key observables in case of $U(2)$ flavor symmetry.

Once deviations from the SM are established, the next question is which quantities are affected by the new physics and how. To consider such questions, it is natural to assume that tree-level processes are not affected much by the new physics. If the Standard Model is a low energy effective theory of some more fundamental theory, the new physics effects will manifest themselves as non-renormalizable higher dimensional operators. In tree-level processes such operators are relatively suppressed, while in loop-induced FCNC processes the higher dimensional operators could compete with the loop effects of the Standard Model.

Therefore, we may proceed in three steps. Firstly, we obtain a constraint on $(\bar{\rho}, \bar{\eta})$ using only tree level processes, *i.e.* $|V_{ub}|$ from the semileptonic decay $b \to u\ell\bar{\nu}$ and ϕ_3 from the DK asymmetry. The result can be considered as the SM value of $(\bar{\rho}, \bar{\eta})$ even in the presence of the new physics. Secondly, the allowed region for $(\bar{\rho}, \bar{\eta})$ is compared with the determination through $B^0 - \bar{B}^0$ mixing, *i.e.* Δm_d and $\sin 2\phi_1$ from $B \to J/\psi K^0_S$. If we assume that the decay amplitude for $B \to J/\psi K^0_S$ is dominanted by the tree level contribution, this value of $(\bar{\rho}, \bar{\eta})$ contains loop effects from $\Delta B = 2$ process. Finally, we consider a parametrization of new physics contributions to $B^0 - \bar{B}^0$ mixing with the amplitude M_{12} expressed as $M_{12} = M_{12}^{\rm SM} + M_{12}^{\rm new}$, and obtain a constraint on $M_{12}^{\rm new}$ [9–11], Such a study of the CKM parameter fit is described in the next section.

The separation of the Standard Model and new physics contributions can also be formulated for radiative and semileptonic B decays: $b \to s\gamma$ and $b \to s\ell^+\ell^-$. As discussed in Section 3.4, in the language of the effective Hamiltonian the new physics contribution can be expressed in terms of Wilson coefficients.

A Similar strategy can be applied to hadronic decay amplitudes. For instance, the difference between the values of $\sin 2\phi_1$ measured by $J/\psi K^0_S$ and ϕK^0_S implies some new physics effect in the $b \to s\bar{s}s$ penguin process. One can parametrize the $b \to s\bar{s}s$ amplitude in terms of SM and BSM amplitudes. In this case, however, the calculation of the decay amplitudes from the fundamental theory is much more difficult and the utility of the parametrization is limited.

5.3 The CKM Fit

We perform a global fit to the CKM parameters $(\bar{\rho}, \bar{\eta})$ using the CKMfitter package [12][1]. If no new physics effect exists, all the measurements should agree with each other in the $(\bar{\rho}, \bar{\eta})$ plane and can be combined to obtain the constraint on them. On the other hand, the effect of new physics may cause discrepancies among these measurements.

The strategy is to look for the new physics effects from only one source at a time, in order to quantitatively identify the new physics contribution. Assuming that the tree-level processes are insensitive to new physics effects, we determine the SM value of $(\bar{\rho}, \bar{\eta})$ using $|V_{ub}|$ from $B \to X_u\ell\nu$ decays and ϕ_3 from $B^\pm \to D^0[\to K^0_S\pi^+\pi^-]K^\pm$ [2]. We then examine the $b \to d$ box diagram, *i.e.* $B^0 - \bar{B}^0$ oscillations, for which the available measurements are $\sin 2\phi_1$ from $B^0 \to c\bar{c}K^0$ and Δm_d.

The input parameters used in the fit are listed in Table 5.1 where the errors are based on the sensitivity studies in the previous sections. The errors for Δm_d are extrapolated from the current measurements with an irreducible systematic error of 0.4% [14]. The current value of $f_{B_d}\sqrt{B_{B_d}}$ is from a recent unquenched lattice calculation $215(11)(^{+\ 0}_{-23})(15)$ MeV [15], where the

[1] We use the CKMFitter package with the *R*-fit option. The parameter values are the default values used in the package if not mentioned explicitly.

[2] There is a possible effect of new physics on the Dalitz distributions through $D^0 - \bar{D}^0$ mixing or CP violation in D^0. However, we can check and measure the effect from the data using soft-pion tagged D^0 decays ($D^{*+} \to D^0\pi^+_s$) [13], and verify whether its effect to the ϕ_3 measurement is small enough.

parameters	central values	errors		
		0.5 ab^{-1}	5 ab^{-1}	50 ab^{-1}
$\sin 2\phi_1$	0.753	$\pm 4.4\%$	$\pm 2.5\%$	$\pm 1.9\%$
ϕ_3 (Dalitz)	65°	$\pm 23\%$	$\pm 7.2\%$	$\pm 2.3\%$
$\lvert V_{ub}\rvert$	3.79×10^{-3}	$\pm 6.9\% \pm 8\%$	$\pm 3.7\% \pm 4.5\%$	$\pm 3.2\% \pm 3\%$
Δm_d	0.496 ps^{-1}	$\pm 0.8\%$	$\pm 0.5\%$	$\pm 0.4\%$
$f_{B_d}\sqrt{B_{B_d}}$	0.230 GeV	$\pm 0.011 \pm 0.026$	$\pm 0.011 \pm 0.026$	$\pm 0.005 \pm 0.015$
ϕ_2	91°	$\pm 9^\circ$	$\pm 2.9^\circ$	$\pm 0.9^\circ$

Table 5.1: Summary of inputs to in the CKM-fit. If two errors are given, the second error is treated as flat in the fit [12]. Otherwise, errors are taken to be Gaussian. $|V_{cb}|$ is fixed at 4.04×10^{-3} in the fit. Central values correspond to $\bar{\rho} = 0.176$ and $\bar{\eta} = 0.376$.

first error is statistical, the second is the uncertainty from the chiral extrapolation and the third is due to other systematic errors. In Table 5.1 the two systematic errors are combined and the error is symmetrized. To improve the accuracy of the lattice calculation, simulations at significantly smaller sea quark masses will be required. With the staggered fermion formulation for sea quarks this is possible, albeit with additional complications, by introducing more flavors (or tastes) of fictitious quarks [16]. Within several years it will also become possible to perform unquenched simulations using lattice fermions with an exact chiral symmetry, such as overlap or domain-wall fermions. The reduction of errors down to a level of several percent is feasible within the time scale of the construction of SuperKEKB.

The constraint on $(\bar{\rho}, \bar{\eta})$ using all these measurements for the SM case is shown in Fig. 5.7 as a reference.

Among those input parameters the measurement of the angle ϕ_3 is not available at present. Therefore, despite the good agreement of $(\bar{\rho}, \bar{\eta})$ from different measurements, there is a possibility that ϕ_3 does not agree with the current world average obtained with the CKM fit. It means that the SM value of $(\bar{\rho}, \bar{\eta})$ could still be different from the current values. To see what could be observed at SuperKEKB, here we show a plot assuming that the central value of the ϕ_3 measurement is 90° instead of the current average 65° (Fig. 5.8). This plot indicates that the theoretical uncertainty in the hadronic matrix element $f_{B_d}\sqrt{B_{B_d}}$ will become the limiting factor for testing the SM using the CKM unitarity.

The effect of new physics on the $b \to d$ box diagram can be expressed as

$$M_{12} = M_{12}^{\rm SM} + M_{12}^{\rm new}, \tag{5.1}$$

where $M_{12}^{\rm SM}$ ($M_{12}^{\rm new}$) is the contribution of the amplitude to the $b \to d$ box diagram from the SM (new physics particles) [9–11]. The result of a fit for the constraints in the (Re $M_{12}^{\rm new}$, Im $M_{12}^{\rm new}$) plane is shown in Fig. 5.9.

Measurements of ϕ_2 using $B^0 \to \pi^+\pi^-$ or $B^0 \to \rho\pi$ decay modes are contaminated by the $b \to d$ penguin diagram. New physics contributes to the $b \to d$ box and penguin amplitudes in a model dependent way. However, the "penguin trapping" technique based on the isospin relation is not affected by the new physics contribution in the penguin-loop as long as the new physics diagrams only contribute to $\Delta I = 1/2$ amplitudes. In this case, the sum of the SM penguin and new physics penguin amplitudes is treated as a penguin amplitude to be trapped out. With this assumption, we examine the additional constraint on new physics parameters from the ϕ_2 measurement. The results are shown in Fig. 5.10.

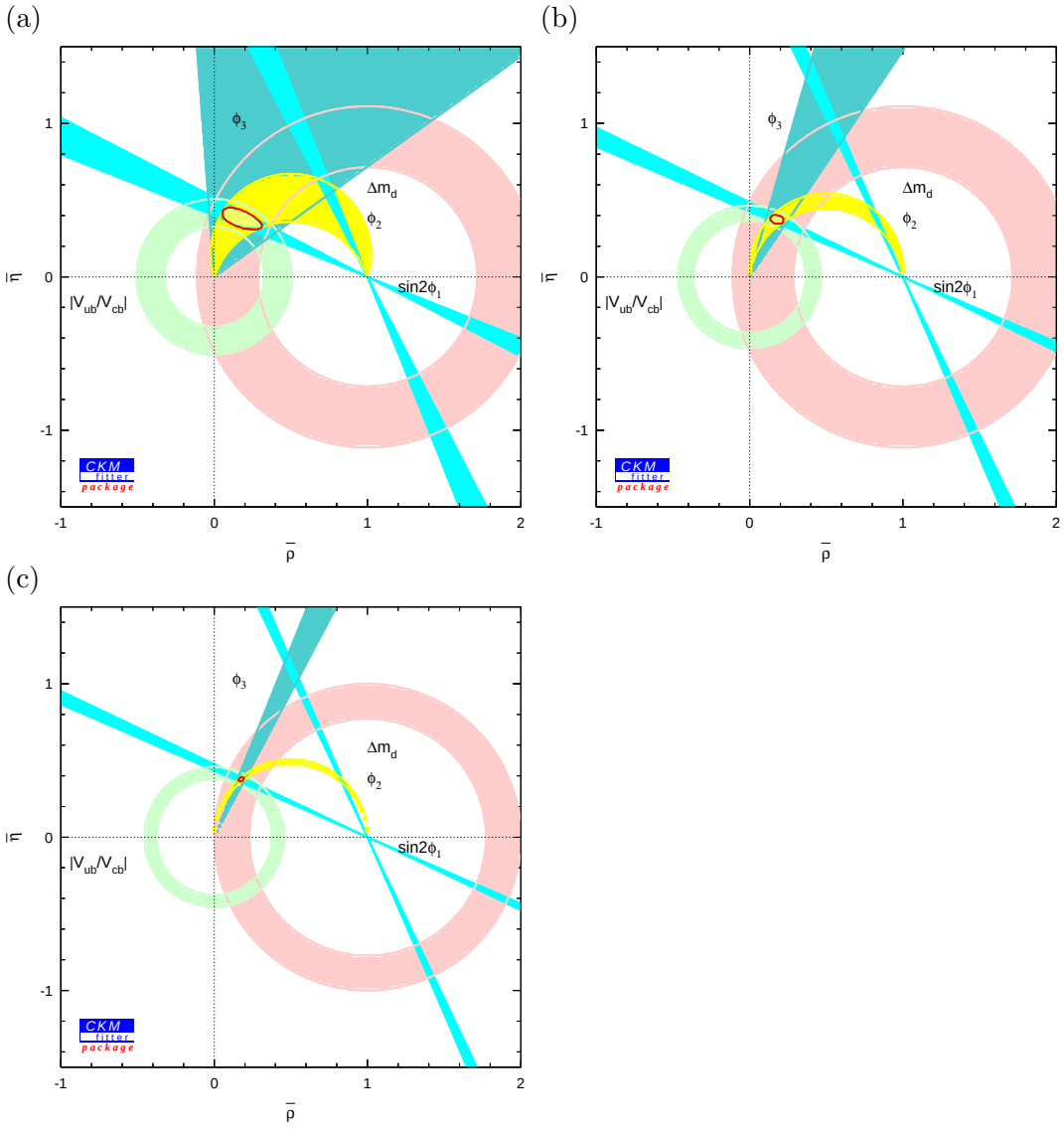

Figure 5.7: Constraints on the CKM unitarity triangle at (a) 0.5 ab^{-1}, (b) 5 ab^{-1}, and (c) 50 ab^{-1}.

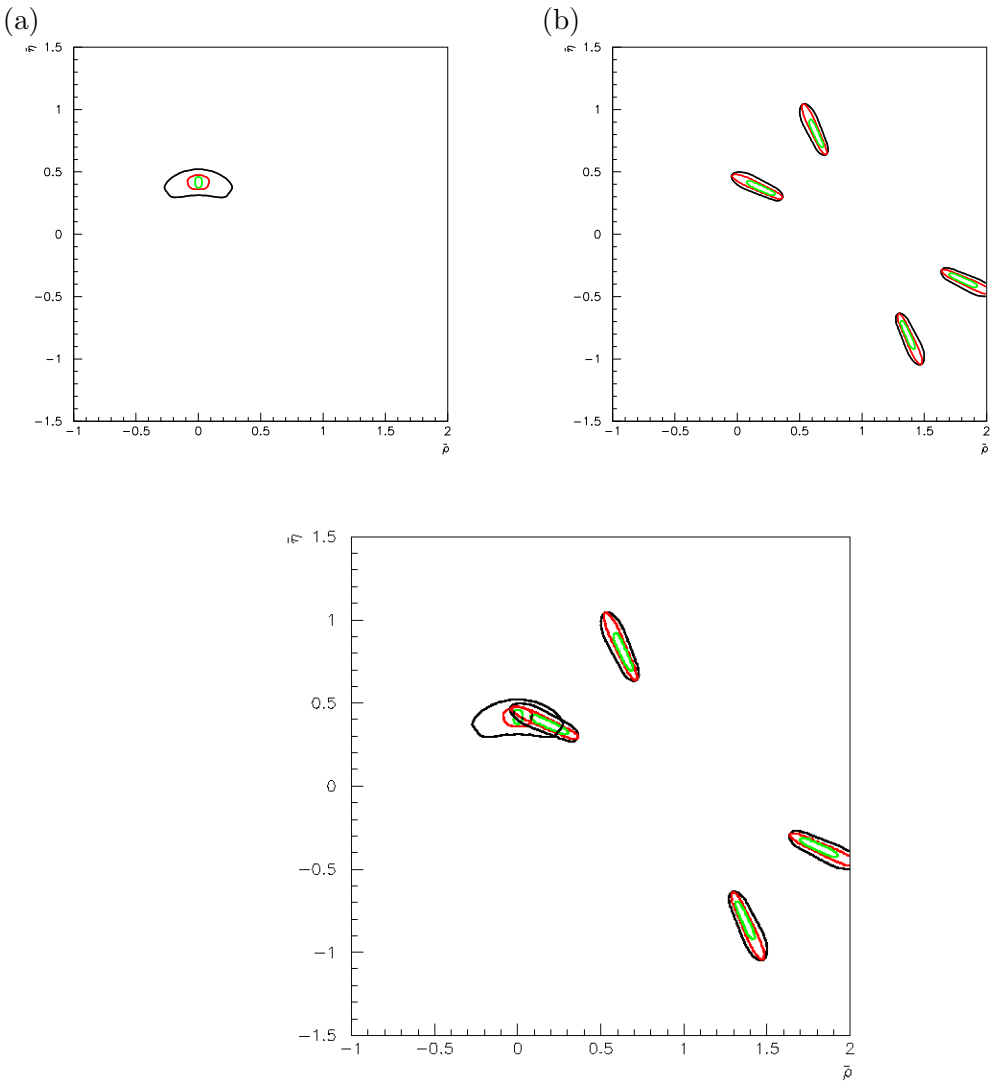

Figure 5.8: (a) Constraints from tree-level processes, *i.e.* $|V_{ub}|$ and ϕ_3 assuming $\phi_3 = 90°$. (b) Constraints from processes induced by the $b \to d$ box diagram, *i.e.* $\sin 2\phi_1$ and Δm_d. Contours correspond to 0.5 ab^{-1} (black), 5 ab^{-1} (red) and 50 ab^{-1} (green). (c) Both contours overlap.

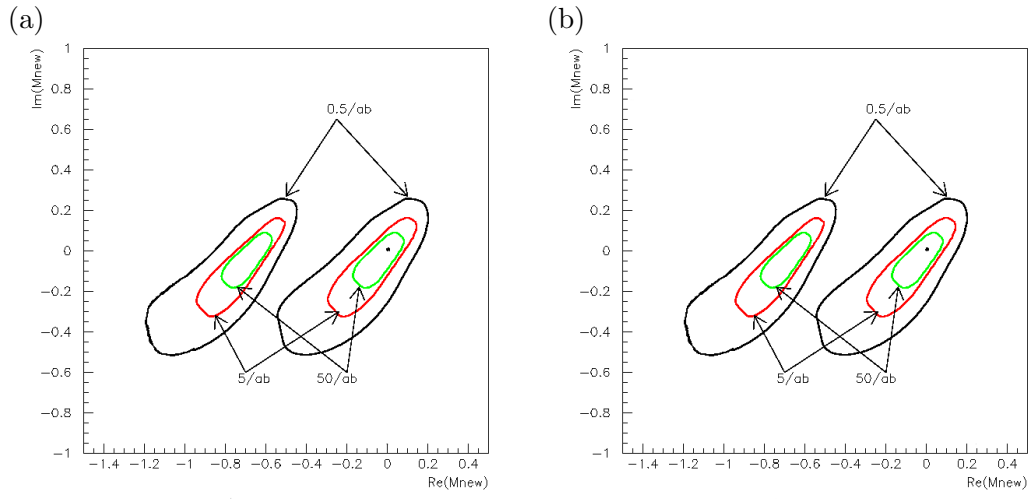

Figure 5.9: Constraints on the new physics contribution to the $b \to d$ box amplitude M_{12}^{new}. Contours correspond to 0.5 ab^{-1} (black), 5 ab^{-1} (red) and 50 ab^{-1} (green). The predictions from SUSY models are indicated by dots in the plots for (a) mSUGRA and (b) for the $SU(5)$ SUSY GUT with right-handed neutrinos.

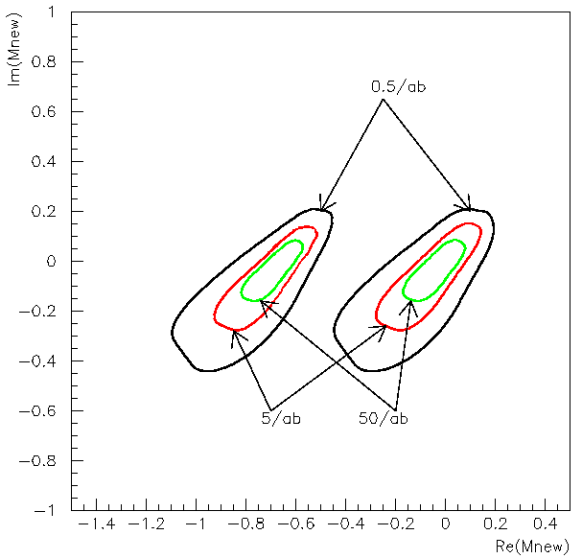

Figure 5.10: Constraints on the new physics contribution to the $b \to d$ box amplitude $M_{12}^{\rm new}$. Contours correspond to 0.5 ab^{-1} (black), 5 ab^{-1} (red) and 50 ab^{-1} (green). The measurement of ϕ_2 is included in the fit.

Figure 5.9 also show the SUSY model predictions for (Re $M_{12}^{\rm new}$, Im $M_{12}^{\rm new}$). For the SUSY models we choose the ones discussed in the previous section. In these models the deviation from the SM is really tiny for M_{12}, which also gives a useful piece of information to investigate the details of the SUSY models.

The method we described above can be extended to the $b \to s$ box diagram (Δm_s) and time dependent CP violation using $B_s^0 \to J\psi\phi$ *etc.*, $s \to d$ box diagram (ϵ_K), and $b \to d$ penguin diagram ($b \to d\gamma$ *etc.*).

References

[1] T. Goto, Y. Okada, Y. Shimizu, T. Shindou and M. Tanaka, "Exploring flavor structure of supersymmetry breaking at B factories," Phys. Rev. D **66**, 035009 (2002) [arXiv:hep-ph/0204081].

[2] T. Goto, Y. Okada, Y. Shimizu, T. Shindou and M. Tanaka, "Exploring flavor structure of supersymmetry breaking from rare B decays and unitarity triangle," arXiv:hep-ph/0306093.

[3] S. Baek, T. Goto, Y. Okada and K. Okumura, "Neutrino oscillation, SUSY GUT and B decay," Phys. Rev. D **63**, 051701 (2001) [arXiv:hep-ph/0002141].

[4] T. Moroi, "Effects of the right-handed neutrinos on $\Delta S = 2$ and $\Delta B = 2$ processes in supersymmetric SU(5) model," JHEP **0003**, 019 (2000) [arXiv:hep-ph/0002208].

[5] T. Moroi, "CP violation in $B_d \to \phi K_S$ in SUSY GUT with right-handed neutrinos," Phys. Lett. B **493**, 366 (2000) [arXiv:hep-ph/0007328].

[6] N. Akama, Y. Kiyo, S. Komine and T. Moroi, "CP violation in kaon system in supersymmetric SU(5) model with seesaw-induced neutrino masses," Phys. Rev. D **64**, 095012 (2001) [arXiv:hep-ph/0104263].

[7] S. Baek, T. Goto, Y. Okada and K. i. Okumura, "Muon anomalous magnetic moment, lepton flavor violation, and flavor changing neutral current processes in SUSY GUT with right-handed neutrino," Phys. Rev. D **64**, 095001 (2001) [arXiv:hep-ph/0104146].

[8] D. Chang, A. Masiero and H. Murayama, Phys. Rev. D **67**, 075013 (2003) [arXiv:hep-ph/0205111].

[9] J. M. Soares and L. Wolfenstein, "CP violation in the decays $B^0 \to \psi K_S$ and $B^0 \to \pi^+\pi^-$: A Probe for new physics," Phys. Rev. D **47**, 1021 (1993).

[10] T. Goto, N. Kitazawa, Y. Okada and M. Tanaka, "Model independent analysis of $B-\bar{B}$ mixing and CP violation in B decays," Phys. Rev. D **53**, 6662 (1996) [arXiv:hep-ph/9506311].

[11] R. N. Cahn and M. P. Worah, "Constraining the CKM parameters using CP violation in semi-leptonic B decays," Phys. Rev. D **60**, 076006 (1999) [arXiv:hep-ph/9904480].

[12] A. Hocker, H. Lacker, S. Laplace and F. Le Diberder, "A new approach to a global fit of the CKM matrix," Eur. Phys. J. C **21**, 225 (2001) [arXiv:hep-ph/0104062].

[13] D. M. Asner *et al.* [CLEO Collaboration], "Search for CP violation in $D^0 \to K_S^0\pi^+\pi^-$," arXiv:hep-ex/0311033.

[14] F. J. Ronga, "Advances in Δm_d measurements," eConf **C0304052**, WG210 (2003) [arXiv:hep-ex/0306061].

[15] S. Aoki *et al.* [JLQCD Collaboration], "$B^0 - \bar{B}^0$ mixing in unquenched lattice QCD," Phys. Rev. Lett. **91**, 212001 (2003) [arXiv:hep-ph/0307039].

[16] C. T. H. Davies *et al.* [HPQCD Collaboration], "High-precision lattice QCD confronts experiment," arXiv:hep-lat/0304004.